
Reliability Analysis of Containment Strength

Sequoyah and McGuire Ice Condenser Containments

Prepared by L. Greimann, F. Fanous, A. Sabri,
D. Ketelaar, A. Wolde-Tinsae, D. Bluhm

Ames Laboratory
Iowa State University

Prepared for
U.S. Nuclear Regulatory
Commission

DISCLAIMER

This book was prepared as an account of work sponsored by an agency of the United States Government. Neither the United States Government nor any agency thereof, nor any of their employees, makes any warranty, express or implied, or assumes any legal liability or responsibility for the accuracy, completeness or usefulness of any information, apparatus, product, or process disclosed, or represents that its use would not infringe privately owned rights. Reference herein to any specific commercial product, process, or service by trade name, trademark, manufacturer, or otherwise, does not necessarily constitute or imply its endorsement, recommendation, or favoring by the United States Government or any agency thereof. The views and opinions of authors expressed herein do not necessarily state or reflect those of the United States Government or any agency thereof.

Available from

GPO Sales Program
Division of Technical Information and Document Control
U. S. Nuclear Regulatory Commission
Washington, D. C. 20555

Printed copy price: \$7.50

and

National Technical Information Service
Springfield, Virginia 22161

Reliability Analysis of Containment Strength

Sequoyah and McGuire Ice Condenser Containments

Manuscript Completed: April 1982
Date Published: August 1982

Prepared by
L. Greimann, F. Fanous, A. Sabri,
D. Ketelaar, A. Wolde-Tinsae, D. Bluhm

Ames Laboratory
Iowa State University
Ames, IA 50011

Prepared for
Division of Engineering
Office of Nuclear Reactor Regulation
U.S. Nuclear Regulatory Commission
Washington, D.C. 20555
NRC FIN A4131

NOTICE

Availability of Reference Materials Cited in NRC Publications

Most documents cited in NRC publications will be available from one of the following sources:

1. The NRC Public Document Room, 1717 H Street, N.W.
Washington, DC 20555
2. The NRC/GPO Sales Program, U.S. Nuclear Regulatory Commission,
Washington, DC 20555
3. The National Technical Information Service, Springfield, VA 22161

Although the listing that follows represents the majority of documents cited in NRC publications, it is not intended to be exhaustive.

Referenced documents available for inspection and copying for a fee from the NRC Public Document Room include NRC correspondence and internal NRC memoranda; NRC Office of Inspection and Enforcement bulletins, circulars, information notices, inspection and investigation notices; Licensee Event Reports; vendor reports and correspondence; Commission papers; and applicant and licensee documents and correspondence.

The following documents in the NUREG series are available for purchase from the NRC/GPO Sales Program: formal NRC staff and contractor reports, NRC-sponsored conference proceedings, and NRC booklets and brochures. Also available are Regulatory Guides, NRC regulations in the *Code of Federal Regulations*, and *Nuclear Regulatory Commission Issuances*.

Documents available from the National Technical Information Service include NUREG series reports and technical reports prepared by other federal agencies and reports prepared by the Atomic Energy Commission, forerunner agency to the Nuclear Regulatory Commission.

Documents available from public and special technical libraries include all open literature items, such as books, journal and periodical articles, and transactions. *Federal Register* notices, federal and state legislation, and congressional reports can usually be obtained from these libraries.

Documents such as theses, dissertations, foreign reports and translations, and non-NRC conference proceedings are available for purchase from the organization sponsoring the publication cited.

Single copies of NRC draft reports are available free upon written request to the Division of Technical Information and Document Control, U.S. Nuclear Regulatory Commission, Washington, DC 20555.

Copies of industry codes and standards used in a substantive manner in the NRC regulatory process are maintained at the NRC Library, 7920 Norfolk Avenue, Bethesda, Maryland, and are available there for reference use by the public. Codes and standards are usually copyrighted and may be purchased from the originating organization or, if they are American National Standards, from the American National Standards Institute, 1430 Broadway, New York, NY 10018.

ABSTRACT

The Sequoyah and McGuire ice condenser containment vessels were designed to withstand pressures in the range of 12 to 15 psi. Since pressures of the order of 28 psi were recorded during the Three Mile Island incident, a need exists to more accurately define the strength of these vessels. A best estimate and uncertainty assessment of the strength of the containments was performed by applying the second moment reliability method. Material and geometric properties were supplied by the plant owners. A uniform static internal pressure was assumed. Gross deformation was taken as the failure criterion. Both approximate and finite element analyses were performed on the axisymmetric containment structure and the penetrations. The predicted strength for the Sequoyah vessel is 60 psi with a standard deviation of 8 psi. For McGuire, the mean and standard deviation are 84 psi and 12 psi, respectively. In an Addendum, results by others are summarized and compared and a preliminary dynamic analysis is presented.

TABLE OF CONTENTS

		<u>Page</u>
	ABSTRACT	iii
I.	INTRODUCTION	1
	1.1 Background	1
	1.2 Objective and Scope	1
	1.3 Containment Description	1
II.	UNCERTAINTY ANALYSIS	3
	2.1 Probabilistic Safety Analysis	3
	2.2 Second Moment Method - One Failure Mode	5
	2.2.1 Invariant Second Moment Method	6
	2.2.2 Non-normal Distributions	11
	2.3 Multiple Failure Modes	14
III.	PARAMETER STATISTICS	16
	3.1 Material Parameters	16
	3.1.1 Yield and Ultimate Stress	16
	3.1.2 Approximate Fracture Stress	16
	3.2 Geometric Parameters	22
	3.3 Resistance Modeling Error - General	23
	3.4 Load Modeling Error	26
IV.	FAILURE CRITERIA	27
	4.1 Containment Shell	28
	4.2 Attached Piping Equipment	29
	4.3 Combined Failure Criterion	30
V.	APPROXIMATE STRUCTURE ANALYSIS	34
	5.1 Stiffened Axisymmetric Shell	34
	5.1.1 Failure Criteria	34
	5.1.2 Modeling Error	36
	5.1.3 Application to Containment Vessels	37
	5.1.4 Sensitivity Analysis	38
	5.2 Penetration Intersections	39
	5.2.1 Failure Criteria	39
	5.2.2 Modeling Error	42
	5.2.3 Application to Containment Vessels	43
	5.2.4 Sensitivity Analysis	44
	5.3 Anchor Bolts	44
	5.4 Combined Failure	46

VI.	FINITE ELEMENT ANALYSIS	47
	6.1 ANSYS Finite Element Program	47
	6.2 Failure Criteria	48
	6.3 Stiffened Axisymmetric Shell	48
	6.3.1 Finite Element Modeling Guidelines	48
	6.3.2 Modeling Error	51
	6.3.3 Applications	53
	6.3.3.1 Finite Element Model	53
	6.3.3.2 Results	54
	6.3.4 Uncertainty Analysis	55
	6.4 Penetration Analysis	56
	6.4.1 Modeling Guidelines	56
	6.4.2 Experimental vs ANSYS Results	57
	6.4.3 Application	58
	6.4.3.1 Finite Element Model	58
	6.4.3.2 Results	60
	6.4.4 Uncertainty Analysis	60
	6.5 Combined Failure Modes	61
VII.	SUMMARY OF RESULTS	63
	7.1 Summary	63
	7.2 Conclusions	63
	7.3 Recommendations	64
VIII.	LIST OF REFERENCES	66
IX.	APPENDIX	71
X.	TABLES	72
XI.	FIGURES	92
XII.	ADDENDUM	122
	12.1 Static Pressure	122
	12.1.1 Ames Laboratory (January 1980)	122
	12.1.2 R&D Associates	123
	12.1.3 TVA	124
	12.1.4 NRC Research	124
	12.1.5 Franklin Research Institute	125
	12.1.6 Offshore Power Systems	126
	12.1.7 Ames Laboratory (September 1980)	127
	12.1.8 Summary	127
	12.2 Dynamic Pressure	128
	12.2.1 Introduction	128
	12.2.2 Preliminary Finite Element Analysis	129
	12.2.3 Approximate Dynamic Analysis	131
	12.2.4 Summary	133
	12.3 List of References for Addendum	139

I. INTRODUCTION

1.1 Background

The purpose of the containment vessel in a nuclear power plant is to prevent the spreading of radioactivity from an event with a low probability of occurrence which may release radioactivity within the vessel. The probability that the containment will not leak radioactivity must be acceptably low. The design pressure for ice condenser containments is typically in the range of 12 to 15 psi. Because the peak pressure recorded during the Three Mile Island (TMI) explosion incident was 28 psi, there is a need to more accurately define the probability of leakage of these containments.

1.2 Objective and Scope

The objective of this work is to review the structural design aspects of the containments at the Sequoyah and McGuire nuclear power plants, as related to the TMI incident pressure pulse.

This objective is accomplished by making a best estimate and uncertainty assessment of the pressure strength of the steel containments at Sequoyah and McGuire. The scope of this assessment was limited to manageable proportions by using:

- . Second moment reliability theory (Sec. 2)
- . Uniform static internal pressures (Sec. 3.4)
- . Gross deformation as the failure criterion (Sec. 4).

Semi-empirical approximate methods are used to analyze the stiffened axisymmetric shell and each penetration (Sec. 5). A more refined non-linear finite element analysis is applied to analyze the axisymmetric stiffened shell and, also, to analyze one penetration in each containment (Sec. 6).

1.3 Containment Description

The steel containment vessels for both the Sequoyah and McGuire nuclear power plants are basically cylindrical shells with hemispherical shell tops. Both vessels have ring (circumferential) and stringer (longitudinal) stiffeners. Figs. 1.1 and 1.2 show the geometry of the axisymmetric vessels (Unit 1 for each plant). At elevations where

thicknesses vary circumferentially, the minimum thickness is shown. Material properties will be discussed in Sec. 3. There are a total of 193 and 258 penetrations in the Sequoyah and McGuire vessels, respectively. Details of these penetrations are not included in this report, but were shown on drawings provided by the plant owners.

II. UNCERTAINTY ANALYSIS

2.1 Probabilist Safety Analysis

Failure of a nuclear power plant containment vessel is considered to occur when radioactivity is released. The probability of such a failure, F , must be acceptably low. If the events, E_n , which may cause the failure event are independent, the probability of containment failure, P_f , can be written approximately (for small probabilities of failure) as [1,2]*

$$P_f = \sum_n P(F/E_n) P(E_n) \quad (2-1)$$

where $P(E_n)$ is the probability of occurrence of event n and $P(F/E_n)$ is the conditional probability of failure given event E_n . Typically, E_n represents severe events with a small probability of occurrence, such as a major earthquake, a direct tornado hit or a loss of coolant accident. It is impractical to design for certain events with a very low probability of occurrence. For these events (core meltdown, geologic fault directly under facility), $P(F/E_n)$ is one.

For the current task, the study is limited to the failure probability for one event - the explosion situation identified in the TMI incident:

$$P_{fTMI} = P(F/E_{TMI}) P(E_{TMI}) \quad (2-2)$$

The study is not concerned with the determination of the probability of occurrence of this event, $P(E_{TMI})$, e.g., human error, equipment malfunction. It is not the purpose of this work to judge the adequacy of the containment designs against the TMI type incident. The work intends only to present information useful in that judgment. The final

*Numbers in brackets refer to entries in the List of References.

[Vertical bars in the right margin indicate changes (expanded remarks and/or corrections) made in this report in response to reviewers' comments to initial draft of November 1980.]

judgment can be made only by bringing this and other factors to bear, e.g., the probability of the event itself and the probability of failure that society is willing to accept. It is, however, aimed at determining the conditional probability of failure $P(F/E_{TMI})$, that is, the probability of failure given the TMI explosion incident. This conditional probability will herein be referred to as

$$p_f = P(F/E_{TMI}) \quad (2-3)$$

The reader will note that the actual probability of failure for the TMI incident is given by Eq. 2-2, i.e., $P_{f_{TMI}} = p_f P(E_{TMI})$.

The failure criteria for a structure can be written as

$$G(x_i) < 0 \quad (2-4)$$

where G is the failure function, which may include several failure modes and x_i are structural parameters such as material properties, geometry, loads and modeling error. The parameters are considered as uncorrelated random variables. Failure does not occur if $G(x_i)$ is greater than zero. The probability of failure p_f can be written as

$$p_f = P(G < 0) = \int_{-\infty}^0 f(G)dG \quad (2-5)$$

in which $f(G)$ is the probability density function of G . Various other forms of this general relationship are given in the literature [3,4,5], e.g.,

$$p_f = P(x_i \text{ in } D) = \int_D f(x_i) d x_i = \int_D dF(x_i) \quad (2-6)$$

where $f(x_i)$ is the joint probability density function of x_i , $F(x_i)$ is the joint probability distribution function and D is the failure domain where $G(x_i)$ is less than zero.

In some cases, the x_i parameters can be separated into two groups: x_r , resistance parameters, and x_q , load parameters. The failure function can then be written as [1,2,3,4,5,6,7,8,9, many others]

$$G(x_i) = R(x_r) - Q(x_q) < 0 \quad (2-7)$$

where $R(x_r)$ is the resistance function and $Q(x_q)$ is the load function. In this form, the probability of failure can be written as

$$P_f = P(R-Q < 0) = \iint_D f_r(R) f_q(Q) dR dQ \quad (2-8)$$

where $f_r(R)$ and $f_q(Q)$ are the probability density functions for R and Q , and D is the failure region where $R-Q < 0$ or $R < Q$. Alternatively,

$$P_f = \int_{-\infty}^{\infty} f_q(Q) \int_{-\infty}^Q f_r(R) dR dQ = \int_{-\infty}^{\infty} f_q(Q) F_r(Q) dQ \quad (2-9)$$

It is generally recognized, even in the most recent literature [2,3,4,5], that the evaluation of the structural safety by the direct evaluation of the above integrals is impractical. First, the required probability distribution functions are seldom, if ever, known, and secondly, the evaluation of the multiple integrals is practically not feasible. In this regard, several investigators have attempted to develop approximate methods to evaluate the failure probability. Since the current task is not research oriented, a summary of these methods will not be made here. Refs. 3, 4 and 5 present a good review of the state of the art. The simplest generally-accepted approach is called the second moment method.

2.2 Second Moment Method - One Failure Mode

The second moment method for probability statements has been advocated for some time [1,2,3,4,5,7,8,9,10,11,12]. The method, as outlined below, follows the developments in these references, principally

Ref. 4. The second moment method has several advantages, the biggest of which is its simplicity. Uncertainty is expressed in terms of the first and second moment of the random variables, x_i . Hence, exact information about the probability density function is not needed - only the first and second moments. The method uses a linearized form of the failure criterion which allows separation of the load and resistance functions as illustrated in Eq. 2-7.

2.2.1 Invariant Second Moment Method

For the second moment method, the failure function is again written as in Eq. 2-4. The uncertainty of the variables x_i is expressed by their mean μ_i (first moment of probability density distribution) and their standard deviation σ_i (square root of second moment). The mean and standard deviation of G are obtained by linearizing G with the first two terms of a Taylor series

$$\mu_G = G(x_i) \tag{2-10}$$

$$\sigma_G^2 = \sum_{i=1}^n \left[\frac{\partial G(x_i)}{\partial x_i} \sigma_i \right]^2 \tag{2-11}$$

Most early approaches performed the linearization at the mean of x_i , i.e., x_i equal μ_i ; however, several investigators have shown that a better approximation is obtained if the linearization is performed at the design (or Rackwitz) point on the failure surface,

$$G(x_i) = 0 \tag{2-12}$$

In this way, the Taylor series expansion of $G(x_i)$ takes place in the upper tail of the load distribution and the lower tail of the resistance distribution [3,4,10,13], which is the design point or most likely region of failure. Linearization of the failure surface at the design point has the additional advantage that the method now becomes invariant under a change in formulation of the failure criteria, e.g., changing a load variable to a resistance variable.

The second moment method does have limitations which should be pointed out. First, if more exact information is available on the parameter distributions, it cannot be logically included. Second, a linear approximation to the failure surface may not be acceptable [3].

A safety index is defined for the second moment method as

$$\beta = \frac{\mu_G}{\sigma_G} \quad (2-13)$$

It is generally assumed that the distribution of G can be approximated as normal in the vicinity of the design point [4] so that the probability of failure can be found as by Eq. 2-5 as

$$p_f = P(G < 0) = \Phi(-\beta) \quad (2-14)$$

where Φ is the standard normal integral.

A more general formulation of the second moment method, equivalent to above, is as a nonlinear minimization problem, [4,10,13,14]

$$\text{minimize } \beta^2 = \sum \left(\frac{\mu_j - x_j}{\sigma_j} \right)^2 \quad (2-15)$$

$$\text{constraint } G(x_j) = 0 \quad (2-16)$$

This formulation can be shown to be, by the Lagrange multiplier method, equivalent to solving the equations [4,14]

$$x_j = \mu_j - \beta \alpha_j \sigma_j \quad (2-17)$$

$$G(x_j) = 0 \quad (2-18)$$

$$\text{where } \alpha_j = \frac{\partial G(x_j)}{\partial x_j} \sigma_j \left[\sum \left(\frac{\partial G(x_j)}{\partial x_j} \sigma_j \right)^2 \right]^{-1/2}$$

All three formulations (Eqs. 2-13, 2-15 and 2-17) are equivalent.

A simple example will illustrate the significance of the design point minimization of the failure function. Suppose the failure function is taken as the nonlinear function

$$G(x) = 1 - \frac{1}{x} = 0 \quad (2-19)$$

If linearization is performed at the mean

$$G_{\mu} \approx G \left|_{x=\mu} + \frac{\partial G}{\partial x} \right|_{x=\mu} (x-\mu) \quad (2-20)$$

$$\approx 1 - \frac{1}{\mu} + \frac{2}{\mu^3} (x-\mu) \quad (2-21)$$

where μ is the mean of x . The mean and standard deviation of G_{μ} are given, using Eqs. 2-10 and 2-11, as

$$\mu_{G_{\mu}} = 1 - \frac{1}{\mu} \quad (2-22)$$

$$\sigma_{G_{\mu}} = \frac{2\sigma}{\mu^3} \quad (2-23)$$

where σ is the standard deviation of x . The safety index, with linearization about the mean, is

$$\beta_{\mu} = \frac{\mu(\mu^2 - 1)}{2\sigma} \quad (2-24)$$

On the other hand, if linearization is performed about the design point x_D on $G(x_D)$ equal zero or

$$x_D = \pm 1 \quad (2-25)$$

the linearized G has the form

$$G_d \approx G \Big|_{x=1} + \frac{\partial G}{\partial x} \Big|_{x=1} (x-1) \quad (2-26)$$

$$\approx 0 \pm 2 (x-1) \quad (2-27)$$

The mean and standard deviation of G_d becomes

$$\mu_{G_d} = 2 (\mu - 1) \quad (2-28)$$

$$\sigma_{G_d} = 2 \sigma \quad (2-29)$$

and the safety index is

$$\beta_d = \frac{\mu - 1}{\sigma} = \frac{2}{\mu(\mu + 1)} \beta_\mu \quad (2-30)$$

The reader will note that β_d is almost always less than β_μ since $G(\mu)$ is almost always greater than zero, i.e., μ is almost always greater than one. Also, the value of β_μ would change if G were formulated as

$$G(x) = x^2 - 1 = 0 \quad (2-31)$$

whereas β_d would not. Thus, as stated previously, β_d is invariant under a coordinate transformation.

If the failure function G is linearized about the design point, careful interpretation of μ_{G_d} and σ_{G_d} is necessary. With reference to Eqs. 2-28 and 2-29 above, μ_{G_d} and σ_{G_d} are not actually the mean and standard deviation of the $f(G)$ but are first order approximations of the mean and standard deviation of $f(G)$. They can also be considered to be the mean and standard deviation of a normal distribution $\phi(G)$ which is a first approximation to $f(G)$ in the vicinity of the design point.[4]

Returning to the formulation of Eq. 2-15, the minimization problem lends itself to a graphical interpretation. If the basic variables are transformed to variables, y_i , with zero mean and unit standard deviation

$$y_i = \frac{x_i - u_i}{\sigma_i} \quad (2-32)$$

the second moment method can be stated as

$$\text{minimize } \beta^2 = \sum y_i^2 \quad (2-23)$$

$$\text{constraint } G(y_i) = 0 \quad (2-34)$$

The equation for β is seen to represent a hypersphere and the minimization process determines the minimum distance between the origin of y_i and the failure surface $G(y_i)$ equals zero. This is illustrated in Fig. 2-1 for a two-parameter failure surface. The $f(G)$ and its approximating normal function $\phi(G)$ are also indicated.

For the special case of a linear failure surface, the derivatives of G are constant. Thus, the distinction between the mean point and design point linearization of the failure function becomes unnecessary. For example, suppose the failure function G is linear in R and Q

$$G = R - Q \quad (2-35)$$

where R and Q are normally distributed. Eqs. 2-10, 2-11 and 2-13 give [6,7,8,9]

$$\beta = \frac{\mu_R - \mu_Q}{\sqrt{\sigma_R^2 + \sigma_Q^2}} \quad (2-36)$$

as the safety index. The formulation of Eq. 2-15 with the Lagrange multiplier method will yield identical results. The probability of failure, by Eq. 2-14, is

$$p_f = P(R-Q < 0) = P(R < Q) = \Phi(-\beta) \quad (2-37)$$

2.2.2 Non-normal Distributions

If the distribution of the variables is non-normal, their distribution can be incorporated by transforming to standard normal variables [4,14]. For example, if z_i is a lognormally distributed structural parameter, the transformation

$$z_i = e^{x_i} \quad (2-38)$$

where x_i is normally distributed, is employed. In many cases, the lognormal distribution assumption is appropriate because it eliminates problems associated with negative values of the parameters. For example, a lognormal distribution assumption for the material yield strength correctly states that the probability of a negative yield strength is zero whereas a normal distribution assumption would provide a finite (but small) probability of negative values. With the transformation of Eq. 2-38, the mean and variance for the normally distributed x_i is given as

$$\mu_x = \ln(\mu_z / \sqrt{V_z^2 + 1}) \quad (2-39)$$

$$\sigma_x^2 = \ln(V_z^2 + 1)$$

where V_z equal to σ_z / μ_z is the coefficient of variation of z . If V_z^2 is small with respect to one (say V_z less than 0.3)

$$\ln(V^2 + 1) = V^2 - \frac{1}{2}V^4 + \frac{1}{3}V^6 \approx V^2 \quad (2-40)$$

$$(V^2 + 1)^{-1/2} = 1 - \frac{1}{2}V^2 + \frac{3}{8}V^4 \approx 1$$

so that

$$\mu_x \approx \ln(\mu_z) \quad (2-41)$$

$$\sigma_x^2 \approx V_z^2$$

are approximate values of the mean and standard deviation of the transformed variables.

For the simple case of G in Eq. 2-35, if R and Q are assumed to be lognormally distributed, the transformation

$$r = \ln R \quad (2-42)$$

$$q = \ln Q$$

will transform the parameters to the normally distributed r and q. Thus, the failure criterion becomes

$$G(r, q) = e^r - e^q = 0 \quad (2-43)$$

where again, G is taken to be normally distributed in the vicinity of the design point. Application of the Lagrange multiplier method to Eq. 2-15 with G from Eq. 2-43 gives

$$\beta = \frac{\mu_r - \mu_q}{\sqrt{\frac{\sigma_r^2}{2} + \frac{\sigma_q^2}{2}}} \quad (2-44)$$

or, in terms of the original variables R and Q [6],

$$\beta = \frac{\ln \frac{\mu_R}{V_R^2 + 1} - \ln \frac{\mu_Q}{V_Q^2 + 1}}{[\ln(V_R^2 + 1) + \ln(V_Q^2 + 1)]^{1/2}} \quad (2-45)$$

where

$$V_R = \sigma_R / \mu_R \quad (2-46)$$

$$V_Q = \sigma_Q / \mu_Q$$

are coefficients of variation of R and Q, respectively. For small V_R and V_Q , the approximations of Eq. 2-40 apply and Eq. 2-45 becomes approximately [8,9]

$$\beta = \frac{\ln(\mu_R / \mu_Q)}{\sqrt{V_R^2 + V_Q^2}} \quad (2-47)$$

Since G is taken to be normally distributed in the vicinity of the design point, the probability of failure is

$$p_f = P(R-Q < 0) = P(R < Q) = \Phi(-\beta) \quad (2-48)$$

Several investigators [6,8,9,10,11] choose to write (for lognormal R and Q)

$$G'(R,Q) = \ln R - \ln Q \quad (2-49)$$

instead of Eq. 2-35. Again, making the transformation of Eq. 2-42 and applying Eq. 2-15 gives results identical to Eq. 2-45. The failure probability for normally distributed G' is understood as

$$p_f = P(G' < 0) = P(\ln R - \ln Q < 0) = \Phi(-\beta) \quad (2-50)$$

which is, of course, the same as Eq. 2-48. The fact that the formulations of G in Eqs. 2-35 and 2-49 give identical results (Eq. 2-45) indicates that the safety index of Eq. 2-15 is invariant under at least this particular coordinate transformation (Eq. 2-42). In general, it is approximately true.

Coordinate transformations for other non-normal distributions are given in Ref. 4. Only lognormal distribution assumptions will be used in this work because of the ease with which they are handled. However, they obviously represent distribution functions of a specific analytical form and, as such, their application is limited.

2.3 Multiple Failure Modes

If a structure can fail by more than one failure mode, estimates of the probability of failure of the structural system can be obtained. In this case, the safe region of the structure is defined by the intersection of the safe regions of the individual failure criteria

$$G_m(x_j) = 0 \quad (2-51)$$

where m denotes the failure mode number. This is illustrated in Fig. 2-2 for three failure modes. For each individual failure mode, the minimum β can be obtained by the minimization method in Eq. 2-15. Let β_m be the minimum β for each failure mode m . If, as before, each G_m is assumed to be normally distributed in the vicinity of the design point, the failure probability for each failure mode is

$$P_{fm} = P(G_m < 0) = \Phi(-\beta_m) \quad (2-14)$$

Bounds on the probability of failure for the structural system are given by [4,10,14,15,16,17,18]

$$\max. p_{fm} = P(G_m < 0) = \Phi(-\beta_m) \quad (2-52)$$

or

$$\Phi(-\min \beta_m) < p_f < \Sigma \Phi(-\beta_m)$$

where the sum is taken over all failure modes and $\max p_{fm}$ denotes the maximum failure probability of all modes. If one mode predominates, the bounds become very close.

Lind [14] suggests that it is often appropriate to derive a safety index for the structural system which includes all failure modes since this may be more convenient in practical design than the probability statements. He defines the generalized safety index $\bar{\beta}$ for the multiple failure mode case as the inverse of the normal error function of the reliability

$$\bar{\beta} = \Phi^{-1}(1-p_f) \quad (2-53)$$

In terms of the probability bounds of Eq. 2-52

$$\Phi^{-1}(1-\Sigma p_{fm}) < \bar{\beta} < \Phi^{-1}(1 - \max p_{fm})$$

or

$$\Phi^{-1}[1 - \Sigma \Phi(-\beta_m)] < \bar{\beta} < \min \beta_m \quad (2-54)$$

as bounds on the generalized safety index.

III. PARAMETER STATISTICS

The formulation in Sec. 2, second-moment reliability theory, requires the first and second moment of the structural parameters (x_i in Eq. 2-4) to approximate the first and second moment of the failure function. In this chapter, these parameter statistics (mean and standard deviation) will be discussed for the Sequoyah and McGuire nuclear power plant containments.

3.1 Material Parameters

3.1.1 Yield and Ultimate Stress

The material for both containment vessels is A516 Grade 60 steel with a specified minimum yield of 32 ksi and a specified ultimate of between 60 and 80 ksi. The mean values of the yield and ultimate strength were furnished by TVA (for Sequoyah) and Duke Power (for McGuire) and are listed in Table 3-1. The standard deviation for these properties was supplied by Duke and assumed to apply to Sequoyah. Assuming that the properties of this steel are similar to those for typical structural steels, e.g., A-36 and A-441, the mean and standard deviation for the other pertinent structural parameters in Table 3-1 [19, pg 1467, and 20, pg 1440] can be used. The distribution type (normal or log-normal) is also indicated. The anchor bolts are SA320-L43 with a minimum specified yield strength of 105 ksi. The mean and standard deviation as given in Table 3-1 are assumed to be similar to A-490 bolts [20, pg 1433].

3.1.2 Approximate Fracture Stress

An additional material property which will be of interest in predicting containment leakage (see Sec. 4) is the fracture stress for the steel. In Sec. 4, it will be shown that the probability of brittle fracture is much smaller than the probability of gross containment deformation. To demonstrate this, an approximate (conservative) value of fracture stress is required. The authors acknowledge that the

following discussion is rather tentative but adequate to serve the purposes of Sec. 4.

Among other items, the fracture stress is dependent upon the fracture toughness of the steel which is frequently characterized by a critical stress intensity factor, K_{IC} . The determination of K_{IC} for a typical ductile steel over a wide temperature range is practically impossible by direct methods. A typical variation of K_{IC} theoretically requires that no plasticity exists at the crack tip [21 (Chap. 3)]. This condition is sufficiently satisfied if plane strain conditions exist at the crack tip, or test specimens are sufficiently thick to prevent significant through thickness straining. ASTM Specifications [22] have translated this into the requirement that

$$\gamma = \frac{1}{B} \left(\frac{K_{IC}}{F_y} \right)^2 < 0.4 \quad (3-1)$$

where B is the specimen width. As γ increases significantly beyond this limit, increasing amounts of through thickness straining occur and a condition of plane stress is approached. Admittedly, the above plane strain conditions do not exist in the containment vessel; however, plane strain conditions do represent a lower bound case.

With reference to Fig. 3-1, it is possible to satisfy the criterion of Eq. 3-1 for ductile steels only at low temperatures - near and below the NDT (nil ductility transition temperature). At these low temperatures, the material is sufficiently brittle (low K_{IC}) that a practical specimen size, B , can be used. At higher temperatures, the behavior becomes increasingly inelastic and B becomes excessively large. In this region, K_{IC} cannot be determined directly. In fact, even to define a K_{IC} in this region is questionable. (K_{IC} in the upper shelf region can be approximated by correlation with other test methods, e.g., Charpy V-Notch tests [21 (Chap. 6)].) In practical terms, this means that at low temperatures (relative to NDT) fracture by crack propagation is possible whereas at temperatures significantly above the NDT, gross yielding of the section will most likely occur even in the presence of a large crack.

Other factors should be mentioned which affect the use of K_{IC} data. In a typical real structure, thicknesses are significantly less than B from Eq. 3.1. Thus, plane strain conditions at the crack tip may not be achieved. In this regard, a K_C is often defined as the critical stress intensity for plane stress. This value depends upon, among other parameters, the material thickness. (The critical stress intensity factor for plane strain, K_{IC} , is the lower bound of K_C , i.e., the value of K_C for large thicknesses.) However, in complex structures with intersecting plates (stiffeners, penetrations) and significant welds in complex geometries and residual stresses, the distinction between plane stress and plane strain cannot be made. In this study, it will be assumed that plane strain conditions of maximum restraint exist near the crack and, hence, that K_{IC} is applicable.

Loading rate also affects values of K_{IC} . At fast loading rates, dynamic K_{IC} values are defined as K_{ID} , the critical stress intensity factor for impact loading and plane strain conditions. A common technique for obtaining K_{ID} curves from K_{IC} data is to shift the curve in Fig. 3-1 to the right by 160°F for mild ductile steels [21 (pg. 129)]. This shift effectively accounts for the reduction in critical stress intensity for impact loadings. For this work, the lower values of K_{ID} will be used instead of K_{IC} for two reasons: (1) the loading is actually dynamic (explosive), and (2) the ASME code adopts this approach through the use of K_{IR} curves [21,23]. (K_{IR} is the lower bound of K_{IC} and K_{ID} .)

Unfortunately, K_{ID} data for the containment vessel steel, A-516 Gr. 60, is not available. However, the ASME code recommendations for K_{IR} [23] are approximately applicable for steels with yield strengths below 50 ksi. As illustrated in Ref. 21 (Fig. 15.1), there is considerable scatter in the experimental data used to develop K_{IR} . Additionally, K_{IR} is a function of the operating temperature relative to the NDT, as in Fig. 3-1. The NDT of the A516 steel is assumed to be -30°F. From Fig. 15.1 of Ref. 21, the mean of the test data for K_{IR} can be represented approximately by (kip, in., and °F units)

$$K_{Id} = x_0 (1.2e^{0.0125(T+250-NDT)} + 26.8) \quad (3-2)$$

which is a shifted form of the ASME equation for K_{IR} . The quantity x_0 accounts for scatter in the data (see Sec. 3.3). Approximately,

$$\mu_{x_0} = 1 \quad (3-3)$$

$$\sigma_{x_0} = 0.17$$

For these containment vessels, the temperature range is approximately 0°F to 100°F. The following statistics of T are used:

$$\mu_T = 50^\circ\text{F} \quad (3-4)$$

$$\sigma_T = 25^\circ\text{F}$$

These temperature statistics are conservative and give a higher than likely probability that the containment will reach a low temperature. Under accident conditions, the temperatures will, most likely, be elevated. With the above statistics for x_0 and T and with Eq. 3-2, the statistics on K_{Id} can be found as

$$\mu_{K_{Id}} = 105 \text{ ksi in} \quad (3-5)$$

$$\sigma_{K_{Id}} = 31 \text{ ksi in}$$

These values are similar to other reported values [24,25]. Also, the required Charpy V-notch impact value for this material is 15 ft-lb at -30°F [26]. This corresponds approximately to a K_{Id} of 47 ksi in at -30°F [21 (Eq. 6.2)] which compares to 54 ksi in given by Eq. 3-2. Again, these are conservative statistics.

Linear elastic fracture mechanics states that a partially through surface crack will propagate through the thickness when

$$K_I = K_{Id} \quad (3-6)$$

K_I is the stress intensity factor for a partially through surface crack, typically written as

$$K_I = Mf \sqrt{\pi a} \quad (3-7)$$

where f is the stress remote from the crack or the stress which would exist in the vicinity of the crack if the crack were not present. (The symbol f is used here for stress since σ has been reserved for standard deviation.) The quantity a represents the crack dimension (crack depth for a partially through crack). The factor M accounts for the different types of stress in the vicinity of the crack (extensional, bending), the shape of the crack (semi-elliptical, semi-circular, straight), and the local geometry of the structure (penetration, weld detail). By their very nature, the crack size a and magnification factor M are random quantities, dependent upon crack shape, local structural geometry, crack location, quality of the material and welds, and inspection and repair techniques.

It is beyond the scope of this work to review possible forms of M except to list a very limited number of references [21,27,28,29,30,31]. Typically, M ranges between about one and two. For this study, the following (conservative) statistics will be assumed for M

$$\mu_M = 1.5 \quad (3-8)$$

$$\sigma_M = 0.15$$

M will be assumed to be lognormally distributed. These estimates are subjective.

Crack size statistics are very difficult to define without a very careful inspection of the vessel, including welds. Such an inspection is probably not feasible at this point. (As will be shown in Sec. 4,

the probability of failure by fracture is very small. Thus, precise determination of fracture properties does not appear necessary.) The vessels were inspected by die penetrant techniques. The maximum allowable crack size is about 3/16 in. [32]. It will be assumed that, before inspection, one crack in ten is greater than 3/16 in. deep. If the inspection is 95 percent effective in detecting these large cracks [33] and the detected cracks have been repaired, approximately one crack in 200 will be greater than 3/16 in. after inspection. This condition, in conjunction with an assumed mean crack size of 1/16 in. gives the following statistics for the crack size a

$$\mu_a = 0.0625 \text{ in.} \tag{3-9}$$

$$\sigma_a = 0.052 \text{ in.}$$

if the crack size is lognormally distributed. Fracture at only one point (a hypothetical crack) is considered here. The probability of fracture at this point will be compared to the probability of gross yielding at this same point in Sec. 4.3.

The fracture criterion of Eq. 3-6 can be formulated as

$$f = F_C \tag{3-10}$$

where F_C , the fracture stress, is defined as [34]

$$F_C = \frac{K_{Ic}}{M \sqrt{\pi a}} \tag{3-11}$$

Statistics for the quantities K_{Ic} , M , and a have been approximated in Eqs. 3-5, 3-8 and 3-9, respectively. Since these quantities are assumed to be lognormally distributed, F_C will also be lognormal distributed. The statistics of F_C are listed in Table 3-1. (Note that the large standard deviation of F_C is caused by the large variations in crack size and K_{Ic} .)

These values of F are quite conservative and serve only as a first approximation for applying fracture mechanics principles. A better approximation can be obtained by collecting actual data for the material fracture properties and crack sizes, shapes and locations. However, as will be discussed in Section 4.3, the values listed here serve the intended purpose, i.e., they demonstrate that the probability of fracture is quite low. The final results are quite insensitive to the particular value of the fracture stress.

3.2 Geometric Parameters

No as-built measurements of the containment vessels exist. However, fabrication and erection tolerances were established and (presumably) met during the construction process. Tolerances on plate thickness and size are given in Ref. 35. Tolerances on erection dimensions were supplied by TVA for Sequoyah and by Duke Power for McGuire during site visits. The nominal values and tolerances are listed in Table 3-2. The mean value of the geometric parameter is taken as the average of the maximum and minimum limits of that parameter as specified by the tolerance extremes. The standard deviation is taken as one-third of the allowable tolerance from the mean [6 (pg 112)]. This is equivalent to assuming that 99.73 percent of the as-built dimensions fall within the prescribed tolerances. The mean and standard deviations of the geometric parameters are listed in Table 3-2. They are assumed to be normally distributed.

The values listed in Table 3-2 imply that quantities such as the thickness are random but uniform throughout. This is, of course, not true. Thicknesses have a spatial variation in actuality and could be idealized as random processes that are functions of the spatial variables. However, the random process approach would be an analytical over-sophistication and would make the following work intractable. The following work (Secs. 5.1.4 and 5.2.4) demonstrates that the results are insensitive to the statistics of the geometric parameters because the coefficient of variation of these quantities is relatively small. The assumption selection (uniform vs random process) is, therefore,

immaterial since either choice will not significantly influence the answer.

3.3 Resistance Modeling Error - General

In the practical case, the failure function G (Eq. 2-4) is not precisely known. At best, a theoretical model is available to predict the failure of a real structure. Variability is introduced into both the prediction of the resistance of the structure and the applied load. In this section, variability in the resistance prediction is considered.

Imperfections in the resistance model result from various sources. First, several assumptions are typically involved in the formulation of a model. Though these assumptions may be relaxed for more sophisticated models, there remains some uncertainty as to their effect. To a limited extent, the uncertainty of the model can be quantified by comparing the theoretical results to results from highly idealized experimental models. However, uncertainty also exists in this experimental work.

Another source of uncertainty of the resistance model is in its application to a real structure. The real structure typically has many details which cannot be accurately modeled analytically or experimentally. Hence, another set of assumptions is introduced into the analysis of the real structure. Typically, application of the prediction model to the real structure involves more uncertainty than in its application to experimental structures.

The resistance modeling error is considered as an additional structural parameter, x_0

$$x_0 = \frac{R}{R_t} \quad (3-12)$$

where R is the actual in-service resistance and R_t is the predicted or theoretical resistance. By the extended reliability formulation [8,9], the modeling error is taken as

$$x_0 = \Delta \delta \tag{3-13}$$

where δ represents the basic variability of the theoretical resistance model with respect to experimental results and Δ represents the variability between experimental results and in-service conditions. Thus, Δ accounts for imperfections in the experimental modeling of real structures, e.g., boundary conditions, welds, residual stresses. (The extended reliability formulation was not introduced into the other parameter variabilities because these variabilities are presumably based upon a large number of samples of in-service conditions.) The random variable Δ and δ are taken to be lognormally distributed so that x_0 is also lognormally distributed.

The mean and standard deviation of Δ cannot be quantified rationally but remain a judgment of the engineer. Actual values can only be determined by testing real, as-built containments which is, of course, prohibitively expensive. In lieu of this, the approach herein will be to adopt the typical values suggested by other investigators [9,36,37]. Hence, the mean of Δ is taken equal to one. This implies that the mean of test data fits the mean of in-service behavior. Typical values of the coefficient of variation of Δ are 0.05 [9], 0.02, 0.05 and 0.07 [36], and 0.05 [37]. A value of 0.05 will be used in this work.

The values of the mean and standard deviation of δ will be determined as the various analytical methods are presented in the following chapters. The general procedure will be to tabulate values of the $\ln \delta$ where δ is the ratio of the experimental resistance of a model to the theoretical resistance. The mean and variance of this tabulation are calculated by usual means as m and s^2 . With 95 percent confidence, one can say (if the error is normally distributed) that

$$m - \frac{t_{0.025} s}{n} < \mu_{\ln \delta} < m + \frac{t_{0.025} s}{n} \tag{3-14}$$

$$\frac{(n-1) s^2}{2} < \sigma_{\ln \delta}^2 < \frac{(n-1) s^2}{2} \tag{3-15}$$

$\times 0.025$
 $\times 0.975$

where n is the number of specimens, $t_{0.025}$ is the value of t such that the area under the Student - t distribution to the right is 0.025, and $\chi^2_{0.025}$ $\chi^2_{0.975}$ are the value of χ^2 for $n-1$ degrees of freedom such that the area under the chi-square distribution to the left and right is 0.025 and 0.975, respectively [38]. For this work, conservative values will be used, i.e.,

$$\mu_{\ln \delta} = m - \frac{t_{0.025} s}{n} \quad (3-16)$$

$$\sigma_{\ln \delta}^2 = \frac{(n-1) s^2}{\chi^2_{0.975}} \quad (3-17)$$

and, by Eq. 2-40,

$$\mu_{\delta} = e^{\mu_{\ln \delta}} \quad (3-18)$$

$$V_{\delta}^2 = \exp(\sigma_{\ln \delta}^2) - 1$$

where V_{δ} is the coefficient of variation of δ .

In summary, the mean and coefficient of variation of the resistance modeling error (lognormally distributed) will be taken as

$$\mu_0 = \mu_{\delta} \quad (3-19)$$

$$V_0^2 = V_{\delta}^2 + (0.05)^2 \quad (3-20)$$

Details for the various analysis methods are presented in the following chapters.

3.4 Load Modeling Error

The exact nature of the pressure loading experienced at TMI is poorly defined. Information supplied to the authors indicate only that the peak recorded pressure was 28 psi and resulted from an explosion incident. The spatial variation and time history of the pulse were not available to us. As a first approximation, the load is assumed to be a uniform, static internal pressure with

$$\mu_p = 28 \text{ psi} \quad (3-21)$$

$$\sigma_p = 0 \quad (3-22)$$

Most likely, the peak pressure was recorded at an interior point of the containment, so that the pressure could be reduced as it radiated to the shell walls. Also, the pulse length may be short so that the dynamic effect of the pressure could be more or less than the static effect depending upon the ratio of the pulse length to the local deformation mode period. In lieu of more specific information and to obtain a first approximation within the project time constraints, the above uniform static pressure is used. In view of the uncertainties of the load information, it is, of course, not consistent to take σ_p equal zero. However, with regard to Eqs. 2-2 and 2-3, this report is aimed at determining a conditional probability; that is, the probability of failure given that the applied pressure is 28 psi. A zero value of σ_p is, thus, appropriate.

IV. FAILURE CRITERIA

The purpose of the containment vessel is to prevent the spreading of radioactivity resulting from an event of low probability (in this case, the TMI explosion incident). Thus, the containment vessel is intended to be a leakproof barrier against release of radioactivity. Failure of the containment is, therefore, considered to occur when radioactivity is released or, in other words, when leakage of the containment occurs. Leakage can occur in at least two areas associated with the containment:

- Leakage of the containment vessel itself either in the shell wall or the penetration intersections;
- Leakage of piping and/or other equipment passing through or attached to the containment shell at locations remote from the containment shell.

Leakage of the containment vessel itself will occur when a crack or defect propagates completely through the wall of the containment shell or penetration intersection. In this study, the forces required to propagate the crack are provided by the internal pressure.

Prior to leakage of the vessel wall or penetration intersection, it is quite possible that leakage could be induced into the attached piping by gross deformation of the vessel wall. Thus, if the vessel wall does not leak, the vessel will continue to expand under increasing internal pressure until the piping or some other attachment is so grossly deformed that it leaks. These failures are considered to occur at locations removed from the shell itself. Additionally, gross deformation of the vessel may induce other types of undesirable behavior such a failure of the equipment in the annular space between the containment and shield building walls, failure of instrumentation and control devices passing through the shell wall, and failure of the anchor bolts and leakage barrier at the containment base. Expansion bellows between the attached equipment and the shield building are provided in each plant. However, these allowances for expansion are limited to the elastic deformation of the containment.

A schematic representation of the pressure-displacement curve for a pressure vessel is shown in Fig. 4-1. In this figure, δ_1 represents the displacement at which leakage (fracture) occurs in the vessel wall or penetration intersection. Leakage of the piping and/or failure of attached equipment at a point removed from the shell is identified as occurring at δ_2 . In all likelihood, δ_2 will be significantly smaller than δ_1 because of the inherent ductility of the large diameter, thin-shell containment vessel. Quantification of these leakage failure is discussed below.

4.1 Containment Shell

The characterization of the fracture of ductile steel structures is still very much in the development stage [21]. No generally recognized technique has established itself among structural analysts. However, two limiting cases are reasonably well agreed upon.

First, fracture of an initially uncracked structure, e.g., tension specimen, will occur when the stresses reach the ultimate tensile strength of the material, F_u (see Table 3-1).

$$f = F_u \quad (4-1)$$

Here f is the applied tensile stress. (Actually, f should be interpreted as the tensile stress on the net area (gross area minus crack area) but for crack areas much smaller than the gross area, f can be interpreted as the tensile stress on the uncracked area.) This limit implies that imperfections in the real structure are smaller than or equal to the imperfections in a machined tensile specimen.

At the other limit, failure of a perfectly elastic structure with an initial crack will occur when the stress intensity K_I reaches the limiting value of the critical stress intensity K_{Ic} . By Sec. 3.1.2, this is equivalent to the failure condition

$$f = F_c \quad (4-2)$$

where F_c is the material fracture strength (see Table 3-1).

Most real cases fall somewhere between these limits depending upon the relative values of the fracture strength and the ultimate tensile strength. Application of the ultimate tensile strength (UTS) limit implies that small cracks and imperfections do not exist or, if they do exist, do not affect the material strength. Application of the linear elastic fracture mechanics (LEFM) implies that no local yielding of the structure occurs, even at the crack tip. Both these implications are obviously incorrect. Ultimate tensile strength is affected by imperfections and local yielding does occur in structures before fracture.

Many techniques have been proposed to account for plasticity at the crack tip (elastic plastic fracture mechanics, EPFM) - the missing link in the above two limits [21 (Chap. 16),34,39,40]. The difference in the theoretical approaches is usually much less than the scatter in the experimental results of fracture tests. In this regard, at least for the current state of the art, a two parameter fracture interaction curved [34] of the form

$$G_1 = 1 - \left(\frac{f}{F_c}\right)^2 - \left(\frac{f}{F_u}\right)^2 < 0 \quad (4-3)$$

is appropriate. This function is used herein as the failure function for fracture of the containment vessel wall.

4.2 Attached Piping and Equipment

Leakage of piping and failure of other equipment passing through or attached to the containment shell wall is probably even more difficult to predict than fracture of the shell itself. However, it can reasonably be assumed that failure of these pieces will not occur if deflection of the containment shell is kept within reasonable limits. To accurately define this limit, it would be necessary to examine individually each component associated with the containment. Because of the large number of such components and their indeterminacy, this is not considered practically feasible.

One approach would be to select some (fairly arbitrary) deflection limit for the shell below which failure of associated components would not occur -- say a few inches. The approach which will be taken here is to assume failure of associated components will occur when "excessive" plastic deformations of the shell occur or when deflections increase "rapidly" for "small" increases in load. In real structures with strain hardening materials and large displacement effects, a plastic pressure would correspond with this large plastic deformation.

Numerous definitions of the plastic pressure have been adopted in the literature [24,41]. Each definition is associated with varying degrees of plastic deformation. The half linear slope method will be adopted here, primarily because it is recommended in the ASME Code [24,41,42]. In this method, the plastic pressure is defined as the pressure at the intersection of the pressure-displacement curve with a straight line having a slope equal to one-half the initial slope (p_C in Fig. 4-2). In other words, the plastic pressure is equal to the pressure which produces deformation twice that of the elastic deformation at the same pressure.

In summary, leakage or failure of the piping and attached equipment at points remote from the containment shell will be taken to be governed by the failure function

$$G_2 = p_C - p < 0 \quad (4-4)$$

where p is the applied pressure and p_C is the plastic pressure as defined by the half linear slope method.

4.3 Combined Failure Criterion

As alluded to in Sec. 3.1 and Fig. 4.1, it is reasonable to expect that leakage of the piping and attachments (general yielding of the containment governed by G_2) will occur before fracture (leakage governed by G_1) of the containment shell itself. In terms of probabilities of failure, one would expect that the probability of leakage of the shell, $P(G_1 < 0)$ (Event A), is much less than the probability of leakage of the piping and attachments, $P(G_2 < 0)$ (Event B), where G_1 and

G_2 are the failure functions in Eqs. 4-3 and 4-4, respectively. This expectation is verified in the following paragraphs.

Now, by the addition and multiplication formulas of probability, the probability of failure can be written as

$$P(A \cup B) = P(A) + P(B) - P(B) \cdot P(A|B) \quad (4-5)$$

in which

$$P(A) = P(G_1 < 0),$$

$$P(B) = P(G_2 < 0)$$

and $P(A|B)$ is a conditional probability that can be referred to as the probability of shell leakage (A) given that attachment leakage (B) has occurred. Now G_2 less than zero (Event B) implies that the plastic pressure p_c of the containment has been reached (see Eq. 4-4). At this condition, the stresses in the containment are greater than or equal to F_y in the region of failure, or

$$P(B) \approx P(f \geq F_y) \quad (4-6)$$

In a similar manner, the fracture criterion of Eq. 4-3 can be approximately written as

$$P(A) \approx P(f \geq F_f) \quad (4-7)$$

in which

$$F_f = \frac{F_c F_u}{X_0 (F_c^2 + F_u^2)}$$

where X_0 has been introduced to represent the modeling error of this failure criterion. Now, the conditional probability in Eq. 4-5 can be written

$$P(A|B) = P(f > F_f | f > F_y) \quad (4-8)$$

Since the stresses cannot be greater than F_y because of the elastic-perfectly plastic assumption, one has

$$P(A|B) = P(f > F_f | f = F_y) = P(F_y > F_f) \quad (4-9)$$

If the modeling error is taken to have a mean of one and a standard deviation of 0.08 [39] and the statistics of F_y , F_u and F_c are as given in Table 3-1 for McGuire (Sequoyah is similar), Eqs. 2-15, 2-16 and 2-14 can be applied to find

$$P(A|B) = 0.020 \quad (4-10)$$

The conditional possibility $P(B|A)$ is also of interest, hence

$$P(B|A) = P(f > F_y | f > F_f)$$

By a Venn diagram

$$P(B|A) > P(f > F_y \cap F_f > F_y | f > F_f)$$

Introducing the multiplication rule for the probability of the intersection gives

$$P(B|A) = P(f > F_y | F_f > F_y \cap f > F_f) \cdot$$

$$P(F_f > F_y | f > F_f)$$

Now the first term on the right is one because of the conditions imposed on f . The second term is simply $P(F_f > F_y)$ since the two events are independent. Hence

$$P(B|A) > P(F_f > F_y) = 1 - P(F_y > F_f)$$

and, by Eqs. 4-9 and 4-10

$$P(B|A) > 0.98 \quad (4-11)$$

Thus, by the multiplication rule,

$$P(A) = P(B) \cdot \frac{P(A|B)}{P(B|A)} < \frac{0.02}{0.98} P(B) \quad (4-12)$$

Eq. 4-5 now becomes

$$P(A \cup B) < 0.9996 P(B) \approx P(B) \quad (4-13)$$

as the approximate probability of failure. Eq. 4-12, indeed, shows that the probability of fracture (A) before yield (B) is very small,* or, the probability of containment leakage is negligible with respect to the probability of attachment leakage. In other words, there is a high probability that the containment vessel has the required ductility to reach the collapse pressure before brittle fracture. This probability of fracture can be neglected in probability calculations. Hence, the results are insensitive to the fracture stress.

In summary, since the probability of containment leakage is negligible, it will be sufficiently accurate for the purposes of this project to consider only leakage of attachments. Thus, the failure criterion to be used is

$$G = p_c - p < 0 \quad (4-14)$$

where, again, p_c is the plastic pressure as defined in Section 4.2.

*There are actually many cracks in the structure, each representing a potential failure mode and, thus, the discussion of Sec. 2.3 applies [43]. However, we are here comparing the probability of fracture at a typical "point" to the probability of yielding at the same typical "point". Only one crack is assumed to occur at this "point".

V. APPROXIMATE STRUCTURAL ANALYSIS

The Sequoyah and McGuire containment vessels are analyzed by approximate methods in this section. In addition to providing approximate results, these methods provide useful guidelines for the more exact finite element analyses described in the following section.

5.1 Stiffened Axisymmetric Shell

5.1.1 Failure Criteria

As discussed in Sec. 4, failure of the containment vessel is assumed to occur when large increases in deflections occur for relatively small increases in pressure, or when the pressure reaches the plastic pressure, p_C (Eq. 4-11). An approximation to the plastic pressure, p_C , is given by limit analysis theory [24], which defines a limit pressure, p_0 , at which a plastic mechanism is formed. Classical limit analysis assumes rigid - perfectly plastic materials and small deflections, i.e., strain hardening and large displacement effects are neglected. For the approximate analysis discussed herein, the limit pressure is reached and a limit mechanism is formed. (A more appropriate definition of the plastic pressure will be used in connection with the finite element analysis in Sec. 6. With the finite element analysis, the theoretical pressure-displacement curve will be available and p_C can be obtained by the half linear slope method. For the simple model discussed here, the pressure-displacement curve would be elastic - perfectly plastic and the half linear slope collapse pressure corresponds to the limit pressure.)

For the approximate analysis, a limit mechanism is assumed to occur when the entire structural system, including stiffeners, yields. The stresses in the shell are assumed to be uniformly distributed at the limit mechanism. For equilibrium in the circumferential and axial directions of a cylindrical shell, respectively,

$$pr s_1 = f_\theta t s_1 + f_1 A_1 \tag{5-1}$$

$$\frac{pr}{2} s_2 = f_x t s_2 + f_2 A_2$$

where

f_x, f_θ = axial and circumferential shell stresses

r = radius

t = shell thickness

p = pressure

s_1, s_2 = ring and stringer spacings

A_1, A_2 = ring and stringer areas

f_1, f_2 = ring and stringer stresses

(The symbol f is used here for stress since σ has been reserved for standard deviation.)

As mentioned above, when the stresses are at yield, a limit mechanism forms. For the stiffeners, this means

$$f_1 = F_y \tag{5-2}$$

$$f_2 = F_y$$

For the biaxial stress state in the shell, yielding is governed by the von Mises yield criterion

$$f_x^2 + f_\theta^2 - f_x f_\theta = F_y^2 \tag{5-3}$$

The assumption that all stresses are at yield implies that sufficient ductility is present in the shell wall to permit a redistribution of load from the shell wall into the stiffeners. This model also assumes that the stringers and rings are totally effective at the limit mechanism.

Introducing the yield criteria, Eqs. 5-2 and 5-3, into Eq. 5-1 gives the theoretical limit pressure p_{0t} for the stiffened cylinder as

$$\frac{p_{0t}r}{tF_y} = \alpha_1 + \sqrt{\frac{4 - (2\alpha_2 - \alpha_1)^2}{3}} \quad (5-4)$$

where

$$\alpha_1 = A_1/ts_1$$

$$\alpha_2 = A_2/ts_2$$

Similar reasoning shows the limit pressure for a stiffened sphere to be

$$\frac{p_{0t}r}{tF_y} = \alpha_1 + \alpha_2 + \sqrt{4 - 3(\alpha_1 - \alpha_2)^2} \quad (5-5)$$

The random value of the limit pressure can be written as (see Eq. 3-12)

$$p_0 = x_0 p_{0t} \quad (5-6)$$

where x_0 is the modeling error relating theory to the actual structure (see Sec. 3.3). Following Eq. 4-11, the failure function becomes

$$G = p_0 - p \quad (5-7)$$

in which p is the applied pressure. The random structural parameters (x_1 in Eq. 2-4) are x_0 , F_y , r , t , A_1 , s_1 , A_2 , s_2 , and p .

5.1.2 Modeling Error

Before proceeding to the application of this analysis to the actual containment vessels, it is appropriate to discuss the statistics of the modeling error, x_0 . Unfortunately, no plastic strength

experimental results for stiffened cylinders with internal pressure could be found. The values of μ_0 and σ_0 are, thus, highly subjective. In the extreme case of unstiffened uniform cylinders of infinite length, the values of μ_δ and σ_δ (see Sec. 3.3) would be one and zero, respectively. (In fact, this experimental situation is frequently used to obtain F_y and/or to verify the von Mises yield criterion. Hence the only variability in the theoretical versus actual would be represented by the variability in F_y .) For this analysis, it will be assumed that most of the experimental results fall within ± 30 percent of the theoretical value. (This is admittedly a crude approximation but one we are forced to accept by the lack of experimental data.) If this limit is taken as two standard deviations, the values of μ_δ and σ_δ are 1.00 and 0.15. By Eqs. 3-19 and 3-20, the statistics of x_0 are

$$\begin{aligned}\mu_0 &= 1.0 \\ \sigma_0 &= 0.16\end{aligned}\tag{5-8}$$

where x_0 is taken to be lognormally distributed.

5.1.3 Application to Containment Vessels

The geometry of the two containment vessels is illustrated in Figs. 1-1 and 1-2. The stringers were neglected in the McGuire vessel (A_2 equals zero) because they are not continuous, i.e., there is a 1/2" gap between each stringer and the ring webs. The statistics of the structural parameters are listed in Sec. 3 and Eq. 5-8. The failure criterion of Eq. 5-7 was used in conjunction with the second moment method of Eq. 2-15 to predict the safety index β at each ring elevation. The minimization procedure of the advanced first order second moment method in Eq. 2-15 is carried out using an iterative numerical procedure based on Eqs. 2-17 and 2-18. Bounds on system failure probability and safety index (Eqs. 2-52 and 2-54) were also calculated. The results are tabulated in Table 5-1. (Note that the safety index and

failure probabilities are associated with an applied pressure of 28 psi - see Sec. 3.4.) Minimum mean limit pressures, which were calculated near Elev. 788 ft. for Sequoyah and Elev. 736 ft. through Elev. 816 ft. for McGuire (Eq. 5-6), are also listed. The safety index, failure probability, and mean limit pressure at each ring elevation are listed in the Appendix.

5.1.4 Sensitivity Analysis

One benefit to be derived from the approximate analysis (besides an approximate safety index) is a sensitivity study. Intuitively, one would expect that, if the coefficient of variation of a particular random parameter x_i is relatively small, the solution for the safety index would be insensitive to this parameter. This is evident when the Taylor series expansion of Eq. 2-11 is examined. In particular, the coefficient of variation of the geometric parameters (Table 3-2) are significantly smaller than the coefficient of variation of the material properties (Table 3-1) and the modeling errors (Sec. 3.3). One would, therefore, expect the reliability of the containment vessels to be relatively insensitive to variations in the geometric parameters. This expectation is verified below.

For this approximate analysis, the failure function is given in Eqs. 5-6 and 5-7. If the randomness of the geometric parameters is neglected (coefficient of variation is small), the formulation for β in Eq. 2-15 can conveniently be solved in closed form. Since the yield strength (F_y), modeling errors (x_0), and applied pressure (p) are taken to be lognormally distributed, this solution is

$$\beta = \frac{\ln \rho}{\sqrt{V_{x_0}^2 + V_{F_y}^2 + V_p^2}} \quad (5-9)$$

where

$$\rho = \mu_{p_0} / \mu_p$$

and V_{x_0} , V_{F_y} and V_p are the coefficient of variation of the modeling error, yield strength, and applied pressure, respectively. Note that p_0 is now lognormally distributed since it is the product of lognormally distributed parameters. Also, note the similarity with Eq. 2-47.

The application of Eq. 5-9 to the two nuclear containment vessels results in the safety indices in Table 5-2. Comparison of these results with those of Table 5-1 shows that, indeed, the safety index and probability of failure is insensitive to the geometric variables. This observation will be very useful in the finite element analysis.

The minimum mean limit pressure is also listed in Table 5-2. Since p_0 is lognormally distributed, the standard deviation of p_0 can be found from Eqs. 5-7 and 5-9 (or, by first order methods from Eq. 5-6) as

$$\sigma_{p_0} = \mu_{p_0} \left[\frac{\ln^2 \bar{p}}{\bar{\beta}^2} - V_p^2 \right]^{1/2} \quad (5-10)$$

where μ_{p_0} is taken as the minimum mean limit pressure and $\bar{\beta}$ is the generalized safety index of Eq. 2-54. Eq. 5-10 defines an upper and lower bound to σ_{p_0} because of the upper and lower bound to $\bar{\beta}$ in Eq. 2-54. These bounds on σ_{p_0} are also listed in Table 5-2. Note that V_p is zero in view of the discussion in Sec. 3.4.

5.2 Penetration Intersections

As a continuation of the approximate structural analysis, the Sequoyah and McGuire penetrations are analyzed using the method outlined in this section.

5.2.1 Failure Criteria

As presented in Sec. 4.2, leakage is assumed to occur in the penetrations at points remote from the containment when excessive plastic deformations take place. The limit pressure is approximately the pressure at which this occurs. For a penetrated vessel, the theoretical

limit pressure p_{ot} is assumed to occur when a yield mechanism is formed [24]. To calculate this pressure, the following two equations [44,45] are used:

Cylinder-Cylinder Intersection

$$p_{ot} = \left\{ \frac{\left[162 \left(\frac{t}{T} \right)^2 + 228 \left(\frac{t}{T} \right) \left(\frac{d}{D} \right) + 210 \right] K + 155}{108K^2 + \left[228 \left(\frac{d}{D} \right)^2 + 228 \right] K + 152} \right\} p_{co} \quad (5-11)$$

Cylinder-Sphere Intersection

$$P_{ot} = P_s P_{so} \quad (5-12a)$$

in which p_s is found from

$$\sqrt{\frac{T}{D} \left\{ \left[1 + \left(\frac{t}{T} \right)^2 \right] (1 - p_s) \right\}} = p_s \frac{d}{D} \sqrt{\left[1 - \left(\frac{d}{D} \right)^2 \right]} - \frac{d}{D} \frac{t}{T} \sqrt{\left[\frac{2t}{d} \left(1 - \frac{2T}{D} \frac{d}{t} p_s \right) \right]} \quad (5-12b)$$

and where

- t = penetration wall thickness
- T = vessel wall thickness
- d = penetration diameter
- D = vessel diameter
- $K = d/D \sqrt{D/T}$
- $p_{co} = 2 F_y T/D$
- $p_{so} = 4 F_y T/D$

Note that p_{co} and p_{so} are the limit pressures of an unstiffened cylinder and sphere, respectively, according to the maximum principal stress failure theory. As indicated by Eqs. 5-4 and 5-5, these limit pressures are conservative because the effects of stiffeners are neglected. Eq. 5-11 gives the theoretical limit pressure of a cylinder-nozzle intersection. Eq. 5-12b is solved by Newton's method to find

p_s . The theoretical limit pressure for a sphere-nozzle intersection is then determined using Eq. 5-12a.

Both Eqs. 5-11 and 5-12 are developed for penetrations which are flush with the inside surface of the vessel. Thus, they neglect any strengthening effect of the penetration wall which intrudes into the vessel -- as is the case for the containment vessels. The effect of the intrusion is investigated in Ref. 45 for nozzles in spherical shells. An expression for the limit pressure is obtained which resembles, in certain respects, Eq. 5-12.

If the intrusion extends significantly into the vessel, the limit mechanism [45 (Mech. No. 6)] includes the formation of a positive and negative plastic hinge in both the interior and exterior portion of the penetration (Fig. 5-1a). Eqs. 5-11 and 5-12 presented herein are based on a mechanism with plastic hinges in only the exterior portion (Fig. 5-1b). The effect of the intrusion can be approximately included by using an equivalent penetration thickness in Eqs. 5-11 and 5-12. If only membrane plastic work is involved, the mechanism in Fig. 5-12b would give the same limit pressure as that in Fig. 5-1a if an equivalent thickness of $2t$ is used. If, at the other extreme, only bending plastic work is involved, the equivalent thickness would be $\sqrt{2}t$. For the present case, both membrane and bending plastic work are involved and the equivalent thickness is somewhere between these two limits. As an approximation, the geometric mean, $2^{3/4}t$ or $1.68t$, will be used here.

The random limit pressure is written as

$$p_0 = x_0 p_{ot} \quad (5-13)$$

in which x_0 is the modeling error relating theory to the actual structure (see Sec. 3.3). Following Eq. 4-11, the failure function becomes

$$G = p_0 - p \quad (5-14)$$

in which p is the applied pressure. The random structural parameters are x_0 , F_y , d , D , t , T and p .

The complex geometry and associated difficulty in fabrication of the penetration intersections are a potential cause of significant undetected cracks. Hence, the probability of fracture relative to the probability of ductile flow is higher than at other locations in the shell. However, the discussion in Sec. 4.3, especially Eq. 4-12, is still appropriate, in the authors' opinion.

5.2.2 Modeling Error

As mentioned previously, the modeling error x_0 is defined as a factor relating theory to the actual structure. Ref. 44 gives some tabulated experimental results of the limit pressure for cylinder-cylinder and sphere-cylinder intersections. Only experimental data for intersection failures (Mode 3, Sec. 5.2.1) were used to find the modeling error. A total of 11 experimental results were used for the cylinder-cylinder intersection and 12 for the sphere-cylinder intersection. Failure of the vessel or penetration wall (modes 1 and 2) is not considered in this section.

The ratio, δ , between the experimental and the theoretical limit pressures can be calculated for the chosen experiments as

$$\delta = \frac{p_{ex}}{p_{ot}} \quad (5-15)$$

Assuming that δ is lognormally distributed, the mean and the standard deviation of $\ln \delta$ for the experimental data are

	<u>Cylinder</u>	<u>Sphere</u>	(5-16)
$m_{\ln \delta}$	0.0323	0.248	
$s_{\ln \delta}$	0.0835	0.111	

Following Sec. 3.3, conservative values for these statistics are found for the 95 percent confidence interval as

	<u>Cylinder</u>	<u>Sphere</u>	(5-17)
$\mu_{\ln \delta}$	-0.017	0.185	
$\sigma_{\ln \delta}$	0.147	0.188	

Using Eq. 2-39, the mean and standard deviation of the lognormally distributed δ becomes

	<u>Cylinder</u>	<u>Sphere</u>	(5-18)
μ_{δ}	0.994	1.23	
σ_{δ}	0.147	0.232	

Referring to Sec. 3.3 (Eqs. 3-19 and 3-20) the statistics for the modeling error x_0 can be found as

	<u>Cylinder</u>	<u>Sphere</u>	(5-19)
μ_0	0.99	1.23	
σ_0	0.16	0.24	

5.2.3 Application to Containment Vessels

The structural parameters for each penetration were obtained from drawings of the containment vessels. The statistics for these parameters are listed in Tables 3-2 and 3-2. Statistics for thicknesses not listed in Table 3-2 were interpolated. Tolerances for the penetration diameters were taken as \pm one percent.

The failure criterion of Eq. 5-14 was used in conjunction with the second moment method of Eq. 2-15 to predict the safety index for each penetration. Bounds on the system failure probability and safety index were also calculated. The results of this analysis are listed in Table 5-3. The minimum mean limit pressures were found to occur at the penetrations at Elev. 767 ft., Az. 266° for Sequoyah and Elev. 758.75 ft., Az. 20° for McGuire. There are several penetrations identical to these

at other locations in the containment shells. Complete results for each individual penetration are listed in the Appendix.

5.2.4 Sensitivity Analysis

As in the discussion of Sec. 5.1.5, the results are expected to be relatively insensitive to the geometric parameters. In the case of the penetrations, this can be verified by using the closed form solution for the safety index in Eq. 5-9. The results for bounds to the safety index and failure probability using Eq. 5-9 are given in Table 5-4. Again, by comparison with Table 5-3, the reliability is seen to be insensitive to the geometric parameters. Minimum mean limit pressure and bounds to the limit pressure standard deviation (Eq. 5-10) are also listed in Table 5-4.

5.3 Anchor Bolts

The Sequoyah and McGuire containment vessels are held down by a number of high strength bolts distributed at about 4° around the containment base. Bolts anchor the containment vessel to the concrete foundation. (Containment weight also acts downward to prevent uplift by internal pressure but this force is relatively small and is neglected here.) The anchor bolts will yield when the internal pressure reaches the limit pressure. Summing vertical forces at the limit pressure when all the bolts have yielded gives

$$P_{ot} \pi r^2 = n A_b F_y \quad (5-20)$$

where

n = number of bolts

A_b = bolt cross-sectional area

F_y = bolt yield strength

r = containment radius

P_{ot} = theoretical limit pressure at bolt yielding.

The random value of the limit pressure can be expressed as (see Eq. 3-12)

$$p_0 = x_0 p_{ot} \quad (5-21)$$

in which x_0 is the modeling error relating theory to the actual structure. For this analysis, it will be assumed that most of the experimental results fall within ± 30 percent of the theoretical value. The modeling error statistics are then the same as in Eq. 5-8, i.e.,

$$\mu_0 = 1.00 \quad (5-22)$$

$$\sigma_0 = 0.16 \quad (5-23)$$

Following Eq. 4-11, the failure function becomes

$$G = p_0 - p \quad (5-24)$$

in which p is the applied pressure. The random structural parameters (x_j in Eq. 2-4) are x_0 , A_b , F_y , r , and p . The statistics of these structural parameters are listed in Tables 3-1 and 3-2 and Eq. 5-23. The second moment reliability method summarized in Sec. 2-2 (Eq. 2-15 and 2-16) is applied. The resulting limit pressure, safety indices, and failure probabilities are tabulated in Table 5-5. (Note that the safety index and the failure probability are associated with an applied pressure of 28 psi.)

Following the discussion of Sec. 5.1.4, the results are expected to be relatively insensitive to the geometric parameters. In the case of the anchor bolts, this can be verified using the closed form solution for the safety index given in Eq. 5-9. The safety index, failure probability and the limit pressure standard deviation are listed in Table 5-6. Comparing these results with those given in Table 5-5, one can see that the anchor bolt reliability is insensitive to the geometric parameters.

5.4 Combined Failure Modes

As discussed in Secs. 5.1, 5.2 and 5.3, each failure mode was studied individually. A sensitivity study demonstrated that the safety index was insensitive to the geometric parameter statistics and could adequately be represented by Eq. 5-9. In this section all the failure modes (shell, penetration intersection and anchor bolts) are combined to predict the bounds for the safety index and failure probability of the complete structure. Thus, the results of Table 5-2 (shell failure modes), Table 5-4 (penetration intersection failure modes) and Table 5-6 (anchor bolt failure mode) are combined using Eqs. 5-9 and 2-54. Bounds on the structure failure probability and the safety index are evaluated and listed in Table 5-7. The minimum mean limit pressure and bounds on its standard deviation (Eq. 5-10) are also listed.

As shown in Tables 5-2 and 5-3, the minimum mean limit pressure for both containments is controlled by the stiffened shell failure modes. Thus, the strength of the penetrated shell is larger than the strength of the unpenetrated shell. (This result is not unexpected and, in fact, provides the basis for the ASME area replacement rule.) However, in the case of McGuire, the strength of the controlling penetration is only slightly larger than the unpenetrated shell. The stiffened shell and the controlling penetration will be analyzed in Sec. 6. In both containments, the anchor bolt limit pressure is relatively high and has no effect on the failure probability.

A word of caution - only the failure modes discussed above were analyzed. They were selected as being the most likely modes. However, many other modes are possible, e.g., welds, expansion bellows, personnel and equipment hatches, seals, and foundation liners. To examine all potential failure modes would require a much more extensive effort. The assumption has been made here that, as shown for the penetration and anchor bolt modes, the strength in all these other modes is greater than the strength in the shell failure modes.

VI. FINITE ELEMENT ANALYSIS

The approximate analyses in the previous section provide useful information in that they indicate critical failure modes which deserve further analysis. Finite element analysis methods are applied in this section to perform a more refined analysis of the stiffened axisymmetric shell and certain controlling penetrations.

6.1 ANSYS Finite Element Program

ANSYS [47] is a large-scale, general purpose computer program for the solution of several classes of engineering analysis problems. The program has the capability of analyzing two and three dimensional structures, piping systems, two dimensional axisymmetric solids, three dimensional solids and nonlinear problems. The ANSYS program is also capable of solving static, dynamic and heat transfer problems. The ANSYS program has the capability of generating and plotting the structural input data for the finite element models. Plotting routines are also available for plotting the distorted geometry.

The ANSYS program has two options available to include geometric nonlinearity. The first is called large displacement analysis and is accomplished by updating nodal coordinates to formulate the element stiffness matrix [48,49]. The second option is called stress stiffening and is accomplished by adding the geometric stiffness matrix [48,49] to the usual linear element stiffness matrix. The stress stiffening matrix depends upon element stresses obtained from the previous iteration. The stress stiffening solution represents a first approximation to large displacement effects.

The ANSYS program provides a plastic material capability with several options for material nonlinearity. The option employed here is called classical bilinear kinematic hardening. An elastic perfectly plastic material property is used (no strain hardening).

To accomplish the nonlinear (material and geometry) solution, an iterative approach is used within the ANSYS program. The procedure is to increase the applied load by small increments, called load steps, and allow the program to iterate until it converges to a final

solution. The solution is said to be converged if the ratio of the change in the plastic strain, $\Delta\epsilon_p$, to the elastic strain, ϵ_e , referred to as the plastic convergence ratio, is less than a specified value. The smaller the load step, the fewer the required number of iterations. In the program, a value of 0.01 is used for this ratio unless otherwise specified.

6.2 Failure Criteria

The nonlinear finite element analysis predicts the theoretical pressure-displacement curve. As discussed in Sec. 4, failure is assumed to occur when the displacements become "large", or the pressure reaches a plastic pressure value as calculated by the half linear slope method [24,41,42]. (See Fig. 4-2.) The theoretical plastic pressure P_{ct} will be used in calculating the structural safety index and probability of failure in conjunction with the sensitivity analysis discussed previously. The random plastic pressure p_c is written as

$$P_c = x_0 P_{ct} \quad (6-1)$$

in which x_0 is the modeling error relating theory to the actual structure (see Sec. 6.3.2).

6.3 Stiffened Axisymmetric Shell

6.3.1 Finite Element Modeling Guidelines

The containment vessel wall (axisymmetric shell) can be modeled by axisymmetric solid elements. The ANSYS program provides two different four-sided isoparametric elements of this type. One has four corner nodes (STIF42) and the other has four corner nodes and four midside nodes (STIF82) as shown in Fig. 6-1.

To study the accuracy of both STIF42 and STIF82 and the various options in ANSYS, a smooth closed end cylindrical shell was analyzed. The following options were employed:

<u>Element</u>	<u>Plastic Convergence Ratio</u>	<u>Geometric Nonlinearity Option</u>
STIF42	0.03	Stress stiffening (SS)
STIF42	0.03	Large displacement(LD)
STIF82	0.03	SS
STIF82	0.05	SS
STIF82	0.10	SS

The cylinder was modeled as shown in Fig. 6-2. For STIF42, an element length (height) of $\sqrt{rt/4}$ was used, in which r and t represent the shell radius and thickness, respectively. Twice this length was used with STIF82. One element was used through the shell thicknesses.

Fig. 6-3 shows the radial deformation of the cylinder at an internal pressure of 35 psi. At this pressure, the structure is in the elastic region. The results using STIF82 and STIF42 without either stress stiffening or large displacements are very close to those found from classical shell theory [50]. Also, STIF82 with the stress stiffening option gives results which are close to those calculated using STIF42 with either the stress stiffening or large displacement options. STIF82 with an element length of about $\sqrt{rt/2}$ will be used in this work.

Fig. 6-4 shows the pressure-displacement curves for the different element types and the different plastic convergence ratios. The results of the theoretical plastic pressure using the half linear slope method are given in Table 6-1. The percentage difference in the theoretical plastic pressures (with respect to p_{ct} for a convergence ratio of 0.03) is listed in Table 6-1. Computer CPU time is also tabulated. Fig. 6-4 and Table 6-1 indicate that there is no significant difference between the results obtained from STIF42 and STIF82. Further, stress stiffening adequately accounts for large displacement effects in the range of interest at a large savings in computer time. Hence stress stiffening will be used in this work.

Table 6-1 illustrates that a higher plastic convergence ratio results in shorter CPU times and a larger error in the theoretical

plastic pressure. Comparing the CPU time used and the difference in P_{ct} , it was decided to use a plastic convergence ratio of 0.1. The error in the theoretical plastic pressure, P_{ct} , will be accounted for, somewhat, in the modeling error x_0 (Eq. 6-1).

The Sequoyah and McGuire containment vessels are reinforced by ring and vertical stiffeners. The vessel in Fig. 6-5 was used to investigate possible finite element models for the stiffeners. The cylinder was modeled by the isoparametric elements mentioned above. The vessel, without stringers, was analyzed using two different ring models. Initially, five isoparametric axisymmetric elements were used to idealize the web and two elements for the flange of the ring. Next, one element was used in the web and one in the flange. Both idealizations gave approximately the same predicted theoretical plastic pressure (within three percent). Due to the noticeable saving in computer time, one-element idealizations of the web and flange will be used.

The stringers obviously introduce a non-axisymmetric character to the problem, i.e., the stringers cause the displacements to vary circumferentially. In principle then, the structural behavior is three-dimensional. However, a three-dimensional idealization of the entire containment vessels is beyond a reasonable scope for this project. To retain the axisymmetric idealization, a stringer is idealized as a beam with properties uniformly distributed around the circumference. The basic assumption, then, is that the circumferential variation of displacement is negligible.

The circumferential variation of displacement for the Sequoyah containment has been independently studied by two investigators [51,52]. Their work is unpublished and summarized here.* Both authors considered the behavior of a typical panel of the Sequoyah containment bounded by two rings and two stringers. At a point midway between the rings, Ref. 51 found that the ratio of the displacement at the stringer to the displacement midway between the stringers (center of panel) is

*Copies of [51,52] are attached in the Addendum.

about 1.08. This ratio is maintained up into the nonlinear range. In Ref. 52, a linear analysis of a slightly different-sized panel showed the ratio to be 1.20.

A two-dimensional beam element (STIF23) was used to model the vertical stiffeners (stringers). This beam element has stress stiffening and nonlinear capabilities. Since no hoop effects are present in the stringers, STIF23 can be used with axisymmetrical elements. Properties are input on a per-radian basis.

The linear constraint equation option in ANSYS was used to idealize the ring and stringer connection to the shell wall. This option relates the displacements of selected nodal points through a specified equation. The cylinder/stringer connection idealization is shown in Fig. 6-6 together with the associated linear constraint equations. In effect, a rigid link connects the stringer node to the shell node.

The cross-section of the ring was assumed to remain rigid and to translate and rotate with the stringer node. Fig. 6-7 shows the ring web connection to the cylinder and to the stringer with the associated constraint equations. Node 4 was constrained to Node 1 only in the vertical direction to prevent any artificial stiffening of the web, e.g., to permit through thickness straining. The ring stiffener flange was also constrained to the stringer node as shown in Fig. 6-8.

Fig. 6-9 illustrates the pressure-displacement curves for the vessel in Fig. 6-5 with and without stiffeners. Using the half linear slope method, there is about a 23 percent increase in the theoretical plastic pressure when the ring and vertical stiffeners are added.

6.3.2 Modeling Error

The modeling error, x_0 , is defined as a factor relating theory to the actual structure (see Sec. 3.3. and Eq. 6-1). Ref. 53 provides some experimental results in the form of pressure-displacement curves for closed-end smooth cylinders. (Unfortunately, no experimental results for stiffened cylinders were found.) A total of six such cylinders (Cylinders 31, 32, 33, 34, 35 and 36) were analyzed using STIF82 with a plasticity convergence ratio of 0.1. The theoretical pressure-displacement relationship was found and the theoretical plastic

pressure was evaluated as discussed in Sec. 6.2. The experimental plastic pressures were obtained from the experimental pressure-displacement curves by the half linear slope method.

The ratio, δ , between the experimental and theoretical plastic pressures was calculated as in Eq. 5-15. Assuming that δ is lognormally distributed, the mean and the standard deviation of $\ln \delta$ is found as

$$\begin{aligned} m_{\ln \delta} &= 0.153 \\ s_{\ln \delta} &= 0.24 \end{aligned} \tag{6-2}$$

Following Sec. 3.3, conservative values for these statistics are found from the 95 percent confidence interval as

$$\begin{aligned} \mu_{\ln \delta} &= 0.123 \\ \sigma_{\ln \delta} &= 0.059 \end{aligned} \tag{6-3}$$

Using Eq. 2.39, the mean and standard deviation of the lognormally distributed δ becomes

$$\begin{aligned} \mu_{\delta} &= 1.13 \\ \sigma_{\delta} &= 0.067 \end{aligned} \tag{6-4}$$

which represents the variability between theoretical and experimental results on smooth cylinders. The experimental models appear to have a plastic pressure about 13 percent larger than that predicted by theory. This increase is not considered reliable and will be conservatively neglected here. The error in the ring and vertical stiffener models is assumed to be incorporated into the factor Δ . Referring to Sec. 3.3 (Eqs. 3-19 and 3-20) the statistics for the modeling error x_0 are taken to be

$$\mu_0 = 1.00$$

(6-5)

$$\sigma_0 = 0.083$$

Admittedly, these values are somewhat subjective. As discussed in Sec. 3.3, more confidence can be developed in these statistics only by analyzing more experimental results and, especially, by testing more full-scale containments. This is beyond the scope of the present study.

6.3.3 Applications

The ANSYS finite element computer program was used to analyze the Sequoyah and McGuire containment vessels shown in Figs. 1-1 and 1-2, respectively. The guidelines outlined in Sec. 6.3.1 were used to model these vessels. The mean dimensions given in Table 3-2 were employed in the finite element analysis.

6.3.3.1 Finite Element Model

For the Sequoyah containment vessel, the stringers are welded to the containment wall and the ring stiffeners. The linear constraint equations discussed in Sec. 6.3.1 were used to model this connection. Two hundred fifty STIF82 elements and 123 STIF23 beam elements were used to idealize the containment vessel. The total number of nodes was 1414. At the time this analysis was performed, the mean material yield strength had not been furnished by the Sequoyah owners. A mean yield strength of 35.2 ksi was used in the ANSYS analysis. The actual mean value was provided later (see Table 3-1). A uniform internal pressure of 35 psi was initially applied to the Sequoyah vessel model and incremented by 5 psi. At a pressure of 50 psi convergence to the specified plastic ratio did not occur within 20 iterations. About 7-1/2 hours of computer time on a PRIME400 minicomputer were used for this analysis.

In the McGuire containment vessel, there is a 1/2" gap between the stringer and the ring webs. Linear constraint equations similar to Fig. 6.6 were used at each end of each stringer to model this gap. Two hundred thirty-eight STIF82 elements and 130 STIF23 elements were used

to model the containment. The number of nodes was 1365. The uniform internal pressure for the McGuire containment was started at 55 psi with increments of 5 psi up to 80 psi. The pressure increment was then changed to 1 psi to ensure convergence within each load step. The solution did not converge to the specified plastic ratio after ten iterations at a pressure of 85 psi. The run time on the PRIME400 was approximately 7-1/2 hours.

6.3.3.2 Results

The results of the finite element analysis are summarized in Figs. 6-10 through 6-15. Figs. 6-10 and 6-11 are plots of the applied pressure versus the maximum radial displacement for the Sequoyah and McGuire containment vessels. This displacement occurs at about Elev. 783' for Sequoyah and about Elev. 751' for McGuire. For the Sequoyah vessel, plastic deformation starts at a pressure of about 40 psi and increases rapidly at a pressure of 45 psi. For the McGuire containment vessel, plastic deformation starts at about 70 psi and increases rapidly at 84 psi. Since convergence did not occur at the last load step, the radial displacement is taken to be very large. This is represented by the nearly horizontal line in Figs. 6-10 and 6-11. Using the half linear slope method, the theoretical plastic pressures, p_{CT} , are 45 psi and 84 psi for Sequoyah and McGuire, respectively. As mentioned above, 35.2 psi was used as the mean yield strength of the Sequoyah containment. The corrected theoretical plastic pressure is obtained by multiplying 45 psi by 47.2/35.2 to obtain 60 psi as the predicted plastic pressure for Sequoyah.

Figs. 6-12 and 6-13 show the applied pressure versus the maximum effective von Mises strain. For Sequoyah, this maximum strain occurred at about Elev. 783' and at about Elev. 751' for McGuire. These plots indicate the strains at the predicted plastic pressures are not excessive - of the order of two times the elastic strain. The ductile steel used in these containments will almost certainly be able to tolerate these strains without fracture [21, pg 529]. In other words, the vessels will almost certainly reach the plastic pressure before leakage. This observation reinforces a similar conclusion in Sec. 4.3.

Fig. 6-14 shows the deflected shape of the Sequoyah containment vessel near the plastic pressure. The maximum displacement occurs at the smallest shell thickness. The deflection between the ring stiffeners is slightly more than at the ring locations. The deflected shape of the McGuire containment vessel near the plastic pressure is shown in Fig. 6-15. Since this vessel has a more uniform thickness, the radial displacement is almost uniform.

An examination of the stress results for both of these analyses indicates, that, as expected, the shell yields first about midway between stiffeners. At this point the rings are below their yield value. However, as the pressure is increased, the ductile shell continues to strain with no change in stress. Forces are, thereby, redistributed to the rings. Eventually, the rings themselves reach their yield stress and, for all practical purposes, a collapse mechanism is formed. In this mechanism, the shell and rings are completely yielded. This corresponds to the last (non-converged) load step of the nonlinear solution. At this point, the stringers are also almost at total yield in tension in the vicinity of the maximum displacement. (The stringer axial loads are 0.96 and 0.89 of the stringer tensile yield strengths for Sequoyah and McGuire, respectively.) This behavior tends to confirm the mechanism assumptions in Sec. 5.1.1.

6.3.4 Uncertainty Analysis

In Sec. 5.1 it was concluded that the safety index is insensitive to the geometric structural parameters and could adequately be predicted using Eq. 5-9. The theoretical plastic pressure, p_{ct} , obtained in Sec. 6.3.3, is used in conjunction with Eqs. 5-9 and 5-10 to perform the uncertainty analysis for the Sequoyah and McGuire containment

vessels. This leads to the standard deviation of the plastic pressure as*

$$\sigma_{p_c} = \mu_{p_c} \sqrt{V_{x_0}^2 + V_{F_y}^2} \quad (6-6)$$

The statistics for material yield strength are given in Table 3-1 and for the modeling error in Eq. 6-5. The mean and the standard deviation of the plastic pressure for the axisymmetric shell failure mode become 60 psi and 5.9 psi, respectively, for Sequoyah and 84 psi and 8.3 psi, respectively, for McGuire.

6.4 Penetration Analysis

The controlling penetration for each containment vessel (see Sec. 5) was analyzed using the finite element method through the ANSYS program.

6.4.1 Modeling Guidelines

The element used for this analysis was STIF48, the only ANSYS shell element possessing both stress stiffening and plasticity characteristics. STIF48 is a three node triangular element with six degrees of freedom per node. Following the suggestion of the ANSYS documentation, a curved shell pressure loading option was utilized which eliminates equivalent nodal moments that cause fictitious bending stresses in the element. Two linear trial runs, with and without this option, proved this to be true.

*Note that the collapse pressure is, to the first order, proportional to F_y . Dimensional analysis principles would give p_c/F_y and F_y/E as the only dimensionless products involving force dimensions. The term, F_y/E , is, typically, considered to be a second order effect so that p_c is proportional to F_y when other parameters are held constant.

In an effort to minimize CPU time without sacrificing accuracy, an attempt was made to develop some modeling guidelines. Parameters felt to warrant study included element size, aspect ratio, mesh characteristics, and model size. An extensive study was not possible, but by linearly analyzing two models - a smooth pressurized cylinder and a pressurized cylinder with a penetration - and comparing their behavior with theoretical and experimental results, some very general guidelines developed.

Element length at the vessel-penetration intersection is controlled not by $rt/2$, but rather by central angle size of the penetration. An arc length of 10 degrees with respect to the penetration is an approximate maximum value. Maximum element size in the penetration remote from the intersection is 30 degrees of arc length. Maximum element size in the vessel remote from the intersection is 20 degrees of arc length with respect to the vessel. Element aspect ratios should approach 1:1 in critical areas of the intersection, but 1:3 is satisfactory in areas remote from the intersection.

Characteristics of the mesh involve two concepts. First, and most obvious, the mesh should have smooth transitions from fine areas around the intersection to coarse areas remote from the intersection. Second, the mesh, wherever possible, should be generated with three sets of parallel lines instead of four [48, pg 245]. The latter mesh gives rise to unequal equivalent nodal forces.

Finally, trial runs indicated that the model of the penetration should extend at least one penetration diameter, d , away from the intersection; similarly, the vessel model should also extend at least a distance, d , away from the intersection.

6.4.2 Experimental vs ANSYS Results

To facilitate some sort of comparison of ANSYS results to predicted results, a nonlinear analysis of a pressure vessel with a penetration was performed using the aforementioned guidelines. The results were compared to an experimental model [54] of the same dimensions ($d = 3.762$ ", $t = 0.125$ ", $D = 5.789$ ", $T = 0.187$ "). The displacement of the point on the vessel-penetration intersection and in the symmetry plane

perpendicular to the vessel axis was plotted versus the internal pressure. Both the experimental and ANSYS curves are shown in Fig. 6-16.

Lack of time and money precluded additional model runs, therefore preventing a more complete error analysis. However, the similarity of the two curves in Fig. 6-16 does indicate certain factors. First, STIF48 appears to give fairly reliable results. Second, the modeling guidelines which were applied appear to be satisfactory. The percent error in the theoretical plastic pressure, p_{ct} , for this particular case is 10 percent. Last, an approximation to the CPU time for a non-linear run was obtained which directly influenced later modeling decisions.

6.4.3 Application

6.4.3.1 Finite Element Model

The finite element model of the controlling Sequoyah penetration (Elev. 767', Az. 266°) was developed with certain considerations. This penetration has a diameter of 24 in. and a thickness of 0.375 in. The containment vessel has a thickness of 0.625 in. in the vicinity of the penetration but is reinforced locally to 1.5 in. To minimize CPU time and still obtain accurate results, as small a portion of the structure as possible was chosen. Since an identical penetration is located 5 degrees (centerline to centerline) away from the modeled penetration, a plane of symmetry was assumed at half that arc length, 2.5 degrees. Also, to minimize the stiffening effect of the circumferential rings and to obtain a conservative result for other similar penetrations, the penetration was assumed to lie midway between two rings. The model, thus, had quarter symmetry. The penetration was modeled with a 24 in. intrusion and a 24 in. protrusion, or one diameter away from the intersection. The model consists of 253 elements and 183 nodes. STIF48 was used for all elements, including the rings. The mesh is shown in Fig. 6-17. All four edge-planes of the vessel, along with the longitudinal symmetry plane of the penetration, were modeled with symmetry boundary conditions. The transverse edges of the penetration were assumed to be free edges.

A uniform pressure was applied in increments to the internal vessel face and the external face of the penetration intrusion. Axial forces were applied to both the penetration intrusion and the vessel to account for pressure end loading. The initial load, 20 psi, was used to establish an initial slope for the pressure/displacement curve. An estimate of the yield pressure was obtained by extrapolating the element stresses to yield. This estimate was 35 psi, which was the second load, or load step. The succeeding load steps were determined by considering the pressure-displacement curve and rate of convergence of the previous load step. Load steps of 5 psi were used successfully. In the interest of saving the time and expense of unnecessary computer processing, the loading was continued only until a minimum acceptable pressure was achieved. For Sequoyah, the plastic pressure of the unpenetrated shell was determined to be 60 psi (see Sec. 6.3). Therefore, the penetration analysis was concluded upon reaching 65 psi successfully. The computer run time was about 9 hours.

The controlling McGuire penetration (Elev. 758.75', Az. 20°) was modeled with similar considerations. The penetration is a Schedule 60, 12.75 in. diameter pipe. The containment shell thickness is 1.0 in. There is no local reinforcement. The penetration is one of several identical penetrations arranged in two parallel rows between two circumferential rings. Again, a symmetry plane was assumed midway between the penetrations (2.5° centerline to centerline) or 1.25° away from the controlling penetration centerline. To conservatively minimize the stiffening effects of the rings, the two rows of penetrations were assumed to lie at one-third points between the rings. A horizontal plane of symmetry was then assumed midway between the two horizontal rows of penetrations. The penetration was modeled with a 12 in. intrusion and a 12 in. protrusion, or one diameter away from the intersection. The McGuire model consists of 455 elements, all using STIF48, and 315 nodes. The finite element mesh is shown in Fig. 6-18. All four edge-planes of the vessel, along with the longitudinal symmetry plane of the penetration, were modeled with symmetry boundary conditions. The remaining transverse edges of the penetration were assumed free edges.

A uniform pressure was applied in increments to the internal vessel face and the external face of the penetration intrusion. Axial forces were applied to both the penetration intrusion and the vessel to account for pressure end loading. Using loading criteria similar to the Sequoyah analysis, the initial load was taken to be 10 psi with an estimated initial yield pressure of 32 psi. Again, varying load steps were applied until a pressure of 88 psi was successfully achieved, well above the controlling theoretical plastic pressure of 84 psi for the axisymmetric shell as determined from the containment analysis (Sec. 6.3). The approximate run time was 22 hours.

6.4.3.2 Results

The pressure versus displacement curves are shown in Fig. 6-19 (Sequoyah) and Fig. 6-20 (McGuire). In each case, the displacement refers to the displacement of the end of the penetration protrusion measured radially from the axis of the vessel [24]. These curves show that the theoretical plastic pressure for the controlling penetrations for Sequoyah and McGuire are greater than 65 psi and 88 psi, respectively.

Plots of the applied pressure versus the maximum effective von Mises strain are shown in Figs. 6-21 and 6-22. In both cases, the strains of the above pressures are not more than six times the yield strain. As discussed in Sec. 6.3.3.2, the ductile steel of this containment will almost certainly tolerate these strains without fracture [21, pg 529].

6.4.4 Uncertainty Analysis

As mentioned above, it did not seem reasonable to spend the computer time and funds which would have been required to continue the pressure-displacement plots of Figs. 6-19 and 6-20 up to the theoretical plastic pressure. An uncertainty assessment of the penetration failure modes can, therefore, not be performed. However, the mean plastic pressures for the controlling penetrations are above 65 psi and 88 psi for Sequoyah and McGuire, respectively. These plastic pressures are significantly above those calculated for the unpenetrated shell in

Sec. 6.3 - 60 psi and 84 psi, respectively. The approximate results show that the standard deviation of the plastic pressure of the penetration analysis (Table 5-4) is not significantly different from the standard deviation of the plastic pressure of the unpenetrated shell (Table 5-2). In terms of the uncertainty analysis of the entire containment, therefore, one can reasonably neglect the probability of failure of the penetrations with respect to the shell. Or, as stated in Sec. 5.4, the strength of the penetrated shell is greater than the strength of the unpenetrated shell.

6.5 Combined Failure Modes

As summarized in the previous portions of Sec. 6, the finite element was used to analyze two failure modes (axisymmetric stiffened shell and one penetration intersection) for each of the two containments. These modes were indicated by the approximate methods of Sec. 5 to be the most likely to occur. A finite element analysis of all the possible failure modes would be well beyond the scope of this project. And yet, failure by these unanalyzed modes is certainly possible. To approximate the effect of the unanalyzed failure modes on the safety index and failure probability, the following approach will be adopted. The system mean failure pressure will be taken to be equal to the minimum mean plastic pressure for the analyzed failure modes: 60 psi and 84 psi for Sequoyah and McGuire, respectively (Sec. 6.3.4). In both cases, the unpenetrated axisymmetric shell has been shown to control, i.e., to have the minimum mean plastic pressure (Sec. 6.4.4). The coefficient of variation of the plastic pressure will be taken as [37]

$$V_{P_C} = \sqrt{V_{x_0}^2 + V_{F_y}^2 + V_m^2} \quad (6-7)$$

where V_m represents the effect of the unanalyzed failure modes. The approach suggested in Eq. 6-7 implies that the effect of the unanalyzed failure modes can be expressed in the form of a multiplying factor similar to the modeling error. The authors realized that this is, at best, a very approximate approach and that it has pitfalls. However,

it is expedient. It is not economically feasible to analyze all failure modes by finite element. In fact, a primary motivation for the development of approximate methods is to be able to analyze many failure modes. The finite element method is here visualized as a means of refining the approximate results. For this reason, no β values or failure probabilities are calculated for the finite element analysis. The coefficient of variation of the modeling error and material yield strength have been discussed previously in conjunction with Eq. 6-6. The difference between the upper and lower bounds to the plastic pressure standard deviation is due to the additional failure modes (see Eq. 2-54 and 5-10). An appropriate value of V_m which approximately accounts for all the shell, penetration and bolt failure modes is

$$V_m = \sqrt{V_{P_{Cu}}^2 - V_{P_{Cl}}^2} \quad (6-8)$$

where $V_{P_{Cu}}$ and $V_{P_{Cl}}$ are the upper and lower bound coefficients of variation for the plastic pressure. For the approximate results in Table 5-7, V_m is 0.037 and 0.099 for Sequoyah and McGuire, respectively. For this work, V_m will be taken as [37]

$$V_m = 0.10 \quad (6-9)$$

With this value of V_m and Eq. 6-7, the final predicted mean and standard deviation of the plastic limit pressure are listed in Table 6-2.

VII. SUMMARY OF RESULTS

7.1 Summary

The Sequoyah and McGuire ice condenser containment vessels were designed to withstand pressures in the range of 12 to 15 psi. Because the peak recorded pressure at TMI was 28 psi, there is a need to more accurately define the strength of these vessels. A second moment reliability method was applied to perform a best estimate and uncertainty analysis of the containment strengths. Material property statistics and geometric tolerances were furnished by the plant owners. The loading was assumed to be a uniform static internal pressure. Gross deformation (displacement twice the elastic value at the same load) was taken to be the failure criteria. Fracture of the vessel wall was shown to have a low probability of occurrence. The final results are insensitive to the ultimate strength and fracture stress and to the randomness of the geometric parameters. However, the calculated mean and standard deviation of the pressure strength are dependent upon the randomness of the yield stress and modeling error.

The complete vessel and all the penetrations were analyzed by approximate methods based on classical limit analysis theory. For Sequoyah, the mean limit pressure was found to be 59 psi with a standard deviation of 10 psi. For McGuire, the mean was 77 psi and the standard deviation was 15 psi.

An axisymmetric finite analysis was performed of each vessel using the ANSYS computer program with nonlinear material and geometric options. Also, the controlling penetration for each vessel, as determined by the approximate analysis, was analyzed using ANSYS. The resulting mean and standard deviation of the plastic pressure for Sequoyah were 60 psi and 8 psi, respectively. For McGuire, the mean and standard deviations were 84 psi and 12 psi, respectively.

7.2 Conclusions

For the failure modes investigated, the mean plastic static pressure strength of the Sequoyah containment vessel is 60 psi with a

standard deviation of 8 psi. The corresponding pressure for McGuire is 84 psi with a standard deviation of 12 psi.

7.3 Recommendations

There are at least four areas where the scope of work presented herein was limited. These limitations could be removed by:

- Dynamic analyses. The TMI pressure pulse is potentially dynamic, i.e., a pulse length of the order of the structural period. (No exact information has been furnished.) In this regard, dynamic analyses should be performed using realistic pressure-time-space relationships.
- Additional failure modes. As mentioned in Sec. 5.3 and 6.5, only a limited set of failure modes was examined in this study. A more comprehensive program could be undertaken to examine other modes.
- Approximate analyses. The approximate analyses appear to give reasonable results for these cases at a large savings in time. The limits of these approximations should be defined.
- Distribution assumptions. The assumption of normal or lognormal distributions for input parameters introduce errors of various amounts in the reliability estimates. The error should be quantified.
- Fracture. The fracture properties of the material (stress intensity factors, crack shapes and size; temperature) should be investigated more thoroughly to establish more certainly the tentative results of Sec. 4.3.
- Experimental results. Perhaps the biggest shortcoming of the analysis reported herein is the lack of correlation with experimental data. No experimental data could be found for stiffened cylinders under internal pressure. Hence, the modeling error which was used was quite subjective. Although extensive experimental data exist for shell penetrations, very little exists for large r/t values. Also, there was not enough time or money to analyze the existing data with the finite element program. Future work should be devoted to: (1) finding (or obtaining) experimental results for stiffened cylinders with internal pressure and correlating these results with

a finite element analysis, and (2) correlating existing penetration experimental results with a finite element analysis.

VIII. LIST OF REFERENCES

1. Schauer, F.P. and Shinozuka, M., "Probabilistic Safety Analysis for Nuclear Power Plant Containment Structures: A Basic Formulation," Reliability Approach in Structural Engineering, Japan-U.S. Joint Seminar on Reliability Approach in Structural Engineering, May 1974, Maruzen, Tokyo, 1975, pp. 347-358.
2. Kiureghian, A.D., "Reliability Analysis Under Stochastic Load," Journal of Structural Division, ASCE, Vol. 106, ST2, Feb. 1980, pp. 411-429.
3. Fiessler, B., Neuman, H-J and Rackwitz, R., "Quadratic Limit States in Structural Reliability," Journal of Engineering Mechanics, ASCE, Vol. 105, EM4, Aug. 1979, pp. 661-676.
4. Rackwitz, R., "Practical Probabilistic Approach to Design," Technical University of Munich, May 1976.
5. Veneziano, D., "New Index of Reliability," Journal of Engineering Mechanics, ASCE, Vol. 105, EM2, April 1979, pp. 277-296.
6. Kapur, K.C. and Lamberson, L.R., Reliability in Engineering Design, John Wiley & Sons, New York, 1977.
7. Freudenthal, A.M., Garrelts, J.M., Shinozuka, M., "The Analysis of Structural Safety," Journal of Structural Division, ASCE, Vol. 90, ST1, Feb. 1966, pp. 267-325.
8. Ang, A.H.-S., "Structural Risk Analysis and Reliability Based Design," Journal of Structural Division, ASCE, Vol. 99, ST9, Sept. 1973, pp. 1891-1910.
9. Ang, A. H-S. and Cornell, C.A., "Reliability Bases of Structural Safety and Design," Journal of Structural Division, ASCE, Vol. 100, ST9, Sept. 1974, pp. 1755-1769.
10. Hasofer, A.M. and Lind, N.C., "Exact and Invariant Second-Moment Code Format," Journal of Engineering Mechanics, ASCE, Vol. 100, EM1, Feb. 1974, pp. 111-121.
11. Ravindra, M.K. and Galambus, T.V., "Load and Resistance Factor Design for Steel," Journal of Structural Division, ASCE, Vol. 104, ST6, Sept. 1978, pp. 1337-1353.

12. Ravindra, M.K. and Singh, A.K., "Reliability Assessment of ASME Code Equations for Nuclear Components," Reliability Engineering in Pressure Vessels and Piping, Second National Conference on Pressure Vessels and Piping, ASME, San Francisco, June 1975, pp. 29-36.
13. Lind, N.C., "Optimal Reliability Analysis by Fast Convolution," Journal of Engineering Mechanics, ASCE, Vol. 105, EM3, June 1979, pp. 447-452.
14. Lind, N.C., "Formulation of Probabilistic Design," Journal of Engineering Mechanics, ASCE, Vol. 103, EM2, April 1977, pp. 273-284.
15. Moses, F., "Reliability of Structural Systems," Journal of Structural Division, ASCE, Vol. 100, ST9, Sept. 1974, pp. 1813-1820.
16. Moses, F. and Stevenson, J.D., "Reliability-Based Structural Design," Journal of Structural Division, ASCE, Vol. 96, ST2, Feb. 1970, pp. 221-244.
17. Cornell, C.A., "Bounds on the Reliability of Structural Systems," Journal of Structural Division, ASCE, Vol. 93, ST1, Feb. 1967, pp. 171-200.
18. Ang, A. H-S. and Ma, H-F., "On the Reliability of Framed Structures," Proceedings of Specialty Conference on Probabilistic Mechanics and Structural Reliability, ASCE, Tucson, Jan. 10-12, 1979, pp. 106-111.
19. Galambos, T.V. and Ravindra, M.K., "Properties of Steel for Use in LRFD," Journal of Structural Division, ASCE, Vol. 104, ST9, Sept. 1978, pp. 1459-1468.
20. Fisher, J.W. et al., "Load and Resistance Factor Design Criteria for Connections," Journal of Structural Division, ASCE, Vol. 104, ST9, Sept. 1978, pp. 1427-1441.
21. Rolfe, S.T. and Barsom, J.M., Fracture and Fatigue Control in Structures--Applications of Fracture Mechanics, Prentice Hall, 1977.
22. "Standard Method of Test for Plane-Strain Fracture Toughness of Metallic Materials," ASTM Designation E399-74, Part 10, ASTM Annual Standards.

23. ASME Boiler and Pressure Vessel Code, Section III, Division 1 - Subsection NA, Appendix G, Article G-2000.
24. Gerdeen, J.C., "A Critical Evaluation of Plastic Behavior Data and a Unified Definition of Plastic Loads for Pressure Vessel Components," draft of final report to Task Group on Characterization of Plastic Behavior of Structures, Pressure Vessel and Research Committees, Welding Research Council, April 9, 1979.
25. Oldfield, W., et al., "Statistically Defined Reference Toughness Curves," Third International Conference on Pressure Vessel Technology, Tokyo, ASME, April 1977, pp. 703-715.
26. ASME Boiler and Pressure Vessel Code, Sec. III, Table I-1.1, 1971.
27. Schmitt, W., Keim, E., Wellein, R. and Bartholome, G., "Linear Elastic Stress Intensity Factors for Cracks in Nuclear Pressure Vessel Nozzles Under Pressure and Temperature Loading," International Journal of Pressure Vessels and Piping, Vol. 8, 1980, pp. 41-68.
28. Cesari, F., "Evaluation of Stress Intensity Factors for Internally Pressurized Cylinders with Surface Flaws," International Journal of Pressure Vessels and Piping, Vol. 7, 1979, pp. 199-227.
29. Merkle, J.G., "A Review of Some Existing Stress Intensity Factor Solutions for Part-Through Surface Cracks," Oak Ridge National Laboratory, Report ORNL-TM-3983, Jan. 1973.
30. ASME Boiler and Pressure Vessel Code, Sec. XI, 1974 ed., App. A.
31. Newman, J.C., "A Review and Assessment of the Stress-Intensity Factors for Surface Cracks," Part-Through Crack Fatigue Life Predictions, ASTM STP 687, 1979, pp. 16-42.
32. ASME Boiler and Pressure Vessel Code, Sec. III, Par. NB535, 1974.
33. Packman, P.F. et al., "Reliability of Defect Detection in Welded Structures," Reliability Engineering in Pressure Vessels and Piping, Second International Conference on Pressure Vessels and Piping, ASME, June 1975, pp. 15-28.
34. Larsson, H. and Bernard, J., "Fracture of Longitudinally Cracked Ductile Tubes," International Journal of Pressure Vessels and Piping, Vol. 6, 1978, pp. 223-243.

35. "Standard Specifications for General Requirements for Steel Plates for Pressure Vessels," ASTM Standards, 1979, Spec. A20, Table 1 and Table 6.
36. Ravindra, M.K., Lind, N.C. and Siu, W., "Illustration of Reliability-Based Design," Journal of Structural Division, ASCE, Vol. 100, ST9, Sept. 1974, pp. 1789-1811.
37. Morales, W.J., Duke, J.M. and Mazumdar, M., "Reliability of Slightly Oval Cylindrical Shells Against Elastic-Plastic Collapse," Reliability Engineering in Pressure Vessels and Piping, Second National Congress on Pressure Vessels and Piping, ASME, San Francisco, June 1975, pp. 37-49.
38. Miller, I. and Freund, J.E., Probability and Statistics for Engineers, Prentice-Hall, Englewood Cliffs, 1977.
39. Harrison, R.P., Darlaston, B.J.L. and Townley, C.H.A., "Failure Assessment of Pressure Vessels Under Yielding Conditions," Third International Conference on Pressure Vessel Technology, Tokyo, ASME, April 1977, pp. 661-668.
40. Adams, N.J.I., "An Analysis and Prediction of Failure in Tubes," Third International Conference on Pressure Vessel Technology, Tokyo, ASME, April 1977, pp. 685-694.
41. Hayakawa, T., Yushida, T. and Mii, T., "Collapse Pressure for the Small End of a Cone-Cylinder Junction Based on Elastic-Plastic Analysis," Third International Conference on Pressure Vessel Technology, Tokyo, ASME, April 1977, pp. 149-156.
42. ASME Boiler and Pressure Vessel Code, Sec. III, Div. 1, Par. II-1430, 1975, Winter Addenda.
43. Okamura, H., Watnabe, K. and Naito, Y., "Some Crack Problems in Structural Reliability Analysis," Reliability Approach in Structural Engineering. Japan-U.S. Joint Seminar on Reliability Approach in Structural Engineering, May 1974, Maruzen, Tokyo, 1975, pp. 243-257.
44. Rodabaugh, E.C. and Cloud, R.L., "Assessment of the Plastic Strength of Pressure Vessel Nozzles," Journal of Engineering for Industry, ASME, November 1968, pp. 636-643.

45. Gill, S.S., "The Limit Pressure for a Flush Cylindrical Nozzle in a Spherical Pressure Vessel," International Journal of Mechanical Science, Vol. 6, 1964, pp. 105-115.
46. Dinno, K.S. and Gill, S.S., "Limit Pressure for a Protruding Cylindrical Nozzle in a Spherical Pressure Vessel," Journal of Mechanical Engineering Science, Vol. 7, No. 3, 1965, pp. 259-270.
47. ANSYS, Engineering Analysis System, User's Manual and Theoretical Manual, Swanson Analysis Systems, Inc., Houston, Pa.
48. Zienkiewicz, O.C., The Finite Element Method, 3rd ed., McGraw-Hill Book Company, Inc., New York, 1977.
49. Gallagher, R.H., Finite Element Analysis Fundamentals, Englewood Cliffs, New Jersey, Prentice Hall, Inc., 1975.
50. Roark, R.J. and Young, W.C., Formulas for Stress and Strain, 5th ed., McGraw-Hill Book Company, Inc., New York, 1975.
51. Orr, Richard, oral presentation at Advisory Committee on Reactor Safety meeting, Washington, D.C., Sept. 2, 1980.
52. Zudans, Z., oral presentation at Advisory Committee on Reactor Safety meeting, Washington, D.C., Sept. 2, 1980, and letter to Dr. R. Savio, U.S. Nuclear Regulatory Commission, Aug. 29, 1980.
53. Augusti, G. and d'Agostino, S., "Experiments on the Plastic Behavior of Short Steel Cylindrical Shells Subject to Internal Pressure," First International Conference on Pressure Vessel Technology, ASME, 1970, pp. 363-375.
54. Ellyin, F., "Experimental Investigation of Limit Loads of Nozzles in Cylindrical Vessel," WRC Bulletin 219, Sept. 1976.

IX. APPENDIX

The limit pressure, safety index and failure probability ($p=28$ psi) from the approximate analysis of each failure mode are listed in this Appendix. The results represent the application of second moment reliability theory in conjunction with the minimization principle of Eq. 2-15 and the statistics of Table 3-1 and 3-2. A computer library subroutine was used to perform the minimization. The results of the approximate axisymmetric shell analysis (Sec. 5.1.3) for Sequoyah and McGuire are presented in Tables 9-1 and 9-2 respectively. The approximate anchor bolt analysis results (Sec. 5.3) are listed in Tables 9-5 and 9-6. All the results are summarized in Sec. 5. Run times and costs are quite small. For example, the results in Table 9-3 (193 failure modes) were obtained for a cost of \$6.97 on an Advanced System 6 computer.

10.0 TABLES

TABLE 3-1. Mean and Standard Deviation of Material Properties

Property	Mean	Standard Deviation
Modulus of elasticity (normal)	29,000 ksi	1740 ksi
Poisson's Ratio (normal)	0.3	0.009
Yield Stress (lognormal)-Sequoyah	47.2 ksi	2.50 ksi
Yield Stress (lognormal)-McGuire	46.9 ksi	2.50 ksi
Ultimate (lognormal)-Sequoyah	66.2 ksi	1.80 ksi
Ultimate (lognormal)-McGuire	67.0 ksi	1.80 ksi
Fracture Stress (lognormal)	197 ksi	102 ksi
Bolt Yield Stress (lognormal)	105 ksi	2.50 ksi

TABLE 3-2. Mean and Standard Deviation of Geometric Properties (Normally Distributed)

Property	Nominal (in)	Tolerance (in)	Mean (in)	Standard Deviation (in)
Thickness	1 1/4"	-0.010,+0.063	1.277	0.012
	1 3/16	-0.010,+0.059	1.212	0.012
	1 1/16	-0.010,+0.053	1.084	0.011
	1	-0.010,+0.050	1.020	0.010
	3/4	-0.010,+0.045	0.768	0.0092
	11/16	-0.010,+0.041	0.703	0.0095
	5/8	-0.010,+0.038	0.639	0.0080
	1/2	-0.010,+0.035	0.513	0.0075
	7/16	-0.010,+0.035	0.450	0.0075
Length & Width	ℓ,b	+ 1/4"	ℓb	0.083
Stiffener Spacing	s	+ 0.005 s	s	0.00167s
Radius (Sequoyah)	690	+ 3.45"	690	1.15
	(McGuire) 690	+ 1.5"	690	0.50
Anchor Bolt Diameter (upset)				
(Sequoyah)	2.58	+ .01	2.58	.0033
(McGuire)	3.75	+ .015	3.75	.005

TABLE 5-1. Reliability Results with Approximate Stiffened Shell Analysis

	Sequoyah	McGuire
Minimum Mean Limit Pressure	59.1 psi	77.5 psi
Safety Index (p = 28 psi)		
Upper Bound	4.5	6.1
Lower Bound	4.4	5.7
Failure Probability (p = 28 psi)		
Upper Bound	5.0 (10 ⁻⁶)	5.6 (10 ⁻⁹)
Lower Bound	3.9 (10 ⁻⁶)	5.4 (10 ⁻¹⁰)

TABLE 5-2. Reliability Results with Approximate Stiffened Shell Analysis-Sensitivity Study

	Sequoyah	McGuire
Minimum Mean Limit Pressure	59.1 psi	77.5 psi
Limit Pressure Standard Deviation		
Upper Bound	10.0 psi	13.8 psi
Lower Bound	9.8 psi	12.9 psi
Safety Index (p = 28 psi)		
Upper Bound	4.5	6.1
Lower Bound	4.4	5.7
Failure Probability (p = 28 psi)		
Upper Bound	4.7 (10 ⁻⁶)	5.2 (10 ⁻⁹)
Lower Bound	3.7 (10 ⁻⁶)	5.1 (10 ⁻¹⁰)

TABLE 5-3. Reliability Results for Approximate Penetration Analysis

	Sequoyah	McGuire
Minimum Mean Limit Pressure	67.2 psi	78.5 psi
Safety Index (p = 28 psi)		
Upper Bound	5.1	6.1
Lower Bound	4.9	5.2
Failure Probability (p = 28 psi)		
Upper Bound	6.1 (10^{-7})	6.9 (10^{-8})
Lower Bound	1.4 (10^{-7})	7.3 (10^{-10})

TABLE 5-4. Reliability Results for Approximate Penetration Analysis--
Sensitivity Study (Eq. 5-9)

	Sequoyah	McGuire
Minimum Mean Limit Pressure	67.2 psi	78.5 psi
Limit Pressure Standard Deviation		
Upper Bound	12.0 psi	15.3 psi
Lower Bound	11.4 psi	13.4 psi
Safety Index (p = 28 psi)		
Upper Bound	5.1	6.1
Lower Bound	4.9	5.3
Failure Probability (p = 28 psi)		
Upper Bound	5.8 (10^{-7})	6.6 (10^{-8})
Lower Bound	1.3 (10^{-7})	7.0 (10^{-10})

TABLE 5-5. Reliability Results for Anchor Bolts

	Sequoyah	McGuire
Minimum Mean Limit Pressure	66 psi	141 psi
Safety Index (p = 28 psi)	5.4	10.1
Failure Probability (p = 28 psi)	4.0 (10 ⁻⁸)	23 (10 ⁻²⁴)

TABLE 5-6. Reliability Results for Anchor Bolts--Sensitivity Study (Eq. 5-9)

	Sequoyah	McGuire
Minimum Mean Limit Pressure	66 psi	141 psi
Limit Pressure Standard Deviation	10.5 psi	22.5 psi
Safety Index (p = 28 psi)	5.4	10.1
Failure Probability (p = 28 psi)	4 (10 ⁻⁸)	2.3 (10 ⁻²⁴)

TABLE 5-7. Reliability Results for Approximate Structural Analysis

	Sequoyah	McGuire
Minimum Mean Limit Pressure	59.1 psi	77.5 psi
Limit Pressure Standard Deviation		
Upper Bound	10.0 psi	15.0 psi
Lower Bound	9.8 psi	13.0 psi
Safety Index (p = 28 psi)		
Upper Bound	4.5	6.1
Lower Bound	4.4	5.3
Failure Probability (p = 28 psi)		
Upper Bound	5.5 (10 ⁻⁶)	7.1 (10 ⁻⁸)
Lower Bound	3.7 (10 ⁻⁶)	7.0 (10 ⁻¹⁰)

TABLE 6-1. Plastic Pressure for Cylinder in Fig. 6-2 With Different ANSYS Options

STIF NO.	42	42	82	82	82
Option	S.S ^a	L.D ^b	S.S ^a	S.S ^a	S.S ^a
Plastic Convergence Ratio	0.03	0.03	0.03	0.05	0-1
P_{c_t} (psi)	71	71	71	73	79
% Difference	---	---	---	3	11
cpu (sec)	1327	2338	1170	765	415

a) S.S = Stress Stiffening Option

b) L.D = Large Displacement Option

TABLE 6-2. Plastic Pressure Results

	Sequoyah	McGuire
Minimum Mean	60 psi	84 psi
Standard Deviation	8 psi	12 psi

TABLE 9-1 SEQUOYAH CONTAINMENT
VESSEL
SHELL LIMIT PRESSURE

RING ELEV.	MEAN LIMIT PRESSURE	SAFETY INDEX	PROBABILITY OF FAILURE
680.80	122.67	8.85	0.4423E-18
691.20	113.25	8.37	0.2782E-16
701.60	107.20	8.04	0.4352E-15
713.50	99.38	7.59	0.1592E-13
721.60	95.46	7.35	0.9908E-13
730.30	75.41	5.93	0.1472E-08
740.60	69.61	5.45	0.2449E-07
750.10	65.13	5.06	0.2135E-06
759.60	65.20	5.06	0.2062E-06
769.10	65.79	5.12	0.1551E-06
778.60	63.60	4.91	0.4472E-06
788.10	59.08	4.47	0.3889E-05
791.40	83.15	6.52	0.3494E-10
796.00	83.86	6.56	0.2607E-10
799.80	85.02	6.64	0.1575E-10
803.80	83.72	6.55	0.2884E-10
809.50	81.96	6.42	0.6697E-10
815.40	81.69	6.40	0.7597E-10
821.40	70.18	5.49	0.1978E-07

SUMMARY
MINIMUM FAILURE LIMIT PRESSURE= 59.077

SAFETY
4.42 < INDEX < 4.47
(BETA)

PROBABILITY
0.3889E-05 < OF < 0.4957E-05
FAILURE

TABLE 9-2 MCGUIRE CONTAINMENT
VESSEL
SHELL LIMIT PRESSURE

RING ELEV.	MEAN LIMIT PRESSURE	SAFETY INDEX	PROBABILITY OF FAILURE
727.83	82.39	6.46	0.5151E-10
736.42	77.94	6.13	0.4427E-09
746.42	77.52	6.10	0.5418E-09
756.92	77.52	6.10	0.5418E-09
766.42	77.52	6.10	0.5418E-09
776.42	77.52	6.10	0.5418E-09
786.42	77.52	6.10	0.5418E-09
796.42	77.52	6.10	0.5418E-09
806.42	77.52	6.10	0.5418E-09
816.42	77.52	6.10	0.5418E-09
826.42	78.08	6.14	0.4129E-09
835.42	78.68	6.19	0.3091E-09
845.00	95.57	7.34	0.1047E-12

SUMMARY
MINIMUM FAILURE LIMIT PRESSURE= 77.520

SAFETY
5.71 < INDEX < 6.10
(BETA)

PROBABILITY
0.5418E-09 < OF FAILURE < 0.5551E-08

TABLE 9-3 SEQUOYAH CONTAINMENT
VESSEL
PENETRATION LIMIT PRESSURE

ELEV.	AZIM.	MEAN LIMIT PRESSURE	SAFETY INDEX	PROBABILITY OF FAILURE
699.71	0 0 0	96.93	7.29	0.1539E-12
822.75	0 0 0	86.44	5.56	0.1343E-07
714.00	4 18 46	81.28	6.26	0.1979E-09
697.00	7 0 0	105.99	7.82	0.2728E-14
708.00	7 38 44	93.46	7.08	0.7380E-12
697.00	8 30 0	105.99	7.82	0.2728E-14
711.42	9 30 0	101.29	7.55	0.2184E-13
716.50	9 30 0	101.29	7.55	0.2184E-13
711.50	17 0 0	111.34	8.11	0.2564E-15
715.50	17 0 0	124.04	8.75	0.1108E-17
715.50	21 0 0	111.84	8.13	0.2069E-15
711.50	21 0 0	111.84	8.13	0.2069E-15
711.50	25 0 0	111.84	8.13	0.2069E-15
715.50	25 0 0	111.84	8.13	0.2069E-15
711.50	29 0 0	111.84	8.13	0.2069E-15
715.50	29 0 0	111.84	8.13	0.2069E-15
712.00	38 30 0	96.93	7.29	0.1539E-12
710.75	56 30 0	124.04	8.75	0.1108E-17
705.50	57 0 0	103.18	7.66	0.9436E-14
696.30	62 0 0	146.89	9.73	0.1100E-21
714.00	65 0 0	105.36	7.78	0.3637E-14
715.00	65 0 0	105.36	7.78	0.3637E-14
697.00	78 30 0	111.84	8.13	0.2069E-15
717.00	90 0 0	104.03	7.71	0.6508E-14
715.50	93 0 0	111.84	8.13	0.2069E-15
715.50	97 0 0	111.84	8.13	0.2069E-15
715.50	101 0 0	111.84	8.13	0.2069E-15
715.00	104 0 0	105.52	7.79	0.3374E-14
714.00	104 0 0	105.52	7.79	0.3374E-14
715.50	114 0 0	111.84	8.13	0.2069E-15
716.67	116 0 0	103.18	7.66	0.9436E-14
711.50	116 30 0	111.84	8.13	0.2069E-15
715.50	118 30 0	111.84	8.13	0.2069E-15
822.75	120 0 0	86.44	5.56	0.1343E-07
712.50	120 30 0	111.34	8.11	0.2564E-15
711.50	151 0 0	111.84	8.13	0.2069E-15
715.50	151 0 0	111.84	8.13	0.2069E-15
711.50	155 0 0	111.84	8.13	0.2069E-15
715.50	155 0 0	111.84	8.13	0.2069E-15

TABLE 9-3 (CONTINUED)

711.50	159	0	0	111.84	8.13	0.2069E-15
715.50	159	0	0	111.84	8.13	0.2069E-15
715.50	163	0	0	124.04	8.75	0.1108E-17
711.50	163	0	0	111.84	8.13	0.2069E-15
697.00	171	30	0	105.99	7.82	0.2728E-14
708.00	172	21	16	93.46	7.08	0.7380E-12
697.00	173	0	0	105.99	7.82	0.2728E-14
714.00	175	41	14	81.28	6.26	0.1979E-09
714.00	184	18	46	81.28	6.26	0.1979E-09
697.00	187	0	0	105.99	7.82	0.2728E-14
708.00	187	38	44	93.46	7.08	0.7380E-12
697.00	189	30	0	105.99	7.82	0.2728E-14
715.50	197	0	0	124.04	8.75	0.1108E-17
711.50	197	0	0	111.84	8.13	0.2069E-15
711.50	201	0	0	111.84	8.13	0.2069E-15
715.50	201	0	0	111.84	8.13	0.2069E-15
711.50	205	0	0	111.84	8.13	0.2069E-15
715.50	205	0	0	111.84	8.13	0.2069E-15
711.50	209	0	0	111.84	8.13	0.2069E-15
715.50	209	0	0	111.84	8.13	0.2069E-15
688.50	209	0	0	105.99	7.82	0.2728E-14
685.50	209	0	0	104.03	7.71	0.6508E-14
688.50	218	0	0	96.93	7.29	0.1539E-12
688.50	222	0	0	96.93	7.29	0.1539E-12
717.00	236	0	0	105.02	7.76	0.4210E-14
705.00	236	0	0	105.02	7.76	0.4210E-14
704.00	236	0	0	105.36	7.78	0.3637E-14
697.00	236	30	0	111.84	8.13	0.2069E-15
714.00	236	30	0	96.93	7.29	0.1539E-12
717.00	237	0	0	105.02	7.76	0.4210E-14
705.00	237	0	0	105.62	7.79	0.3238E-14
716.50	240	0	0	124.04	8.75	0.1108E-17
710.00	240	0	0	111.84	8.13	0.2069E-15
697.00	243	30	0	124.04	8.75	0.1108E-17
716.00	243	30	0	124.04	8.75	0.1108E-17
748.50	248	30	0	111.84	8.13	0.2069E-15
752.50	248	30	0	111.84	8.13	0.2069E-15
822.75	245	0	0	86.44	5.56	0.1343E-07
756.50	248	30	0	124.04	8.75	0.1108E-17
773.50	248	30	0	111.84	8.13	0.2069E-15
767.00	248	30	0	124.04	8.75	0.1108E-17
707.50	249	0	0	111.84	8.13	0.2069E-15
728.33	252	30	0	96.93	7.29	0.1539E-12
737.30	255	0	0	146.89	9.73	0.1100E-21
775.92	261	0	0	67.21	5.14	0.1365E-06
748.50	262	0	0	103.18	7.66	0.9436E-14
688.23	261	51	10	67.21	5.14	0.1365E-06

TABLE 9-3 (CONTINUED)

748.50	265	0	0	103.18	7.66	0.9436E-14
767.00	266	0	0	67.21	5.14	0.1365E-06
748.50	268	0	0	103.18	7.66	0.9436E-14
710.00	277	30	0	104.03	7.71	0.6510E-14
706.00	277	30	0	93.46	7.08	0.7380E-12
697.50	277	30	0	102.27	7.61	0.1412E-13
700.00	278	0	0	100.26	7.49	0.3467E-13
709.00	278	30	0	104.03	7.71	0.6510E-14
719.50	280	0	0	96.93	7.29	0.1539E-12
697.50	280	0	0	104.00	7.70	0.6566E-14
706.50	280	30	0	105.69	7.80	0.3133E-14
700.00	281	30	0	101.29	7.55	0.2184E-13
709.00	281	30	0	94.63	7.15	0.4360E-12
704.50	281	30	0	99.18	7.43	0.5616E-13
706.00	283	0	0	105.02	7.76	0.4210E-14
697.50	282	30	0	101.29	7.55	0.2184E-13
695.00	282	30	0	103.84	7.70	0.7064E-14
741.63	285	0	0	274.55	13.40	0.3066E-40
705.50	286	30	0	104.36	7.72	0.5634E-14
697.00	286	30	0	102.44	7.61	0.1321E-13
700.50	287	0	0	105.62	7.79	0.3238E-14
695.00	287	0	0	101.29	7.55	0.2184E-13
698.00	287	30	0	105.02	7.76	0.4210E-14
709.00	287	30	0	96.93	7.29	0.1539E-12
700.50	288	0	0	105.02	7.76	0.4210E-14
699.50	288	0	0	105.34	7.78	0.3660E-14
697.00	288	30	0	104.36	7.72	0.5634E-14
775.92	289	0	0	96.93	7.29	0.1539E-12
785.00	289	0	0	103.55	7.68	0.8062E-14
705.50	298	30	0	98.07	7.36	0.9242E-13
700.50	289	0	0	105.02	7.76	0.4210E-14
712.50	290	0	0	105.02	7.76	0.4210E-14
786.00	290	0	0	102.63	7.63	0.1212E-13
718.00	290	0	0	105.02	7.76	0.4210E-14
718.00	291	0	0	105.02	7.76	0.4210E-14
700.50	291	0	0	105.02	7.76	0.4210E-14
709.00	291	30	0	96.93	7.29	0.1539E-12
697.50	291	30	0	101.29	7.55	0.2184E-13
718.00	292	0	0	104.36	7.72	0.5634E-14
700.50	292	0	0	103.84	7.69	0.7110E-14
704.00	292	0	0	104.36	7.72	0.5634E-14
705.50	292	0	0	104.36	7.72	0.5634E-14
700.50	293	0	0	103.84	7.69	0.7110E-14
726.25	293	0	0	96.93	7.29	0.1539E-12
718.00	293	0	0	104.36	7.72	0.5634E-14
785.50	293	0	0	97.06	7.30	0.1462E-12
705.50	293	30	0	104.36	7.72	0.5634E-14

TABLE 9-3 (CONTINUED)

704.00	293	30	0	104.36	7.72	0.5634E-14
700.50	294	0	0	103.84	7.69	0.7110E-14
718.00	294	0	0	104.36	7.72	0.5634E-14
710.00	294	0	0	104.03	7.71	0.6508E-14
696.50	294	0	0	104.36	7.72	0.5634E-14
707.25	294	45	0	99.18	7.43	0.5616E-13
785.50	296	30	0	97.06	7.30	0.1462E-12
705.50	298	30	0	98.07	7.36	0.9242E-13
711.50	299	30	0	106.20	7.83	0.2496E-14
697.50	299	30	0	104.03	7.71	0.6508E-14
707.50	299	30	0	104.36	7.72	0.5634E-14
699.50	299	30	0	104.36	7.72	0.5634E-14
727.25	299	30	0	104.36	7.72	0.5634E-14
725.25	299	30	0	104.36	7.72	0.5634E-14
752.00	300	0	0	99.18	7.43	0.5616E-13
688.00	300	0	0	105.54	7.79	0.3356E-14
748.50	300	0	0	99.18	7.43	0.5616E-13
737.00	300	0	0	104.36	7.72	0.5634E-14
735.00	300	0	0	104.36	7.72	0.5634E-14
711.50	300	30	0	106.20	7.83	0.2496E-14
694.96	300	30	0	93.46	7.08	0.7380E-12
714.00	301	0	0	96.93	7.29	0.1539E-12
704.50	301	C	0	99.18	7.43	0.5616E-13
710.00	301	0	0	100.26	7.49	0.3467E-13
700.50	301	0	0	104.36	7.72	0.5634E-14
698.50	301	0	0	104.36	7.72	0.5634E-14
687.00	301	0	0	105.99	7.82	0.2728E-14
770.50	301	15	0	105.41	7.78	0.3543E-14
771.50	301	15	0	105.41	7.78	0.3543E-14
772.50	301	15	0	105.41	7.78	0.3543E-14
773.50	301	15	0	105.41	7.78	0.3543E-14
774.50	301	15	0	105.41	7.78	0.3543E-14
775.50	301	15	0	105.41	7.78	0.3543E-14
776.50	301	15	0	105.41	7.78	0.3543E-14
777.50	301	15	0	105.41	7.78	0.3543E-14
725.25	301	30	0	104.36	7.72	0.5634E-14
727.25	301	30	0	104.36	7.72	0.5634E-14
697.50	301	30	0	104.36	7.72	0.5634E-14
832.33	301	30	0	82.09	5.31	0.5568E-07
830.33	304	0	0	82.09	5.31	0.5568E-07
832.33	306	0	0	84.69	5.46	0.2372E-07
698.50	306	0	0	104.36	7.72	0.5634E-14
700.00	306	0	0	104.36	7.72	0.5634E-14
696.00	306	30	0	124.04	8.75	0.1108E-17
700.00	307	30	0	104.36	7.72	0.5634E-14
698.50	307	30	0	104.36	7.72	0.5634E-14
830.33	308	0	0	84.69	5.46	0.2372E-07

TABLE 9-3 (CONTINUED)

711.50	331	0	0	111.84	8.13	0.2069E-15
711.50	335	0	0	111.84	8.13	0.2069E-15
711.50	339	0	0	111.84	8.13	0.2069E-15
711.50	343	0	0	111.84	8.13	0.2069E-15
715.50	343	0	0	124.04	8.75	0.1108E-17
711.50	346	30	0	104.36	7.72	0.5634E-14
713.50	346	31	0	104.36	7.72	0.5634E-14
716.50	350	30	0	101.29	7.55	0.2184E-13
711.42	350	30	0	101.29	7.55	0.2184E-13
697.00	351	30	0	105.99	7.82	0.2728E-14
708.00	352	21	16	93.46	7.08	0.7380E-12
697.00	353	0	0	105.99	7.82	0.2728E-14
714.00	355	41	15	81.28	6.26	0.1979E-09

SUMMARY

MINIMUM FAILURE LIMIT PRESSURE= 67.208

SAFETY

4.85 < INDEX < 5.14
(BETA)

PROBABILITY

0.1365E-06 < OF < 0.6095E-06
FAILURE

TABLE 9-4 MCGUIRE CONTAINMENT
VESSEL
PENETRATION LIMIT PRESSURE

ELEV.	AZIM.	MEAN LIMIT PRESSURE	SAFETY INDEX	PROBABILITY OF FAILURE
715.75	5 0 0	149.31	9.82	0.4720E-22
750.50	5 58 43	113.15	8.20	0.1218E-15
753.00	14 10 0	117.84	8.43	0.1658E-16
764.00	16 0 0	118.27	8.46	0.1378E-16
754.75	17 30 0	78.46	6.05	0.7308E-09
758.75	20 0 0	78.46	6.05	0.7308E-09
758.75	22 30 0	78.46	6.05	0.7308E-09
754.75	22 30 0	78.46	6.05	0.7308E-09
758.75	25 0 0	78.46	6.05	0.7308E-09
754.75	25 0 0	78.46	6.05	0.7308E-09
754.75	27 30 0	78.46	6.05	0.7308E-09
758.75	27 30 0	78.46	6.05	0.7308E-09
758.75	30 0 0	78.46	6.05	0.7308E-09
754.75	30 0 0	78.46	6.05	0.7308E-09
754.75	36 0 0	78.46	6.05	0.7308E-09
758.75	36 0 0	78.46	6.05	0.7308E-09
762.75	36 0 0	78.46	6.05	0.7308E-09
752.17	57 30 0	78.46	6.05	0.7308E-09
755.65	57 30 0	78.46	6.05	0.7308E-09
670.58	57 30 0	78.46	6.05	0.7308E-09
755.65	60 0 0	78.46	6.05	0.7308E-09
741.60	62 0 0	137.59	9.34	0.4602E-20
755.65	62 30 0	78.46	6.05	0.7308E-09
760.75	62 30 0	78.46	6.05	0.7308E-09
755.65	65 0 0	78.46	6.05	0.7308E-09
760.75	65 0 0	78.46	6.05	0.7308E-09
755.65	68 0 0	78.46	6.05	0.7308E-09
760.75	68 0 0	78.46	6.05	0.7308E-09
752.17	68 0 0	78.46	6.05	0.7308E-09
752.17	74 0 0	78.46	6.05	0.7308E-09
755.46	74 0 0	78.46	6.05	0.7308E-09
761.58	75 59 48	78.46	6.05	0.7308E-09
755.46	77 30 0	78.46	6.05	0.7308E-09
752.16	77 30 0	78.46	6.05	0.7308E-09
755.46	80 0 0	78.46	6.05	0.7308E-09
752.16	80 0 0	78.46	6.05	0.7308E-09
755.46	82 30 0	78.46	6.05	0.7308E-09
752.16	82 30 0	78.46	6.05	0.7308E-09
755.46	85 0 0	78.46	6.05	0.7308E-09

TABLE 9-4 (CONTINUED)

752.16	85	0	0	78.46	6.05	0.7308E-09
761.50	90	59	48	78.46	6.05	0.7308E-09
748.67	91	30	0	78.46	6.05	0.7308E-09
755.65	91	30	0	78.46	6.05	0.7308E-09
748.67	94	0	0	78.46	6.05	0.7308E-09
755.65	94	0	0	78.46	6.05	0.7308E-09
748.67	96	30	0	78.46	6.05	0.7308E-09
755.65	96	30	0	78.46	6.05	0.7308E-09
748.67	99	0	0	78.46	6.05	0.7308E-09
755.65	102	0	0	78.46	6.05	0.7308E-09
755.65	99	0	0	78.46	6.05	0.7308E-09
748.67	102	0	0	78.46	6.05	0.7308E-09
761.58	102	0	0	78.46	6.05	0.7308E-09
758.67	110	0	0	78.46	6.05	0.7308E-09
762.25	110	0	0	78.46	6.05	0.7308E-09
730.25	111	0	0	149.31	9.82	0.4720E-22
734.00	111	0	0	149.31	9.82	0.4720E-22
758.67	112	30	0	78.46	6.05	0.7308E-09
762.25	112	30	0	78.46	6.05	0.7308E-09
734.00	115	0	0	149.31	9.82	0.4720E-22
758.67	115	0	0	78.46	6.05	0.7308E-09
762.25	115	0	0	78.46	6.05	0.7308E-09
768.67	117	30	0	78.46	6.05	0.7308E-09
762.25	117	30	0	78.46	6.05	0.7308E-09
734.00	119	0	0	149.31	9.82	0.4720E-22
734.00	120	0	0	78.46	6.05	0.7308E-09
762.25	120	0	0	78.46	6.05	0.7308E-09
734.00	123	0	0	149.31	9.82	0.4720E-22
734.00	129	0	0	149.31	9.82	0.4720E-22
734.00	134	0	0	149.31	9.82	0.4720E-22
734.00	138	0	0	149.31	9.82	0.4720E-22
750.75	141	30	0	78.46	6.05	0.7308E-09
754.75	141	30	0	78.46	6.05	0.7308E-09
758.75	141	30	0	78.46	6.05	0.7308E-09
762.75	141	30	0	78.46	6.05	0.7308E-09
750.75	144	0	0	78.46	6.05	0.7308E-09
754.75	144	0	0	78.46	6.05	0.7308E-09
758.75	144	0	0	78.46	6.05	0.7308E-09
762.75	144	0	0	78.46	6.05	0.7308E-09
730.25	145	0	0	149.31	9.82	0.4720E-22
734.00	145	0	0	149.31	9.82	0.4720E-22
730.25	149	0	0	149.31	9.82	0.4720E-22
734.00	151	0	0	150.73	9.87	0.2777E-22
754.75	152	30	0	78.46	6.05	0.7308E-09
758.75	152	30	0	78.46	6.05	0.7308E-09
739.00	153	0	0	97.20	7.31	0.1383E-12
744.17	153	0	0	97.20	7.31	0.1383E-12

TABLE 9-4 (CONTINUED)

730.25	154	0	0	149.71	9.83	0.4044E-22
754.75	155	0	0	78.46	6.05	0.7308E-09
738.75	155	0	0	78.46	6.05	0.7308E-09
734.00	156	0	0	150.73	9.88	0.2635E-22
758.75	157	30	0	78.46	6.05	0.7262E-09
762.75	157	30	0	78.46	6.05	0.7308E-09
739.75	157	30	0	117.59	8.42	0.1822E-16
744.17	157	30	0	97.20	7.31	0.1383E-12
750.75	160	0	0	78.46	6.05	0.7308E-09
754.75	160	0	0	78.46	6.05	0.7308E-09
758.75	160	0	0	78.46	6.05	0.7309E-09
762.75	160	0	0	78.46	6.05	0.7308E-09
730.25	162	0	0	149.71	9.83	0.4044E-22
734.00	162	0	0	150.73	9.88	0.2635E-22
758.75	162	30	0	78.46	6.05	0.7308E-09
761.50	164	0	0	118.27	8.46	0.1378E-16
730.25	166	0	0	149.31	9.82	0.4720E-22
734.00	166	0	0	149.31	9.82	0.4720E-22
739.00	166	0	0	97.20	7.31	0.1383E-12
744.17	166	0	0	117.59	8.42	0.1822E-16
753.00	166	0	0	117.84	8.43	0.1658E-16
744.17	171	30	0	97.20	7.31	0.1383E-12
730.25	172	0	0	149.36	9.82	0.4624E-22
734.00	172	0	0	149.36	9.82	0.4624E-22
744.17	172	0	0	117.59	8.42	0.1822E-16
760.50	174	1	7	113.15	8.20	0.1218E-15
726.00	175	0	0	97.20	7.31	0.1383E-12
751.75	175	0	0	149.31	9.82	0.4720E-22
744.17	175	0	0	118.27	8.46	0.1378E-16
734.00	177	0	0	150.73	9.88	0.2635E-22
730.25	177	0	0	149.31	9.82	0.4720E-22
726.00	184	0	0	193.75	11.34	0.4339E-29
744.50	184	0	0	97.20	7.31	0.1383E-12
740.35	184	0	0	118.27	8.46	0.1378E-16
751.75	184	30	0	149.31	9.82	0.4720E-22
760.50	183	58	9	113.15	8.20	0.1218E-15
730.25	185	0	0	149.31	9.82	0.4720E-22
734.00	185	0	0	149.31	9.82	0.4720E-22
739.75	188	0	0	97.20	7.31	0.1383E-12
730.25	189	0	0	149.31	9.81	0.4978E-22
734.00	189	0	0	149.31	9.81	0.4978E-22
744.17	189	0	0	97.20	7.31	0.1383E-12
730.25	194	0	0	149.31	9.82	0.4720E-22
739.75	194	0	0	149.31	9.82	0.4720E-22
734.00	194	0	0	150.73	9.88	0.2635E-22
744.17	194	0	0	117.59	8.42	0.1822E-16
753.00	0	0	0	117.84	8.43	0.1658E-16

TABLE 9-4 (CONTINUED)

761.50	196	0	0	118.27	8.46	0.1378E-16
730.25	201	0	0	149.31	9.82	0.4720E-22
734.00	202	0	0	149.31	9.82	0.4720E-22
755.00	203	0	0	149.31	9.82	0.4720E-22
761.50	203	0	0	149.31	9.82	0.4720E-22
730.25	205	0	0	149.31	9.82	0.4720E-22
734.00	206	0	0	117.59	8.42	0.1822E-16
755.00	207	0	0	97.32	7.31	0.1314E-12
739.75	208	0	0	149.31	9.82	0.4720E-22
744.17	208	0	0	149.31	9.82	0.4720E-22
761.50	209	0	0	117.59	8.42	0.1822E-16
730.25	210	0	0	149.31	9.82	0.4720E-22
734.00	210	0	0	150.73	9.88	0.2635E-22
755.00	211	0	0	149.31	9.82	0.4725E-22
762.75	215	0	0	149.31	9.82	0.4720E-22
751.50	216	30	0	117.59	8.42	0.1822E-16
730.25	217	0	0	149.31	9.82	0.4720E-22
734.00	219	0	0	150.73	9.88	0.2635E-22
761.50	220	0	0	117.59	8.42	0.1822E-16
730.25	221	0	0	149.31	9.82	0.4720E-22
752.00	221	0	0	78.46	6.05	0.7308E-09
730.25	225	0	0	149.31	9.82	0.4720E-22
734.00	225	0	0	149.31	9.82	0.4720E-22
730.25	229	0	0	149.31	9.82	0.4720E-22
734.00	231	0	0	150.73	9.88	0.2635E-22
730.75	236	0	0	149.31	9.82	0.4720E-22
734.00	236	0	0	149.31	9.82	0.4720E-22
739.75	236	0	0	97.20	7.31	0.1383E-12
744.17	236	0	0	97.20	7.31	0.1383E-12
761.50	236	0	0	97.20	7.31	0.1383E-12
755.00	237	0	0	97.20	7.31	0.1383E-12
751.50	239	0	0	117.59	8.42	0.1822E-16
730.25	240	0	0	149.31	9.82	0.4720E-22
734.00	240	0	0	149.31	9.82	0.4720E-22
739.75	240	0	0	97.20	7.31	0.1383E-12
744.17	240	0	0	117.59	8.42	0.1822E-16
760.50	242	0	0	113.80	8.23	0.9629E-16
739.75	244	0	0	97.20	7.31	0.1383E-12
744.17	244	0	0	97.20	7.31	0.1383E-12
730.25	248	0	0	149.31	9.82	0.4720E-22
734.00	248	0	0	149.31	9.82	0.4720E-22
739.75	248	0	0	97.20	7.31	0.1384E-12
744.17	248	0	0	97.20	7.31	0.1384E-12
769.50	249	0	0	168.78	10.52	0.3502E-25
799.75	249	0	0	230.26	12.33	0.3260E-34
809.75	249	0	0	230.26	12.33	0.3260E-34
760.50	250	0	0	117.59	8.42	0.1822E-16

TABLE 9-4 (CONTINUED)

814.25	250	30	0	158.78	10.52	0.3502E-25
818.25	250	30	0	168.78	10.52	0.3502E-25
824.25	250	30	0	168.78	10.52	0.3502E-25
730.25	252	0	0	149.31	9.82	0.4720E-22
734.00	252	0	0	149.31	9.82	0.4720E-22
739.75	252	0	0	97.20	7.31	0.1383E-12
744.17	252	0	0	97.20	7.31	0.1383E-12
769.50	252	0	0	90.99	6.91	0.2347E-11
810.50	254	0	0	90.99	6.91	0.2347E-11
814.50	254	0	0	90.99	6.91	0.2347E-11
818.67	254	0	0	90.99	6.91	0.2347E-11
822.50	254	0	0	90.99	6.91	0.2347E-11
800.50	254	0	0	90.99	6.91	0.2347E-11
804.50	254	0	0	90.99	6.91	0.2347E-11
769.50	254	30	0	90.99	6.91	0.2347E-11
782.19	255	0	0	137.59	9.34	0.4602E-20
769.50	257	0	0	90.99	6.91	0.2347E-11
819.75	258	0	0	168.78	10.52	0.3502E-25
824.25	258	0	0	170.04	10.57	0.2055E-25
799.75	258	30	0	170.04	10.57	0.2055E-25
804.75	258	30	0	163.78	10.52	0.3502E-25
809.75	259	0	0	170.04	10.57	0.2055E-25
814.25	259	0	0	168.78	10.52	0.3502E-25
769.50	259	30	0	90.99	6.91	0.2347E-11
733.50	261	51	44	165.82	10.43	0.9304E-25
812.00	265	0	0	173.64	10.69	0.5563E-26
819.75	265	0	0	170.04	10.57	0.2055E-25
824.25	265	0	0	170.04	10.57	0.2055E-25
750.75	278	30	0	78.46	6.05	0.7308E-09
754.75	278	30	0	78.46	6.05	0.7308E-09
750.75	281	0	0	94.67	7.15	0.4281E-12
754.75	281	0	0	78.46	6.05	0.7308E-09
760.00	281	0	0	168.78	10.52	0.3502E-25
769.42	281	0	0	90.99	6.91	0.2347E-11
769.42	283	30	0	90.99	6.91	0.2347E-11
769.42	286	0	0	90.99	6.91	0.2347E-11
787.25	288	0	0	248.17	12.80	0.7907E-37
769.42	288	30	0	90.99	6.91	0.2347E-11
754.75	291	0	0	78.46	6.05	0.7308E-09
760.00	291	0	0	168.78	10.52	0.3502E-25
769.42	291	0	0	90.99	6.91	0.2347E-11
822.42	291	30	0	230.26	12.33	0.3260E-34
754.75	293	30	0	78.46	6.05	0.7308E-09
769.42	293	30	0	90.99	6.91	0.2347E-11
818.67	295	0	0	90.99	6.91	0.2347E-11
822.42	295	0	0	90.99	6.91	0.2347E-11
754.75	296	0	0	78.46	6.05	0.7308E-09

TABLE 9-4 (CONTINUED)

760.00	296	0	0	170.04	10.57	0.2055E-25
818.67	297	30	0	90.99	6.91	0.2347E-11
822.42	297	30	0	90.99	6.91	0.2347E-11
754.75	298	30	0	94.67	7.15	0.4410E-12
818.67	300	0	0	90.99	6.91	0.2498E-11
822.42	300	0	0	90.99	6.91	0.2498E-11
754.75	301	0	0	94.67	7.15	0.4281E-12
760.00	301	0	0	168.78	10.52	0.3502E-25
810.50	301	0	0	230.26	12.33	0.3260E-34
761.58	307	0	0	230.26	12.33	0.3260E-34
754.75	323	0	0	78.46	6.05	0.7308E-09
758.75	323	0	0	78.46	6.05	0.7308E-09
754.75	332	30	0	78.46	6.05	0.7308E-09
758.75	332	30	0	78.46	6.05	0.7308E-09
754.75	335	0	0	78.46	6.05	0.7308E-09
758.75	335	0	0	78.46	6.05	0.7308E-09
754.75	337	30	0	78.46	6.05	0.7308E-09
761.58	339	0	0	118.27	8.46	0.1378E-16
754.75	340	0	0	78.46	6.05	0.7308E-09
754.75	342	30	0	78.46	6.05	0.7308E-09
762.75	345	0	0	78.46	6.05	0.7308E-09
758.75	345	0	0	78.46	6.05	0.7308E-09
751.75	355	30	0	149.31	9.82	0.4720E-22
760.50	356	0	51	113.15	8.20	0.1218E-15
753.00	0	0	0	117.84	8.43	0.1658E-16
872.75	211	0	0	123.28	7.32	0.1270E-12
872.75	218	0	0	123.28	7.32	0.1270E-12
872.75	225	0	0	123.28	7.32	0.1270E-12
872.75	232	0	0	123.28	7.32	0.1270E-12
872.75	240	0	0	123.28	7.32	0.1270E-12
872.75	247	0	0	123.28	7.32	0.1270E-12

SUMMARY

MINIMUM FAILURE LIMIT PRESSURE= 78.459

SAFETY

5.27 < INDEX < 6.05

(BETA)

PROBABILITY

0.7309E-09 < OF < 0.6875E-07

FAILURE

TABLE 9-5 SEQUOYAH CONTAINMENT VESSEL
ANCHOR BOLTS LIMIT PRESSURE

ANCHOR BOLT LIMIT PRESSURE	=	66.061
SAFETY INDEX	=	5.369
PROBABILITY OF FAILURE	=	0.3960E-07

TABLE 9-6 MCGUIRE CONTAINMENT VESSEL
ANCHOR BOLTS LIMIT PRESSURE

ANCHOR BOLT LIMIT PRESSURE	=	141.112
SAFETY INDEX	=	10.116
PROBABILITY OF FAILURE	=	0.2343E-23

11.0 FIGURES

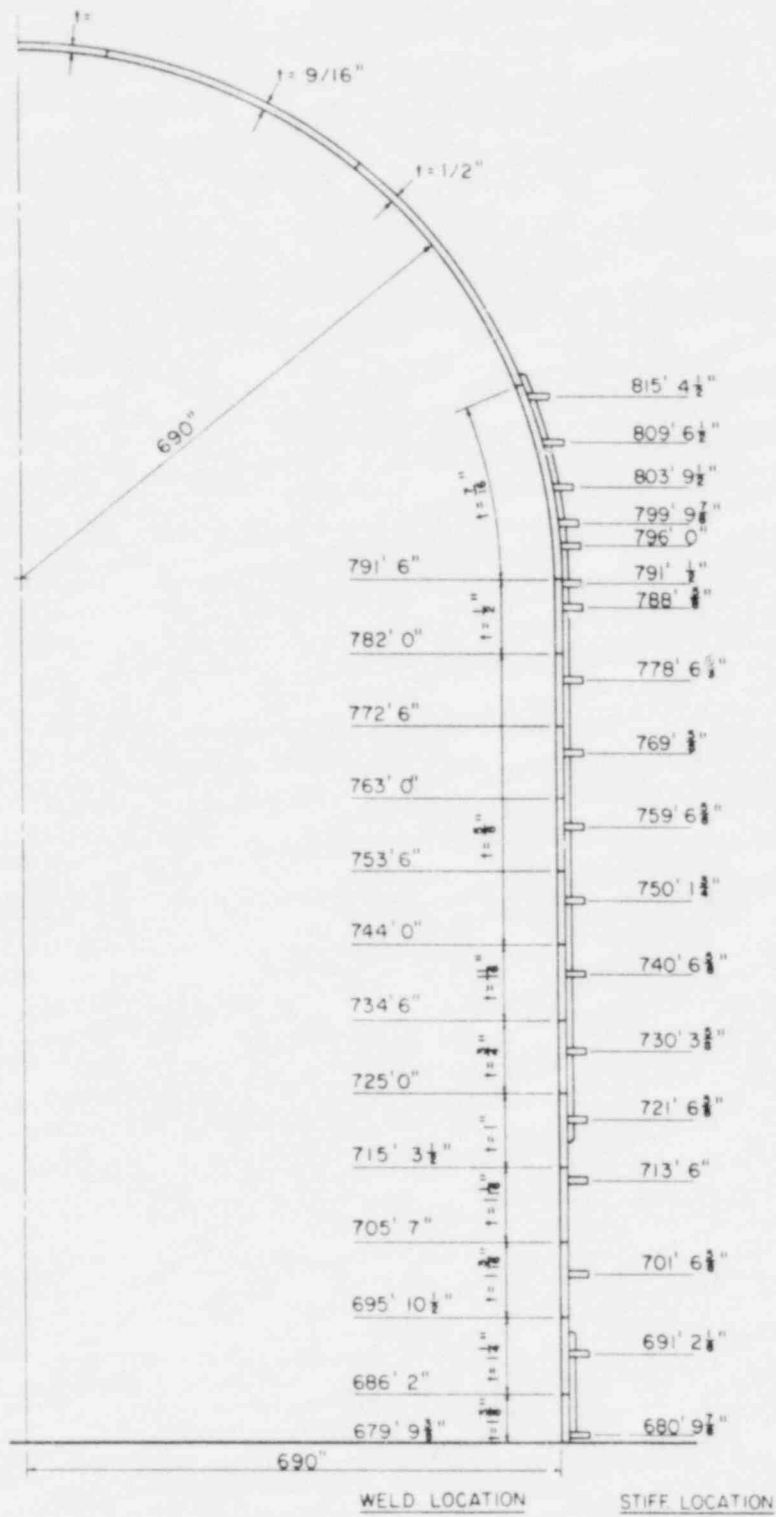


Figure 1-1. Sequoyah Containment Vessel Geometry

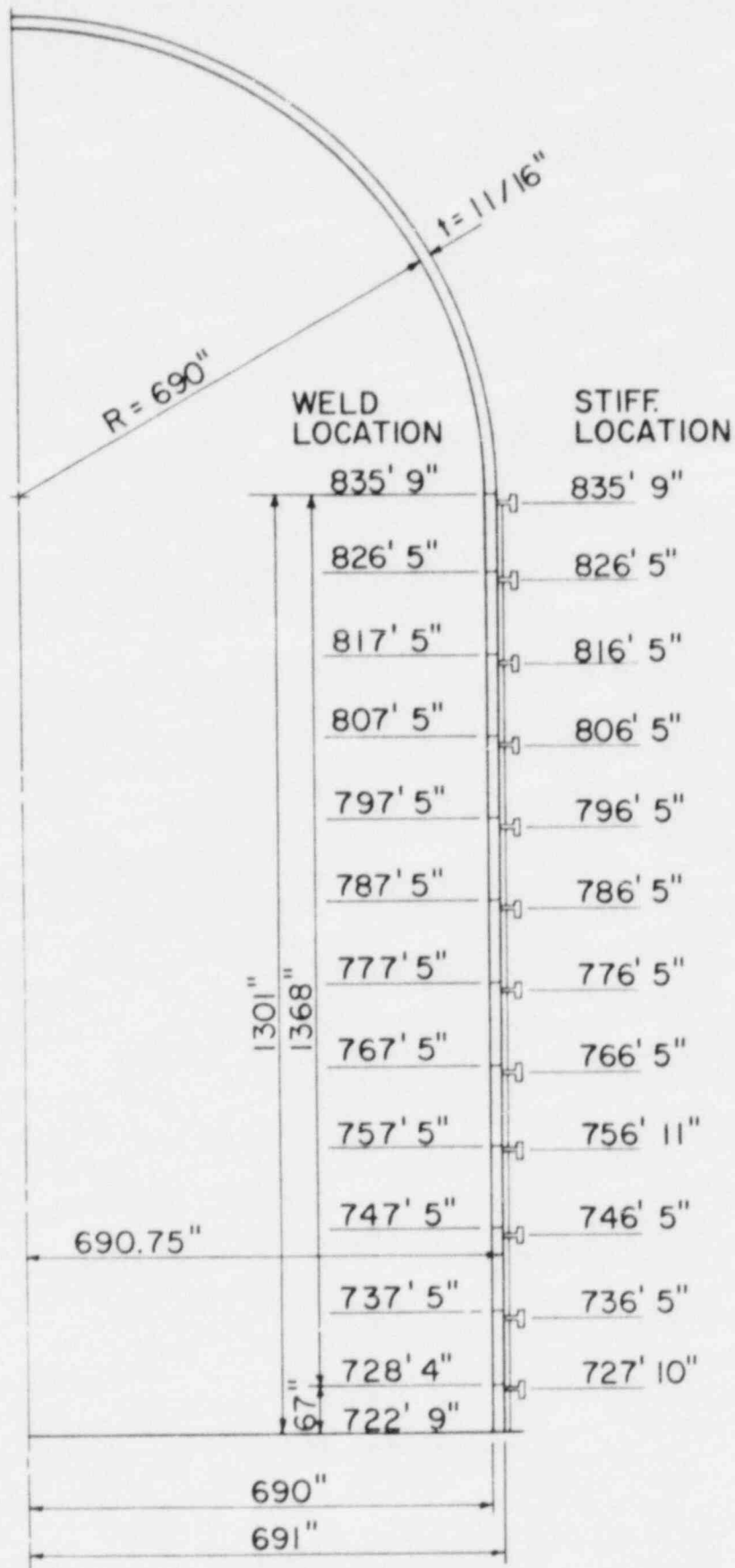
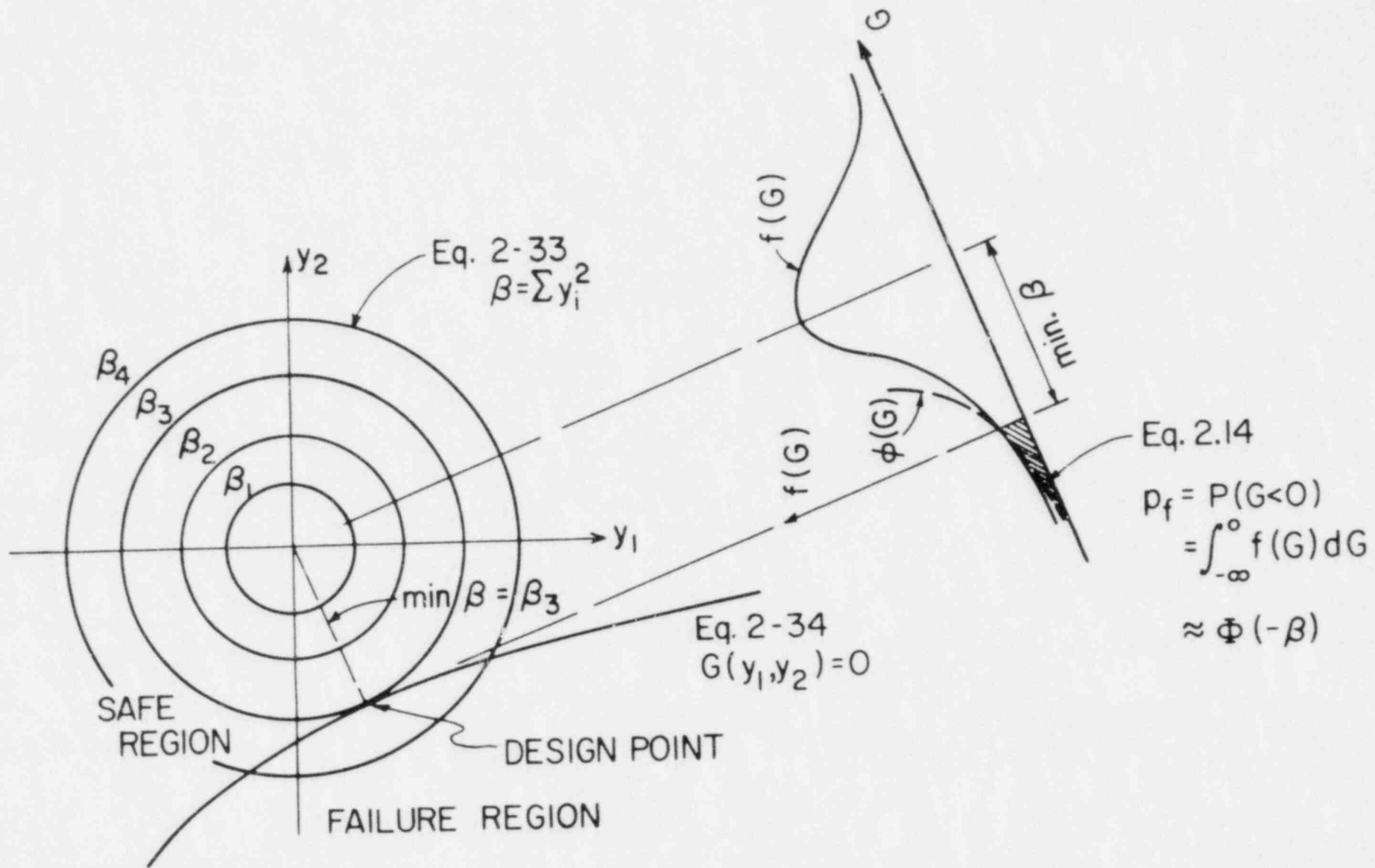


Figure 1-2. McGuire Containment Vessel Geometry



(a) Failure Function in Design Parameter Space

(b) Probability Density of Failure Function

Figure 2-1. Graphical Representation of Safety Index

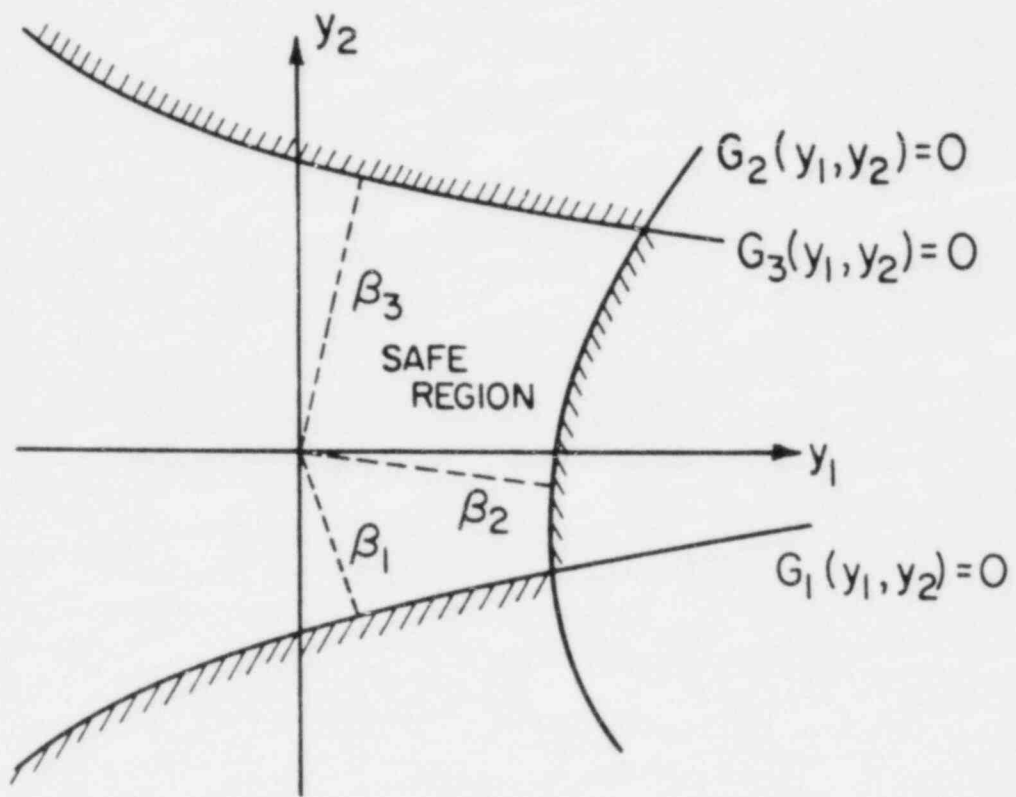


Figure 2-2. Safe Region for Multiple Failure Modes

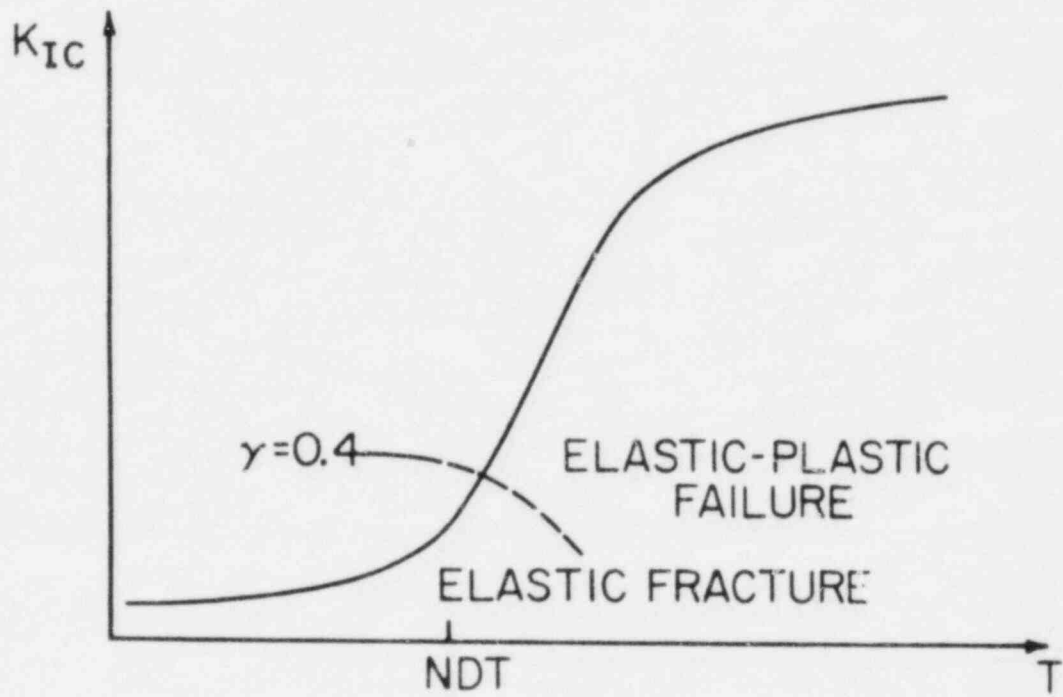


Figure 3-1. Effect of Temperature on Critical Stress Intensity Factor

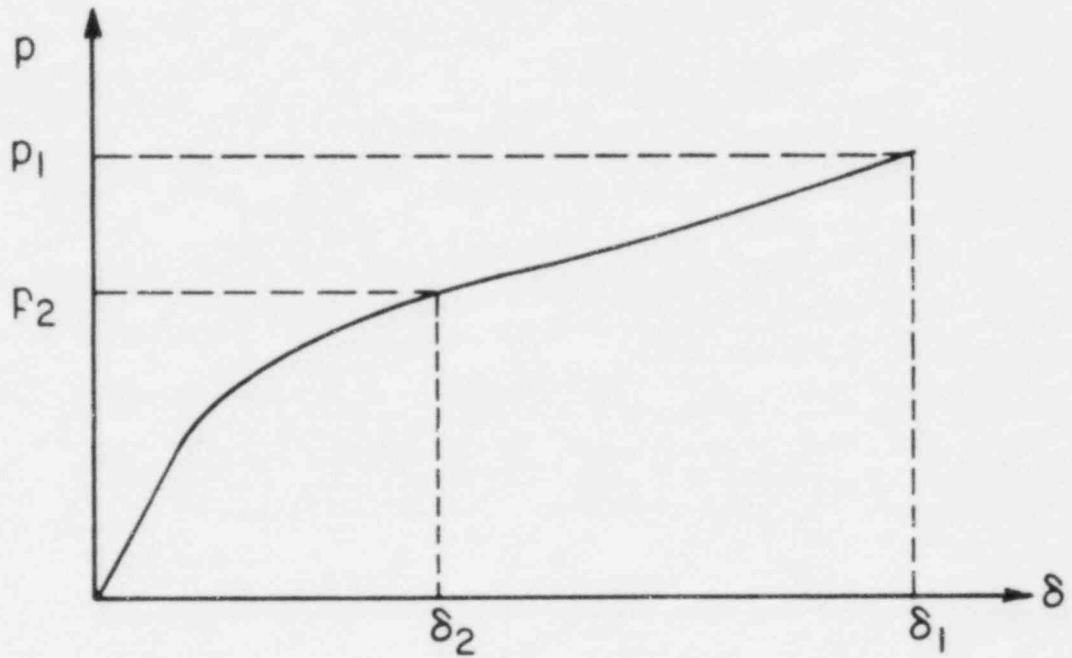


Figure 4-1. Pressure-Displacement Curve for Pressure Vessel

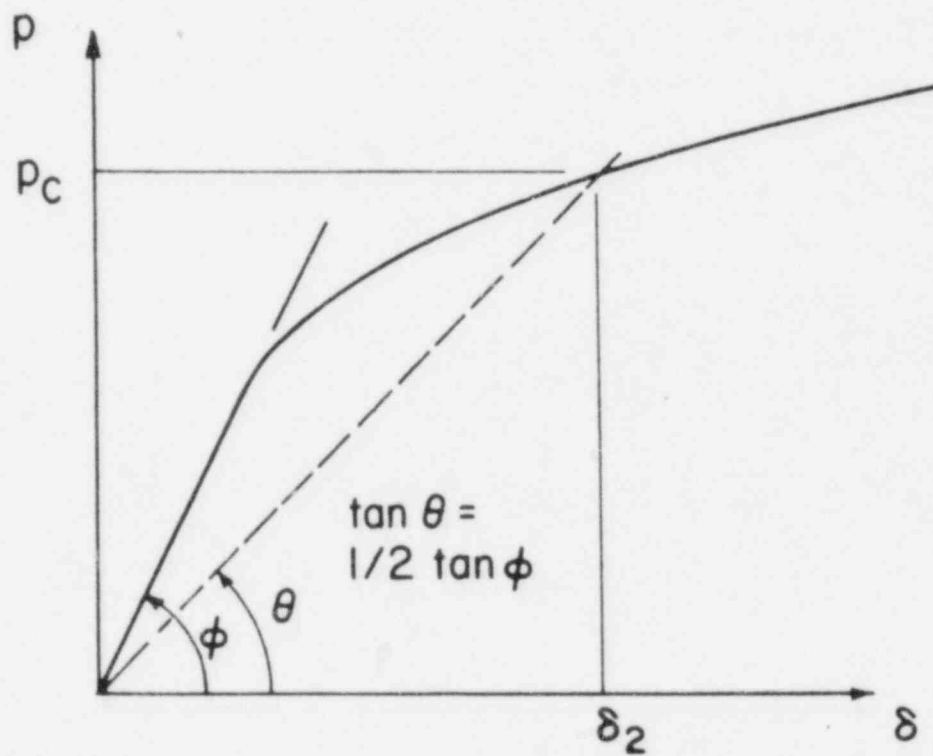
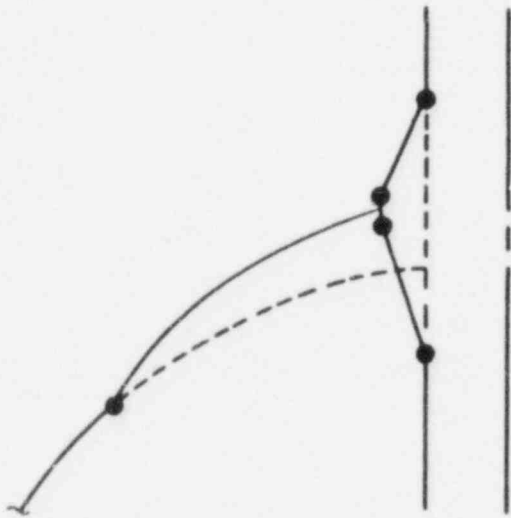
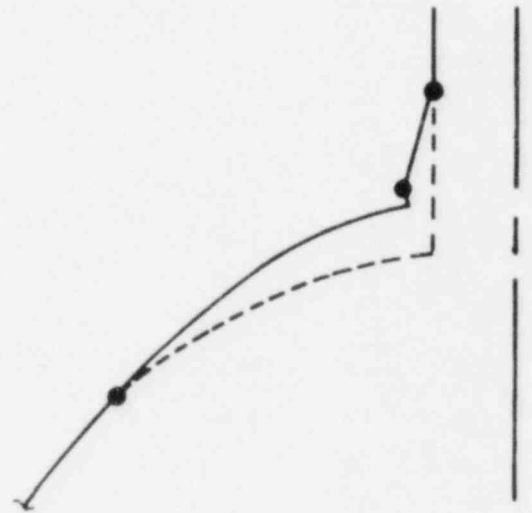


Figure 4-2. Definition of Half-Elastic Slope Plastic Pressure



(a) Protruding Penetration



(b) Flush Penetration

Figure 5-1. Limit Mechanism for Cylindrical Penetration in Spherical Shell

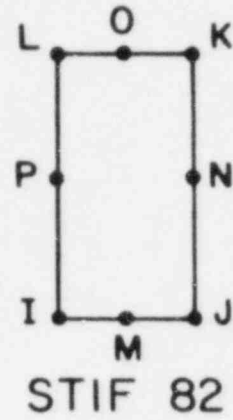
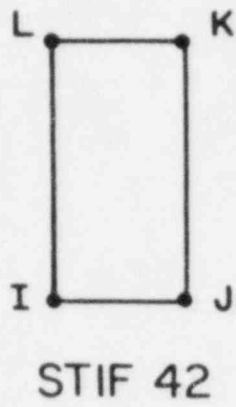


Figure 6-1. Axisymmetric Shell Element

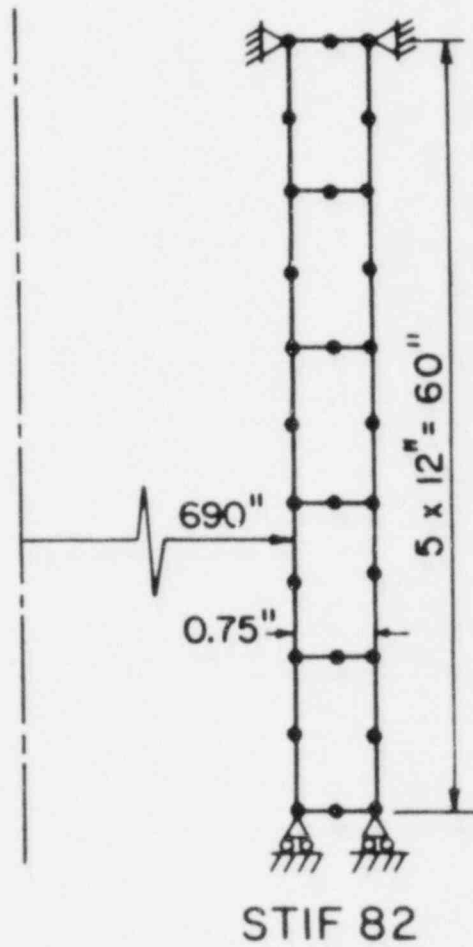
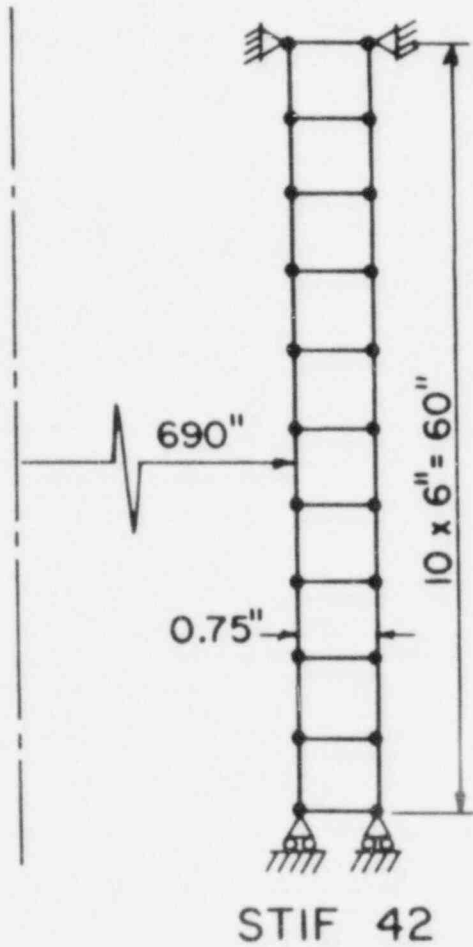


Figure 6-2. Finite Element Model for Closed End Cylinder

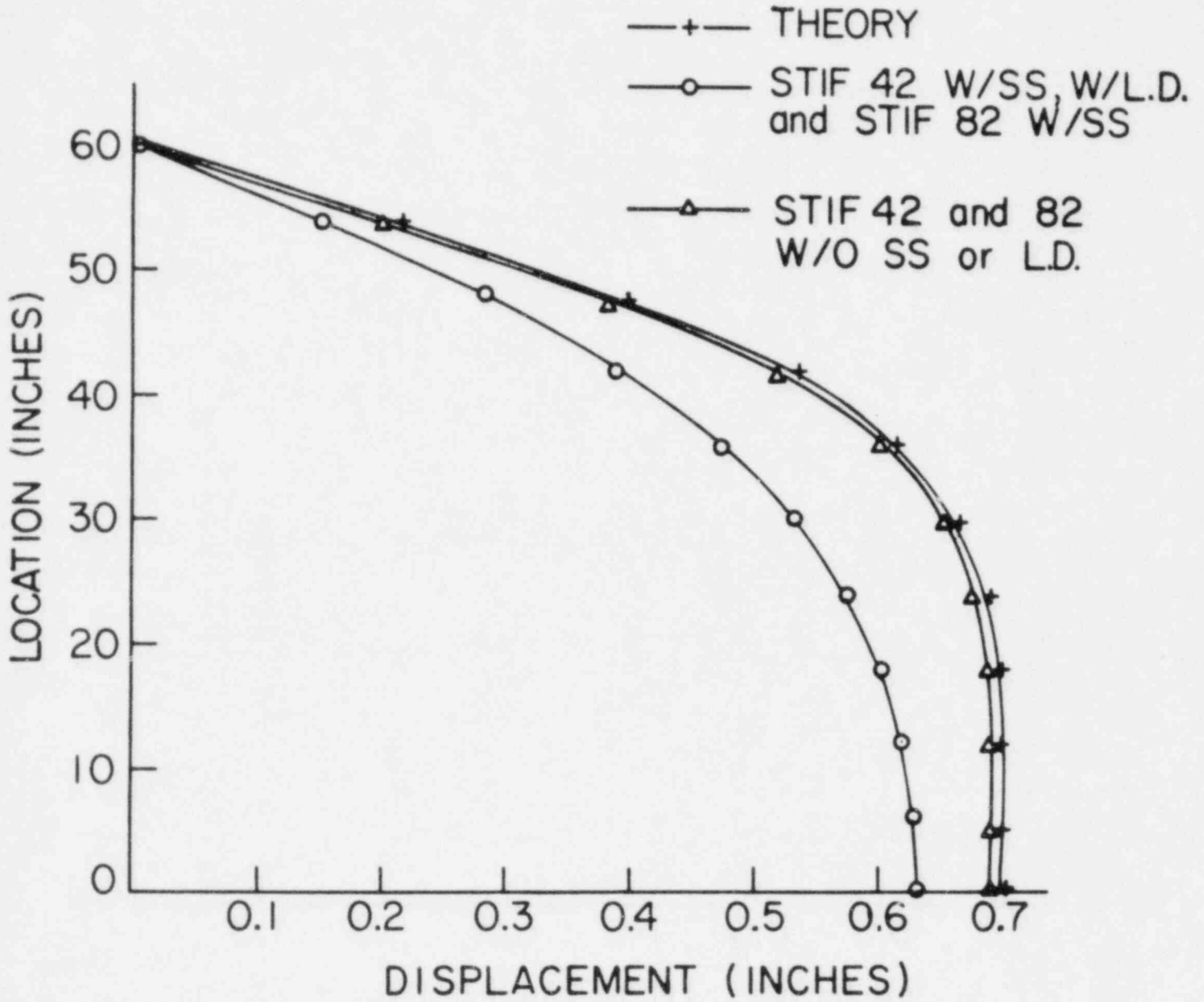


Figure 6-3. Radial Deformation vs Location (at p = 35 psi)

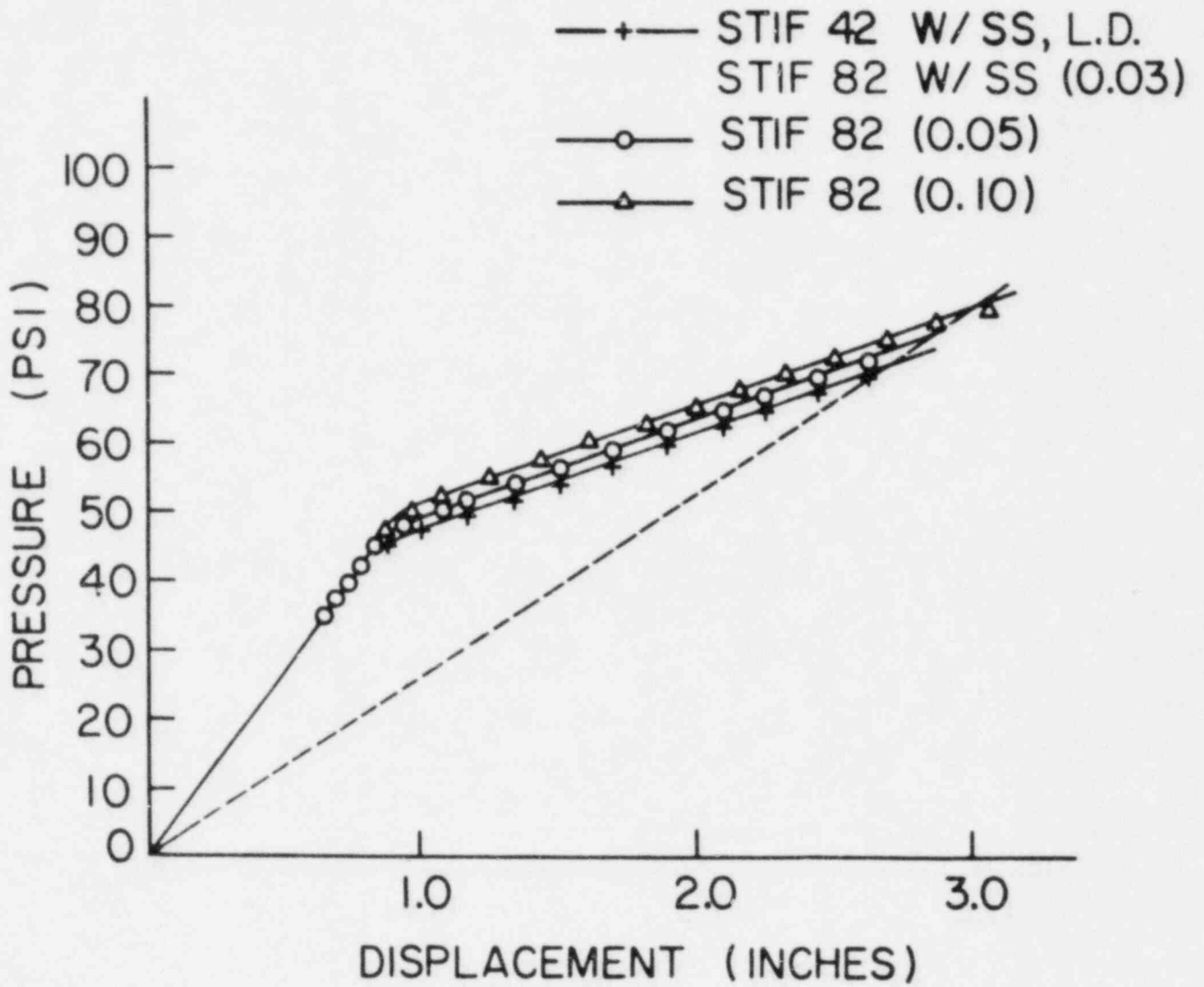


Figure 6-4. Pressure-Displacement Using Different Element Type and Convergence Criteria

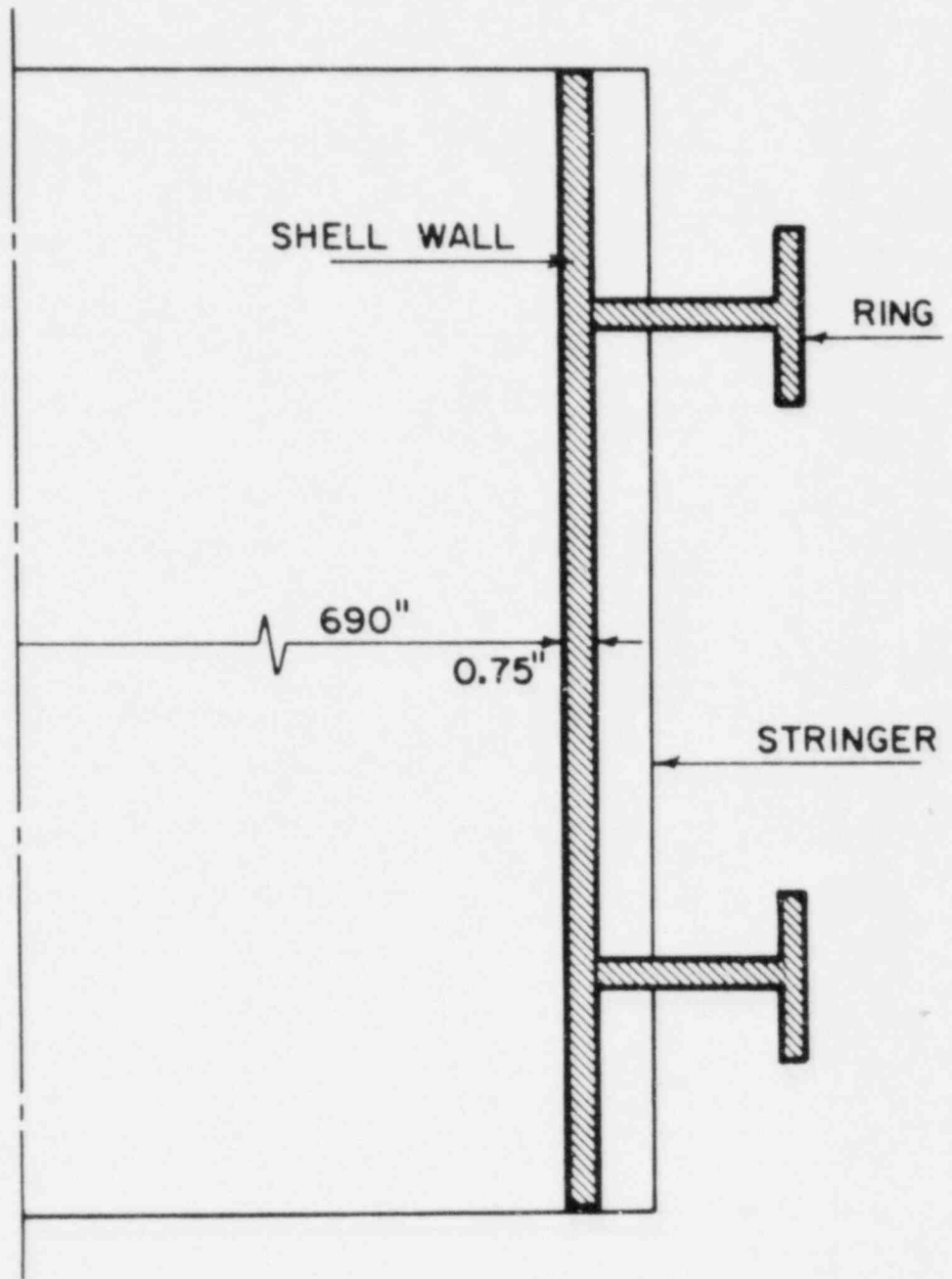
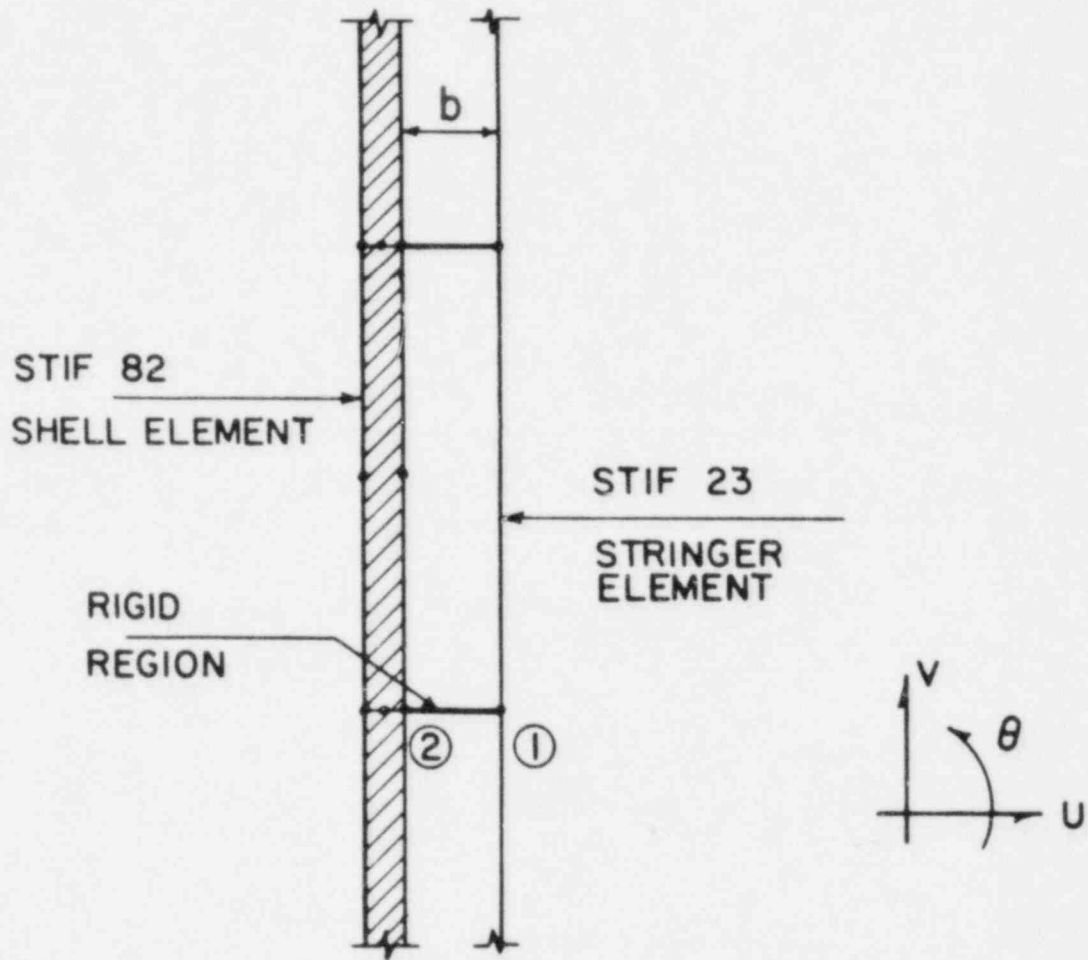


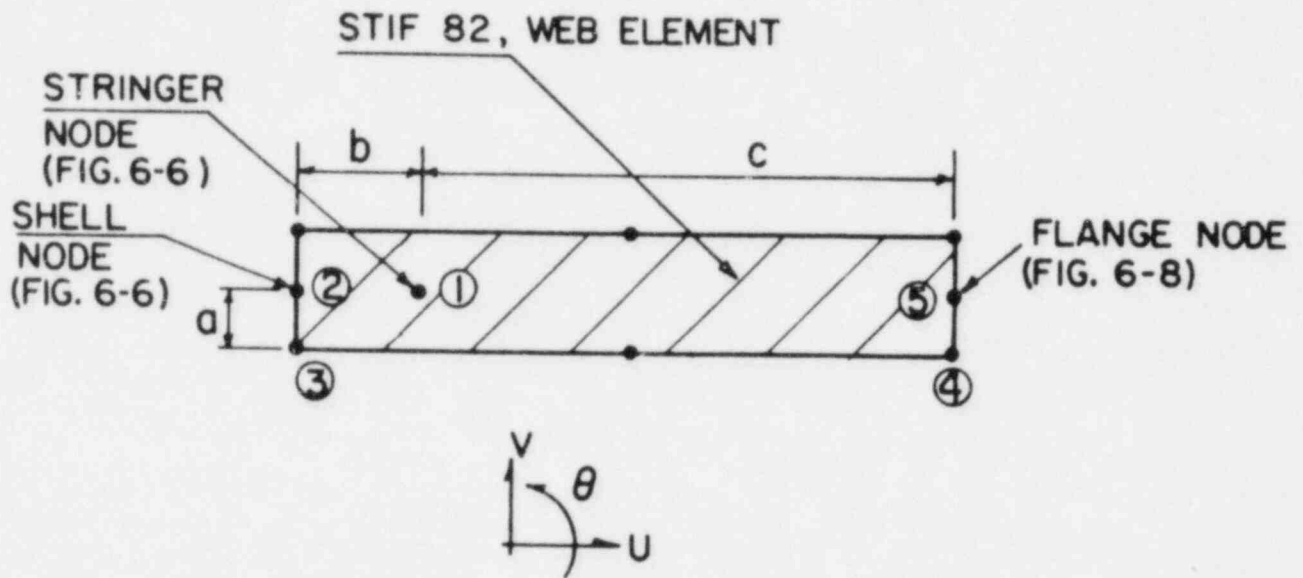
Figure 6-5. Vessel with Ring and Vertical Stiffeners



CONSTRAINT EQUATIONS

$$U_2 = U_1$$
$$V_2 = V_1 - b\theta_1$$

Figure 6-6. Cylinder-Stringer Connection Idealization



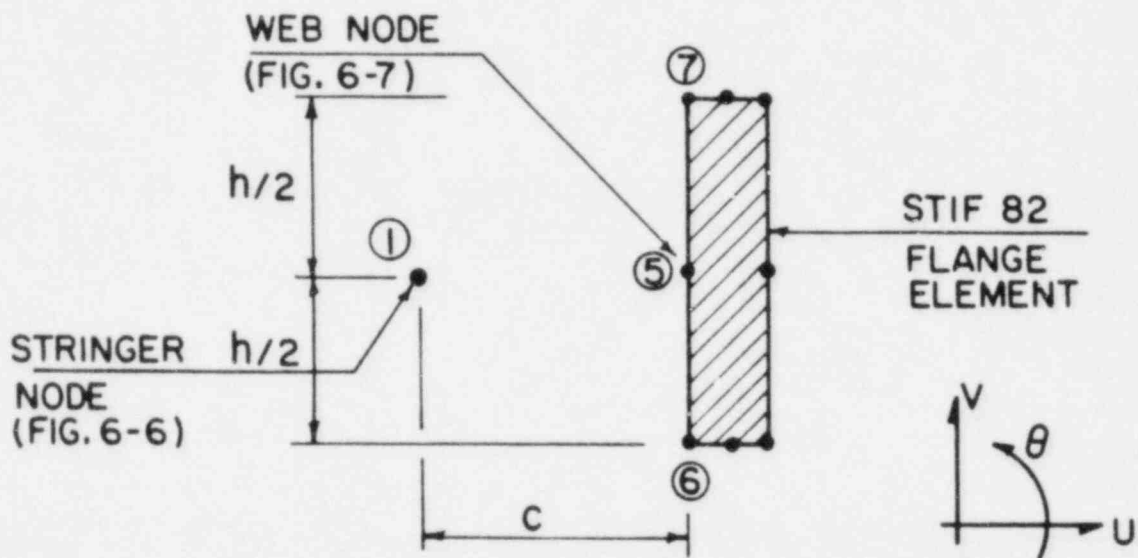
CONSTRAINT EQUATIONS

$$U_3 = U_1 + a\theta_1$$

$$V_3 = V_1 - b\theta_1$$

$$V_4 = V_1 + c\theta_1$$

Figure 6-7. Ring Web Connection Idealization



CONSTRAINT EQUATIONS

$$U_6 = U_1 + h/2 \theta_1$$

$$V_6 = V_1 + c \theta_1$$

$$U_7 = U_1 - h/2 \theta_1$$

Figure 6-8. Ring Flange Connection Idealization

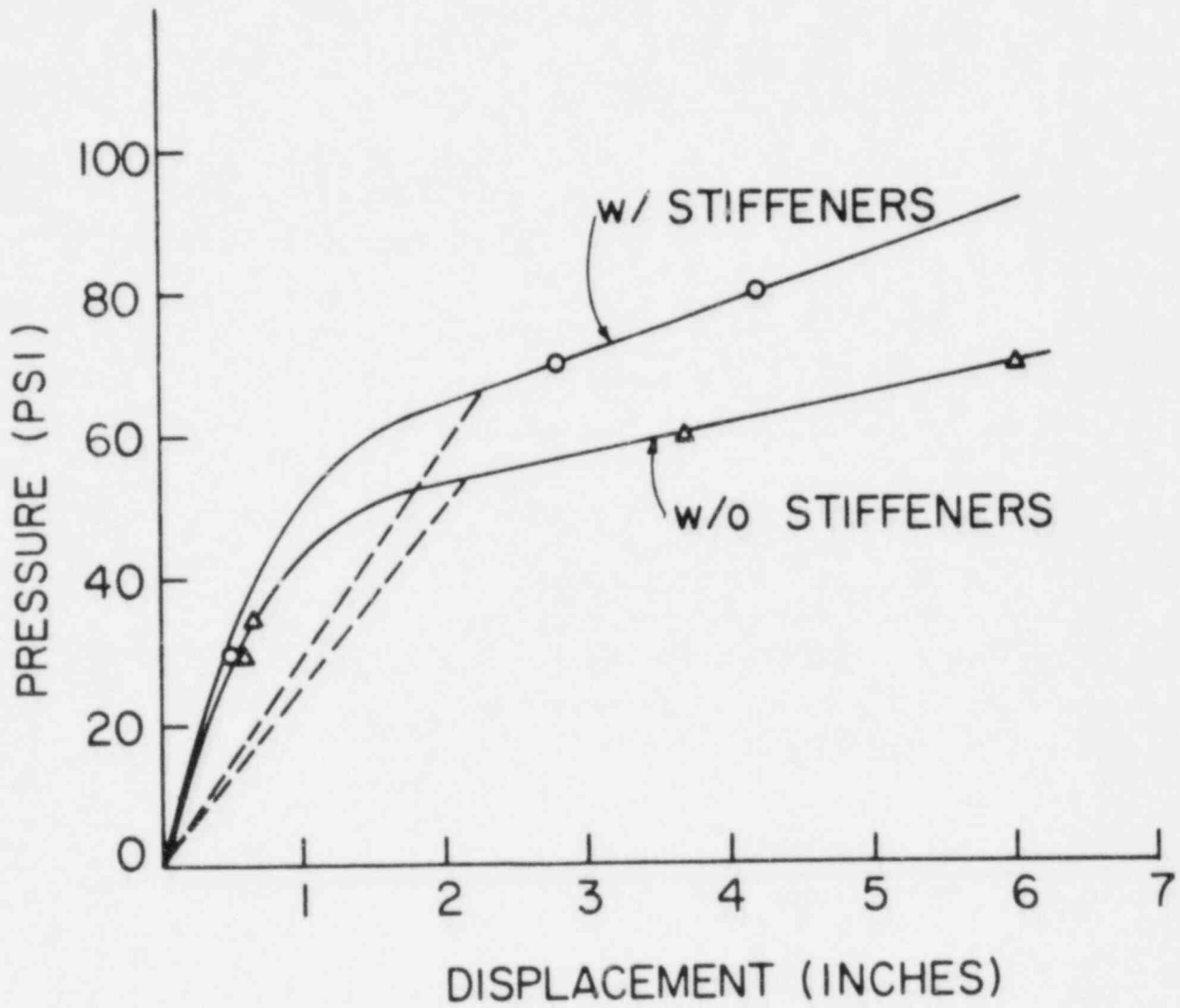


Figure 6-9. Pressure-Displacement for the Vessel in Fig. 6-5

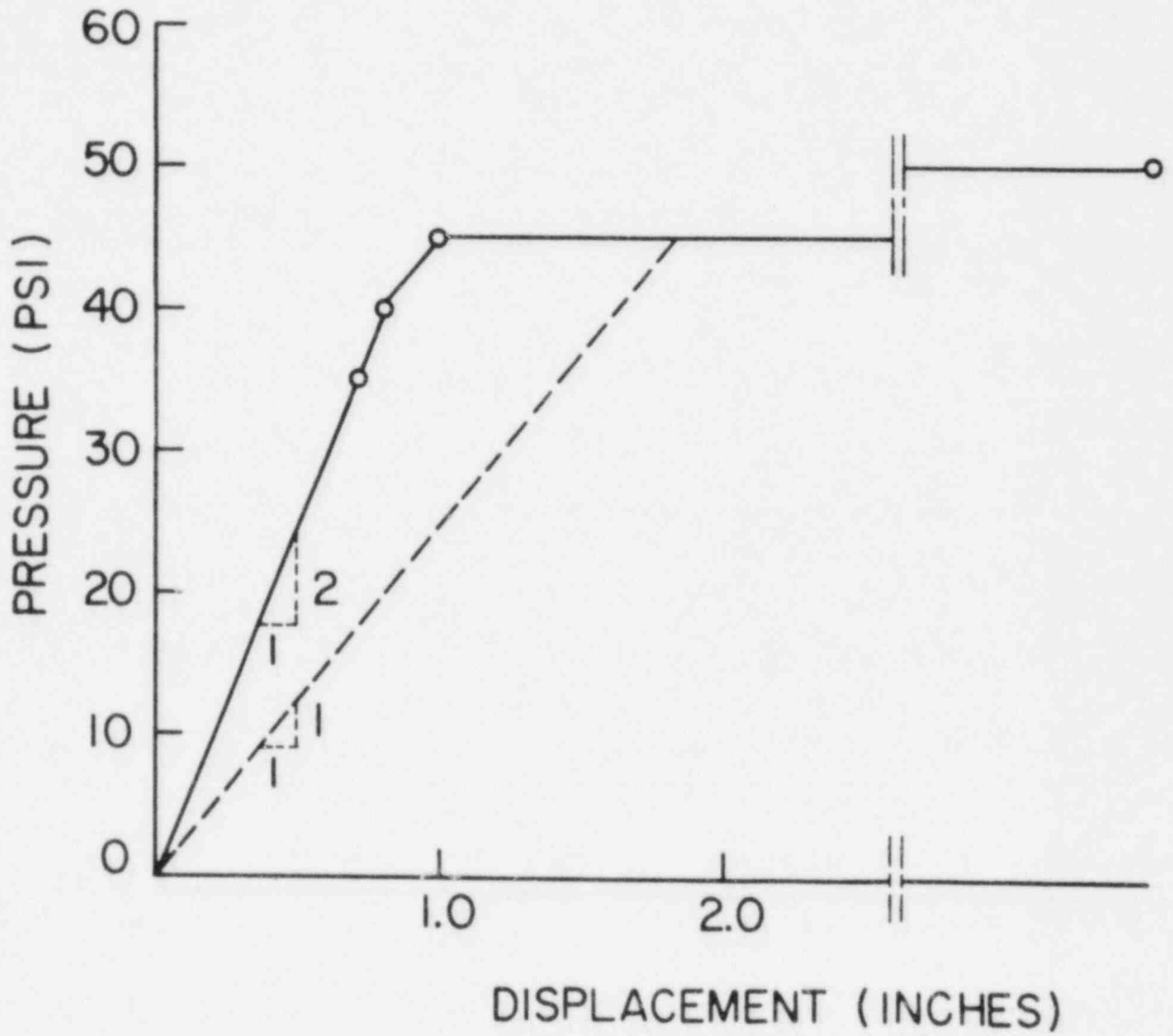


Figure 6-10. Pressure-Maximum Displacement Curve, Sequoyah Containment ($F_y = 35.2$ ksi)

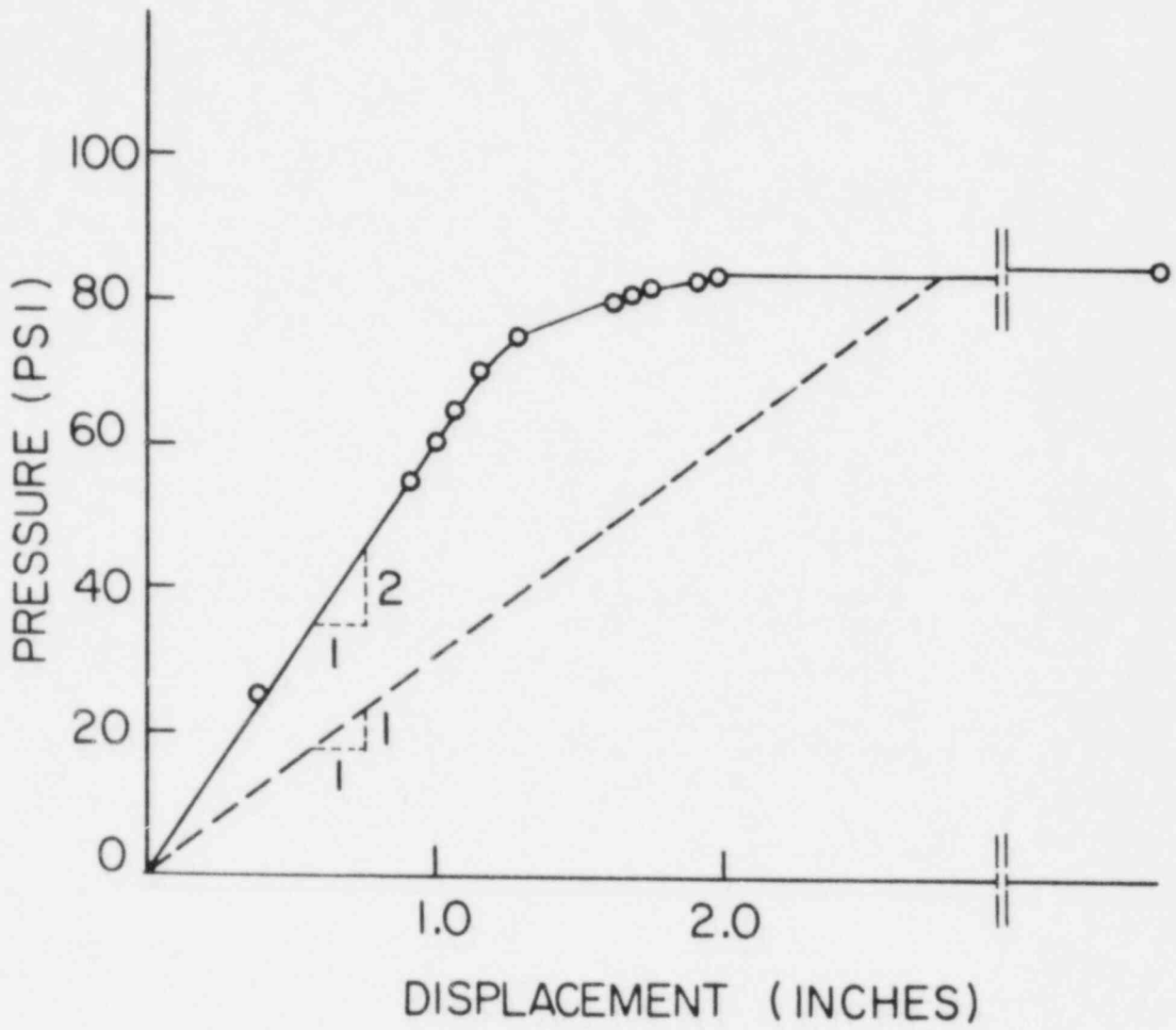


Figure 6-11. Pressure-Maximum Displacement Curve - McGuire Containment

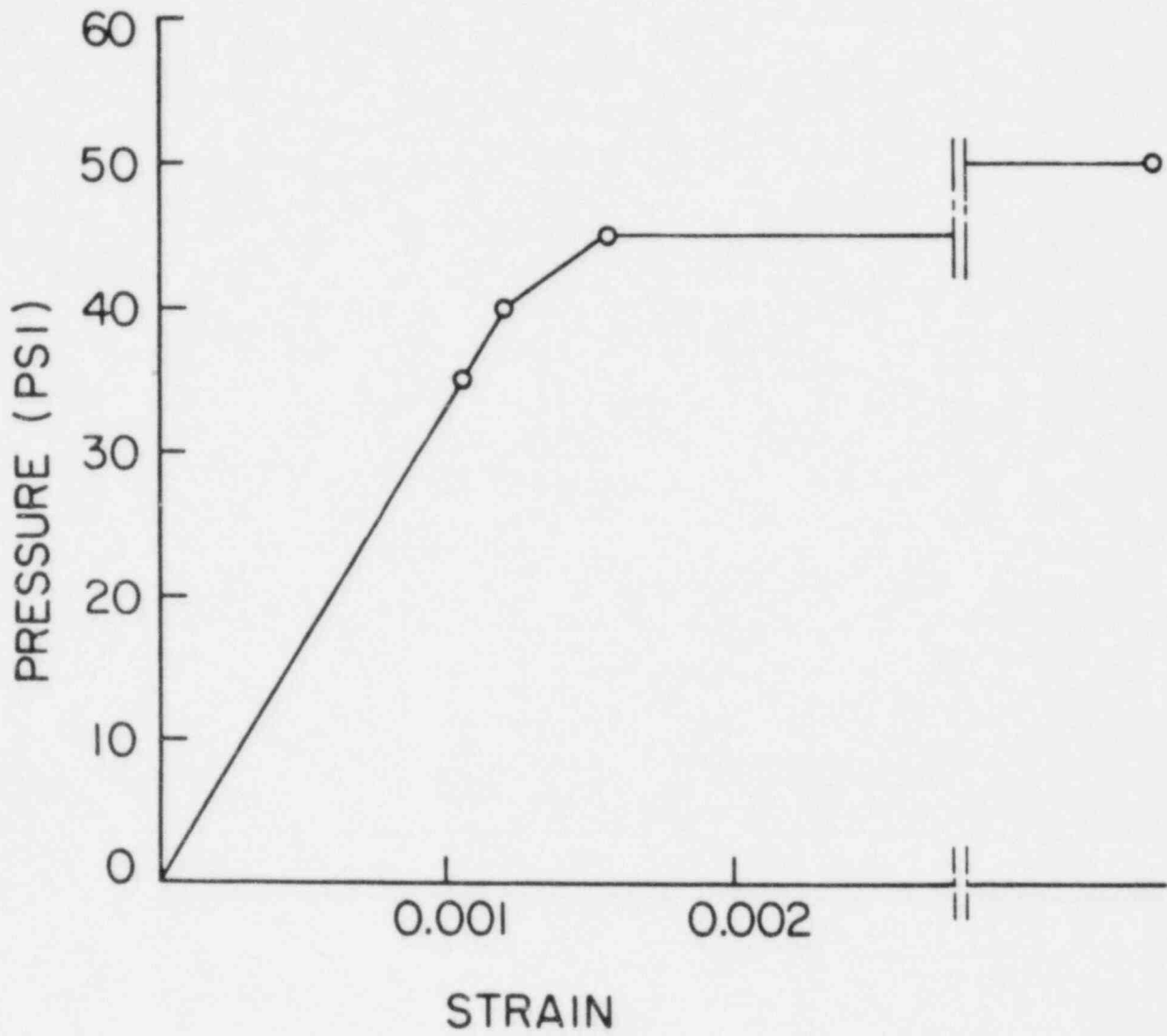


Figure 6-12. Pressure-Maximum Effective Membrane Strain Curve - Sequoyah Containment Vessel

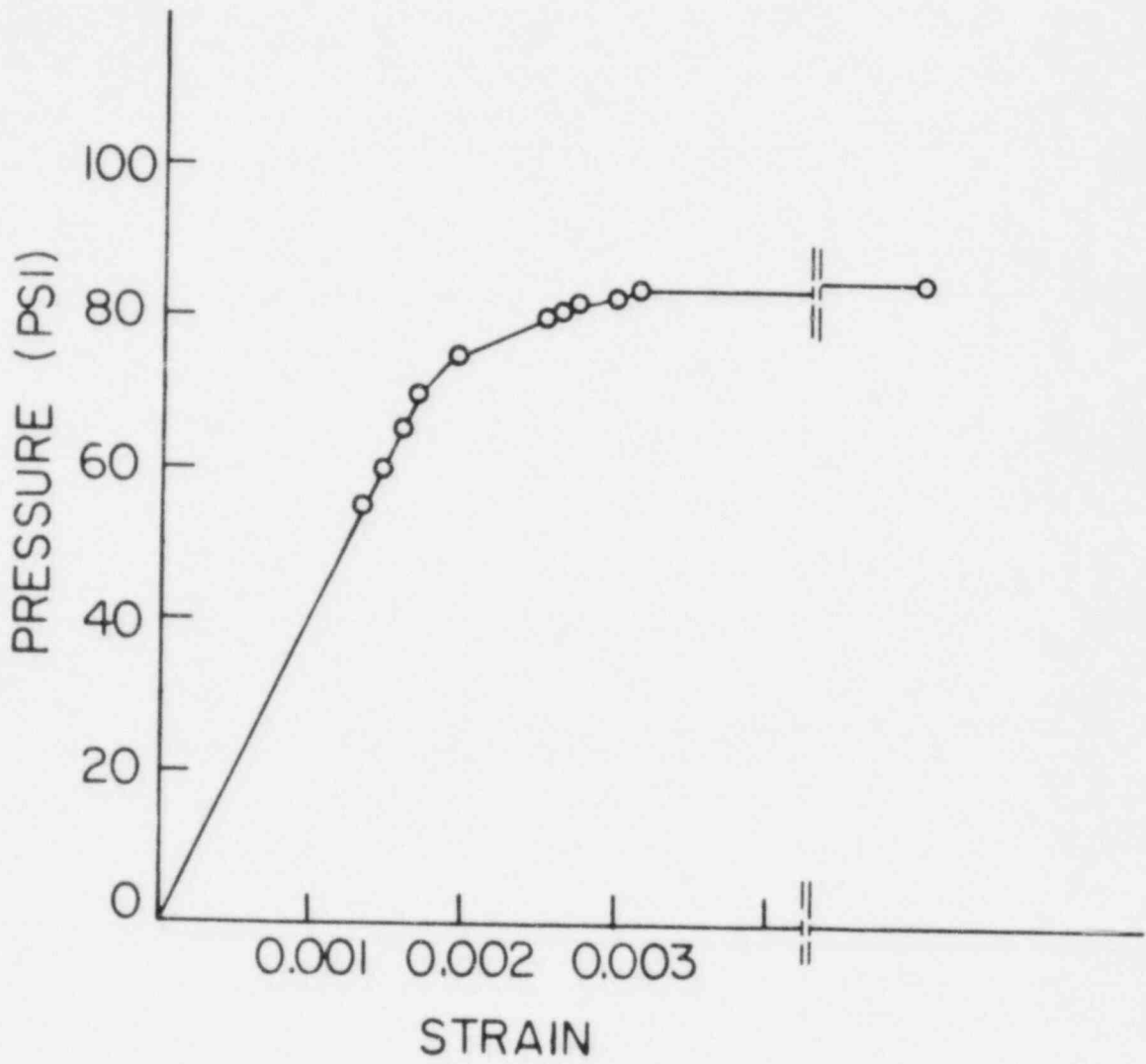


Figure 6-13. Pressure-Maximum Effective Membrane Strain Curve -
McGuire Containment Vessel

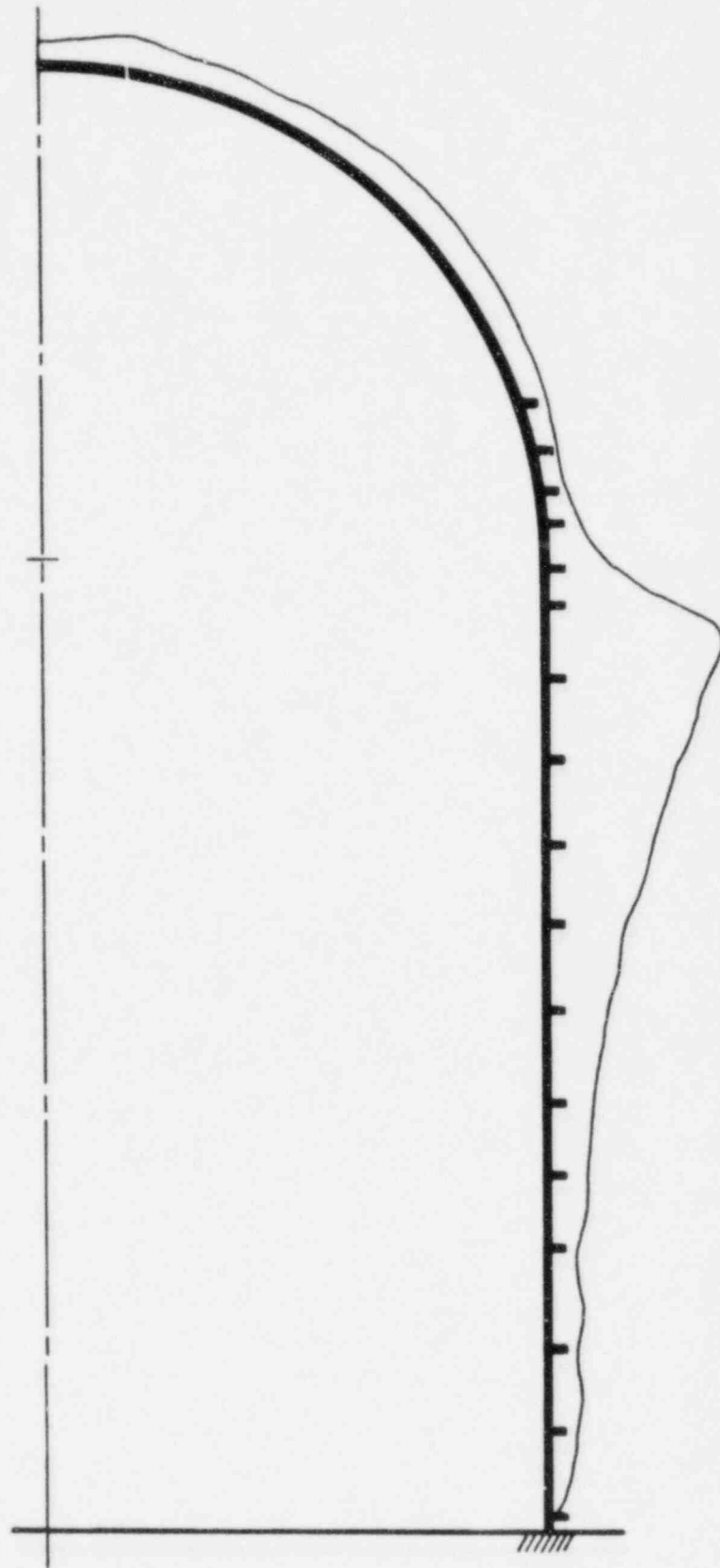


Figure 6-14. Deflected Shape of Sequoyah Containment Vessel Near Plastic Pressure



Figure 6-15. Deflected Shape of McGuire Containment Vessel
Near Plastic Pressure

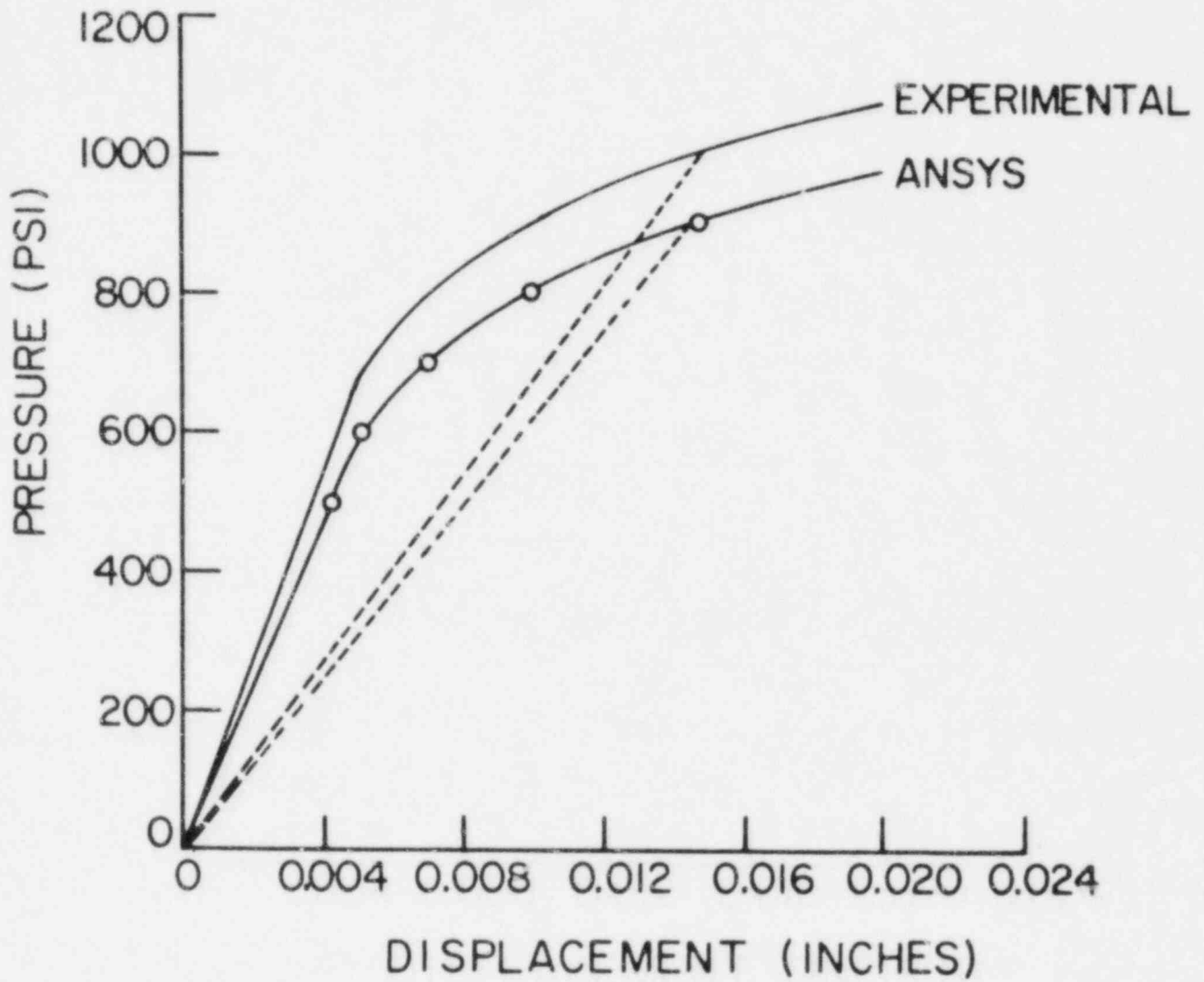


Figure 6-16. Pressure-Displacement for Experimental Model

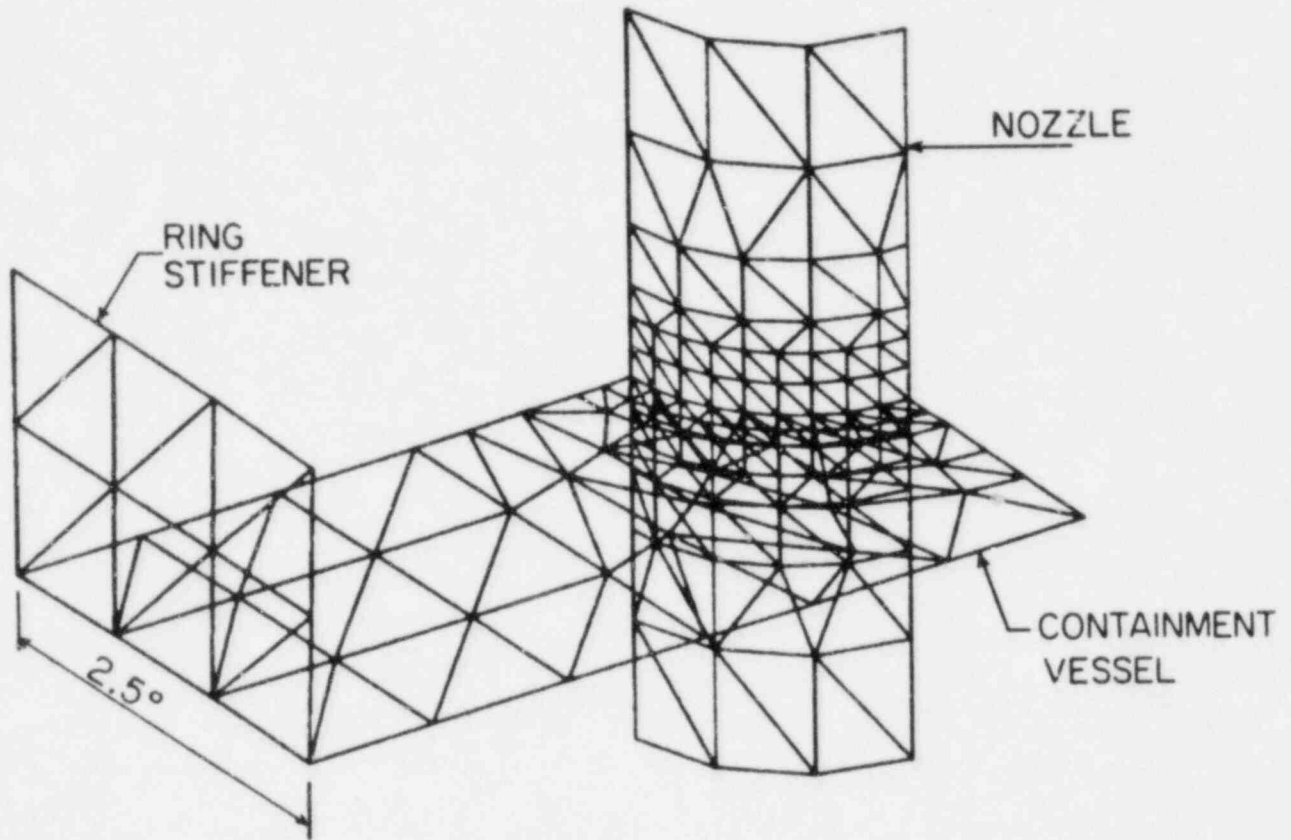


Figure 6-17. Ring Stiffener, Penetration and Containment Vessel Mesh Layout (Sequoyah vessel)

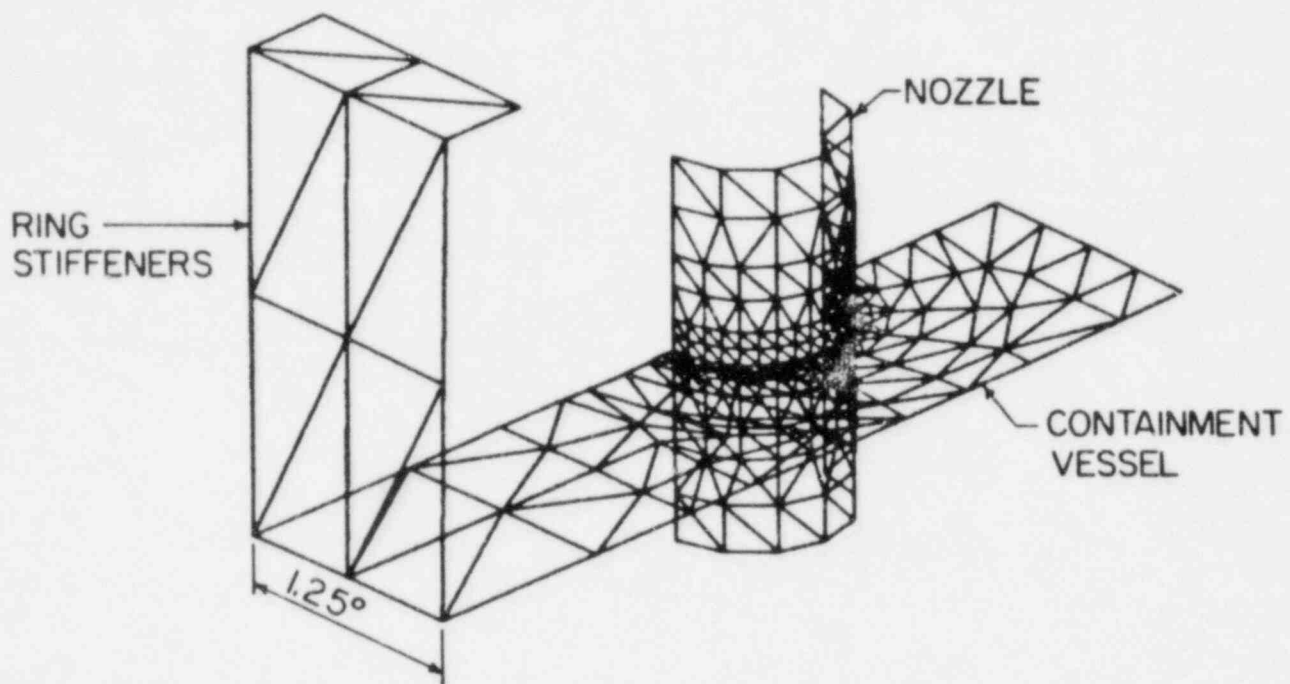


Figure 6-18. Ring Stiffener, Penetration and Containment Vessel Mesh Layout (McGuire Vessel)

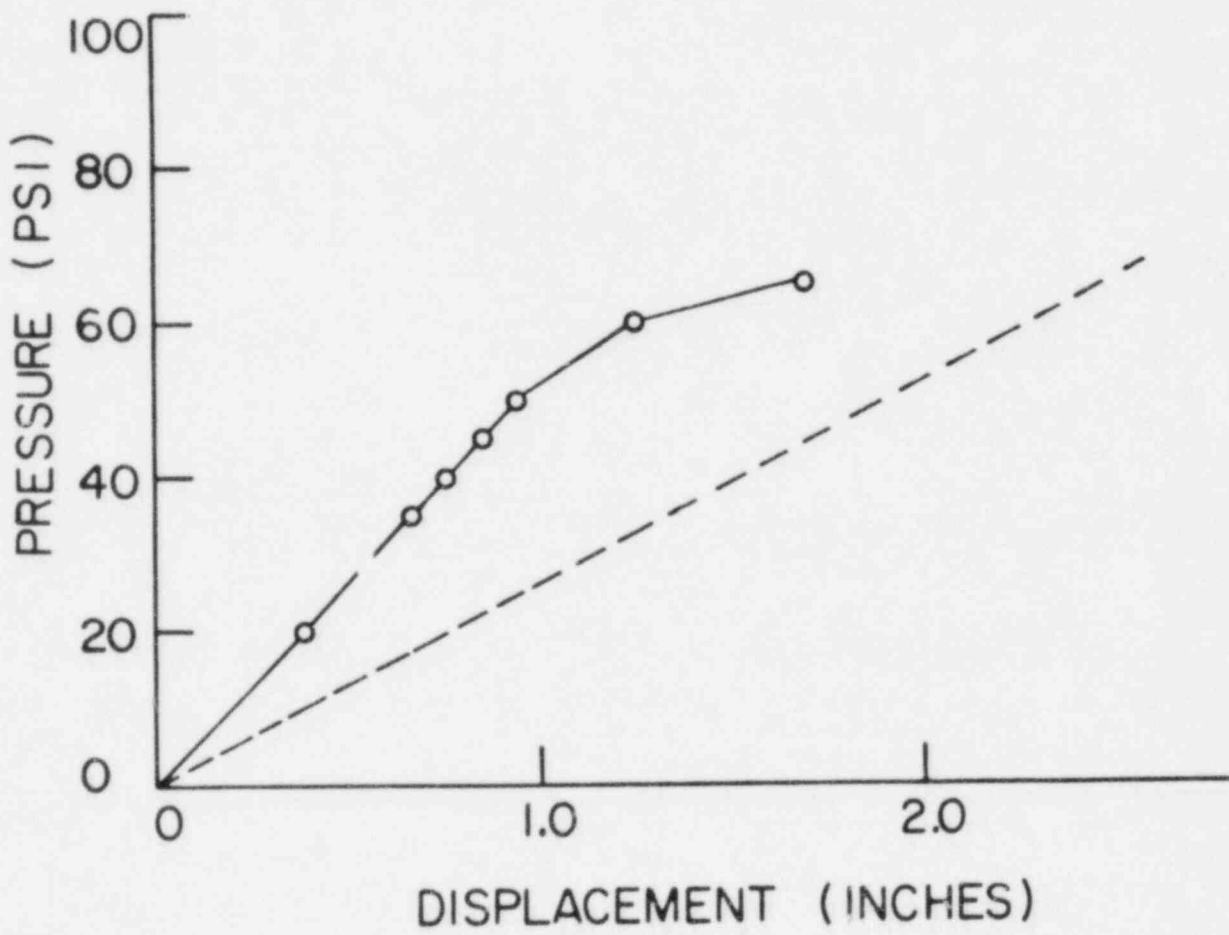


Figure 6-19. Pressure-Displacement of Penetration End - Sequovah Vessel

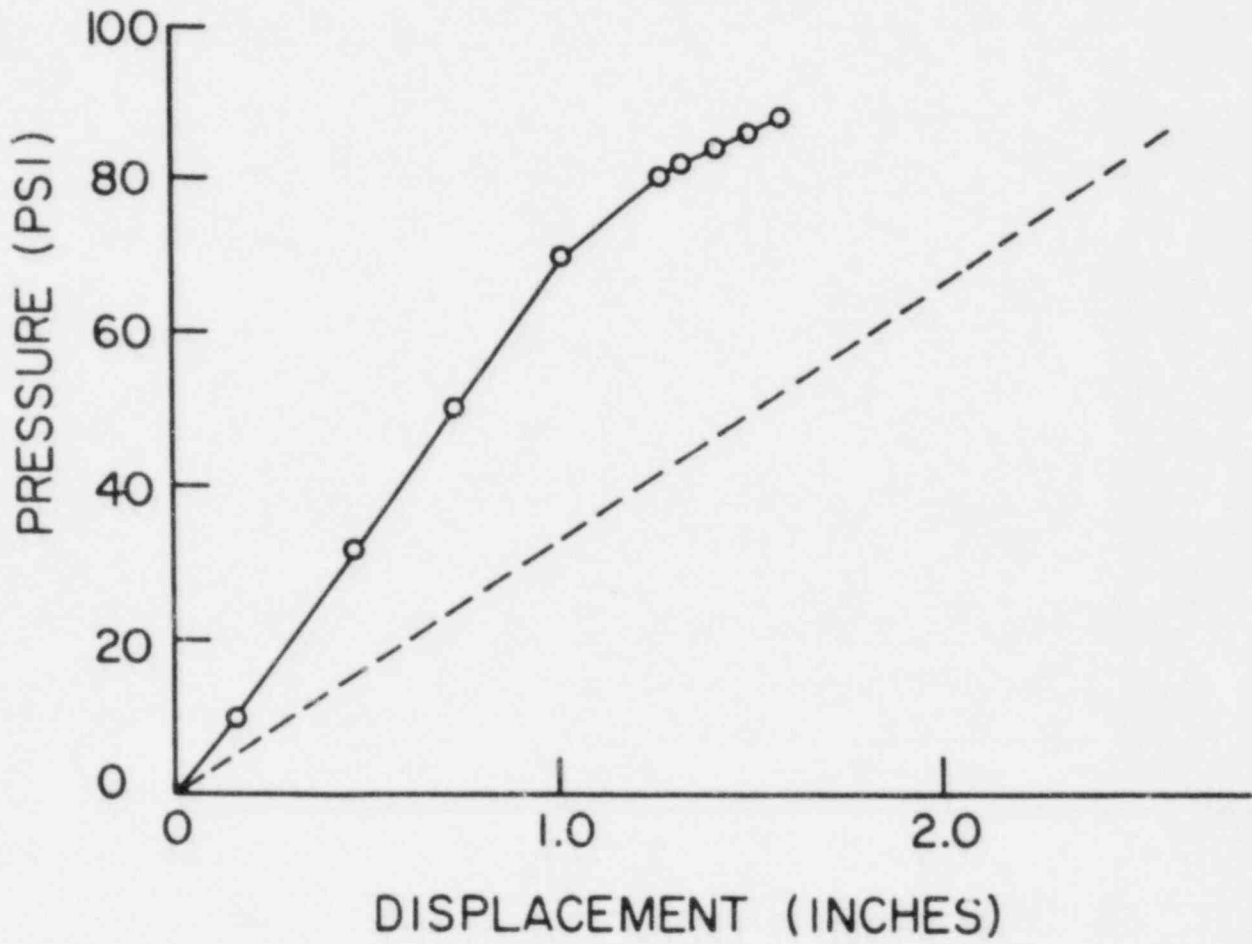


Figure 6-20. Pressure-Displacement of Penetration End - McGuire Vessel

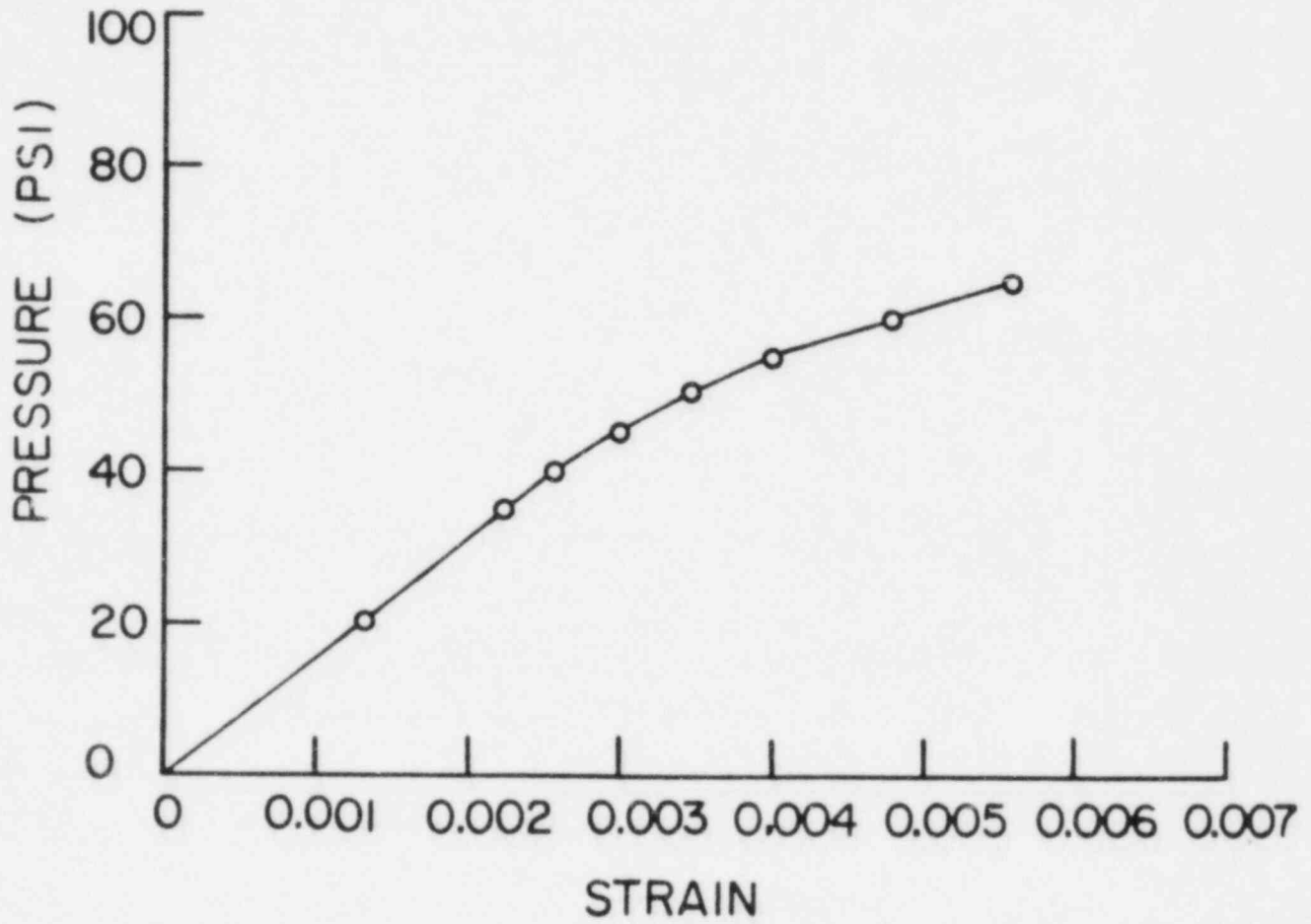


Figure 6-21. Pressure - Maximum Strain - Sequoyah Penetration

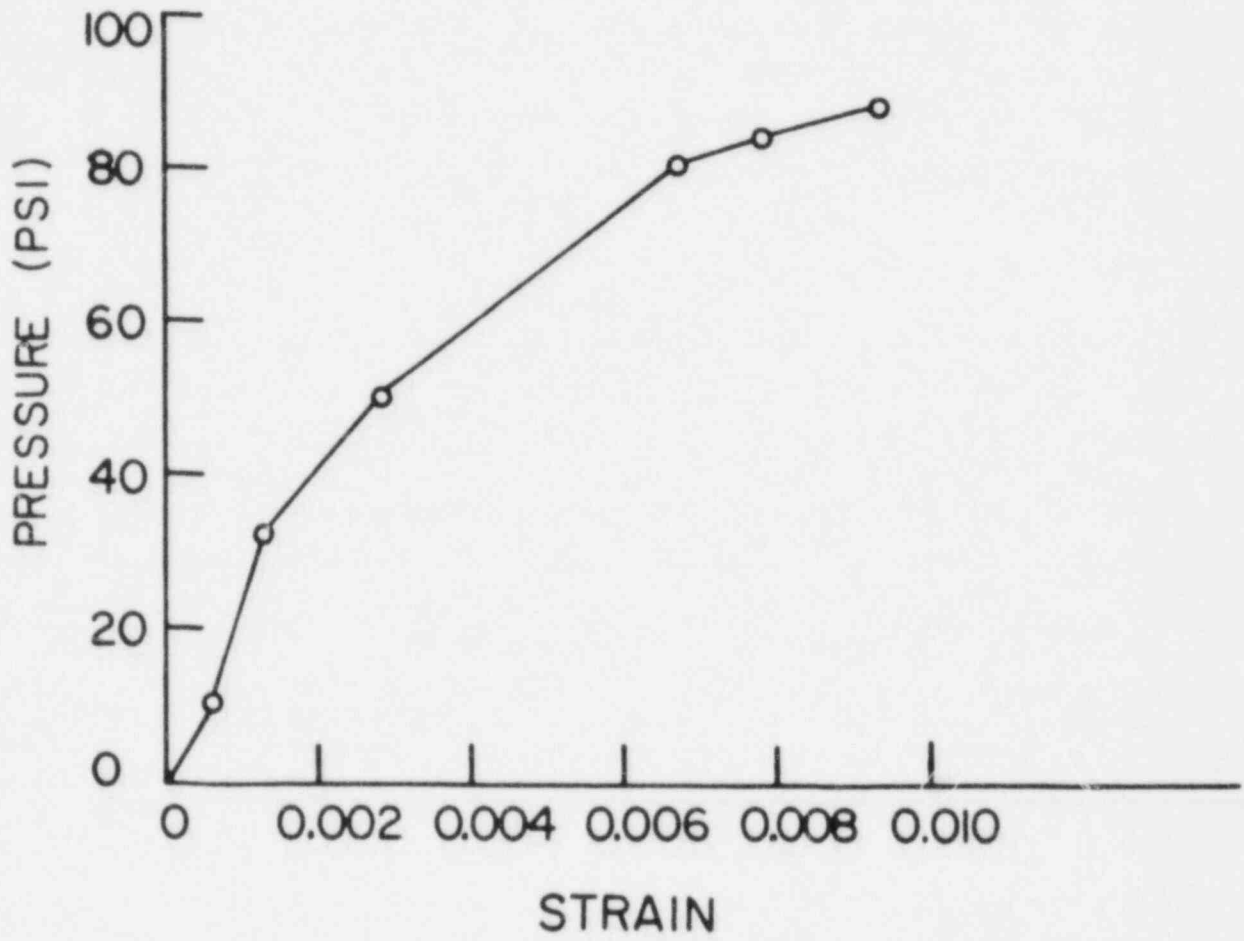


Figure 6-22. Pressure - Maximum Strain - McGuire Penetration

12.0 ADDENDUM

SUMMARY AND CRITIQUE OF INDEPENDENT ANALYSES OF SEQUOYAH CONTAINMENT

On September 2, 1980, a meeting of the Advisory Committee on Reactor Safeguards (ACRS) subcommittee on Structural Engineering was held in Washington, D.C. At that meeting, the results of several independent analyses of the Sequoyah containment vessel were presented. A summary of these results and a critique by this author are presented herein. All of these analyses examined the strength of the vessel under uniform static internal pressure. The results of a first order approximation to the dynamic strength obtained by this author are also presented in this Addendum.

12.1 Static Pressure

12.1.1 Ames Laboratory (January 1980)

On January 16, 1980, Ames Laboratory was requested to make a first order approximation to the static strength of the Sequoyah containment. In this analysis, the total ring and stringer areas were "smeared" to form an equivalent shell [A]*. Stresses in the equivalent shell were assumed to be uniform at

$$f_x = \frac{pr}{2t_{ex}} \quad (12-1)$$

$$f_\theta = \frac{pr}{t_{e\theta}} \quad (12-2)$$

*References for the Addendum are listed at the end. Copies of the references are attached

where $t_{e\theta} = t(1 + \alpha_1)$

$t_{ex} = t(1 + \alpha_2)$

are the equivalent thicknesses and the other terms are defined in Sec. 5.5.1. The von Mises yield criterion is applied to the biaxial stress state in the shell. Since the rings are under axial stress, the limit strength was obtained when Eq. 12-1 is set equal to the yield stress, F_y (taken to be 32 ksi in this work). The ASME area replacement rule was assumed to be satisfied so that penetrations did not control. The static pressure was reported to be 36 psi (+30, -10 percent). Burst pressure predictions were not considered reliable because of the limited ductility of the stiffened shell.

Comments: The assumption of uniform stress in the equivalent "smeared" shell at the maximum pressure is not consistent with a limit mechanism. Since the shell and stiffeners are in biaxial and uniaxial stress states, respectively, stresses will not be the same in the stiffeners and shell at the limit load (nor in the linear elastic range). Local bending effects are not included nor are they demonstrated to be unimportant, i.e., the limits of "smearing" are not defined. However, the report, submitted four working days after it was requested, did serve its intended purpose.

12.1.2 R&D Associates

The above results by Ames Laboratory were presented to the Commissioners of the Nuclear Regulatory Commission. Commissioner Victor Gilinsky requested R&D Associates to critique the Ames Laboratory (January 1980) analysis. Their work employed a linearly elastic analysis to show that the stringers are only about 40 percent effective and the rings are totally ineffective [B]. Locally high bending stresses were shown to exist near the rings and stringers but they were shown not to affect the vessel strength. A burst analysis is not appropriate for this vessel since other features, such as holddown bolts, will fail first. The predicted strength, based on an F_y of 32 ksi and the

von Mises yield criterion, was 27 psi. A more detailed finite element analysis and an experimental panel test were recommended.

Comments: This work represents a reasonable approximation to the linear behavior of the stiffened shell. In essence, the analysis calculates the strength of an unstiffened shell of infinite length. Locally high bending stresses are, indeed, not important insofar as the limit state is concerned. However, the results certainly are a lower bound to the limit pressure. If the shell has any ductility capacity whatsoever (which it most certainly does), stress redistribution will occur between the stiffeners and shell and pressures beyond 27 psi will be obtained.

12.1.3 TVA

The analysis by TVA [C] considered several failure modes: anchorage, penetrations (bellows and valves), personnel locks/equipment hatch, seals and shell plate. The shell plate was shown to control. The shell was conservatively analyzed as an unstiffened cylinder with a material yield stress of 45.7 ksi (lowest value of actual mill tests). The von Mises failure criterion gave a pressure strength of 38.2 psi.

Comments: The TVA analysis is conservative and gives essentially the same results as the R&D Associates analysis. Similar comments apply.

12.1.4 NRC Research

NRC Research personnel submitted a critique of the Ames Laboratory (January 1980) and the R&D Associates analyses [D]. This memorandum states that the stiffeners should be expected to add some strength to the shell. An independent analysis was performed in which the stringers were idealized as beams spanning between ring stiffeners. Pressure applied to the inside shell surface was assumed to be resisted by circumferential tension in the shell plus bending of the stringer. Local shell bending effects were ignored. The maximum pressure was assumed to occur when a plastic beam mechanism formed in the stringer and the shell yielded in tension. For an assumed F_y of 32 ksi and the von Mises yield criterion, a predicted strength was given as 34 psi.

Comments: This analysis represents an interesting approach to incorporating stringer bending effects. It gives results similar to the Ames Laboratory (January 1980) results. However, the results are conservative in that transverse meridional shear forces are neglected in the shell free body diagram. The net result is that no force is assumed to be transmitted from the shell directly to the rings. The effect of the ring on the circumferential shell stresses is, consequently, neglected. Additionally, at the limit load, the stringer is predominately an axial force member, rather than a bending member (See Sec. 6.3.3.2). Also, radial deflection of the rings at the ends of the stringers may not permit the development of the full stringer beam mechanism hypothesized here.

12.1.5 Franklin Research Institute

Zenons Zudans of the Franklin Research Institute reported on his critique of the Ames Laboratory (January 1980) and R&D Associates work [E]. He concluded that both analyses are incorrect in the manner in which the rings and stringers are treated. Of the Ames Laboratory work, for example, he stated that the "calculations of limit pressure . . . are meaningless. Accordingly, the conclusion, that the ring will yield first (at 35.7 psi) is not realistic." Mr. Zudans proposed a model of his own which includes four separate analyses:

- (1) Axisymmetric, ring stiffened shell (5/8 in.) without stringers. This elastic analysis demonstrated that the rings have no effect on the elastic stresses in the shell midway between rings if no stringers are present.
- (2) Axisymmetric, ring stiffened shell (5/8 in.) with smeared stringers. The hoop stresses in the shell with the stringers were shown to be almost uniform in the elastic range and significantly below those of Analysis (1).
- (3) Curved shell panel (5/8 in.) with one ring and one stringer. The elastic panel analysis demonstrated that the "smearing" technique used in Analysis (2) above is valid. Thus, the bending and membrane stiffnesses of the stringer can be smeared circumferentially.

- (4) Axisymmetric, ring stiffened shell (1/2 in.) with smeared stringers. (Same as Analysis (2) except 1/2 in. shell). The pressure at which the average hoop stress midway between rings reached the yield stress was predicted to be 30.3 psi. An F_y at 32 ksi with the maximum shear stress criterion was used.

Comments: This analysis confirms at least two aspects of the original Ames Laboratory work: (a) stringers can be "smeared" if their axial and bending stiffnesses are included (Analysis (3) above), and (b) the hoop stresses in the shell with the stringers are almost uniform between rings (Analyses (2), (3), and (4) above). Thus, although the author strongly objects to the Ames Laboratory assumptions, he tends to confirm them. Beyond initial yielding, i.e., with large displacement and force redistribution effects, and near the limit load, the Ames Laboratory assumptions become even more realistic. At this stress level, stringer bending strength and stiffness are negligible and only axial effects need to be incorporated into the smearing process. The above direct quote from the Franklin Research Institute report indicates that they may not have understood that the analysis by Ames Laboratory was intended to be an approximate limit analysis. Certainly, the ring will not yield first but, as confirmed by the current report (Sec. 6.3.3.2), the limit strength is certainly controlled by the rings.

The results of this analysis were very useful in confirming the stringer smearing process used in the finite element analysis reported in the text of this report (Sec. 6.3.1).

12.1.6 Offshore Power Systems

Offshore Power Systems performed a nonlinear analysis of a typical 1/2 in. curved panel bounded by two stringers and two rings (a geometry very similar to Analysis (3) by Franklin Research Institute) [F]. The nonlinear finite element analysis was performed using ANSYS and an F_y of 45 ksi. These results demonstrated that the circumferential variation of displacement in the panel is negligible - even in the nonlinear range. Additionally, the ring and shell stress vary little circumfer-

entially. No maximum pressure strength was predicted from the finite element results. An analysis with "smeared" rings, independent of the finite element analysis, gives predicted strength of 50.8 psi and 56.8 psi for 9'6" and 6'6" ring spacings, respectively.

Comments: As with the Franklin Research Institute results, the finite element results confirm the stringer in the original Ames analysis. The Offshore Power Systems work is also referred to in the text of this report as verification of the smeared stringer technique used in the nonlinear finite element analysis (Sec. 6.3.1). The predicted strengths from the "smeared" analysis are based on essentially the same assumptions as the original Ames work.

12.1.7 Ames Laboratory (September 1980)

The latest complete Ames Laboratory analysis is summarized in the text of this report. Preliminary results were presented at the ACRS meeting. The approximate analysis reported herein is a revised version of the January 1980 work. A complete mechanism was assumed to form with stiffeners and shell at yield (see Sec. 5.1). The approximate limit pressure is 59 psi. An axisymmetric, nonlinear finite element analysis of the complete containment was also performed (see Sec. 6.3). The plastic pressure was shown to be 60 psi. An F_y of 47.2 ksi (mean value) was used in each of these analyses.

Comments: The finite element model employed here appears to give the most complete analysis of the containment. The stringer smearing process is confirmed by the Franklin Research Institute and Offshore Power Systems' analyses.

12.1.8 Summary

To provide some basis for a comparison of the various approaches summarized above, it is useful to: (1) convert each result to an F_y of 47.2 ksi by a direct ratio, (2) use the von Mises yield criterion (multiply the result of Franklin Research Institute by $2/\sqrt{3}$), and (3) classify results. This process gives:

R & D Associates	40 psi	first yield w/o stiffeners
TVA	40 psi	first yield w/o stiffeners
NRC Research	50 psi	stringer beam mechanism
Franklin Research	51 psi	membrane yield
Ames Laboratory (Jan. 1980)	53 psi	yield w/smeared stiffeners
Offshore Power Systems	53 psi	yield w/smeared stiffeners
Ames Laboratory (Sept. 1980)	59 psi	limit mechanism
Ames Laboratory (Sept. 1980)	60 psi	finite element

In spite of the apparent large variation in the predictions for the Sequoyah strength, there is, in essence, really only one practical question to be answered: How much ductility capacity does the existing containment have? If the ductility is such that the membrane strains must remain below yield, then a pressure based on first yield is appropriate. First yield will probably occur between 40 psi (if stiffeners are neglected) and 50 psi (if stiffeners are included). Figs. 6-10 and 6-12 of the current report also confirm this. If, on the other hand, the containment vessel has a ductility capacity of at least two, force redistribution will be permitted to occur and the stiffening will become more effective. The strength of the vessel could then be taken as 60 psi. As documented in this report (Chap. 4 and Fig. 6-12), a ductility capacity of two is certainly probable (see also [21, pg. 529]) so that a 60 psi strength is reasonable. The statistical distribution of the ductility capacity of the containment vessel should be determined to quantitatively define this probability.

12.2 Dynamic Pressure

12.2.1 Introduction

As mentioned elsewhere in this report, the explosion incident identified at TMI may have produced dynamic pressures which varied with time. In particular, if a hydrogen explosion occurs within the relatively confined volume of a lower compartment, significant dynamic pressure could develop. A preliminary estimate of the dynamic pressure capacity of the Sequoyah containment is presented in this section. An

explosion in the upper compartment or in the ice condenser compartment is assumed to be relatively unconfined and of little significance. Dynamic pressures were considered in only the lower compartments (Elev. 693' to 719.5') listed in Table 12-1. No information was furnished to us regarding the actual time and spatial variation of the potential explosive pressures for Sequoyah. The analyses summarized below are intended to be very preliminary. In this regard, several simplifying assumptions have been made. More effort should be devoted to this work; see Recommendations in Sec. 7.3.

12.2.2 Preliminary Finite Element Analysis

On July 3, 1980, Ames Laboratory was requested to make a preliminary calculation of the strength of the Sequoyah containment vessel subject to a dynamic pressure [G (copy of report is attached)]. A dynamic pressure was assumed to act in a lower compartment over an arc length of 60 degrees. The pressure in the compartment was assumed to vary from a maximum pressure, p_v , at time zero to a zero pressure at 0.030 sec. The pulse magnitude and length are quite arbitrary and would be dependent upon compartment size, explosion characteristics and venting properties. (An initial pulse representing the detonation phase of the explosion was also included, but its momentum was shown to be relatively insignificant.)

Since the pressure loading is not axisymmetric, the response will not be axisymmetric. The non-axisymmetric response was assumed to be dominated by the rings. A typical ring (Elev. 713.5') with an effective shell width was idealized by STIF23 nonlinear beam finite elements (see Sec. 6.3.1). Elastic springs, tangential to the ring, were used to model the resistance of the shell below the ring. An F_y of 39 ksi was used for the dynamic analysis. A dynamic transient solution was obtained using ANSYS with material and geometric nonlinearities. Three separate analyses were performed with three separate maximum dynamic pressures, i.e., for p_v equal to 10, 50 and 100 psi.

The resulting maximum strains and displacements are summarized on page 12 of the attached Ref. G. They can be summarized in a non-dimensional form as

$1000 p_v/F_y$	Ductility Demand	
	μ_ϵ	μ_δ
0.26	0.4	0.3
1.28	4.8	2.2
2.56	24.9	11.7

where the maximum dynamic pressure has been non-dimensionalized with respect to the material yield strength, the strain ductility demand is

$$\mu_\epsilon = \frac{\text{maximum strain}}{\text{yield strain}} \quad (12-3)$$

and the displacement ductility demand is

$$\mu_\delta = \frac{\text{maximum displacement}}{\text{yield displacement}} \quad (12-4)$$

The non-dimensionalization of the maximum pressure is convenient for extending the results to other material yield strengths. The yield strain is 39/29000 or 1345 micro in./in. The yield displacement is, quite arbitrarily, taken as the elastic displacement at the ASME half-linear-slope pressure (Sec. 4.2). From page 10 of Ref. G, the yield displacement for an F_y of 32 ksi is 35 psi/(20 psi/in.) or 1.75 in. For an F_y of 39 ksi the yield displacement is 2.13 in. which was used to calculate the above μ_δ .

The predicted strength of the vessel is dependent upon the ductility capacity of the vessel -- as in the static case (Sec. 12.1.8). In Ref. G, a maximum dynamic pressure was conservatively predicted, based upon a strain ductility capacity of two. However, a ductility capacity of two for displacement seems more consistent with the ASME definition of the static plastic pressure by the half-linear-slope method. For a displacement ductility capacity of two, a $1000 p_v/F_y$ ratio of 1.2

is interpolated from the above table. Using the actual mean material yield stress of 47.2 ksi gives a predicted dynamic pressure strength of 57 psi.

12.2.3 Approximate Dynamic Analysis

A simple approximate analytical model for estimating the strength of the Sequoyah steel containment vessel under a dynamic pressure acting in a lower compartment over some arc length is presented in this section.

The transient response of the ring which was obtained in Sec. 12.2.2 indicated that most of the energy absorbed is predominately due to membrane action. A nonlinear static analysis of the ring was also performed in Ref. G. The results showed that, as the limit load is approached, the cross sections in the vicinity of α equal zero (Fig. 12-1) went into pure plastic tension. What may be termed complex hinges formed in the vicinity of α_0 (actually, slightly beyond α_0) on either side of the centerline shown in Fig. 12-1. The energy absorbed at each end of the complex hinges is the summation of the work done by the reduced plastic moment and the tensile force at the section. The results obtained in Sec. 12.2.2 suggest that a simpler analytical model may provide a first approximation to the strength of the containment vessel. A section of the containment vessel will be modeled by a single degree-of-freedom system.

To obtain a simple analytical model, it is assumed that, at the limit load, a typical ring section with an effective shell width collapses by the formation of plastic hinges on either side of the centerline at α_0 and a fully plasticized section in pure axial tension at α equal zero. The reactive stresses are assumed to be shearing stresses as shown in Fig. 12-1. The deformation of the mechanism under constant pressure during plastic collapse is shown in Fig. 12-2. The arc curvature is assumed to remain constant during collapse. Secondary effects like the influence of large deformations on the limit load are neglected. The work done by the external loads is assumed to be absorbed by

the two plastic hinges (assuming no reduction in the plastic moment, M_p) and by axial extension at α equal zero. The contribution of the shearing stresses to the strain energy is neglected.

From Fig. 12-2, for a virtual displacement, θ , the axial extension, δ , is

$$\delta = 4\theta R_0 \sin^2 \frac{\alpha_0}{2} \quad (12-5)$$

where R_0 is the radius of the containment wall. The external work done by the distributed load acting on arc ABD may be taken as,

$$\text{external work} = 4\theta R_0^2 \left(\sin^2 \frac{\alpha_0}{2}\right) p_0 s_r$$

where p_0 is the limit pressure and s_r is the ring spacing. Equating internal work with external work, we obtain

$$2M_p \theta + P_y \delta = 4\theta R_0^2 \left(\sin^2 \frac{\alpha_0}{2}\right) p_0 s_r \quad (12-6)$$

where M_p is the plastic moment and P_y is the axial yield load of the effective ring section.

Substitution for δ in Eq. 12-6, gives

$$2M_p + P_y 4R_0 \sin^2 \frac{\alpha_0}{2} = 4R_0^2 \left(\sin^2 \frac{\alpha_0}{2}\right) p_0 s_r \quad (12-7)$$

The limit load of the ring considered in Sec. 12.2.2 will now be estimated using the simple analytical model described above and the results will be compared with those obtained from the nonlinear (material and geometric) finite element analysis of Sec. 12.2.2. Using the same geometric and material quantities as in Sec. 12.2.2 [G, pg 3] and a steel yield stress, F_y , equal 32 ksi, the static limit pressure estimated by Eq. 12-7 is 30 psi as compared with 35 psi from Sec. 12.2.2 [G, pg 10].

The nonlinear finite element analysis of Sec. 12.2.2, using the actual mean material yield stress of 47.2 ksi and a displacement ductility capacity of two, predicted a dynamic pressure strength of 57 psi. For a yield stress of 47.2 ksi, Eq. 12-7 predicts a static limit pressure, p_0 , of 44 psi. Assuming t_d/T is still 0.75 as in Ref. G, and the displacement ductility capacity is two as in Sec. 12.2.2, Fig. 12-3 gives p_v/p_0 of 0.88 for the one degree-of-freedom model with a linearly decaying pressure. Therefore, the maximum dynamic pressure predicted by this model is 50 psi. Again, the one degree-of-freedom model yields a more conservative maximum dynamic pressure. This may partly be attributed to the omission, in the one degree-of-freedom model, of the strain energy due to shearing stresses. In the finite element study the shearing stresses were approximated by linear springs.

A hydrogen explosion in a lower compartment may be assumed to impose a dynamic pressure consisting of a detonation phase followed by a venting phase. As stated in Sec. 12.2.2, the impulse may be idealized to consist of only the venting phase. For the dynamic analyses to be performed in the remainder of this section, the venting time is assumed to be infinite (conservative). Thus, the hydrogen explosion in a lower compartment has been idealized as a suddenly applied constant pressure (Fig. 12-4) acting on the arc of the containment vessel subtended by the compartment in question. With this approximation and a displacement ductility capacity of two, Fig. 12-4 gives p_v/p_0 as 1.33 where p_0 is found from Eq. 12-7. Data and the estimated maximum dynamic pressures, p_v , for the lower level compartments are summarized in Table 12-1. A ring spacing of 120 inches and a yield stress of 47.2 ksi were used in computing the approximate maximum dynamic pressures. The minimum value is 33 psi.

12.2.4 Summary

Preliminary estimates of the dynamic pressure capacity of the lower compartment region in the Sequoyah containment were made. A dynamic, transient finite element analysis of a typical ring with a linearly decaying dynamic pressure was performed. For a displacement

ductility capacity of two, the predicted dynamic pressure strength is 57 psi. An approximate, one degree-of-freedom analysis of a typical ring was also conducted. For this analysis, the dynamic pressure was assumed to be suddenly applied and constant with time. The predicted strength is 33 psi for a given displacement ductility capacity of two. Both of these analyses must be considered quite approximate and, in the authors' opinion, conservative. In particular, the results obtained from the one degree-of-freedom analyses can be considered very conservative since the venting times were assumed to be infinite. More sophisticated analysis techniques with fewer assumptions should be applied.

Table 12-1. Estimated Maximum Dynamic Pressures (Lower Level Compartments)

Compartment	Azimuth (degrees) (approx.)	Arc (degrees)	Shell thickness (in.)	Limit Pressure (psi)	Max. Dyn. Pressure (psi)
Accumulator Room	270-326	56	1 1/2	73	55
Fan Room	326- 34	68	1 1/2	73	55
Accumulator Room	34- 54	20	1 1/2	87	65
Instrument Room	54-126	72	1 1/16	44	33
Accumulator Room	126-146	20	1 1/16	47	43
Fan Room	146-214	68	1 1/16	44	33
Accumulator Room	214-270	56	1 1/16	44	33

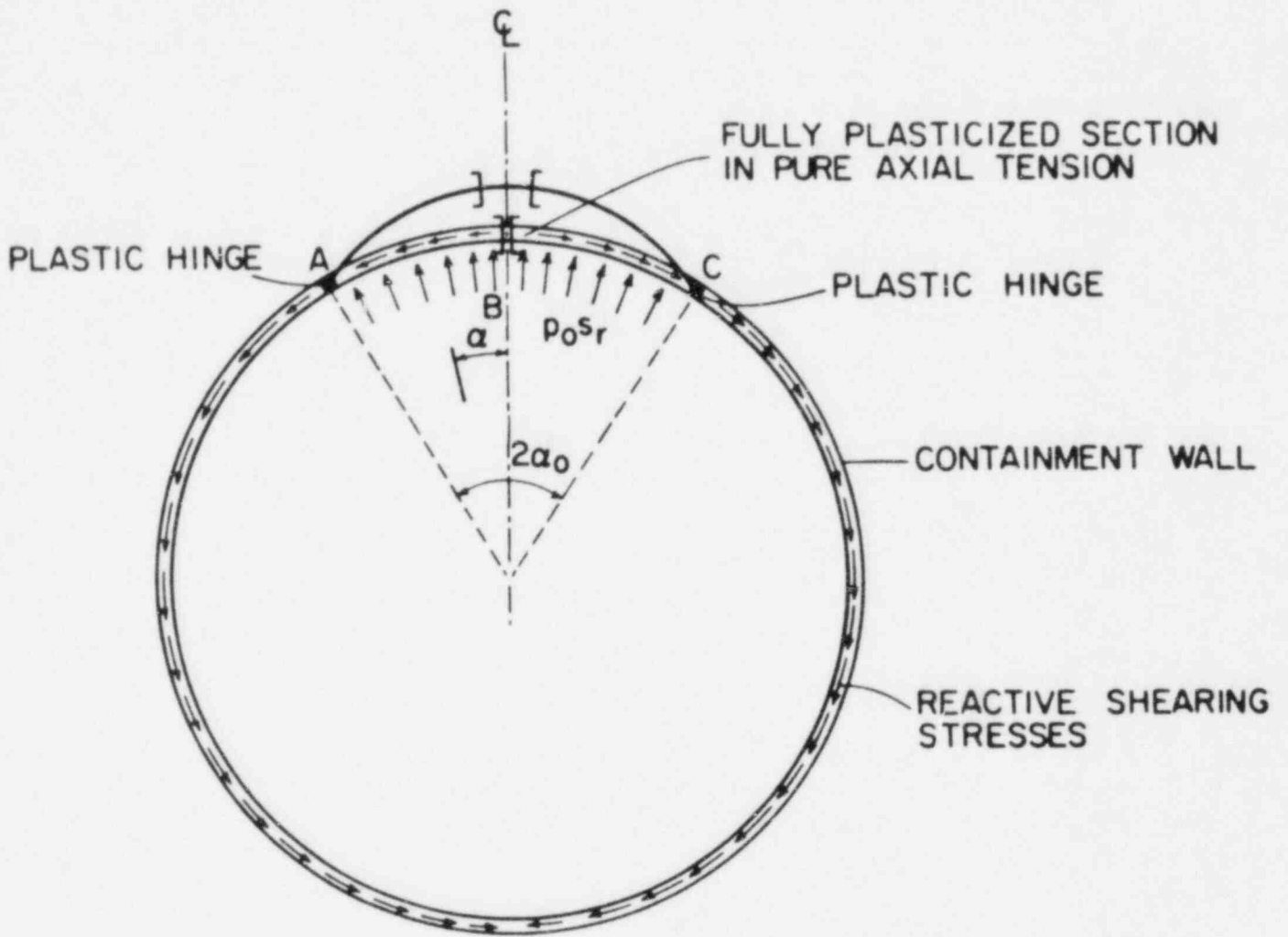


Fig. 12-1. Collapse Mechanism for Ring Section with Effective Shell Width

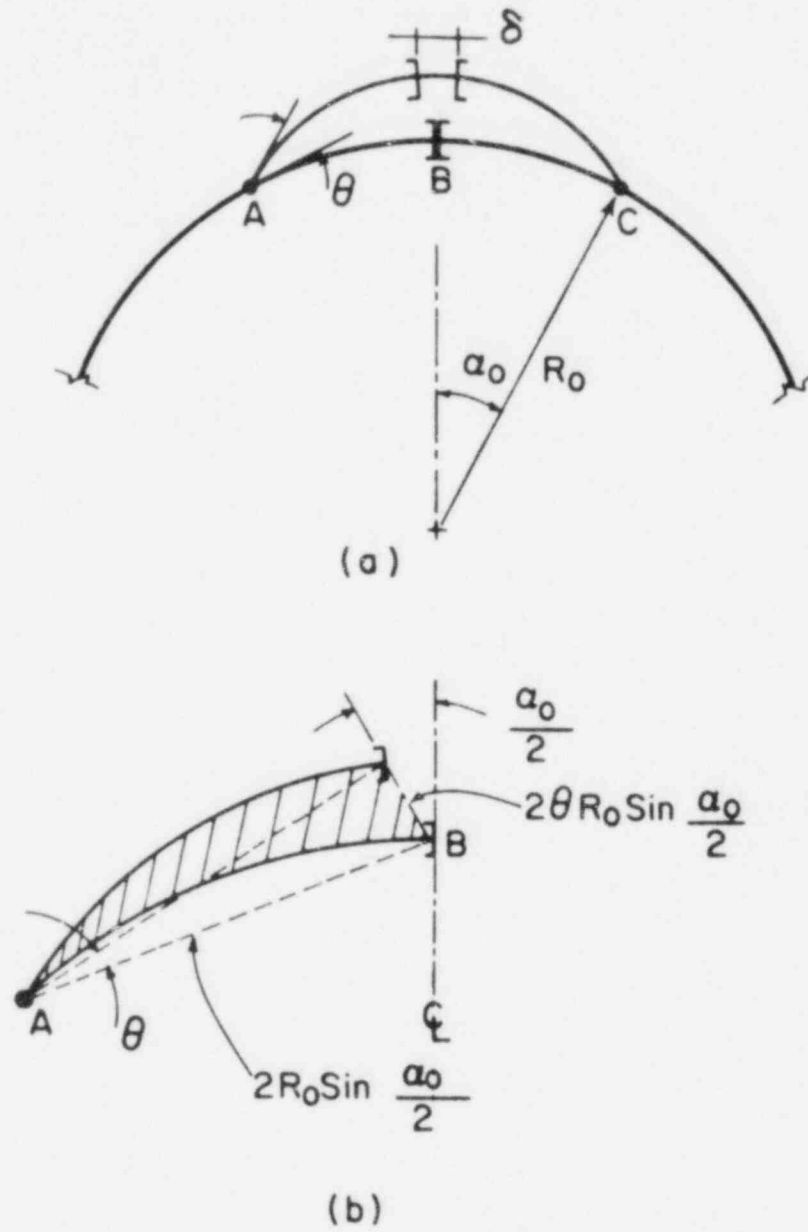


Fig. 12-2. Deformation at Collapse

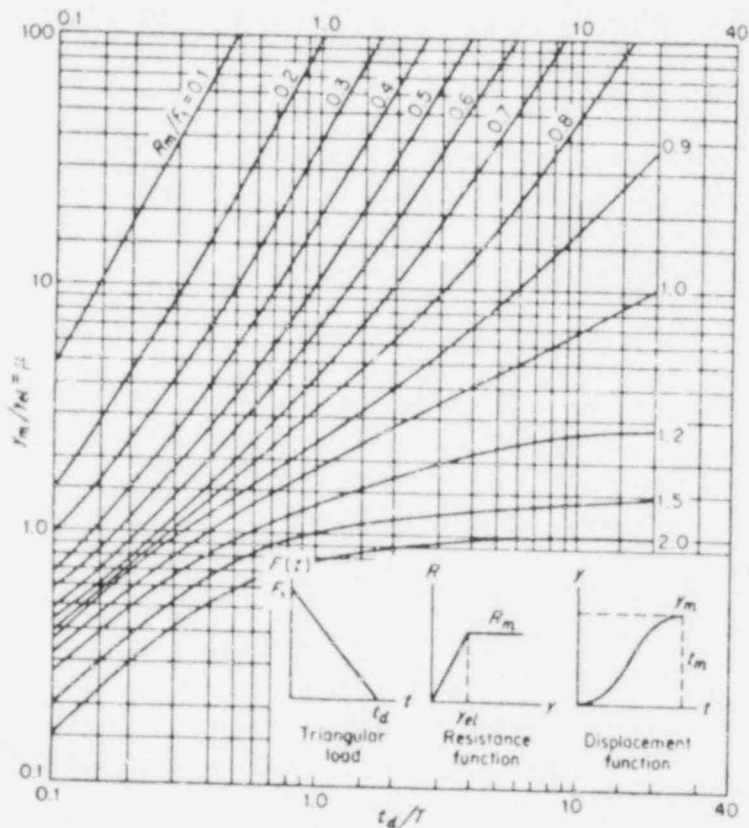


Fig. 12-3. Maximum response of elasto-plastic one-degree systems (undamped) due to triangular load pulses with zero rise time. (U.S. Army Corps of Engineers: "Design of Structures to Resist the Effects of Atomic Weapons," Manual EM 1110-345-415, 1957.)

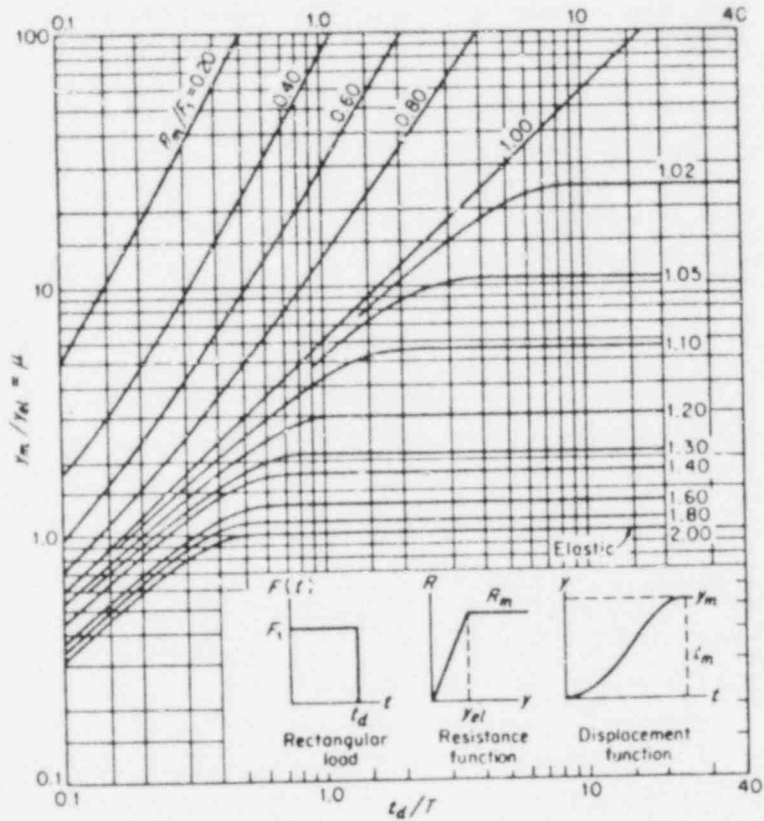


Fig. 12-4. Maximum response of elasto-plastic one-degree systems (undamped) due to rectangular load pulses. (U.S. Army Corps of Engineers: "Design of Structures to Resist the Effects of Atomic Weapons," Manual EM 1110-345-415, 1957.)

12.3 LIST OF REFERENCES FOR ADDENDUM

Copies of References attached following this page.

- A. Greimann, L.F. (Ames Lab.), Letter report to Dr. F.P. Schauer, NRC, Washington, DC, January 22, 1980.
- B. Hubbard, H.W. (R&D Associates), Letter report to Dr. R.L. Tedesco, 8913 Wooden Bridge Road, Potomac, Washington 20851, July 25, 1980 (presented orally at ACRS meeting, September 2, 1980, by F. Parry).
- C. TVA, oral presentation at ACRS meeting, September 2, 1980.
- D. Bagchi, G. (NRC Research), Memorandum to F.P. Schauer, NRC, Washington, DC, August 17, 1980.
- E. Zudans, Z. (Franklin Research Institute), letter report to Dr. R. Savio, NRC, Washington, DC, August 29, 1980.
- F. Orr, R. (Offshore Power Systems), oral presentation at ACRS meeting, September 2, 1980.
- G. Greimann, L.F., letter report to Dr. F.P. Schauer, NRC, Washington, DC, July 18, 1980 and supplement of July 30, 1980.

REFERENCE A

Greimann, L.F. (Ames Lab.), letter report to Dr. F.P. Schauer,
NRC, Washington, DC, January 22, 1980.



ames
laboratory

Energy & Mineral Resources Research Institute

January 22, 1980

Dr. F. P. Schauer, Branch Chief
Division of Systems Safety
Office of Nuclear Reactor Regulation
Nuclear Regulatory Commission
Washington, DC 20555

SUBJECT: AMES LABORATORY TECHNICAL ASSISTANCE TO THE DIVISION OF SYSTEM SAFETY, NUCLEAR REACTOR REGULATION - "REVIEW OF NUCLEAR PLANTS STRUCTURAL DESIGN" (FIN NO. A-4131). PRELIMINARY CALCULATION OF ULTIMATE STRENGTH OF SEQUOYAH AND MCGUIRE CONTAINMENT VESSELS

Dear Dr. Schauer:

As you requested in our telephone conversation of January 16, 1980, I have performed a preliminary calculation of the ultimate strengths of the Sequoyah and McGuire Containment Vessels. The following assumptions and limitations apply to these calculations:

- (1) Uniform static internal pressure loading.
- (2) Shell stiffeners are "smeared" for stress calculation.
- (3) Von Mises failure criterion applies.
- (4) Penetrations do not control; i.e., ASME area-replacement rule is satisfied.
- (5) Ultimate strength is defined as the pressure at which stresses in the equivalent "smeared" shell reach the minimum specified yield stress. (Burst pressures are not considered reliable at this time because of the potentially limited ductility of the vessel.)

Copies of the calculations are enclosed. In summary, the preliminary calculated ultimate strengths are 36 psi for the Sequoyah and 47 psi for the McGuire containment vessel. In my judgment, the actual ultimate strengths are probably between -10 percent and +30 percent of these values. The actual value may be less because Assumption (1) underestimates the shell stresses, although the shell does not control. The actual value may be greater because Assumption (1) overestimates the ring stresses, which do control; Assumption (5) is conservative; and the actual material yield strength is probably greater than the minimum specified.

Dr. F. P. Schauer

- 2 -

January 22, 1980

As per the statement of work on the subject project, we intend to continue to refine the above estimates of the ultimate strength and the associated uncertainties. If you have any questions, please contact me.

Sincerely,

Lowell F. Greimann
Project Engineer

Enclosure

cc: Director, Division of System Safety (Attn: B. L. Grenier) w/encl.
Delwyn D. Bluhm, Head, Project Engineering w/encl.

Sequoyah Containment
Ultimate Strength

Dr. L. F. Greimann

F. Farous

JAN. 21, 1980

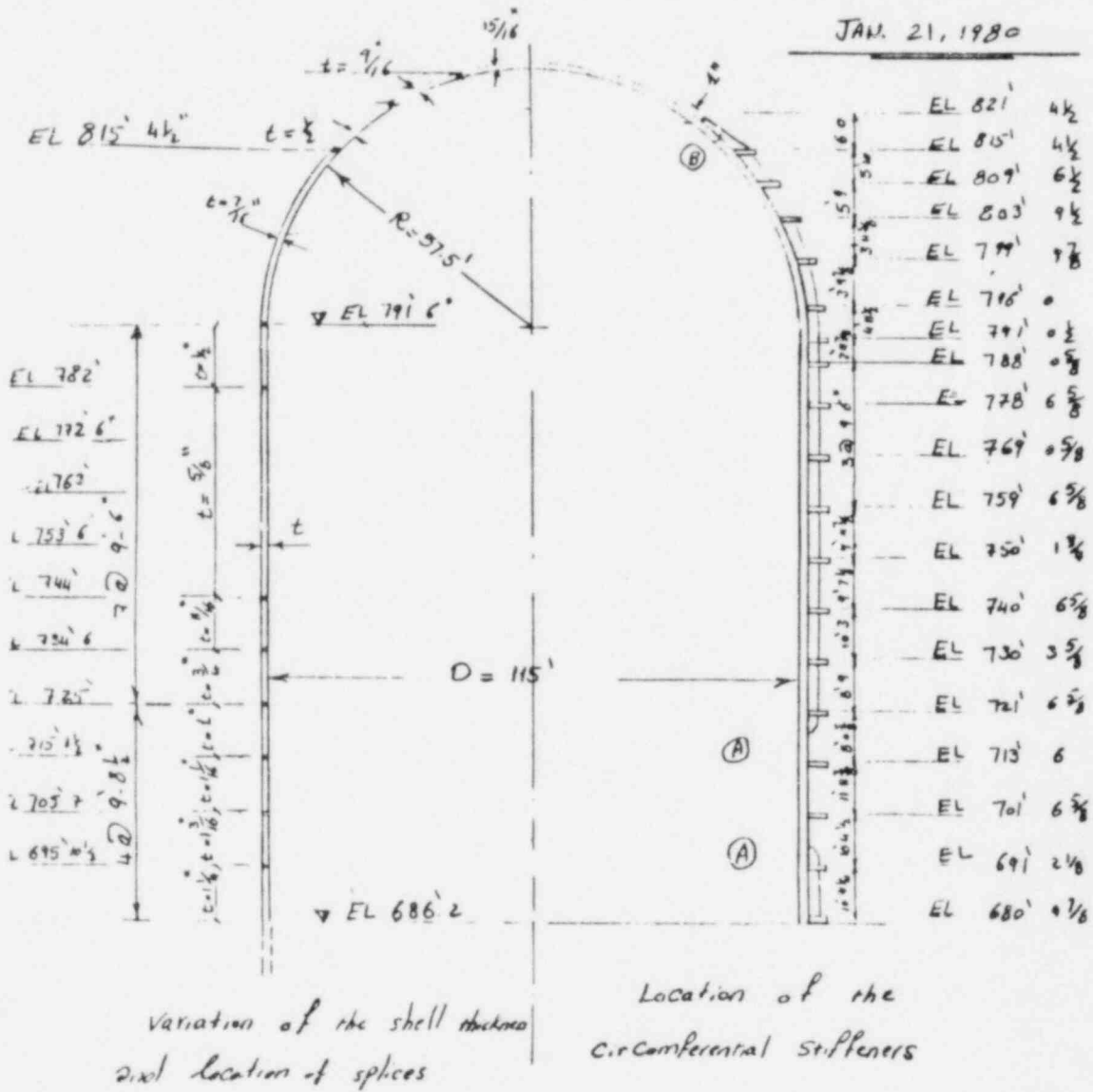


Figure 1

Not to scale

Assumptions

↳ Stresses in ring/stringer stiffened shell are approximately equal to stresses in equivalent shell with "smeared" stiffeners. For example, in cylinder

$$\sigma_{\theta} = \frac{Pr}{t_{e\theta}} \quad (\text{Circumferential stresses})$$

$$\sigma_v = \frac{Pr}{2t_{ev}} \quad (\text{Vertical stresses})$$

where:

$$t_{e\theta} = t + \frac{A_r}{s_r} \quad \text{"equivalent circumferential thickness"}$$

$$t_{ev} = t + \frac{A_s}{s_s} \quad \text{"equivalent meridional thickness"}$$

A_r, A_s = Area of ring and stringer stiffeners, respectively

s_r, s_s = spacing of ring and stringer stiffener respectively

This assumption predicts stresses too low in the shell and too high in the stiffeners.

2- Von Mises failure criteria applies in regions of two dimensional stresses.

3- The limit pressure was assumed to occur when the stresses reached the specified material yield stress. This is a conservative assumption because:

- a) The material yield stress is, most likely, greater than the minimum specified yield stress.
 - b) Yielding does not necessarily imply failure (although by assumption (1), gross yielding is implied)
- 4- Burst pressures were calculated by setting the calculated stresses equal to the material ultimate strength. This calculation is not very reliable because burst pressures imply large deformations. Thus,
- a) Assumption (1) and (2) are not confirmed
 - b) The containment may contact the shield building
 - c) Weld and joints may not have the required ductility
- 5- The ASME area replacement rule is satisfied for all penetrations and, hence, the strength of the penetrated shell is greater than the strength of the unperforated shell.

Equivalent Circumferential for the
Containment vessel

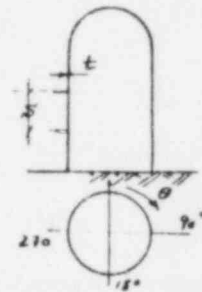


Table 1.

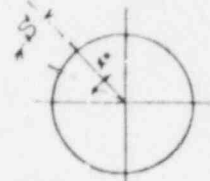
EL	St. FT. DIM. IN.	Ar IN ²	Sr IN.	Ar/S ₂ IN.	t IN.	t _{eq} IN.	
691	2 1/8	18 x 1 1/4	22.5	124.375	0.1809	1 1/4	1.4309
701	6 5/8	17 15/16 x 1 1/4	22.42	133.938	0.1674	1 3/16	1.3549
713	6	19 7/8 x 1 1/4	24.2968	120	0.2025	1 1/16	1.2650
721	6 5/8	17 3/4 x 1 1/4	22.19	100.813	0.2201	1	1.2201
730	3 5/8	19 1/4 x 1 1/4	24.06	114	0.2111	3/4	0.9611
740	6 5/8	19 3/16 x 1 1/4	23.98	119.063	0.2014	1/16	0.8809
750	1 3/4	19 1/8 x 1 1/4	23.91	114	0.2097	5/8	0.8347
759	6 5/8	19 1/8 x 1 1/4	23.91	113.438	0.2108	5/8	0.8356
769	0 5/8	20 x 1 1/4	25.0	114	0.2193	5/8	0.8443
778	6 5/8	17 1/2 x 1 1/4	21.41	114	0.1878	5/8	0.8128
788	0 5/8	16 x 1 1/4	20	74.938	0.2669	1/2	0.7669
791	0 1/2	16 x 1	16	47.453	0.335	7/16	0.7725
796	0	18 x 1 1/4	22.5	53.3125	0.4220	7/16	0.8595
799	9 7/8	16 x 1	16	48.2032	0.3319	7/16	0.7694
803	9 1/2	16 x 1	16	60.750	0.2634	7/16	0.7009
809	6 1/2	16 x 1	16	74.9063	0.2136	7/16	0.6511
815	4 1/2	16 x 1	16	77.125	0.2075	7/16 + 1/2	0.645
> 815 4 1/2 to Crown	0	0	—	0	smallest t = 0.5	0.5	0.5

Cylinder
↑
Head

Notes:-

- 1- Dimensions of the stiffeners were found from drawing sheet # 48N410
- 2- Since the same ring dimensions varied around the circumference, the smallest dimensions were to find A_r
- 3- The smallest shell thickness was used to find t , if the shell thickness varies between two stiffeners
- 4- The distance S_r was calculated along the sphere perimeter for the shell head.
- 5- Drawings # 36, 90, 91, 92, 48N409 and 48N410 were used to find the information needed to calculate the equivalent thickness.

Equivalent meridional thickness for
the Containment Vessel



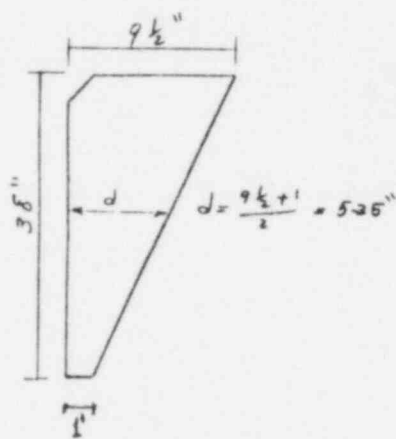
- 1- $S_3 = R \theta \frac{\pi}{180} = 48.171 \text{ IN.}$
- 2- ALL vertical stiffeners = PL. $9\frac{1}{2} \times \frac{1}{2} \text{ IN}$
- 3- There are no vertical stiffeners between EL. $691' 2\frac{1}{8}''$ and EL. $721' 6\frac{5}{8}''$
- 4- $A_s = \text{Area of vertical stiff} = 4.75 \text{ IN}^2$
 $A_s/S_3 = 0.09861 \text{ IN}$

Table 2

Cylinder			Head		
EL	t IN	t _v IN	EL	t	t _v
691' 2 $\frac{1}{8}$ "	1 $\frac{1}{4}$	1.25	796	7/16	0.5361
701' 6 $\frac{5}{8}$ "	1 $\frac{3}{8}$	1.1875	799' 4 $\frac{7}{8}$ "	7/16	0.5361
713' 6"	1 $\frac{1}{8}$	1.0625	803' 7 $\frac{1}{2}$ "	7/16	0.5361
721' 6 $\frac{5}{8}$ "	1	1	809' 6 $\frac{1}{2}$ "	7/16	0.5361
730' 3 $\frac{5}{8}$ "	3/4	0.8486	815' 4 $\frac{1}{2}$ "	7/16	0.514
740' 6 $\frac{5}{8}$ "	1 $\frac{1}{8}$	0.78611	> 815' 4 $\frac{1}{2}$ "	1/2"	0.5
750' 1 $\frac{3}{4}$ "	5/8	0.7236	To Crown	smallest the others	
759' 6 $\frac{5}{8}$ "	5/8	0.7236			
769' 0 $\frac{5}{8}$ "	5/8	0.7236			
778' 6 $\frac{5}{8}$ "	5/8	0.7236			
788' 0 $\frac{5}{8}$ "	1/2	0.59861			
791' 0 $\frac{1}{2}$ "	1/2	0.59861			

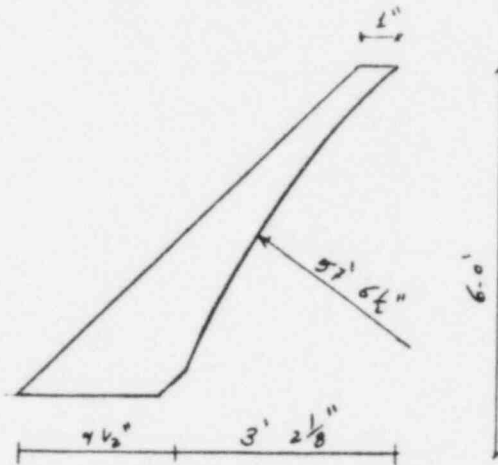
Note:-

- 1- The stiffeners Dimension were found from Drawings number 48N409 and 48N410
- 2- Details of stiffeners A, B (see Figure 1)



DET. A.

Not to scale



DET B

Not to scale

- 3- The effect of the vertical stiffener is neglected at EL. 691 2 1/8 & EL 721 6 5/8, since it doesn't pass the midpoint of ELs 691 2 1/8, EL 701 6 5/8 and EL 713 6 and 721 6 5/8
- 4 - AT EL. 815' 4 1/2"

$$t_c = 0.098 \frac{1}{2} + \frac{((9\frac{1}{2} + 1)/2) \cdot \frac{1}{2} + \frac{7}{16}}{48.171} = 0.514$$

Material Properties

material used is SA 516 Gr 60

minimum specified yield stress = 32 ksi

ultimate stress = 60 ksi

Calculation of limit pressure

Using Von Mises Equation

$$\sigma_y = [\sigma_\theta^2 + \sigma_v^2 - \sigma_\theta \sigma_v]^{1/2}$$

where

$$\sigma_\theta = \frac{P_r r}{t_{e\theta}} \quad ; \quad \sigma_v = \frac{P_r r}{2t_{ev}} \quad \text{Cylindrical shell}$$

$$\sigma_\theta = \frac{P_r r}{2t_{e\theta}} \quad ; \quad \sigma_v = \frac{P_r r}{2t_{ev}} \quad \text{Hemispherical shell}$$

$$\sigma_\theta = 0 \quad ; \quad \sigma_v = \frac{Pr}{2t_{ev}} \quad \text{Vertical stiff.}$$

$$\sigma_\theta = \frac{P_r r}{t_{e\theta}} \quad ; \quad \sigma_v = \text{zero} \quad \text{Ring stiff. on "cylinder"}$$

Burst Pressure

use σ_u instead of σ_y in the above Eq.
(Reference 1), pg 6

Ref. 1

EC. Rodabaugh, "Interpretive Report on Limit Analysis and Plastic Behavior of Piping Products" to Test Group on Characterization of Plastic Behavior of Structures, PVCC, October 1976.

Limit Pressure For
cylinder & sphere

	EL.	Limit Pressure P _{si}	Burst Press. P _{si}		
cylinder ↑	691	2 1/8	76.3605	72.442 Controls.	
	701	6 7/8	72.3176		
	717	6	67.3360		
	721	6 5/8	64.8167		
	730	3 5/8	51.3181		
	740	6 7/8	42.0037*		
	750	1 3/4	38.6358*		
	759	6 5/8	44.5799		
	769	0 5/8	45.0052		
	778	6 5/8	43.4167		
	788	0 5/8	40.5380		
	791	0 1/2	40.7986		
	796	0	56.8406		
	799	7 7/8	55.9906		
	803	7 1/2	56.0095		
	809	6 1/2	53.7901		
	815	4 1/2	52.0755		
	>815	4 1/2'	46.3768		
		To crown			

* These results were presumed in the original report. They are in error and should be 47.5 and 44.5, respectively.

Yield Pressure for Stiffeners

1- Ring stiff.

$$\text{cylinder: } \rightarrow \sigma_y = \frac{P_y r}{t_{c\theta}} \quad ; \quad \text{sphere } \sigma_y = \frac{P_y r}{2t_{c\theta}}$$

In the ring direction use min. $t_{c\theta}$, From table 1

$$t_{c\theta \text{ min}} = 0.7669 \text{ in} \quad \text{cylinder @ Elev. } 790' \text{ } 0.5\%$$

$$t_{c\theta \text{ min}} = 0.645 \text{ in} \quad \text{sphere}$$

$$P_y = \frac{32000 \times 0.7669}{690} = \underline{\underline{35.566 \text{ Psi}}}$$

$$\text{OR } P_y = \frac{32000 \times 0.645}{690} = 59.827 \text{ Psi}$$

2. Vertical stiff.

$$\text{cylinder} \quad \sigma_y = \frac{P_y r}{2t_{cv}}$$

$$\text{sphere} \quad \sigma_y = \frac{P_y r}{2t_{cv}}$$

use min t_{cv} which is 0.514 (see table 2)

$$\therefore P = \underline{\underline{47.675 \text{ Psi}}}$$

To calculate the burst Pressure

use σ_u instead of σ_y , and the stress in the Ring stiffness controls

$$\begin{aligned} P_b &= \frac{\sigma_u t_{cs}}{r} \\ &= \frac{60000 \times 7669}{690} = \underline{\underline{66.687 \text{ Psi}}} \end{aligned}$$

REFERENCE B

Hubbard, H.W. (R&D Associates), letter report to Dr. R.L. Tedesco, 8913 Wooden Bridge Road, Potomac, Washington 20851, July 25, 1980 (presented orally at ACRS meeting, September 2, 1980, by F. Parry)

25 July 1980

Dr. Robert L. Tedesco
8913 Wooden Bridge Road
Potomac, Maryland 20854

Dear Dr. Tedesco:

The enclosed document is a critique of the Ames analysis of the Sequoyah containment structure. The critique was performed by R & D Associates at the request of Commissioner Victor Gilinsky, who asked that a copy be supplied to you on its completion.

Very truly yours,

Harmon W. Hubbard

HWH/dl

Enclosure: "Sequoyah Containment Analysis," July 1980,
(1 cy).

SEQUOYAH CONTAINMENT ANALYSIS

1. INTRODUCTION

This letter report is in response to a request from the U.S. Nuclear Regulatory Commission to review and critique the ultimate strength analyses of the Sequoyah containment.

The description of the containment vessel and the analysis for review were provided in the NRC Information Report dated 22 April 1980, Ref. SECY-80-107A. The tasks requested in the work statement were as follows:

1. To what extent are the assumptions in the analyses conservative?
2. To what extent is the calculated ultimate strength conservative?
3. What are the uncertainties in the analyses, methods, and models?
4. To what extent is there assurance of no gross leakage from the vessel at stresses above the design stress and yield stress?
5. How would the analyses and results be altered if the stresses are caused by ignition/detonation of 300-600 kg of hydrogen distributed uniformly and nonuniformly in the containment?
6. To what extent can distributed ignition sources mitigate the effects of hydrogen?

This report will cover the first four tasks of the work statement. A report on the hydrogen problem, tasks 5 and 6, will be issued separately. A preliminary briefing of the analyses conducted by RPA was given to Commissioner Gilinsky and Dr. J. Austin at RPA on 18th July 1980.

2. BACKGROUND - SEQUOYAH CONTAINMENT VESSEL DESIGN

The containment vessel for Sequoyah is a low-leakage, free-standing steel structure consisting of a cylindrical wall, a hemispherical dome, and a bottom liner plate encased in concrete. Figure 1 shows the outline and configuration of the containment vessel.

The structure consists of side walls measuring 113 feet 8-5/8 inches in height from the liner on the base to the spring line of the dome and has an inside diameter of 115 feet. The bottom liner plate is 1/4 inch thick, the cylinder varies from 1-3/8 inch thickness at the bottom to 1/2 inch thick at the spring line and the dome varies from 7/16 inch thickness at the spring line to 15/16 inch thickness at the apex.

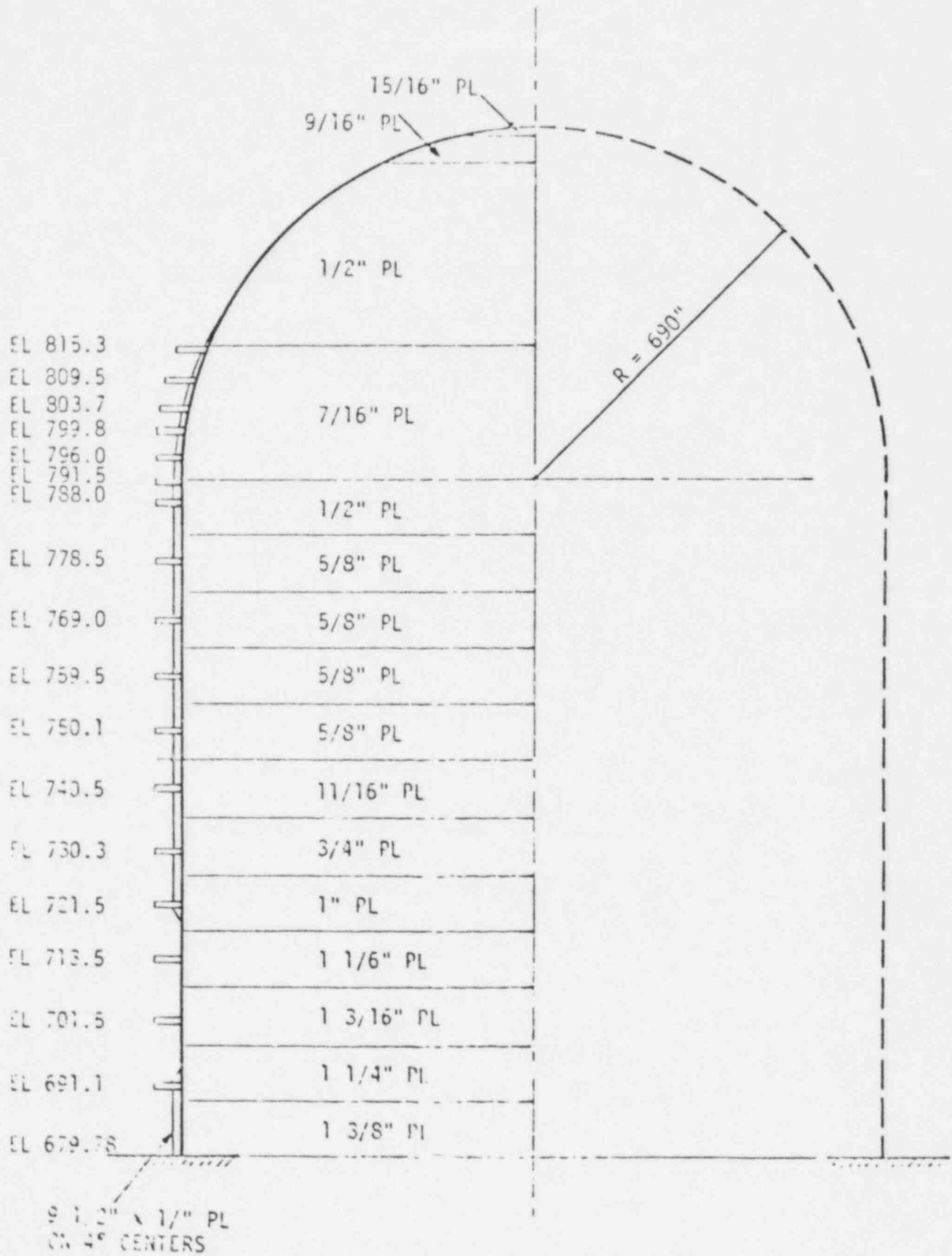
The containment vessel is provided with both circumferential and vertical stiffeners on the exterior of the shell. These stiffeners are required to satisfy design requirements for expansion and contraction, seismic forces, and pressure transient loads. The circumferential stiffeners were installed on approximately 20-foot centers during erection to insure stability and alignment of the shell. Vertical stiffeners are spaced at 4 degrees and other locally stiffened areas are provided for penetration, etc., as required.

The design of the containment vessel was to the requirements of the ASME Code, Section III, Subsection B. The Code includes cases 1177-5, 1290-1, 1330-1, 1413, 1431, and the Winter 1968 Addenda.

The following pressures and temperatures were used in the design of the vessel:

Overpressure test (1)	13.5 psig
Maximum internal pressure (2)	12.0 psig at 200°F
Design internal pressure (2)	10.8 psig at 220°F

Figure 1. Sequoyah Containment Vessel



Leakage rate test pressure	12.0 psig
Design external pressure	0.5 psig
Lowest service metal temperature	30° F
Operating ambient temperature	120° F
Operating internal temperature	120° F

- (1) 1.25 times design internal pressure as required by ASME Code, UG-100(b).
- (2) See Paragraph N-1312(2) of Section III of the ASME Code which states that the "design internal pressure" of the vessel may differ from the "maximum containment pressure" but in no case shall the design internal pressure be less than 90 percent of the maximum containment internal pressure.

The steel plate used is to ASME specifications SA-516 grade 60 with a yield stress of 32,000 psi, an ultimate stress of 60,000 psi and a Young's Modulus, E, of 28×10^6 psi at 70°F. For the above code, the maximum shear stress criterion yields an equivalent maximum membrane principal stress, in the hoop direction, given by:

$$\text{hoop stress} = \frac{PR}{t} = \text{allowable stress, where } P = 10.8 \text{ psi}$$

$R = 690 \text{ in.}$

(the given allowable stress in the 1977 version of the code is 16,500 psi (i.e., approximately 1/2 the yield stress)).

Hence,

$$t = \frac{10.8 \times 690}{16,500} = 0.452 \text{ in.}$$

Thus, the minimum plate thickness of 1/2 inch satisfies the basic code requirements.

Originally the vessel was designed with only seven ring stiffeners and local vertical stiffeners at penetration

regions. Detailed buckling analysis and acoustic excitation analysis showed, however, that additional rings and vertical stiffeners would be required and the final configuration of Figure 1 resulted. It should be noted that the longitudinal, or meridional, stresses in a cylindrical membrane are only half of the hoop stress and hence do not contribute to the maximum shear criterion of the ASME Code. Further the dome stresses are all of the same type ("meridional" as opposed to "hoop") and hence with the plate thicknesses used the dome membrane stresses are much less than the critical cylindrical stresses.

3. THE ANALYSIS OF A SHELL WITH RING AND STRINGER STIFFENERS

The application of rings and stiffeners to a membrane structure is well known in aircraft structural analysis and must be treated with caution since local bending stresses can be induced. It was noted that the analysis provided in the reference document SECY-80-107A used a "smearing" technique whereby the rings and longitudinal stiffeners (or "stringers") are smeared out over the membrane thickness thereby increasing the effective thickness of the membrane and hence its pressure capability. It is well known, however, in aircraft structural analysis that in general this cannot be done. The problem is succinctly described in the following extract from "Analysis and Design of Flight Vehicle Structures," E. F. Bruhn, Purdue University, Tri-State Offset Company, 1965. (Library of Congress Card #64-7896).

Because of functional requirements over and above those of a simple pressure vessel, the pressurized cabin shell of an airplane has a number of stress analysis problems peculiar to its configuration. Several of the more general of these will be considered here.

To stabilize the shell wall in transmitting heavy tail loads through the fuselage, longitudinal stringers are added. These same stringers will also help to carry the meridional

pressure loads. The skin and stringers must, of course, have equal strains in the longitudinal directions but, because the skin is in a two-dimensional state of stress, they cannot have equal longitudinal stresses: hence the following analysis.

Let the meridional (longitudinal) stresses in the skin and stringers be S_M and S_L , respectively. S_t will be the tangential (hoop) stress in the skin. We have

$$S_t = \frac{PR}{t}$$

If N is the total number of stringers, each of cross sectional area A_L , then equilibrium longitudinally requires

$$P \pi R^2 = 2 \pi R t S_M + N A_L S_L.$$

The condition of equal longitudinal strain in the skin and stringers yields

$$E \epsilon = S_L = S_M - \mu S_t$$

where μ is Poisson's ratio (= .27 for steel).

Solving these three equations one finds

$$S_t = \frac{PR}{t}$$

$$S_M = \frac{PR}{2t} \frac{(1 + 2\mu\alpha)}{(1 + \alpha)} = \frac{PR}{2t} \frac{(1 + 0.54 \alpha)}{(1 + \alpha)}$$

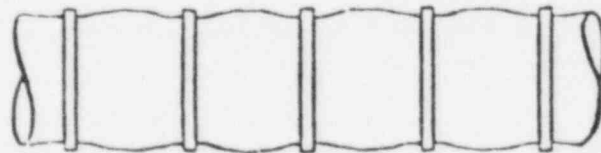
$$S_L = \frac{PR}{2t} \frac{(1 - 2\mu)}{(1 + \alpha)} = \frac{PR}{2t} \frac{0.46}{(1 + \alpha)}$$

where $\alpha = N A_L / 2\pi R t$ is the ratio of total stringer area to skin area. A little study will show that $t(1 + \alpha)$ is a sort

of "effective shell wall thickness": it is the result of taking all the cross sectional area (skin plus stringers) and distributing it uniformly around the perimeter. On this basis, the results are a little disappointing: the stringers are carrying only 40% of the stress one might expect if the net longitudinal load ($p \pi R^2$) were distributed evenly over the entire cross sectional area ($2 \pi R t (1 + \alpha)$). Thus the meridional skin stresses are reduced by the factor $(1 + .6 \alpha) / (1 + \alpha)$ from what they would be without the stringers.

Because of the necessity for transmitting various concentrated loads from within the cabin and from the wings and tail to the main shell and because it is also necessary to provide some lateral restraint which will stabilize the stringers and skin against an overall instability failure, the pressurized fuselage of an airplane contains a considerable number of rings and frames distributed along the length of the shell. These rings are seldom, if ever, spaced closely enough such that they can be considered effective in carrying a part of the hoop stresses (in the way the stringers were effective in carrying part of the meridional stress). Rather, they act more like widely spaced restraining bands having the effect shown exaggerated in Figure 2.

Figure 2. Restraining rings along a pressurized tank. The action is representative of a fuselage with widely spaced rings inside.



It is obvious that the rings in this case will produce secondary bending stresses in the skin and hence may have a detrimental effect on the simple membrane stress system.

equally harmful are the tensile loadings developed in the rivets joining the skin and rings. (End of Extract)

4. STRINGER EFFECTIVENESS

Following the method of Section 3 above and Figure 3 illustrates the application of the longitudinal stiffeners to the Sequoyah vessel. In calculating the meridional stresses an "effective" pressure is used, which is the internal pressure of the container less that pressure which is needed to support the structural weight above the section under consideration. Thus, at the critical 1/2 inch plate section (top of the cylinder) a dome weight of about 550,000 lb has to be supported and this is equivalent to an internal pressure of about 0.37 psi, and the internal pressure has to exceed this value before a meridional tension stress can be achieved. At the base the equivalent pressure to offset the overall weight of the container (about 2.3 million lb) is 1.54 psi.

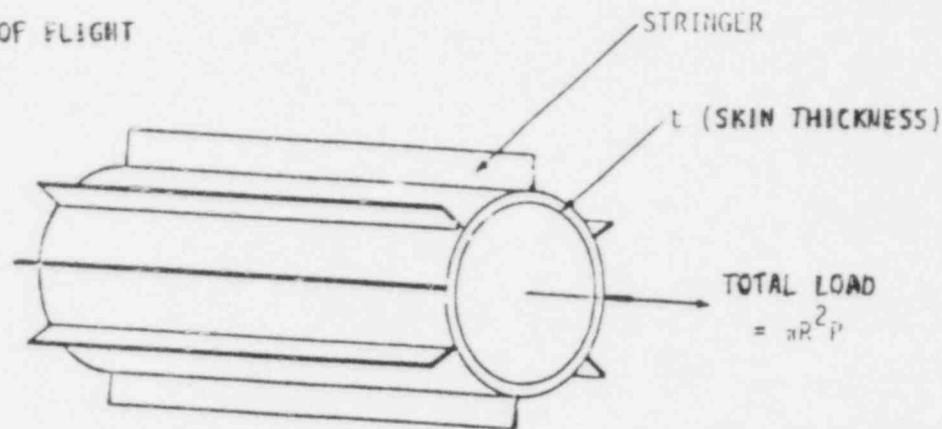
It is seen from Figure 3 that the stringers are stressed to only about 40% of the amount of the meridional stress in the membrane. Of the total longitudinal load the membrane carries 93% and the stringers only 7%. It is therefore clearly incorrect to assume that the stringer cross sectional area can be "smeared" out fully over the membrane - the smearing technique can be used but by using about 40% of the stringer cross sectional area.

5. RING STIFFENER EFFECT

The analysis of thin walled cylinders with ring stiffeners is treated in detail in "Beams on Elastic Foundation" by M. Hetenyi (University of Michigan Press 1946) pages 83-84. Figure 4 shows the results of this analysis applied to the cylindrical section of the Sequoyah vessel. It is seen that the ring stiffeners have to be spaced very much closer than 80 inches to have any appreciable reduction on the membrane

Figure 3. Stringer Effectiveness

- REF "ANALYSIS AND DESIGN OF FLIGHT VEHICLE STRUCTURES" BRUHN



TOTAL STRINGER C.S. AREA = A, STRESS = S_L

SKIN STRESS (MEMBRANE): S_t (HOOP) = PR/t , S_M (MERIDIONAL) = ?

LONGITUDINAL EQUILIBRIUM: $\pi R^2 P = 2\pi R t S_M + A S_L$

EQUAL LONGITUDINAL STRAIN $\epsilon = \frac{S_L}{E}$ (STRINGER)

$= \frac{S_M - \mu S_t}{E}$ (SKIN) ($\mu = 0.3$, POISSONS RATIO)

SOLUTION: $S_M = \frac{PR}{2t} \left[\frac{1 + 0.6a}{1 + a} \right]$

$S_L = \frac{PP}{2t} \left[\frac{0.4}{1 + a} \right]$ $a = \frac{A}{2\pi R t}$

$R = 690''$ $t = 1/2''$

$P = 12$ PSI (EFFECTIVE)

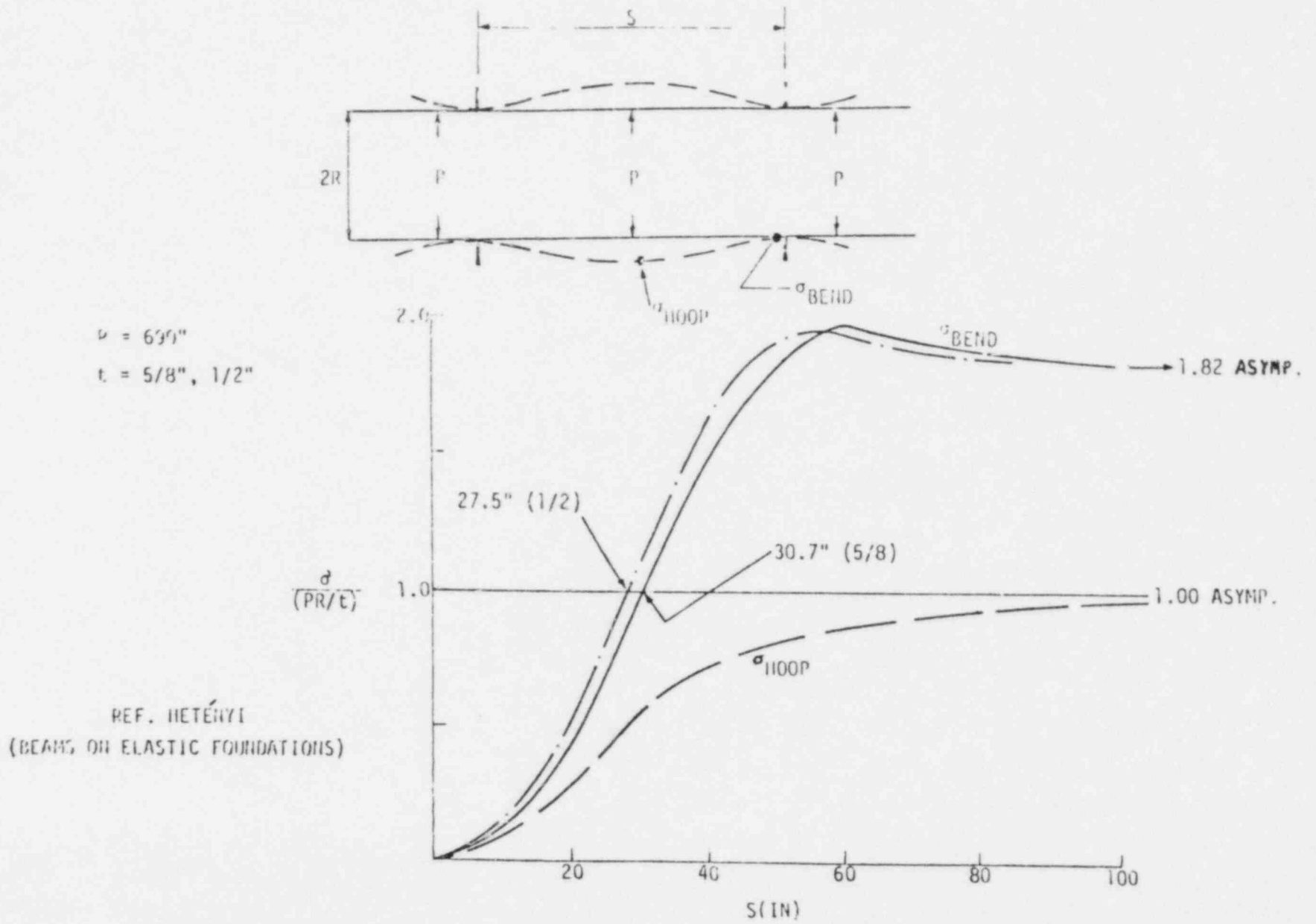
$A = 90 \times 4.75 = 427.5$ in

$a = 0.197$

$PR/2t = 8280$
$S_M = 7235$
$S_L = 2767$

NOTE: SKIN CARRIES 16.8 MILLION LB (93%) STRINGERS 1.2 MILLION LB (7%) OF TOTAL LOAD OF 18 MILLION LB.

Figure 4. Ring Stiffener Effect



hoop stress. Further local bending stresses at the attachment to the ring which are greater than the unmodified hoop stress are generated when the ring spacing is in excess of 27.5" to 20.7" (respectively for 1/2" and 5/8" plate). Since the actual design ring spacings are at 10 ft two conclusions may be drawn:

- a. Membrane hoop stresses in a considerable region between the ring stiffeners is for practical purposes not influenced by the ring stiffeners.
- b. A local bending stress at the ring attachment to the shell is induced and this stress is some 80% higher than the simple membrane hoop stress.

Thus, the critical region for hoop stress will be the 1/2 inch plate midway between the two rings. (This occurs between rings at elevations 778.5 and 788.0 shown in Figure 1). This section has the upper 2/3 of 1/2 inch plate and the lower 1/3 of 5/8 inch plate, and hence the mid-section area of criticality is in the 1/2 inch plate). In this case the critical internal pressure may be calculated as follows:

$$\begin{aligned} \text{yield stress (= 32,000 psi)} &= PR/t \\ (R = 690 \text{ in.}, t = 1/2 \text{ in.}) & \\ \text{giving } P &= 23.2 \text{ psi} \end{aligned}$$

This corresponds to the Boiler Code Max Shear Stress Criterion for yield. If ultimate strength is used then this pressure would be scaled up in the ratio of ultimate to yield stresses (60,000 to 32,000 psi) giving a value of 43.5 psi.

The corresponding longitudinal stress would be half the hoop stress in a simple unstiffened cylinder. As shown in Section 4, the membrane longitudinal stress is reduced by a factor of 0.87 due to the presence of the stringers. An alternative method to the minimum shear stress method of the Boiler Code is to use Von Mises criteria which determines the critical

stress as a function of both the hoop stress (σ_t) and the longitudinal or meridional stress (σ_M). This is given by:

$$\sigma_{crit} = \sqrt{c_M^2 + \sigma_t^2} - \sigma_M \sigma_t$$

In this case $\sigma_M = 0.5 \times 0.87\sigma_t = 0.435 \sigma_t$

Hence $\sigma_{crit} = 0.868\sigma_t$

Hence, for the Von Mises criteria the critical pressures corresponding to yield and ultimate stresses are respectively 26.8 and 50.3 psi.

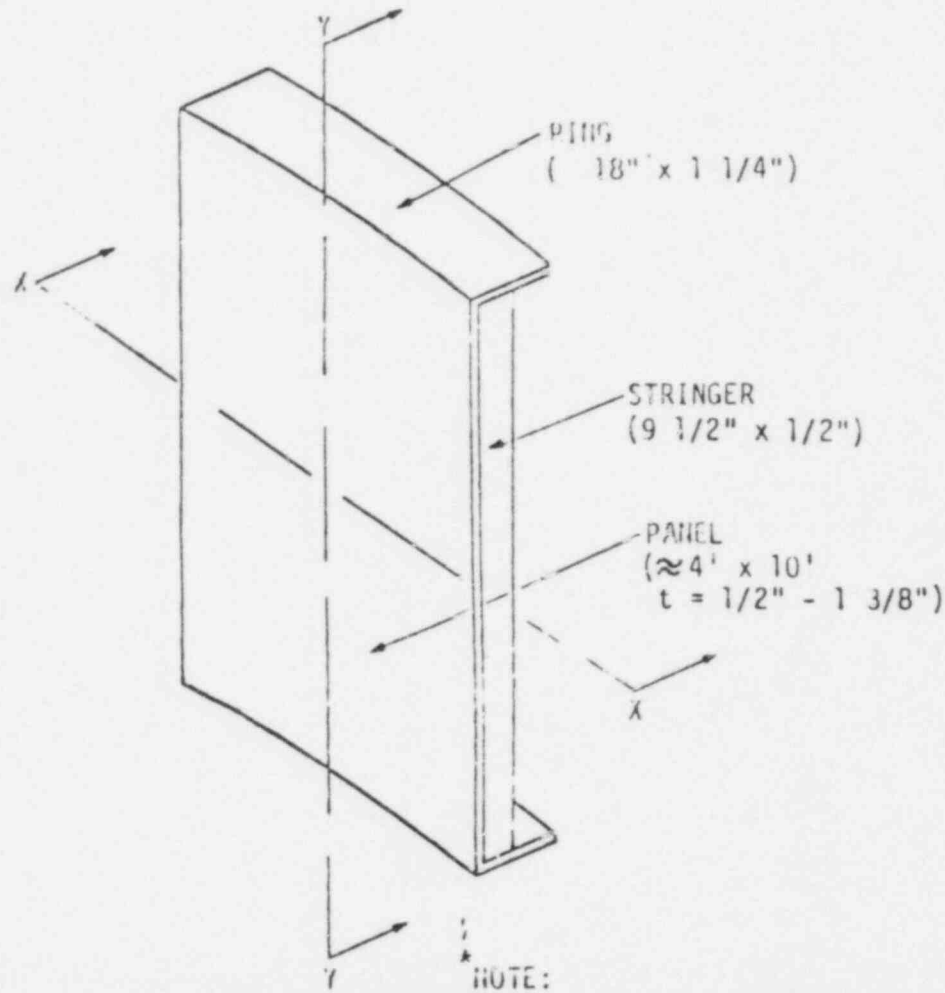
6. ALTERNATIVE PANEL ANALYSES

An alternative approach, in order to determine local stress regions induced by the rings and stringers, is to consider the cylinder to be a number of rectangular panels framed by ring sectors and stringer sections as shown in Figure 5. Thus, the cylinder is composed of a number of panels approximately 4 ft by 10 ft as shown with thicknesses varying from 1/2 in. to 1 3/8 in. A comparison of the bending stiffness of the panel and the rings and stringers is shown in Figure 5. The cross sectional moment of inertia about the bending axis is a measure of the stiffness of a beam. In the case of a panel bending as a beam there is an additional term due to a Poisson's Ratio (ν) contribution. This is, however, only a 10% effect (proportional to $1 - \nu^2$, and $\nu = 0.27$) and is neglected in calculating the moment of inertia of the panel.

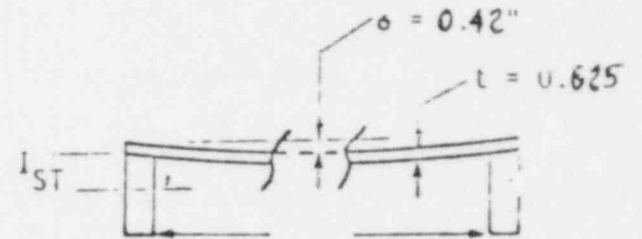
From Figure 5 it is seen that in bending about the XX axis the stringers are over twenty times as stiff as the skin, even though the skin is curved across the bending axis thereby increasing its effective moment of inertia by some 50%. For bending about the longitudinal axis YY the relative stiffness

Figure 5. Panel Arrangement

• NOT TO SCALE



NOTE:
 $1-\nu^2$ NEGLECTED (10% EFFECT)

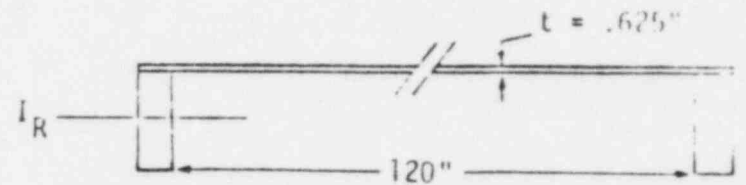


$$I_{\text{STRINGER}} = 35.73 \text{ in}^4$$

$$* I_{\text{SKIN}} = 0.98 + 0.47 = 1.45 \text{ in}^4$$

(AREA) (CURV)

SEC'N X-X



$$I_{\text{RING}} = 607.5 \text{ IN}^4$$

$$* I_{\text{SKIN}} = 2.44 \text{ IN}^4$$

SEC'N Y-Y

is even higher (about 250 to 1). The analysis of Figure 5 were carried out for a 5/8 inch thick skin. The relative stiffness will be even higher for a 1/2 inch thick skin since the skin moment of inertia involves a t^3 term.

It is clear from these considerations that an analysis of the skin as a panel held rigidly at the boundaries should be made (i.e., encastré edges). The legitimacy of this encastré assumption is strengthened when one considers that adjacent panels help in keeping the ring and stringer edges from twisting. For example, symmetry in the cross section across a stringer in the XX direction ensures that the stringer cannot twist for panel bending in about the YY axis.

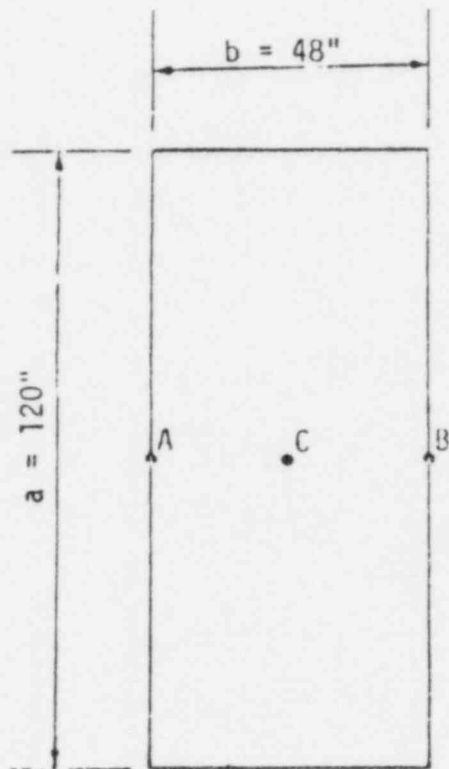
Two flat plate analysis have been carried out following the methods of "Formulas For Stress and Strain" - R. J. Roark, 5th Edition McGraw-Hill Book Co. (1975), pages 392 and 408.

a. Simple flat plate analysis

This is presented in Figure 6. For an encastré edged plate Table 8a on page 392 of the reference volume gives a value for the maximum bending stress at A & B (the midpoints of the long sides) as $\sigma = 0.5 Pb^2/t^2$. For the plate under consideration this gives initial stresses for yielding at a pressure of 6.94 psi. At this pressure the inner plate fibers at A & B will just begin to yield in tension, and the outer plate fibers in these locations will be compressed to a stress of 32,000 psi. At a value of about 1.5 times this pressure (or 10.4 psi) yielding will occur through the entire plate section at A & B. (This is known as a "plastic hinge"). Ultimate yielding stresses of the surface fibers at A & B will be reached at a pressure of 13.0 psi.

The table, referenced above, shows that the stress at the midpoint of the plate (C in Figure 6) is half that occurring at A & B, and is in the opposite sense (i.e., tensile on the outside, compression on the inside). However the plate is not

Figure 6. Flat Plate Analysis



• REF: ROARK "FORMULAS FOR STRESS AND STRAIN" PAGE 39

$$\begin{aligned} \text{MAX. } \sigma_{M} \text{ (AT A, B)} & \quad \left(\begin{array}{l} b = 48'' \\ t = 1/2'' \end{array} \right) \\ & = \frac{0.5 P b^2}{t^2} \end{aligned}$$

$$\begin{aligned} \text{FOR } \sigma &= 32,000 \text{ PSI} & \sigma &= 60,000 \text{ PSI} \\ P &= 6.94 \text{ PSI} & P &= 13.0 \text{ PSI} \end{aligned}$$

$$\text{CENTER } \sigma_C = 0.5 \sigma_M$$

$$\begin{aligned} \text{FOR } \sigma &= 32,000 \text{ PSI} & \sigma &= 60,000 \text{ PSI} \\ P &= 13.9 \text{ PSI} & P &= 26.0 \end{aligned}$$

NOTE: FULL PLASTIC HINGE DEVELOPS AT A, B
AT $1.5 \times 6.9 = 10.4 \text{ PSI}$

a truly "flat" plate and the analysis of Section 4 is more appropriate to the center of the plate which is mainly subject to the hoop tension. There would undoubtedly be some complex combination of bending stresses due to the ring and stringer constraints coupled with the hoop and meridional membrane stresses. A careful analysis with a finite element code would be required to resolve this point and this is beyond the scope of this review.

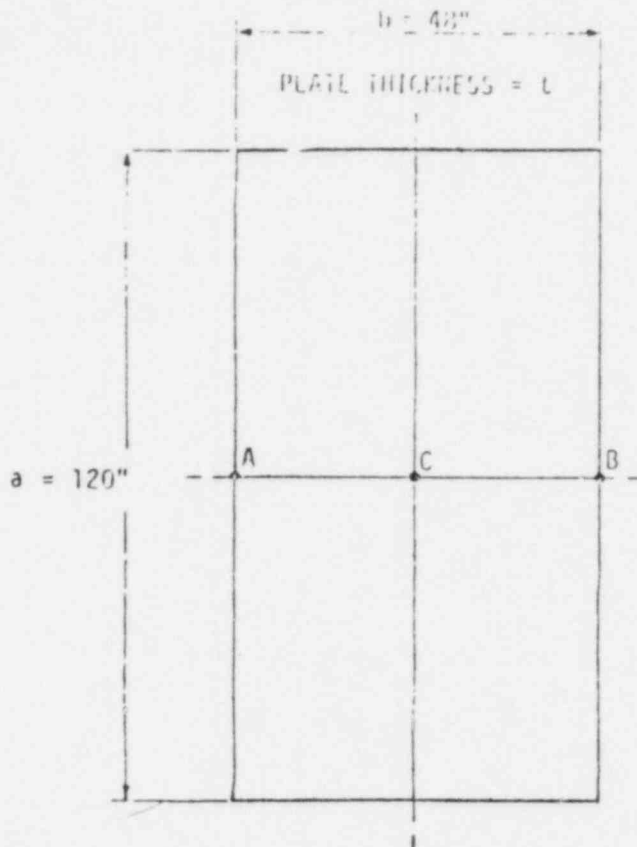
b. Large deflection plate analysis ("quilting" effect)

The analysis of (a) assumes a flat plate and makes no allowance for the finite deflections of the plate. The formula of page 408 of the referenced work makes allowance for the plate deflection. These results are summarized in Figure 7. Again maximum stresses occur at the midpoints of the long sides. The resulting stress is a combination of bending and membrane stresses. Yielding (at 32,000 psi stress) of the inner fibers at A & B begins at an internal pressure of 7.8 psi. Only 6 1/2% of the total stress is due to the membrane contribution.

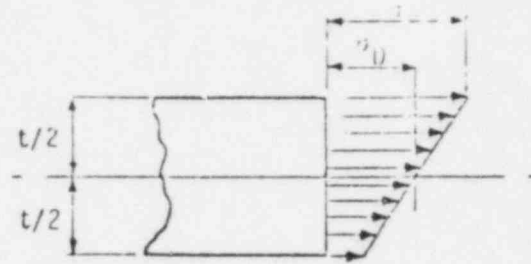
c. Comments on the maximum stress loading at A & B

The onset of yield could occur at the inner fibers at the midpoints of the long edges of the half inch plate sections at an internal pressure of 7.8 psi, assuming the more realistic "quilting" analysis. However, this is at local points only and full plastic hinging would not occur until about 11.7 psi. Even then local stress relief might well occur and for a "one-shot" pressurization it is not clear whether this would result in leakage. It would be a serious problem if many cycles of pressurization were encountered when cracking due to "LCF" (low cycle fatigue) might well occur. More serious, however, is the pure membrane stress induced in the 1/2 inch skin at 26.8 psi. This is a tension over the whole cross section of the panel and would occur over several inches of the vertical panel centerline.

Figure 7. Large Deflection Flat Plate Analysis
("Quilting Effect")



• REF: ROARE "FORMULAS FOR STRESS AND STRAIN" 5th EDITION,



STRESS FIELD → COMBINED TENSION AND BENDING

σ_D = DIAPHRAGM (MEMBRANE) STRESS AT A AND B

σ = TOTAL STRESS BENDING AND DIAPHRAGM AT A AND B

Y_{MAX} = OUT OF PLANE PLATE DEFLECTION AT C

$$Y/t = F_1 (Pb^4/Et^4)$$

$$\sigma_D b^2/Et^2 = F_2 (Pb^4/Et^4)$$

$$\sigma b^2/Et^2 = F_3 (Pb^4/Et^4)$$

DEFLECTION AND
STRESS COEFFICIENTS
 $E = 28 \times 10^6$ PSI

	$t = 1/2''$		$t = 5/8''$	
σ PSI	32,000	60,000	32,000	60,000
σ_D PSI	2100	5000	1500	4100
P PSI	7.8	15.9	11.8	23.2
Y_{MAX} INS	.24	.40	.20	.35

7. HOLD DOWN BOLT STRESSES

Figure 8 depicts the tension stress in the hold down bolts as the internal pressure is increased. The bolts are pre-stressed to a level of 25,000 psi and this bolt tension is not increased until the internal pressure overcomes the container weight as well as the preload tension. This occurs at an internal pressure of 17.3 psi. Increasing pressure will produce bolt yield stress at 64.5 psi and the ultimate bolt stress of 125,000 psi would be reached at an internal pressure of 77.1 psi. The latter, however, could not realistically be achieved since gross leakage would occur as soon as the bolts yield.

8. SUMMARY OF STRESS ANALYSES, CONCLUSIONS AND RECOMMENDATIONS--

Figure 9 summarizes the stress analyses described above together with the AMES "smeared" shell/stiffener analyses of SECY-80-107A.

The RDA analysis leads to the following conclusions.

- a. The AMES analysis is optimistic.
 1. The ring stiffeners are not amenable to the smearing technique--the spacing is such that the hoop stress in the mid-region between the rings is essentially unaffected.
 2. The stringers are only partially amenable to smearing--the stringers only carry 40% of the load that would be expected with "equal" area effectiveness between membrane and stringers.
 3. Having "smeared out" the rings and stringers they cannot be put back in to carry load. This leads to the rather surprising case of one of the rings being the "weak" element in the system.
 4. The ultimate burst analysis is clearly incorrect--the hold down bolts would yield first.

Figure 8. Hold Down Bolt Stresses

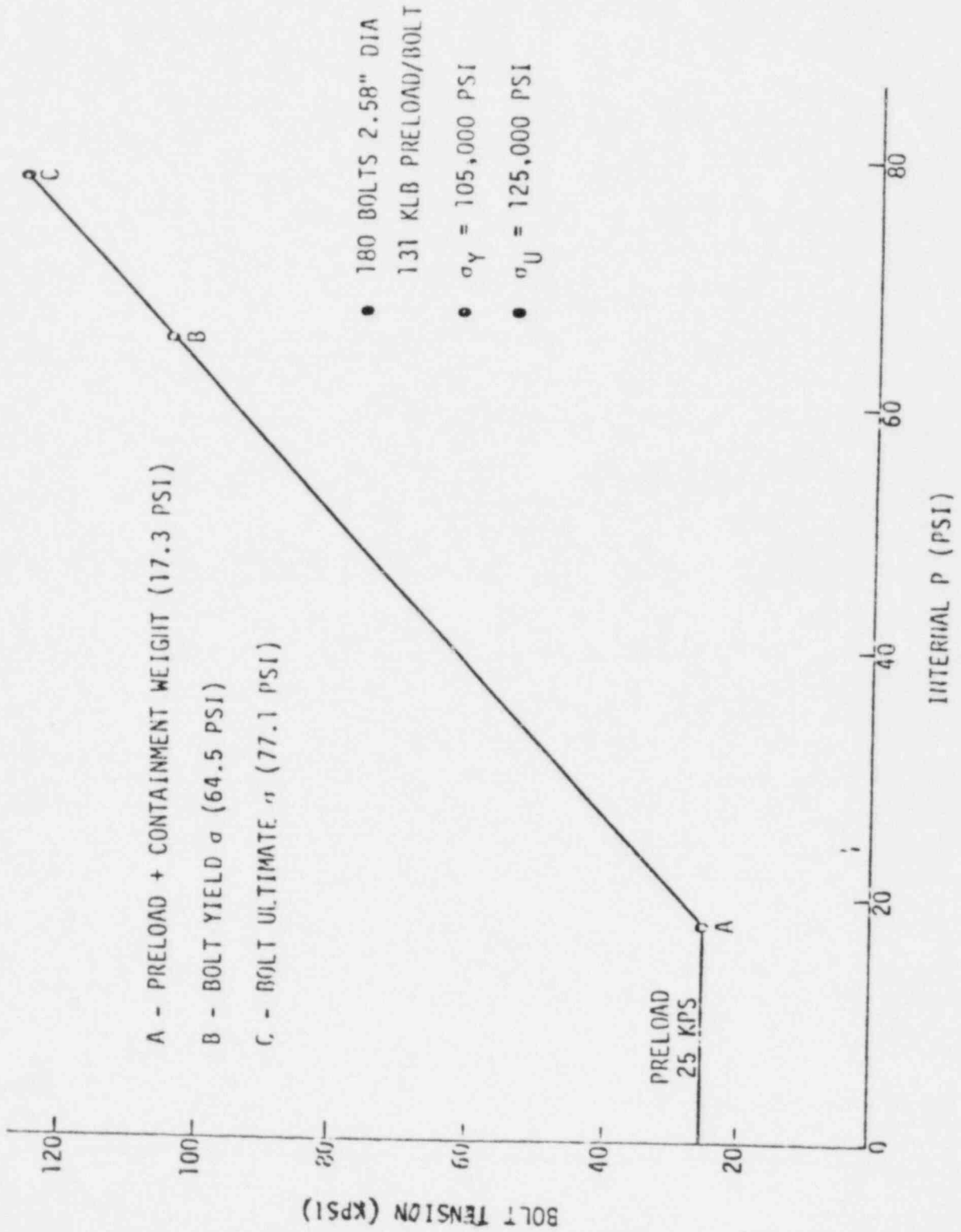


Figure 9. Sequoyah Containment Vessel - Summary of Stresses

	METHOD	CRITICAL ELEMENT	STRESSES	PRESSURE FOR YIELD STRESS PSI	PRESSURE FOR ULT. STRESS PSI
1	AMES "SHEARED" SHELL/STIFFENER ANALYSIS	1 RING STIFFENER 2 5/8" SKIN	PURE MEMBRANE (VON MISES)	1 35.6 2 38.6	1 66.7 2 72.4
2	RDA SHELL/STIFFENER ANALYSIS	1/2" SKIN	PURE MEMBRANE (BOILER CODE-MAX. SHEAR STRESS/ VON MISES)	23.2/26.8	43.5/50.3
3	RDA FLAT PLATE ANALYSIS (ENCASTRE' EDGES)	1/2" SKIN 1 MIDDLE OF LONG- EDGE 2 CENTER OF PLATE	PURE BENDING (BOILER CODE-MAX SHEAR STRESS) A) YIELD AT MAX FIBER B) FULL PLASTIC HINGE	1 A) 6.9 B) 10.4 2 A) 13.9 B) 20.85	1 13.0 2 26.0
4	RDA LARGE DEFLECTION FLAT PLATE ANALYSIS (ENCASTRE' EDGES)	1/2" SKIN MIDDLE OF LONG- EDGE	COMBINED BENDING AND TENSION (BOILER CODE- MAX SHEAR STRESS) A) YIELD AT MAX FIBER B) FULL PLASTIC HINGE	A) 7.8 B) 11.7	15.9

MATERIAL ASME SA 516 GRADE 60

- o YIELD STRESS 32,000 PSI
- o ULTIMATE STRESS 60,000 PSI
- o E 28 X 10⁶ PSI @ 70°F

b. The above four conclusions answer the first three tasks of the work statement. A preliminary answer to the fourth task--the question of leakage above the design point is given by the following summary of the panel/membrane analysis. Recommendations are also presented to refine these answers.

1. Onset of local yielding could occur at about 8 psi, but this is not considered a problem since local yielding could lead to stress relief. Full plastic hinging would not theoretically occur until 12 psi. This could lead to local cracking for a repeated pressurizing case (low cycle fatigue) but may not be important for a "one-shot" loading.
2. Gross membrane yielding could occur at about 27 psi. This corresponds to the ASME code value of 23 psi limit loading. It is interesting to note that an elastic-plastic analysis carried out by Sandia* gives a nominal failure pressure of 27 ± 3 psi.

It appears from this simplified analysis that the progression of events with increasing pressure, begins with pure bending resistance and small local elastic fiber deformations and progresses through combined bending and tensile resistance (quilting) with larger elastic deformations. Eventually local zones of plastic yielding will culminate in a state such that the final resistance mode is pure membrane tension in the skin material alone. This final state will only occur if the skin material is sufficiently ductile to avoid local rupture by tearing or cracking with the internal bending resistance nullified by yielding. Furthermore this final state will be reached independently of the properties of the stiffeners

* "Report On Systems Analysis Task, Reactor Safety Study Methodology Applications Program, Sequoyah #1 Power Plant," Draft Report 1978, Asselin, Carlson, Gramond, Hickman, Fedele, Cybulskis and Wooton.

(from zero to infinitely stiff) so long as the spacing of the ring stiffeners is greater than about 60 inches for the 1/2 inch plate. The final state would then be pure membrane resistance with an equivalent longitudinal thickness which includes the partial effect of longitudinal stiffeners and with hoop thickness equal to the unmodified plate thickness. The resulting limit load pressure about 27 psi is thus probably a reasonable estimate of failure onset. The structure may fail locally below this value but will probably not survive much above this value whatever the properties of stiffeners as currently spaced.

Based on these analyses and conclusions it is recommended that further analyses and experimental verification be carried out:

- a. A detailed finite element code analysis should be carried out to clarify the location, extent and profile of stress concentrations.
- b. A full scale excastrate panel should be pressurized to failure including a full strain gage and stress coat instrumentation. This would not be difficult or expensive since the panel size is only 10 ft by 4 ft, and the severity and effect of the local stress concentrations could be readily evaluated. The pressurization should be carried out in two stages.
 1. Up to 13.5 psi and back to zero (to simulate the containment acceptance pressure test). The panel should then be examined carefully for local deformations, etc. These would likely be shown up by stress coat or crack detection methods.
 2. Pressurization to failure with full instrumentation reading at selected pressure increments.

REFERENCE C

TVA, oral presentation at ACRS meeting, September 2, 1980 .

PRESENTATION OUTLINE

I. OVERVIEW OF PRESENTATION

II. DESIGN OF CONTAINMENT VESSELS

ORIGINAL DESIGN -

REVISED DESIGN -

DESIGN/CONSTRUCTION PROCEDURES

DESCRIPTION OF CONTAINMENT

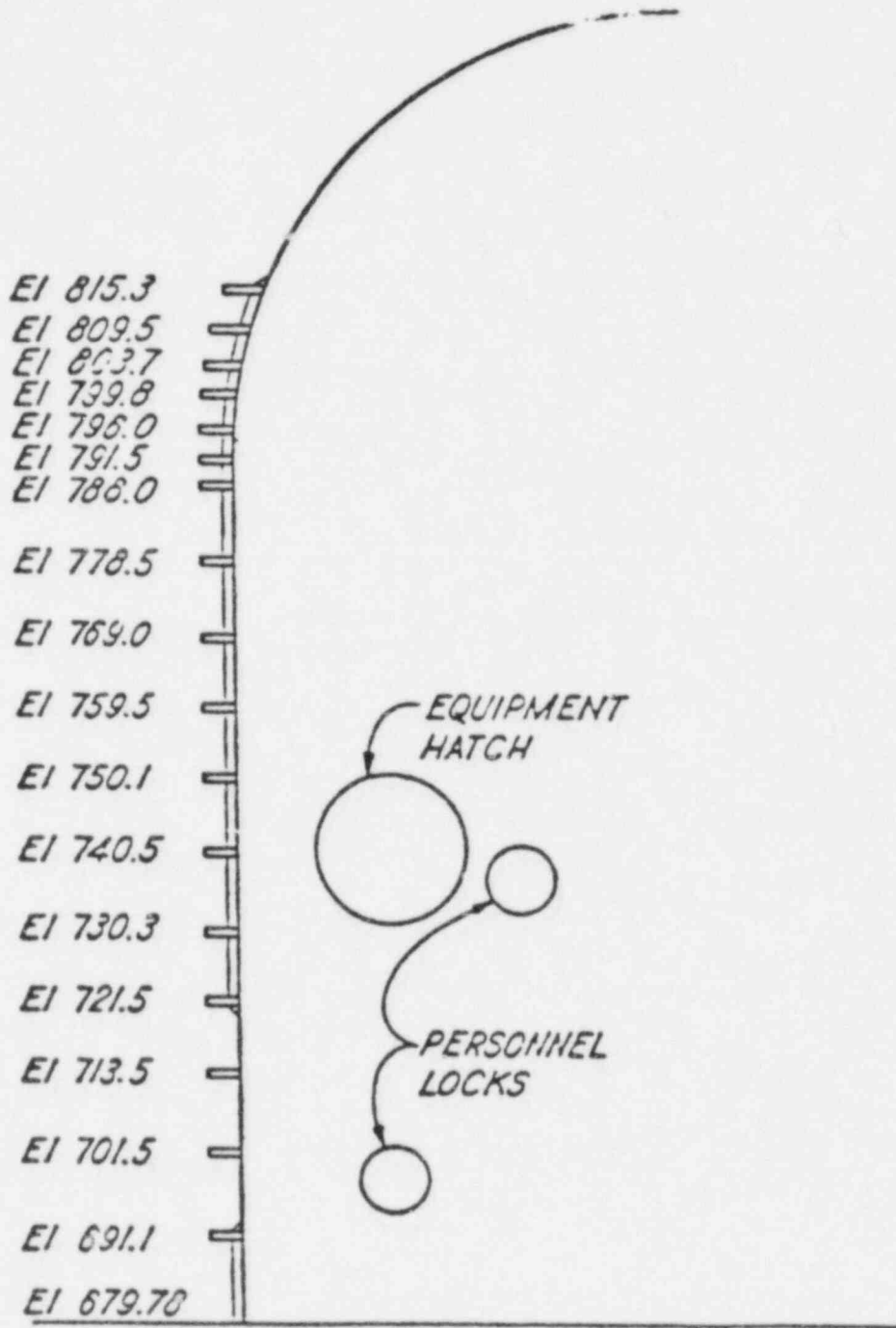
III. CONTAINMENT CAPACITIES -

CRITICAL SECTIONS

EVALUATION OF THE CRITICAL SECTION

RESULTS

IV. CONCLUSIONS & RECOMMENDATIONS -



Steel Containment Vessel

DETERMINATION OF CRITICAL SECTIONS

ANCHORAGE

PENETRATIONS (PIPING)

BELLOWS

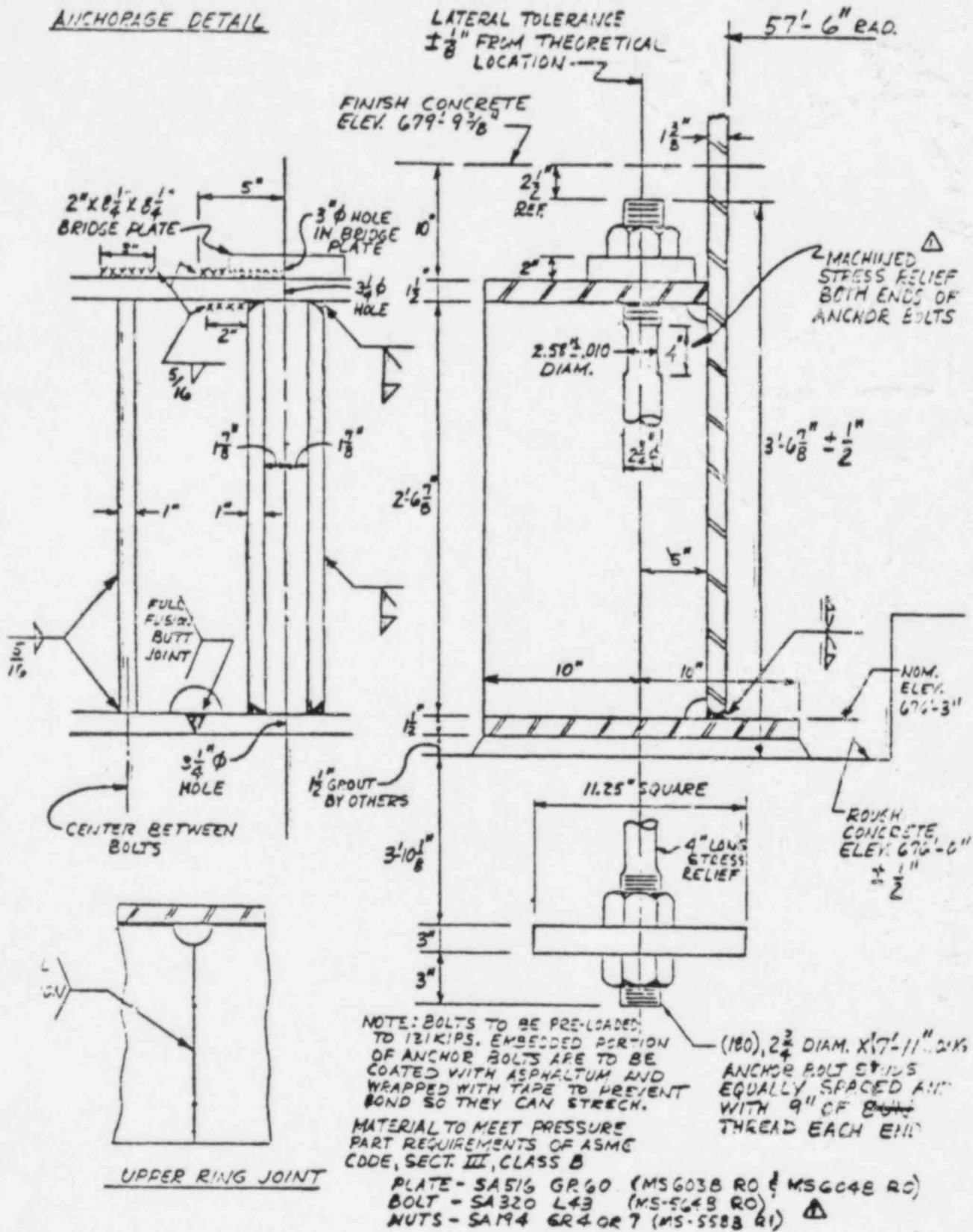
VALVES

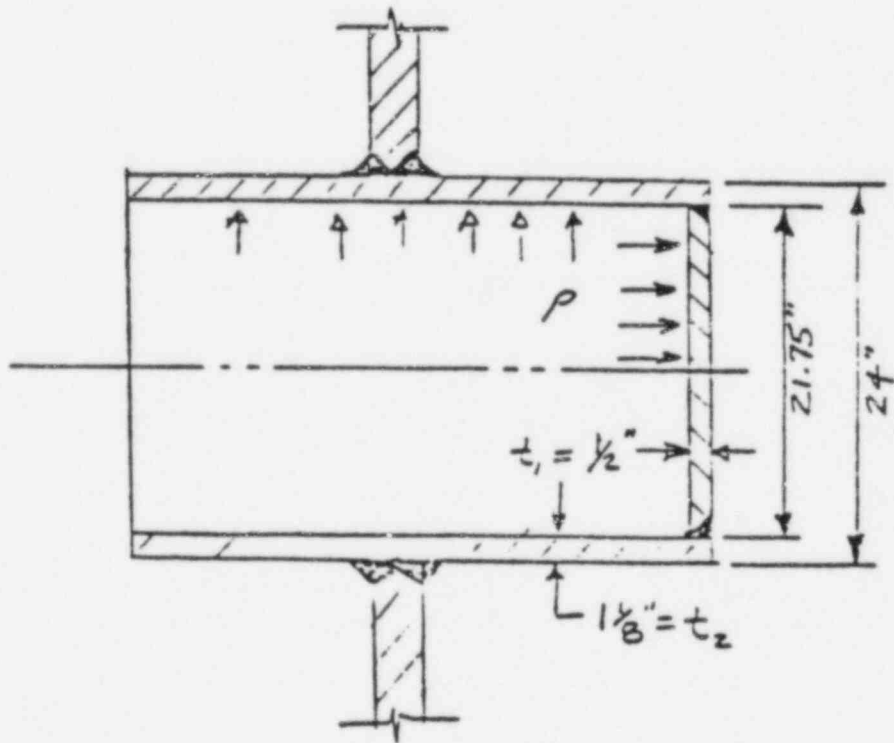
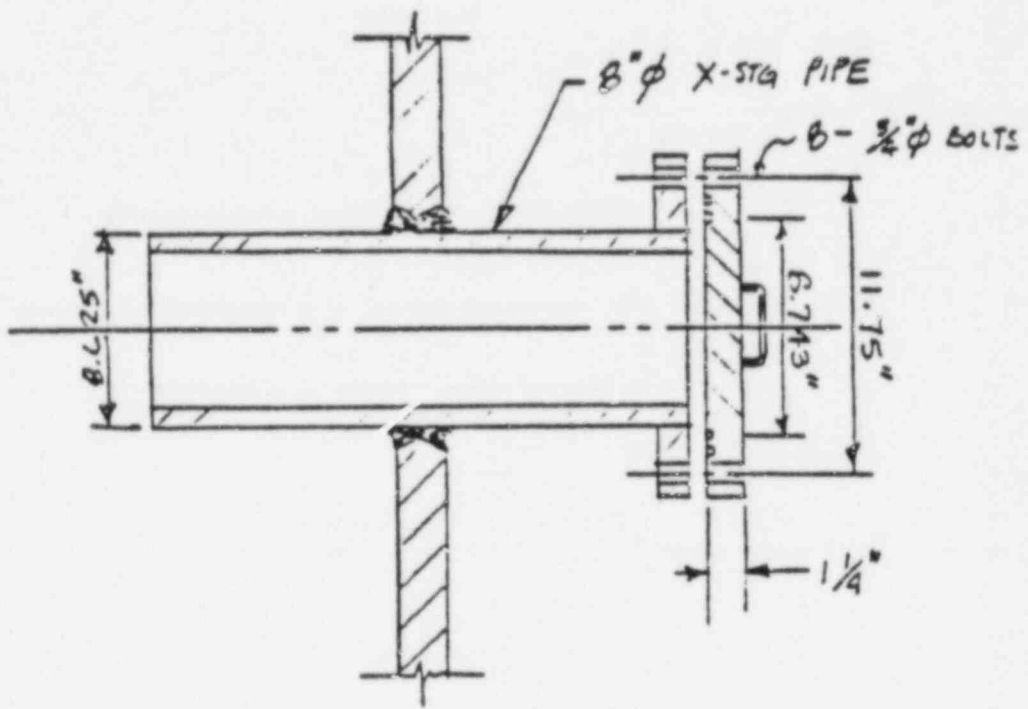
PERSONNEL LOCKS/EQUIPMENT HATCH

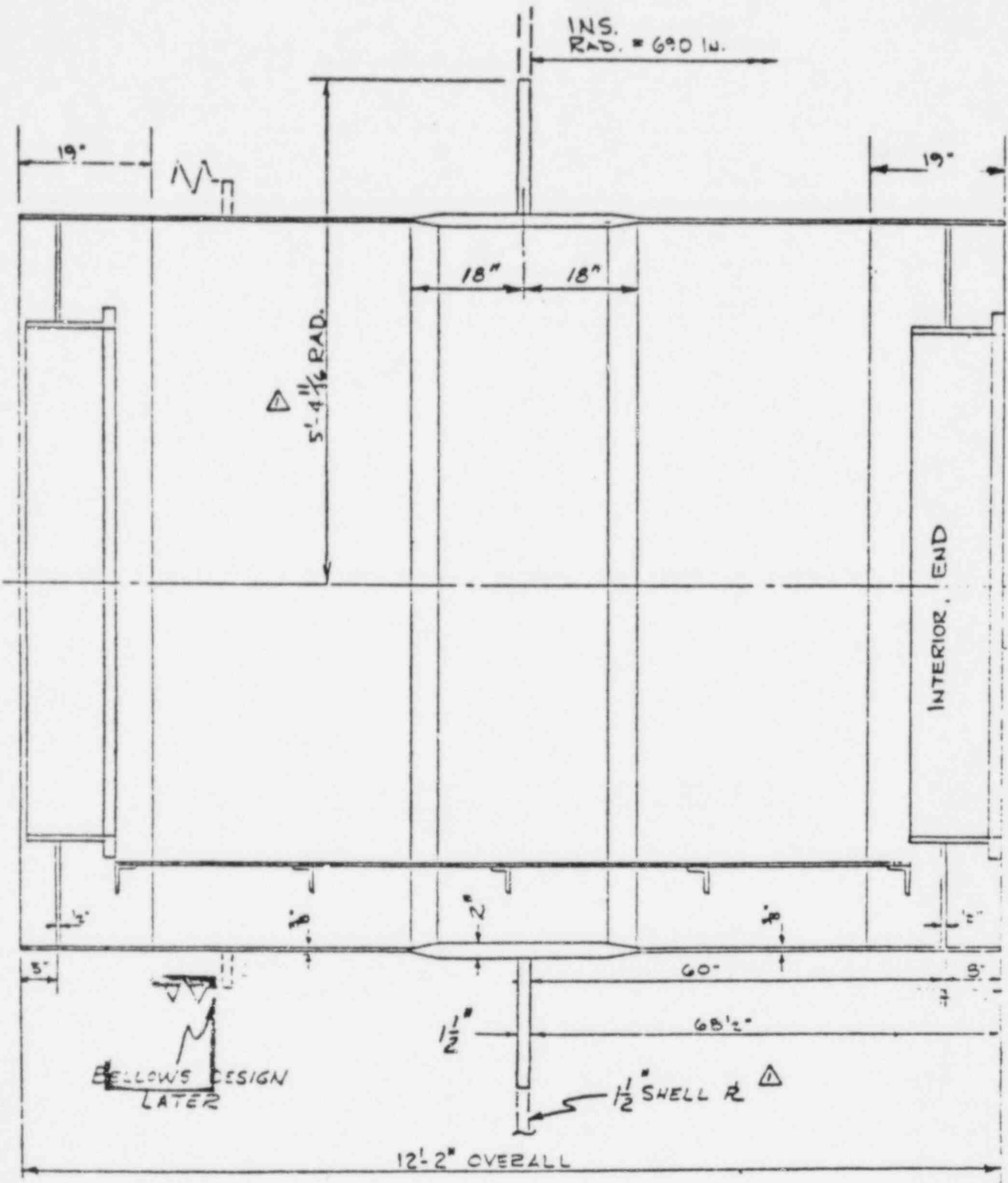
SEALS

SHELL PLATE

ANCHORAGE DETAIL

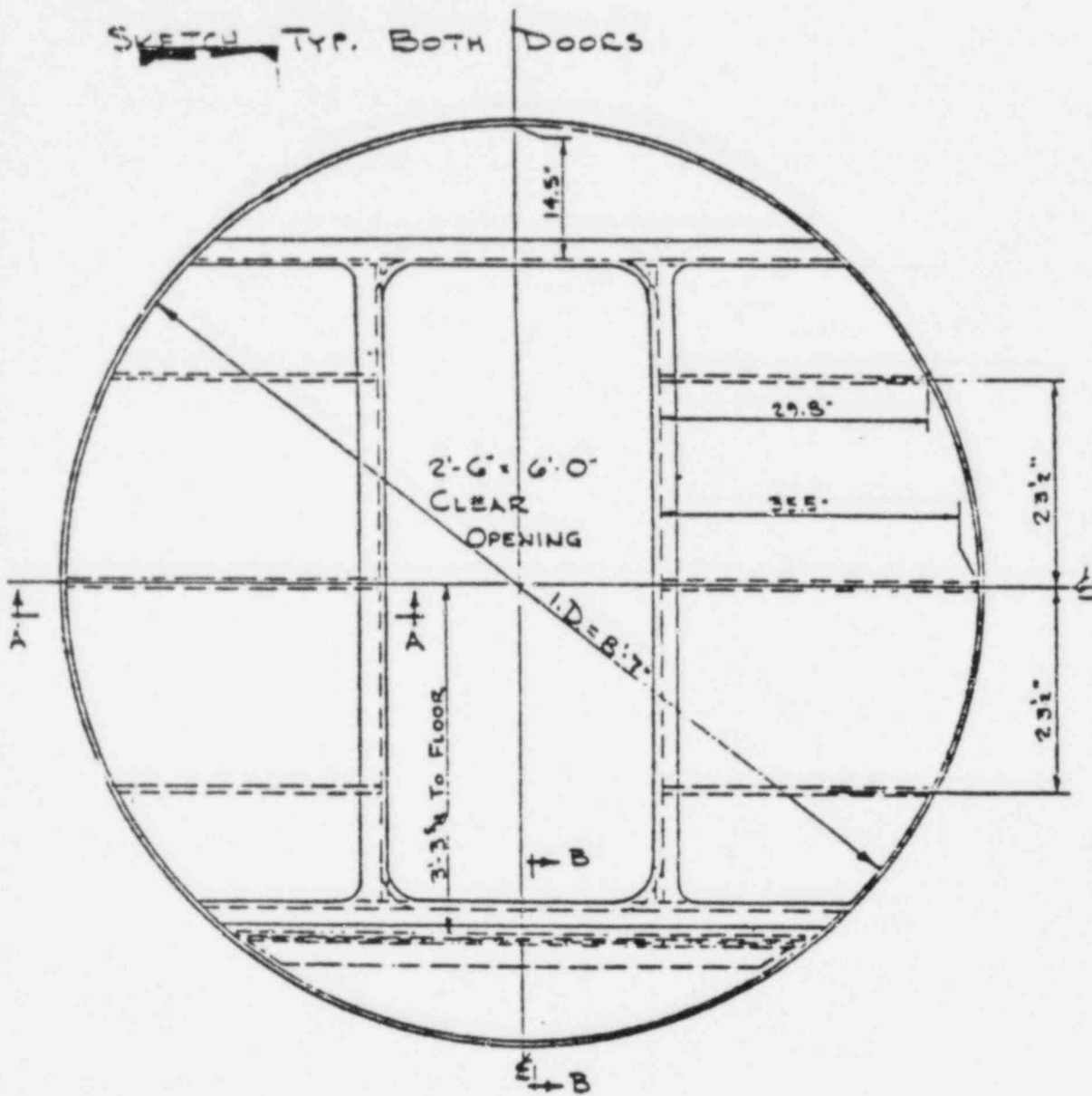






PERSONNEL LOCK

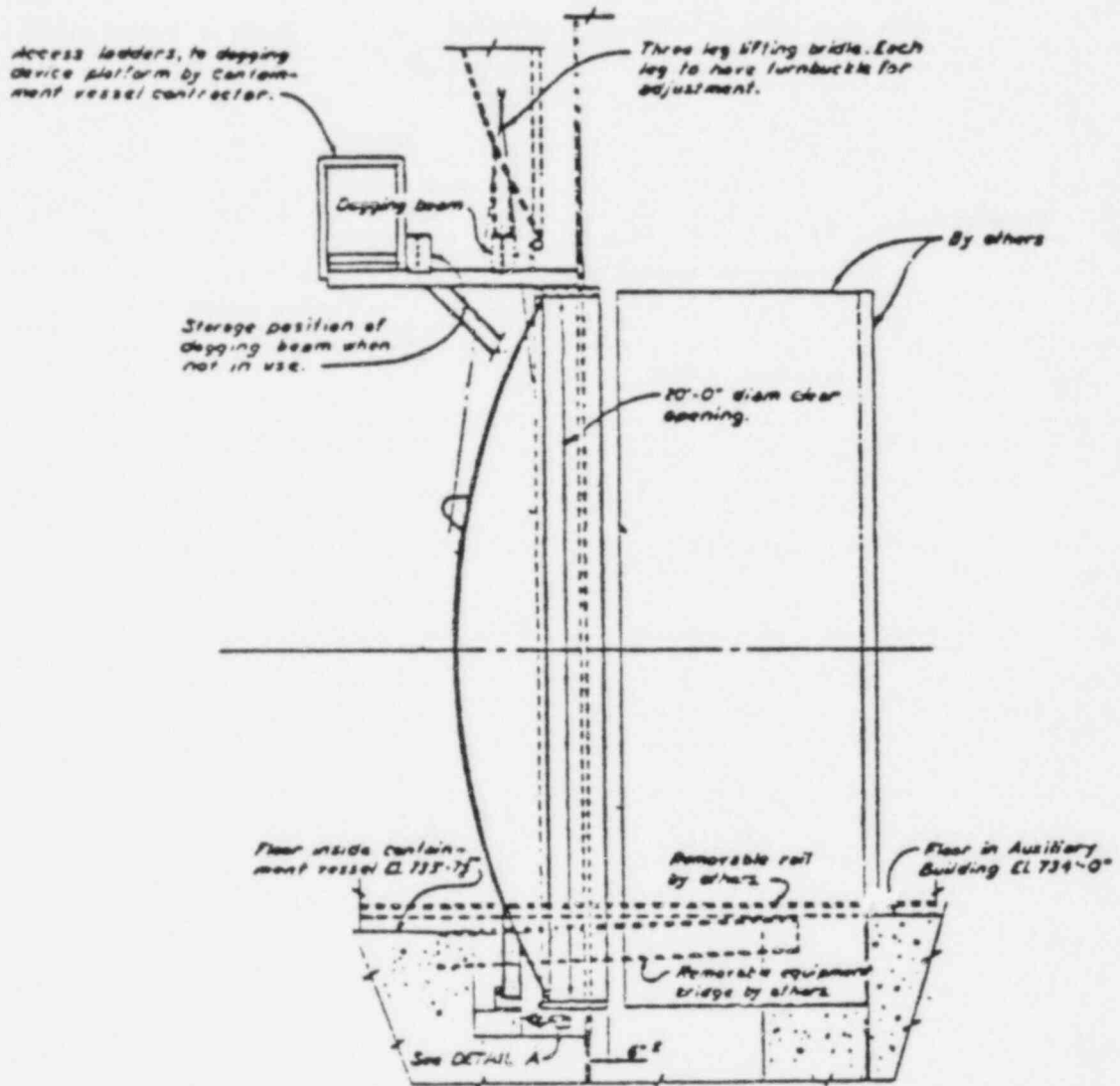
SKETCH TYP. BOTH DOORS



LOADS: 10.8^{PSI} INTERNAL PRESSURE
 .5^{PSI} EXTERNAL PRESSURE
 100^{PSI} OR 1000^{LB} POINT LOAD ON FLOOR

MATERIALS: $\frac{1}{2}$ " - SA 516 GR 60 $S_m = 15000^P$, $F_y = 28350^P$, @ 100^F
 $\frac{1}{4}$ " - A 36 $F_y = 32000^P$, @ 100^F
 NON-SKID FLOOR $\frac{1}{2}$ " - USS 2EG QUALITY CARBON STEEL FLOOR $\frac{1}{2}$ " (S-400)
 BOLTS - A 307 $F_y = 36000^P$, @ 100^F

DESIGN TEMPERATURE - 220^F



SECTION B-B

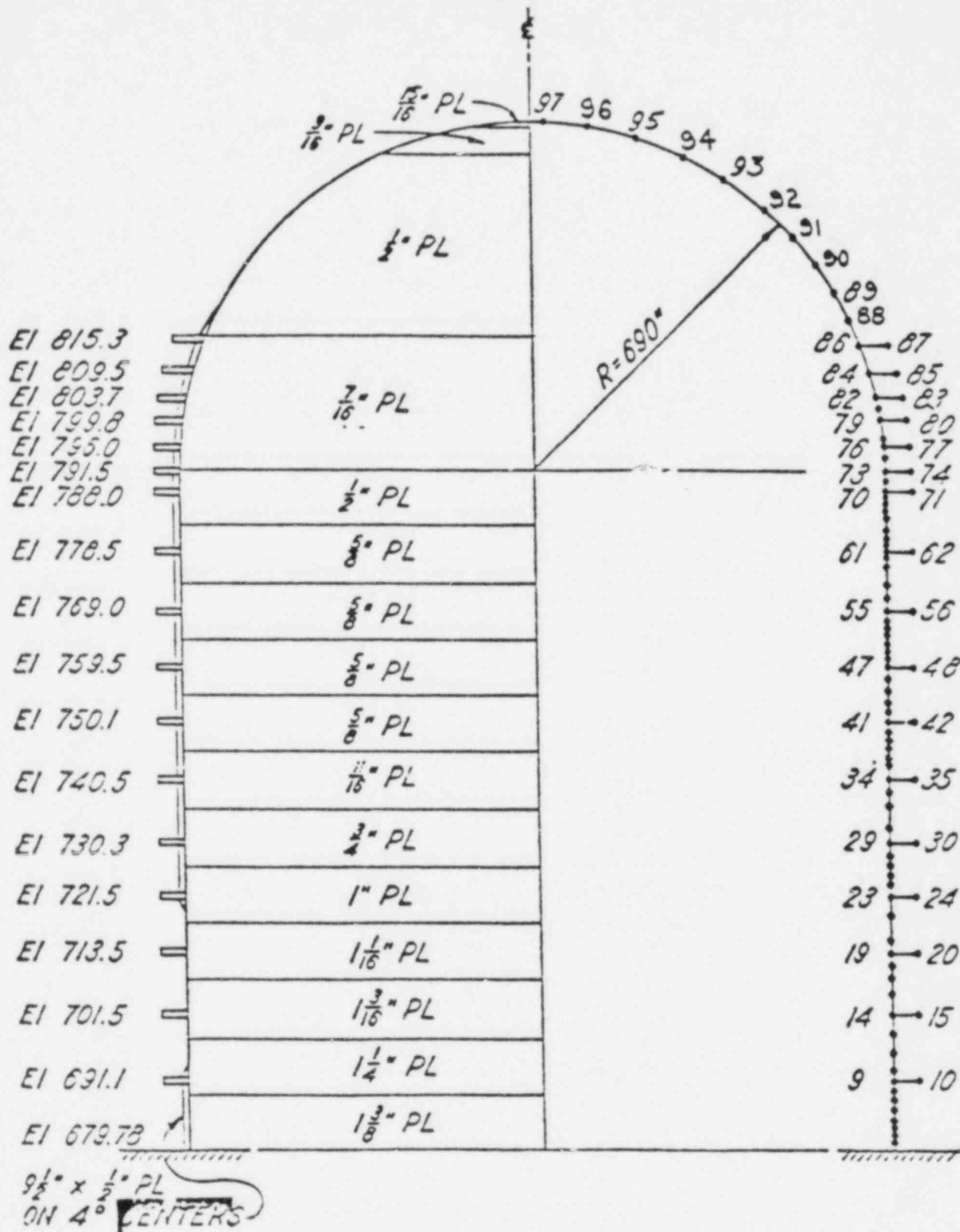


Figure 3.8.2-7

Steel Containment Vessel
Finite Element Model

EVALUATION OF CONTAINMENT VESSEL BETWEEN STIFFENERS AT ELEVATIONS 778'-6" AND 778'

MATERIAL -

PLATE - SA 516 6R 60
STIFFENERS - SA 516 6R 60
WELD - E7018

MATERIAL PROPERTIES -

		STRESSES		
		<u>YIELD</u>	<u>TENSILE</u>	
SHELL PLATE & STIFFENERS	{	SPECIFIED CODE MINIMUM	<u>32 KSI</u>	<u>60 KSI</u>
		LOWEST TEST VALUE	<u>45.7 KSI</u>	<u>65.7 KSI</u>
		MEAN TEST VALUE	<u>47.2 KSI</u>	<u>66.2 KSI</u>
WELD	SPECIFIED CODE MINIMUM	<u>60 KSI</u>	<u>72 KSI</u>	

SEQUOYAH NUCLEAR PLANT (UNIT 1)

1/2 INCH CYLINDRICAL SHELL PLATE
BETWEEN ELEVATIONS 782 & 791-6

<u>TENSILE TEST</u>	<u>NUMBER OF PLATES</u>	<u>YIELD STRENGTH</u>	<u>TENSILE STRENGTH</u>	<u>PERCENT. ELONGATION</u>
1	3	46,100 PSI	65,800 PSI	25
2	2	46,600 PSI	65,000 PSI	24
3	3	46,800 PSI	66,300 PSI	23
4	1	47,900 PSI	66,700 PSI	25
5	3	48,400 PSI	67,100 PSI	26

3111 10-3-54

21
JW

BETHLEHEM STEEL CORPORATION
METALLURGICAL DEPARTMENT
REPORT OF TESTS AND ANALYSIS

PLANT BURNS TOWER	SHIPMENT NO. 803-18159	DATE SHIPPED 11-27-70	CAR OR VEHICLE NO. PC-EVANSVILLE-LN W CNV 042711	PAGE
----------------------	---------------------------	--------------------------	---	------

SOLD TO CHICAGO BRIDGE & IRON CO BOX 277 BIRMINGHAM AL 35202	SHIP TO CHICAGO BRIDGE & IRON CO BOYLES AL
---	--

DESCRIPTION & SPECIFICATION CUSTOMER ORDER NO. B.C.O. ORDER NO.	SERIAL NUMBER	HEAT NUMBER	THICKNESS		SIZE & QUANTITY		LENGTH		YIELD STRENGTH	TENSILE STRENGTH	ELONG. IN %	BEND	HARDNESS	
			No. Pcs	XXXX	Width or Dia.	XXXXXX	Weight	Type					V	
STEEL PLATES- MS-601-B REV 0 GPS-516 REV 4 ASME CHARPY V NOTCH IMPACT OF 15 FT LB AT CO# 5546 SHEET 17 GH 025-3547														
	B 31908 -1	802804870	1	11/16	114- 1/2	362	8073	48100	70200	8	27	B		
	B 31856 -1	802806530	1	11/16	114- 1/2	362	8073	49600	69100	8	25	B		

-192-

HEAT NUMBER	CHEMICAL ANALYSIS										
	C	Mn	P	S	Si	Ca	Ni	Cr	Mo	V	Ti
802804870	0.15	1.09	.010	.019	.25						
802806530	0.15	1.06	.009	.030	.25						

SUBSCRIBED AND SWORN TO BEFORE ME
THIS 18th DAY OF December 1970.
Jerry D. Bowles
NOTARY PUBLIC
LA PORTE COUNTY INDIANA
MY COMMISSION EXPIRES DECEMBER 12, 1973

METHODS OF ANALYSES

FINITE ELEMENT SHELL MODEL
PANEL
MEMBRANE

FAILURE CRITERIA

MAXIMUM SHEAR STRESS
VON MISES

CONTAINMENT PRESSURE (PSIG)

CRITICAL SECTIONS		CRITICAL PRESSURE	SPECIFIED CODE MIN. STRESSES		LOWEST ACTUAL TEST STRESSES	
			MAX SHEAR	VON MISES	MAX SHEAR	VON MISES
SHELL PLATE	ULTIMATE YIELD		43.5 23.2	50.2 26.8	47. 33.1	5 38.2
PENETRATIONS						
WELDED SPARE	YIELD		83.0			
BOLTED HEAD	YIELD		1355.0			
BELLOWS	YIELD		100.9			
ELECTRICALS	ULTIMATE	100.0				
VACUUM RELIEF VALVES	ULTIMATE	47.8				
PERSONNEL LOCK	YIELD		31.1			
EQUIPMENT HATCH	ULTIMATE	73.0				
ANCHORAGE	ULTIMATE	73.0				

REFERENCE D

Bagchi, G. (NRC Research), Memorandum to F.P. Schauer, NRC,
Washington, DC, August 17, 1980.

UNITED STATES
NUCLEAR REGULATORY COMMISSION
WASHINGTON, D. C. 20555



AUG 7 1980

MEMORANDUM FOR: F. P. Schauer, Chief
Civil Engineering Branch

FROM: Goutam Bagchi, Chief
Structural Engineering Research Branch

SUBJECT: ANALYSIS OF SEQUOYAH CONTAINMENT CAPACITY

I reviewed two separate analyses of the Sequoyah Containment Structure referenced below:

- (1) Analysis by Anes as a part of SECY-80-107A
- (2) Critique of SECY-80-107A by R&D Associates

I feel that the critique in Reference 2 above treated the effects of meridional stiffeners independently of the ring stiffeners and vice versa. The network of stiffeners should serve as another strength element to provide resistance to the shell membrane beyond its first yield capacity. I tried to take an independent look at this and developed a force equilibrium model to utilize both the ring and meridional stiffeners. Enclosed is a copy of calculations for your review. I hope you will find them useful for your safety evaluation.

My conclusions are that the containment strength is 34 psi at gross yield and is governed by the thinnest section. This value is closer to that calculated in Reference (1), 35.5 psi than the 27 psi estimated in Reference (2).

It is my opinion that the ultimate capacity of the containment is around 45 to 50 psi internal pressure, considerably higher than the strength at gross yield.

A handwritten signature in cursive script that reads "Goutam Bagchi".

Goutam Bagchi, Chief
Structural Engineering Research Branch
Division of Reactor Safety Research

Enclosure: Calculations

cc: T. E. Murley, RES
L. C. Shao, RES
D. G. Eisenhut, NRR
J. P. Knight, NRR
C. N. Kelber, RES
J. F. Costello, RES
C. P. Siess, ACRS
M. Bender, ACRS

CAPACITY OF CONTAINMENT SHELL REINFORCED BY RING AND MERIDIONAL STIFFENERS

G. Bajaj
8-1-60

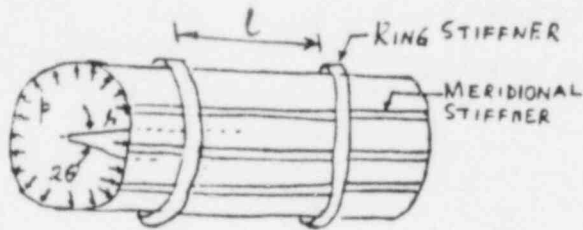
ASSUMPTIONS :

- (1) Ignore local bending effects
- (2) Shell resists pressure load by tension
- (3) Meridional stiffeners act as beams between ring stiffeners, and support a portion of pressure loading when the shell radial deflection becomes high enough to deform the meridional stiffeners in a flexural mode.
- (4) Ring stiffeners are stretched by the end reactions from meridional stiffeners.
- (5) Deformations are symmetric circumferentially
- (6) Ignoring the shell ends, meridional deflections v.c. symmetric about equally spaced ring stiffeners.

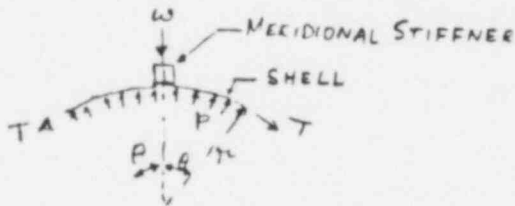
CONTAINMENT SHELL REINFORCED BY RING AND MERIDIONAL STIFFENERS

G. BAGCHI
8-1-80

ANALYSIS FOR INTERNAL PRESSURE LOADING :



EQUILIBRIUM OF A SEGMENT OF THE CYLINDRICAL SHELL



In the figure above, let T = membrane tension of shell,

p = internal pressure, w = load per unit length of the meridional stiffener due to the internal pressure,

2θ = angle subtended by the spacing of meridional stiffeners,

r = radius of the shell.

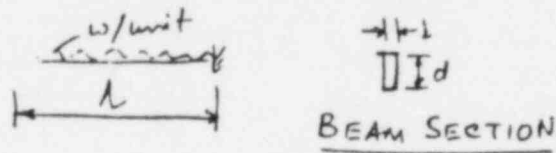
for equilibrium in the vertical direction,

$$\int_0^\theta p r d\theta \cos\theta = T \sin\theta + \frac{w}{2} \quad \text{or} \quad p r \sin\theta = T \sin\theta + \frac{w}{2}$$

$$\therefore p = \frac{T}{r} + \frac{w}{2r \sin\theta} \quad \text{--- (1)}$$

MERIDIONAL STIFFNER AS A BEAM

G. Bapoli
P-580



For fully restrained ends,

$W_c = \frac{16 M_p}{L}$ where M_p = fully plastic moment of the beam section, L = span length, and W_c = total collapse load.

There will be some influence of axial load on the plastic moment capacity of the stiffeners due to longitudinal loading. This can be treated as follows:

For a rectangular section,

$\frac{M_N}{M_p} = 1 - \left(\frac{N}{N_p}\right)^2$ where M_N = fully plastic moment capacity of the section in combination with an axial load N , N = applied axial load, and N_p = axial load capacity of the section at yield stress without bending.

Reference: The Plastic Methods Of Structural Analysis
by B.G. Neal, published by Chapman & Hall Ltd
London, Second Edition, pages 44, 212

Assuming that the longitudinal force causes stresses equal to half of the fully yield stress (since longitudinal stress is half the hoop stress)

$$W_c = \frac{16}{L} M_N = \frac{16}{L} M_p \left[1 - \left(\frac{N}{N_p}\right)^2\right] = \frac{16}{L} M_p \left[1 - \left(\frac{1}{2}\right)^2\right]$$

$$\therefore W_c = \frac{16}{L} M_p \times \frac{3}{4} = 12 \frac{M_p}{L}$$

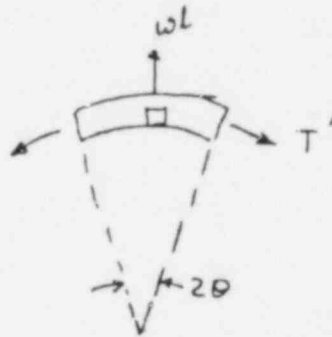
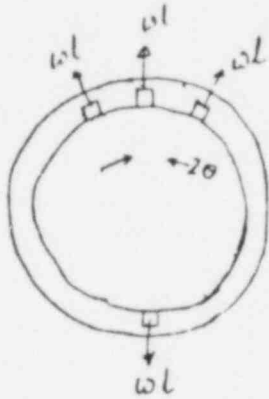
Using $W_r = wl$, and $M_r = \frac{bd^2}{4} f_y$,
 where $f_y = \text{yield stress}$

G. Bagel:
 P-5-83

$$w = \frac{12}{l^2} \times \frac{bd^2}{4} f_y = 3 \frac{bd^2}{l^2} f_y \quad \dots (2)$$

$$\text{End shear} = \frac{wl}{2} \quad \dots (3)$$

RING STIFFENER CAPACITY:



$$\frac{wl}{2} = T' \sin \theta \quad \therefore T' = \frac{wl}{2 \sin \theta} \quad \dots (4)$$

Substituting the value of w from equation (2) in equation (3)
 we get

$$P = \frac{T}{2} + \frac{3bd^2}{l^2} f_y \times \frac{1}{2 \sin \theta} \quad \dots (5)$$

The last term in equation (5) is clearly the additional resistance obtained from the stiffener network at gross yield.

REINFORCED SHELL ANALYSIS :

G. Bag. 1.
8-5-80

Meridional Stiffener as a beam :

$$b = 0.5 \text{ in}, d = 9.5 \text{ in}, f_y = 32,000 \text{ psi}$$

using equation (2),

$$w = \frac{3 \times (0.5) \times (9.5)^2 \times 32,000}{(120)^2} = 300.83 \text{ lbs}$$

Using this value of w which accounts for the axial load and the fully plastic moment capacity of the cross section of the meridional stiffener,

from equation (1)

$$p = \frac{T}{r} + \frac{300.83}{2r \sin \theta}, \quad T = 32,000 \times \frac{1}{2} \times 1 = 16,000 \text{ lbs}, n = 690$$

$$2\theta = 4^\circ, \sin \theta - \sin 2^\circ = 0.0349$$

$$p = \frac{16,000}{690} + \frac{300.83}{2 \times 690 \times 0.0349} = 23.18 + 6.25 = 29.43 \text{ psi}$$

Using Von Mises Criteria, the circumferential stress being denoted by σ , $f_y^2 = [\sigma^2 + (\frac{1}{2}\sigma)^2 = \sigma^2 + \frac{1}{4}\sigma^2]_{\therefore} \sigma = f_y \times \frac{1}{\sqrt{1.25}}$

$$\therefore p = 29.43 \times \left(\frac{1}{\sqrt{1.25}}\right) = \underline{33.98 \text{ psi}}$$

Checking of shear :

$$\text{Shear yield stress} = \frac{32,000}{\sqrt{3}} = 18,475 \text{ psi} = f_y \tau$$

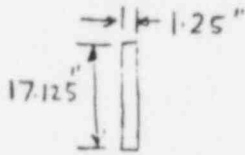
Using equation ③

G. Bagchi
8-5-50

$$\text{Applied shear} = \frac{\omega l}{2} = \frac{300 \times 120}{2} = 18050 \text{ lbs}$$

$$\begin{aligned} \text{Shear capacity} &= f_y \times \text{shear area} = 18475 \times b \times d = 18475 \times 5 \times 9.5 \\ &= 27,756 \text{ lbs} > 18050 \text{ lbs} \\ &\text{O.K.} \end{aligned}$$

Ring Stiffener Capacity:



Cross Section

$$\text{From equation ④, } T' = \frac{\omega L}{2.5 \sin \theta} = \frac{300 \text{ psi} \times 120}{2 \times 5 \sin 2^\circ} = 517,194 \text{ lbs}$$

$$\text{Capacity} = 17.125 \times 1.25 \times 32 = 685,000 \text{ lbs} > 517,194 \text{ lbs O.K.}$$

Conclusion:

Based on the thinnest section of the shell, and assuming that both the ring and meridional stiffeners are effective, the Sequoyah steel containment capacity at yield = 34 psi.

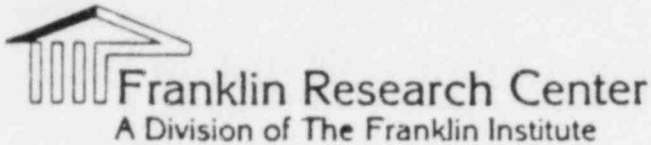
Due to the high ultimate strength of the material, the ultimate strength based on the thinnest section of the shell should be around 30% above the gross yield strength. This will work out to 45 psi internal pressure.

Although this estimate is purely judgmental, it does not seem to be unreasonable, since the material ductility around 200 in tension.

G. Beal
8-5-40

REFERENCE E

Zudans, Z. (Franklin Research Institute), letter report to
Dr. R. Savio, NRC, Washington, DC, August 29, 1980



August 29, 1980

Dr. R. Savio
Staff Engineer
Advisory Committee on Reactor Safeguards
U.S. Nuclear Regulatory Commission
Washington, D.C. 20555

- References: 1) Dr. L. Greimann, Ames Laboratory: Ultimate Strength Characteristics of the Sequoyah and McGuire Containments, January 21, 1980.
- 2) R&D Associates Report: "Sequoyah Containment Analysis," July 25, 1980.

Subject: Review of Sequoyah Containment Structural Analyses by Ames and R&D Associates and an Independent Analyses of a Portions of Sequoyah Containment.

Dear Dr. Savio:

As per your instructions I reviewed the analyses and conclusions reached in subject referenced Reports. Detailed findings of this review are given in the Enclosures 3 and 4.

In summary neither of the two reports support their conclusions with argument of adequate rigor.

Ames conclusion (for 5/8" thick section) that plastic limit load is reached at $p = 35.6$ psi is derived from an erroneous assumption which results in ring yielding at this pressure!

Similarly, R&D Associates conclusion that full membrane hoop stress will develop in a considerable region of 1/2" section between the rings at $p = 23.2$ psi is based on neglecting the effect of the stringers.

To offer a rational estimate of the containment strength, I performed four (4) independent analyses using a reduced model of the Sequoyah containment.

The first three (3) analyses addressed the 5/8" thick section (considered critical by Ames). The conclusion based on these three (3) analyses, indicates that: 5/8" thick shell section full yielding will occur at 34.3 psi, and that essentially an entire panel (between the stringers and stiffeners) will yield at 38.6 psi. These are conservative numbers, non-linearities will stiffen the structure and higher pressures will likely be required to produce gross distortion.

Dr. R. Savio
ACRS

- 2 -

August 29, 1980

The fourth analysis addressed the area of 1/2" thick shell (considered critical by R&D Associates). The conclusion based on the fourth analysis indicates that the first yielding of 1/2" thick section will occur at the point where 1/2" thick shell joins the 5/8" thick shell at 30.3 psi, and that essentially the entire panel between elevations 778' 0-5/8" and 691' 0-1/2" will yield at 34.7 psi.

Details of four (4) analyses are given in the Enclosures 1 through 5. Briefly, these analyses were performed in the following manner.

First analyses modelled a portion of the containment building between Elev. 730' to 769' with circumferential ring stiffeners, but neglected the meridional stiffeners (stringers). The reason for this analysis was to demonstrate the response of a shell without meridional stiffeners. Results of this analysis confirmed the fact that given the spacing of the rings as per Sequoyah design in this area, full hoop stresses would develop in the region couple feet away from the ring and cause membrane yielding of 0.625 in. thick shell at about 28 psi. The stresses for this case are shown in Figure 2, Enclosure 1. It is also clear that plastic hinges would develop in the shell at a considerable lower pressure.

The second analysis was performed (for the same area as the first analysis) with added stiffeners in the model. While the rings were modelled exactly within the linear elastic theory, the stringers were smeared out to represent their axial stiffness and meridional bending stiffness in an average manner. Pertinent details of this analysis are given in Enclosure 1. Figure 3, Enclosure 1, shows the hoop and axial stress distribution for this case. It is noted that the hoop stress is much more uniform than in the previous case, Figure 2, Enclosure 1, and that the average axial stress varies along the meridian. The largest hoop stress in this case predicts total cross section plasticity at 36 psi (see Page 6, Enclosure 1). The results further indicate that the entire shell section between the elevation 740' to 759' would yield with the internal pressure loading in the range from 36 to 38 psi.

The third analysis was performed to prove the validity of the method used for "smearing out" meridional stiffener. This was a finite element analysis of a portion of the containment between El. 744' and 755'. Here, symmetry boundary conditions were imposed on all sides of the model and axial loads applied at one end of the model such that the end remained flat. Details of this analysis are given in Enclosure 2.

This analysis confirmed the shell of revolution analysis results as obtained with rings and smeared out stiffeners. It further showed that hoop stresses generated in the midspan between the rings and stringers are slightly higher than those produced by shell of revolution analysis. However, the basic finding that the stringers are significant in reducing the hoop stress remained. The results of this analysis indicate that a gross shell yielding at this location will occur over essentially the entire span of this model between rings and stiffeners in the range of the internal pressure 34.3 to 38.6 psi.

Dr. R. Savio
ACRS

- 3 -

August 29, 1980

Another interesting result is that essentially full axial stress is developed in the shell at the rings since the stringers at that location contribute very little to axial stiffness due to significant bending stress developed in the stringers. Figure 5 of Enclosure 2 shows this case.

Fourth analysis was performed for the region between elevations 778' to 791' by using shell of revolution method with rings and smeared out meridional stiffeners. Pertinent details of this analysis are given in Enclosure 5. Figure 7, Enclosure 5 shows hoop and axial stress distribution for this case. The largest hoop stress in this case predicts total cross section plasticity at 31.9 psi (see Page 5, Enclosure 5).

The results further indicate that the entire section between the ring at elevations 778' 0-5/8" and 791' 0-1/2" will yield at 34.7 psi. There was no finite element analysis done for this region, however, the same amount of stress change (from shell to finite element) can be anticipated here as was found in comparing the second and third analysis. Accordingly, a reasonable plastic limit load in this region is 30.3 psi.

Because of the structural discontinuities, the local stress at the shell surface vary significantly from the average stress upon which gross plasticity pressure was derived. However, formation of plastic hinges locally is not a significant contributor to failure for a one time loading.

To define a pressure at which the structure would reach its ultimate capacity, it is first necessary to select the mode of failure of concern. If the leakage is the concern, R&D Associates computed value of $p = 64.5$ psi (producing hold down bolt yielding) is a reasonable value. Other design details around the penetrations and at discontinuities, however, may produce leakage path at a pressure lower than 64.5 psi.

The ultimate structural capacity of the Sequoyah is strongly dependent on as built condition of the specific details and requires nonlinear inelastic analysis under consideration of strain hardening and strain rate effects. Generally, however, dynamic structural capability exceeds the static capability, in particular, if the loading is of impulsive type with short load application time as compared to the length of the lower natural period of the containment. Also previous analyses of pressure vessel closures indicate that the collapse pressure (defined collapse pressure in ASME Code is equal to the load which produces deformation twice that of the elastic deformation at the same load) usually occurs at pressures in excess of the pressure to produce first plasticity in a cross section.

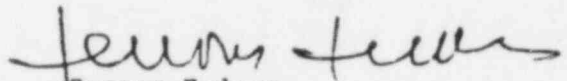
Dr. R. Savio
ACRS

- 4 -

August 29, 1980

Accordingly, the computed internal pressure for plastic limit at p = 30.3 psi can be considered a reasonable lower limit.

Very truly yours,



Zenons Zudans
Senior Vice President, Engineering

ces

encls.

Enclosure 1

SHELL OF REVOLUTION ANALYSIS
FOR EL. 730' TO 769' REGION

Shell of revolution model representing portion of containment between A-A and B-B, Figure 1 was made. It was assumed that the meridional rotation was zero at Sections A-A and B-B to simulate the fact that, due to approximately uniform distance between the rings, such rotation would be zero in a full containment model. This is deemed to be a good assumption. At A-A it was further assumed that the shell was fixed axially and free to expand radially. At B-B, axial force per unit length of meridian, equal to the end closure pressure loading of 20 psi was applied, and free radial expansion allowed.

The rings were modelled as circular plates, hence represented exactly within the linear theory of shells. The meridional stiffeners (stringers) were included in one analysis, such that their contribution to meridional bending and axial stiffness is correctly represented. For another analysis these meridional stiffeners were ignored.

Analysis with rings and meridional stiffeners produced stresses shown in Figure 3. Analysis with rings, but without meridional stiffeners produced stresses shown in Figure 2.

As anticipated, if stiffeners are neglected, full membrane stress is developed some distance away from the rings. This is due to the fact that distance between the rings is in the order of 5 to 7 times the characteristic length of the cylinder, i.e., edge effects at the ring do not propagate in the shell. Full yield would develop at locations between the rings at a pressure

$$p = \frac{32,000t}{R}$$

For locations shown in Figure 3,

$$p = \frac{20}{22,851} \times 32,000 \approx 28 \text{ psi}$$

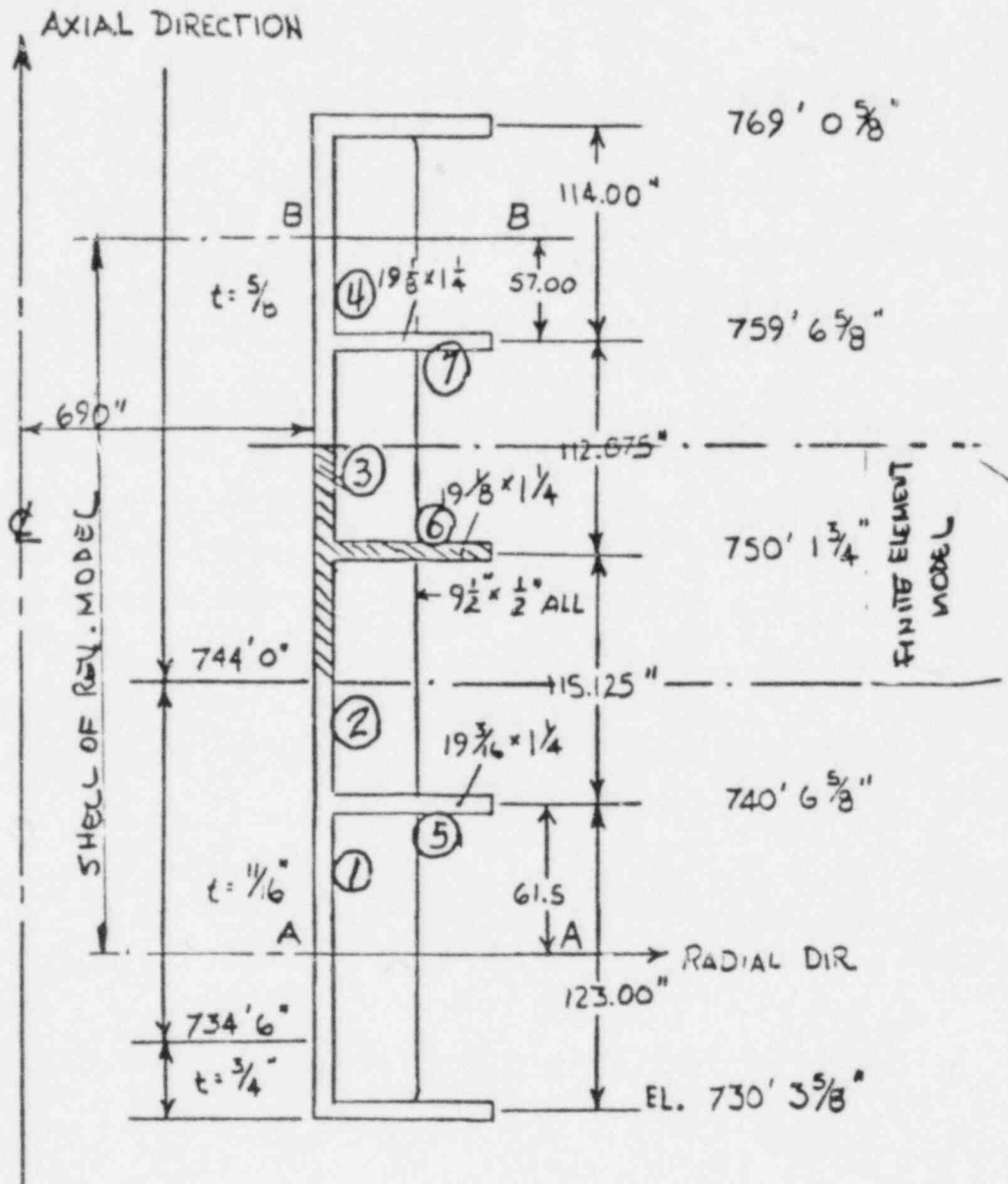


Figure 1. Portion of Sequoyah Containment Analyzed

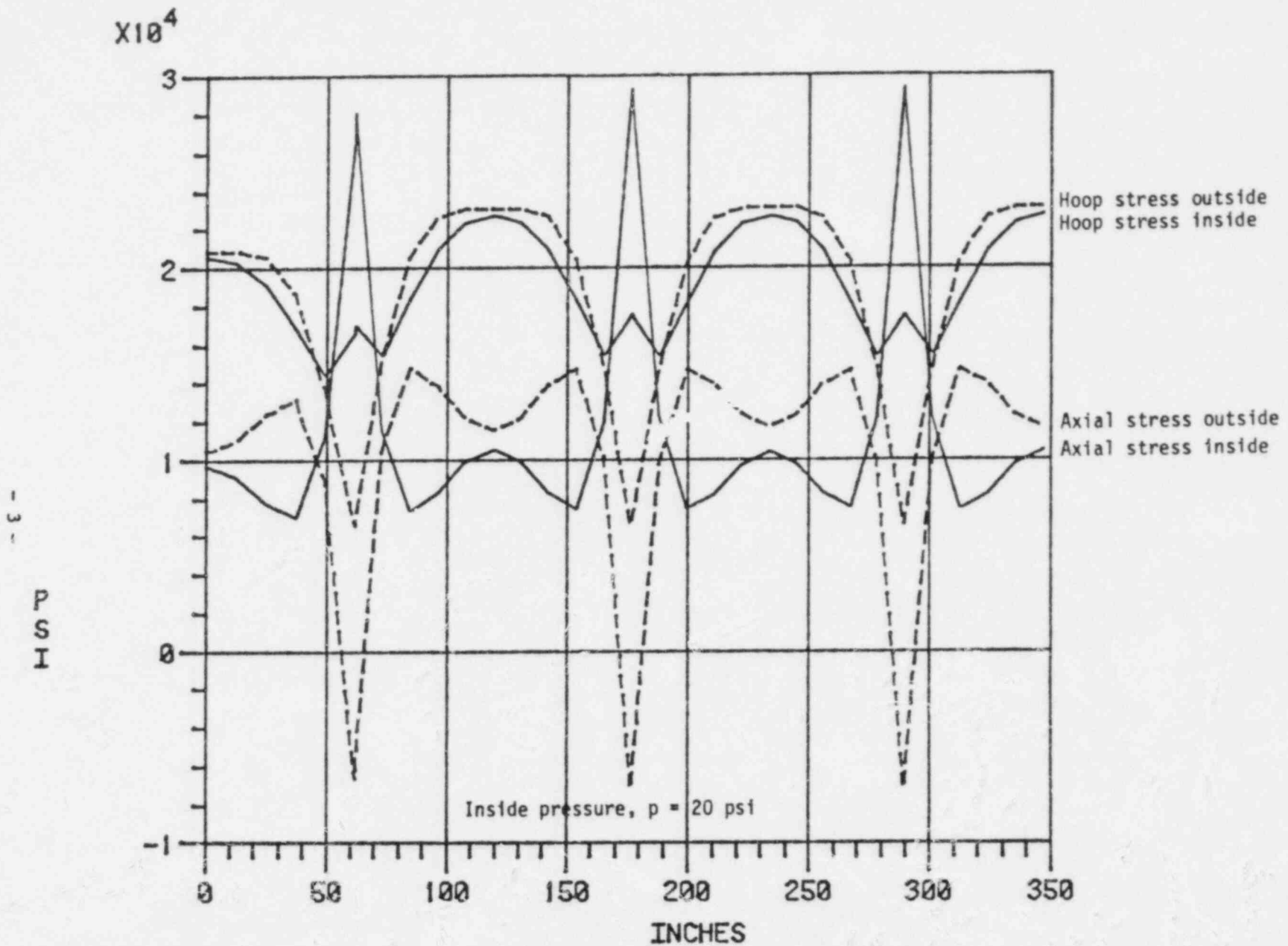


Figure 2. Stresses in Sequoyah Containment Portion Analyzed (without Stiffeners)

- 3 -

-211-

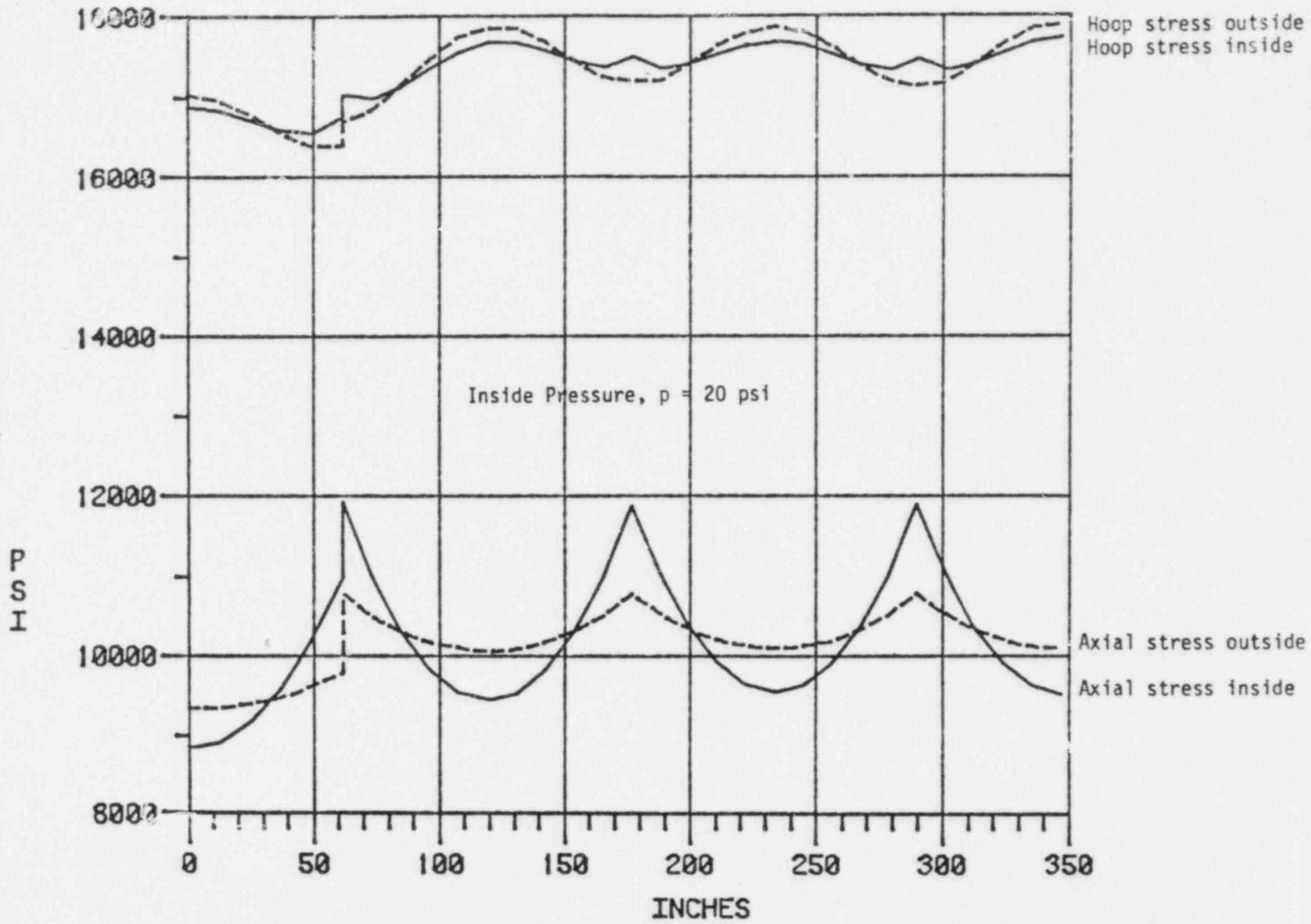


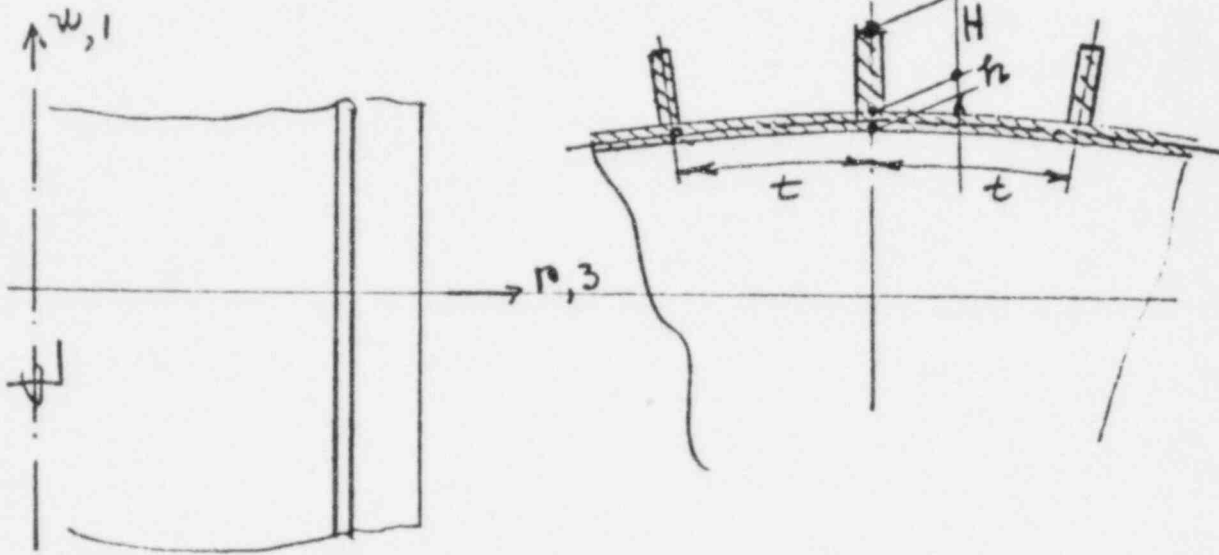
Figure 3. Stresses in Sequoyah Containment Portion Analyzed (with Stiffeners)

Full plastic hinges, however, would develop at the rings considerably earlier. For a single loading cycle such hinges would not represent failure if weldings is done appropriately. The results just discussed, however, do not represent a good approximation to the limit load corresponding to gross plastic strain development.

The second analysis of the same section with consideration of meridional stiffeners (stringers) produced stresses shown in Figure 3. Here stringer axial and bending stiffnesses are "smeared out," but in a more rigorous manner than in Ames analysis.

The basic assumption here is that stringers are forced to assume the deformation shape of the shell meridian. This means that the stringer meridional strain is derived from

$$e_{11} = p_{11} + zq_{11} \quad (1)$$



where p_{11} is the shell axial membrane strain and q_{11} is the shell curvature strain. The strain energy density in the stringer is then

$$2W = Ee_{11}e_{11} = E (p_{11}p_{11} + 2z p_{11}q_{11} + z^2 q_{11}q_{11}) \quad (2)$$

Total strain energy per unit of circumference is obtained by integrating (2) over the volume of stringers. Given consideration to the fact that stringers occupy only b/t fraction of the circumference, the total strain energy is obtained from

$$U = \int_{\tau} W d\tau = \int_{\sigma} \left(\frac{b}{t} \int_{h/2}^{\frac{b}{2}+H} W dz \right) d\sigma = \int_{\sigma} \bar{W} d\sigma$$

$$\begin{aligned} \bar{W} = \frac{1}{2} E \frac{b}{t} \left\{ H P_{11} P_{11} + \left[\left(\frac{H+h}{2} \right)^2 - \left(\frac{h}{2} \right)^2 \right] P_{11} q_{11} \right. \\ \left. + \frac{1}{3} \left[\left(\frac{H+h}{2} \right)^3 - \left(\frac{h}{2} \right)^3 \right] q_{11} q_{11} \right\} \end{aligned} \quad (3)$$

Equation 3 will contribute to the stress resultants and final constitutive relations used in the program are

$$\begin{pmatrix} N_{11} \\ N_{22} \\ M_{112} \\ M_{22} \end{pmatrix} = \frac{E}{1-\nu^2} \begin{pmatrix} h + \beta \frac{b}{t} H & \nu h & \beta \frac{b}{2t} \left[\left(\frac{H+h}{2} \right)^2 - \left(\frac{h}{2} \right)^2 \right] & 0 \\ \nu h & h & 0 & 0 \\ \beta \frac{b}{2t} \left[\left(\frac{H+h}{2} \right)^2 - \left(\frac{h}{2} \right)^2 \right] & 0 & \frac{h^3}{12} + \frac{1}{3} \beta \frac{b}{t} \left[\left(\frac{H+h}{2} \right)^3 - \left(\frac{h}{2} \right)^3 \right] & \frac{\nu h^3}{12} \\ 0 & 0 & \frac{\nu h^3}{12} & \frac{h^3}{12} \end{pmatrix} \begin{pmatrix} P_{11} \\ P_{22} \\ q_{11} \\ q_{22} \end{pmatrix}$$

Note that $\beta = 1-\nu^2$, however, the numerical results of Figure 3, are produced with $\beta=1$. Results, Figure 3, with meridional stiffeners indicate that stringers transfer significant amount of loading to the rings and that the average membrane stresses in the shell is reduced to 17,722 psi. This results in the pressure causing yield in the shell equal to

$$P = \frac{20}{17,722} \times 32,000 = 36 \text{ psi}$$

The fact that this number is close to that indicated by Ames Analysis is pure coincidence. For comments on Ames Analysis, see Enclosure 3.

Are the effects of the stiffeners realistically determined in Figure 3 analysis? It is noted from Figure 3 that axial stress average varies along the cylinder. At the ring locations the average stress in the shell increases and it is reduced towards the middle of the span between the rings. This indicates that the axial stresses in the stringer likewise vary along the meridian, being the smallest at the ring. This behavior is qualitatively correct due to the increased bending effect at the rings. For more detailed explanation, see Enclosure 2, Finite Element Analysis Results.

FINITE ELEMENT ANALYSIS OF A PORTION
OF SEQUOYAH CONTAINMENT

A portion of the model shown in Figure 1, Attachment 1 (identified by "Finite Element Model") was modelled over 2° of circumference using finite elements. This model is shown in Figure 4.

This analysis was performed to clarify the behavior of the containment due to shell, ring, and stringer interactions. The solution was constructed such that the top of the model displaced uniformly in axial direction and was free in radial direction. Symmetry condition where imposed in the x-plane, and 2° away from the x-plane, Figure 4. Bottom of the model was fixed axially (z-direction) and both bottom and top boundaries where subject to symmetry condition (free radial expansion, zero meridian rotation).

The results of this analysis confirmed the behavior of the structure as in general found in shell of revolution analysis. The radial deflections at the four corners of the model, for internal pressure $p = 20$ psi and corresponding end load of 166,190 lbs, where found to be, Figure 4,

	<u>Finite Element</u>	<u>Shell of Revolution</u>
Corner A	0.3487 in.	0.3661
Corner B	0.4155	0.3661
Corner C	0.3518	0.3661
Corner D	0.4227	0.3661

which indicates that the panel deflects somewhat more at the midplane of the span than the stiffener does. In all cases values of shell of revolution analysis fell in between those of the finite element results.

Axial stretching of the finite element model was 0.02015 in as compared to 0.02034 in. found in the shell of revolution analysis.

The highest average hoop stress was found to be 18,660 psi, which corresponds to pressure

$$p = 20 \frac{32,000}{18,660} = 34.3 \text{ psi}$$

required to produce yield through the entire thickness of the shell. It is noted that a substantial bending is superimposed over the average membrane stress (see Appendix for details). Near the stiffener, element 1, Figure 4; inside surface sees higher tensile stresses due to restraint offered by the stringer (inside 25,500 psi, outside 11,790 psi). Progressing towards midspan, outer fibers of the shell see larger tensile stresses than the inside (inside 13,570 psi outside 23,400 psi). Average hoop stress in the entire panel stays rather constant reducing to approximately 16,590 psi only at the ring stiffener. This indicates that yielding of the essentially entire span between the ring and stiffeners can occur in the range of pressures 34.3 to 38.6 psi. Surface yielding will occur prior to the overall yielding.

It is noted that ring, shell and stiffener interaction did not allow full hoop stress of 22,080 psi ($= 20 \times 690 / 0.625$) to be developed anywhere in the panel.

Another interesting observation is depicted in Figure 5. Here, the axial loads carried in stiffener and in the shell are compared. At the circumferential ring location, the stiffener carries only 2710 lb while at the midspan its contribution is increased to 16,990 lb of the total end load of 166,190 lb. This behavior is qualitatively confirmed as follows: at the ring location, significant bending is introduced in the stringer, since the ring moves radially less than the shell midspan between the rings does (ring 0.3234, shell 0.3487). In fact element 102 shows compressive axial stress, while element 83 has a higher tensile stress than the the element 81.

Further details of the finite element analysis are found in the Appendix.

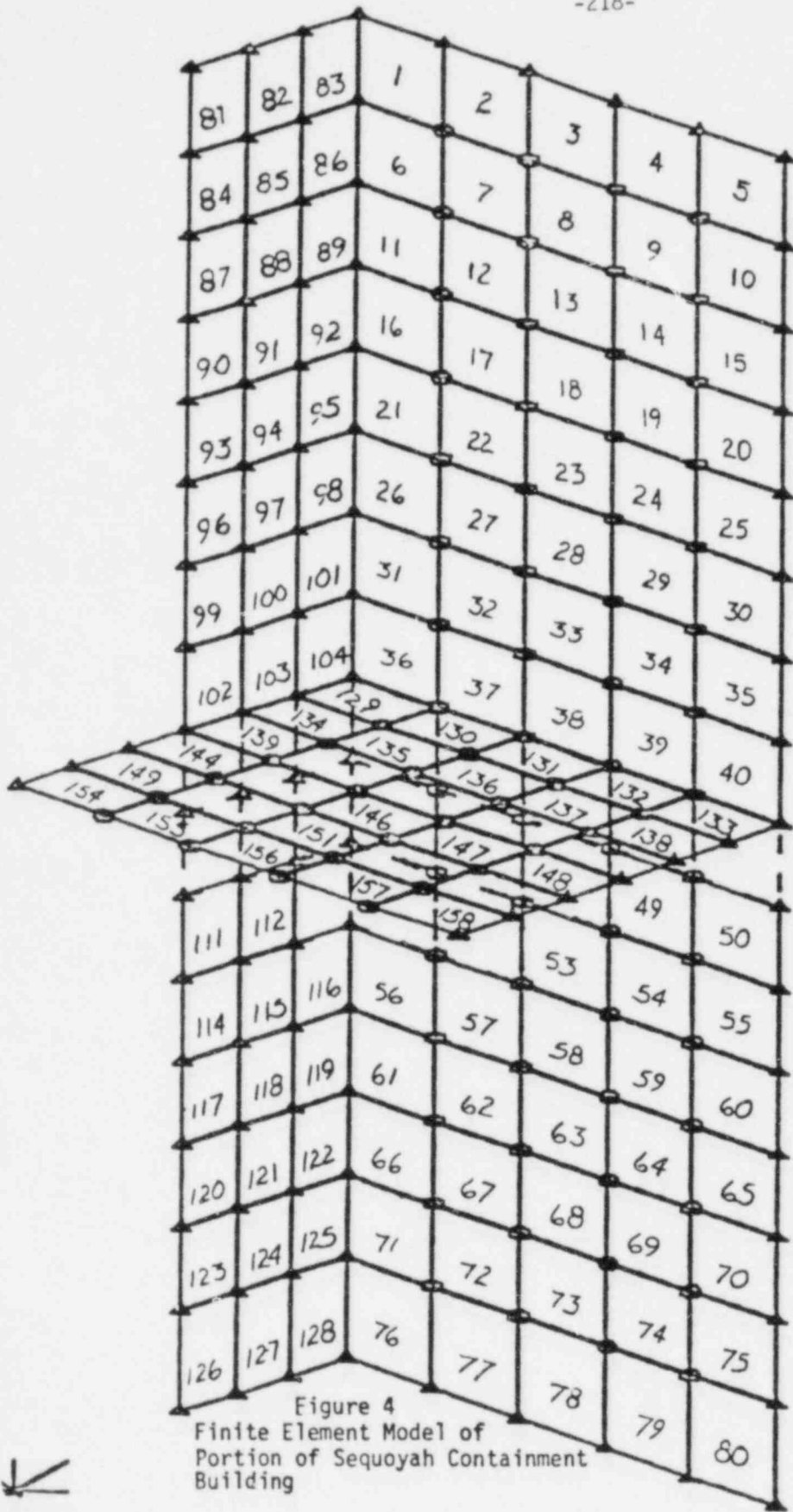
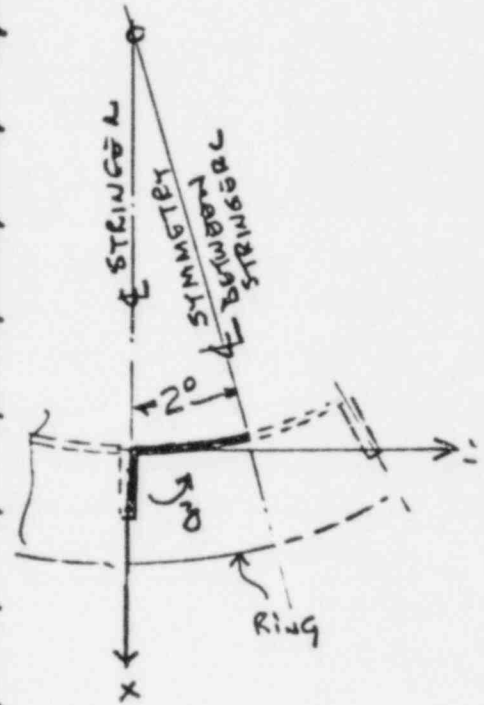
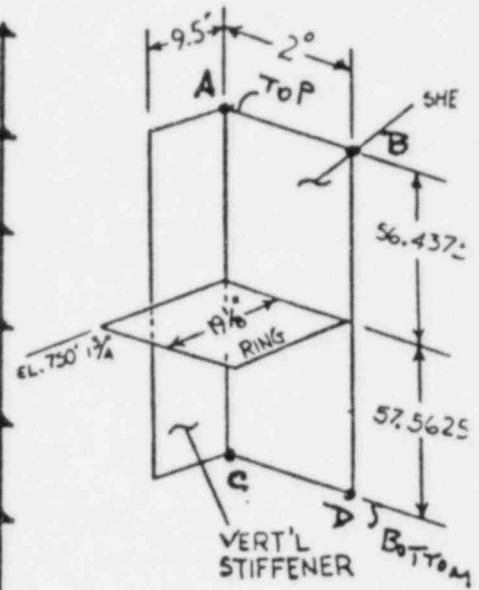


Figure 4
Finite Element Model of
Portion of Sequoyah Containment
Building



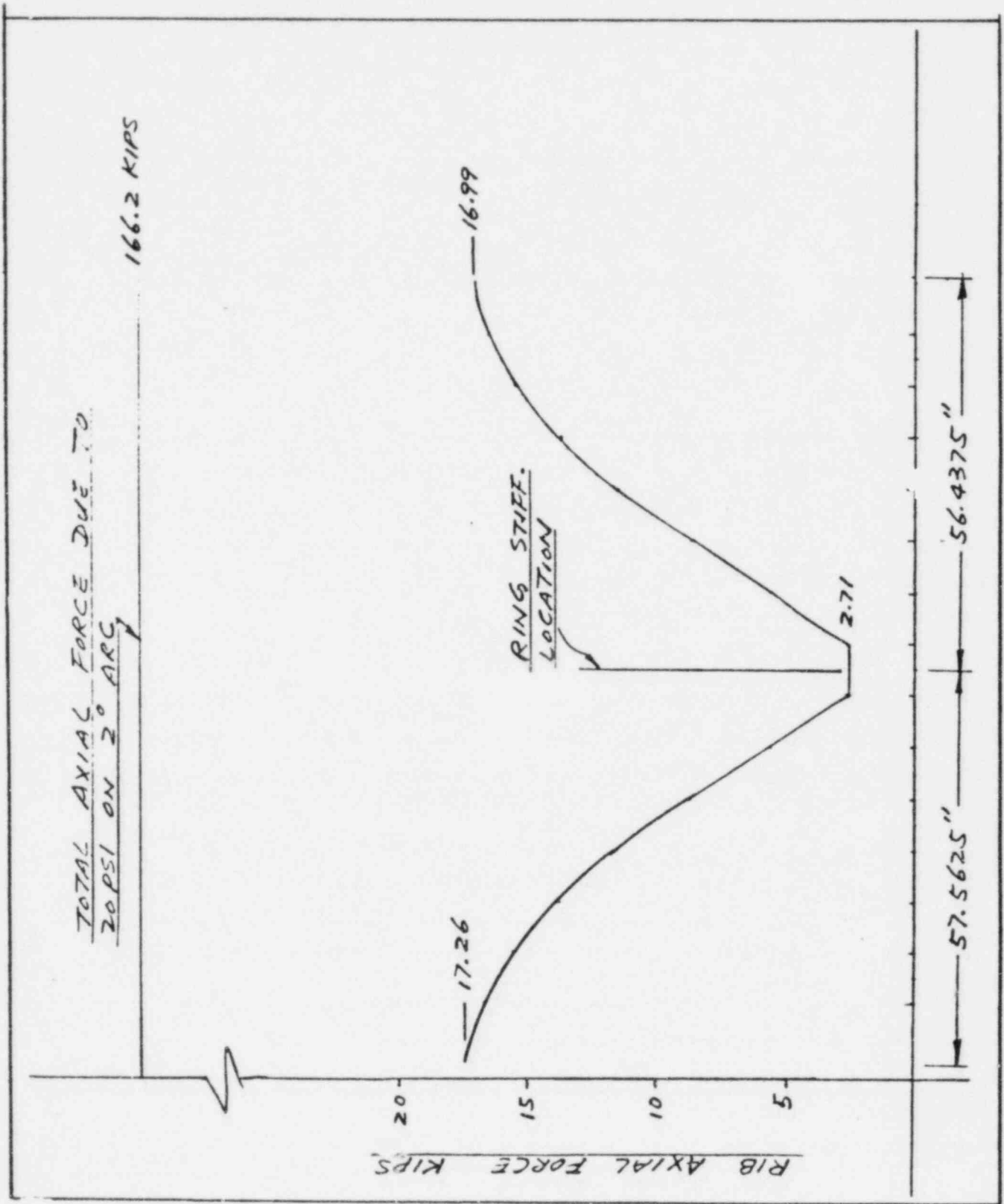


Figure 5. Axial Load Sharing Between Stiffener and Shell

Comments to:

Dr. L. Greimann, Ames Lab. Analysis:
"Ultimate Strength Characteristics of the Sequoyah and McGuire
Containments," January 21, 1980.

1. Assumption of "smeared out rings" by use of an equivalent circumferential thickness

$$t_{e\theta} = t + A_r/S_r$$

is not conservative since the distance between the rings range from 4 to 7 characteristics length of the cylinder. All edge effects (at the ring) will decay completely towards midspan between the rings and full hoop stress will develop as if the rings were not there. This is confirmed in Figure 2 of the Shell of Revolution Analysis, Page 3, Enclosure 1.

2. Assumption of "smeared out" meridional stiffeners (stringers) is a common practice of the industry when shell of revolution type of the analysis is used. However, a correct "smearing out" method considers the bending stiffness of the stringer in addition to the axial stiffness. Since the bending stiffness of stringers is significant as compared to the shell bending stiffness, stringers transfer loads to rings and, if properly spaced, can reduce the hoop stress in the shell considerably. Typical "smearing out method" normally used in shell of revolution analysis is shown in Pages 5 to 7 of Attachment 1, Ames method not acceptable.

3. Assumptions used in Ames report will not yield a reliable burst pressure. Burst pressure depends strongly on load history, fracture characteristics of welds, local geometry (as built), materials hardening parameters, all of which can be considered (approximately) by use of a large deformation, inelastic analysis or by testing.

4. Calculations of limit pressure for stringers and ring stiffeners as described in the report are meaningless. Accordingly, the conclusion, that the ring stiffeners will yield first (at 35.57 psi) is not realistic. Hoop stresses in ring stiffeners are considerably lower than those in the shell (see Attachments 1 and 2).

5. Penetration replacement area calculation is not in compliance with the ASME Code. Paragraph NB-3334.2 (Page 73- 1980 edition) requires that the reinforcing normal to the shell wall shall be within

$$0.5 \sqrt{121.5(3)} = 9.5 \text{ in.}$$

of the wall and 75% of the reinforcing must be located at most (NB-3334.1)

$$0.5 \sqrt{690(0.75)} = 11.37 \text{ in.}$$

from the finished diameter of the equipment hatch. Using these limits we find that the available reinforcing is only

$$\begin{aligned} 2 \times (9.5 \times 3) &= 57.00 \text{ in}^2 \\ 2(1.5 - 0.75) 11.37 &= \frac{17.01}{74.01 \text{ in}^2 < 135 \text{ (75\% of 180)}} \end{aligned}$$

Accordingly, the conclusion reached in the report is not substantiated.

Comments to:

R&D Associates Report: "Sequoyah Containment Analysis," 25 July 1980.

R&D report presents an interesting discussion of stringer and skin interaction (Page 6). The results would be exact if: 1) full hoop stress $s_c = p R/t$ can be developed and if one deals with an infinite cylinder without ring stiffeners. As shown in Enclosure 2, rings and stringers will cause significant reduction of hoop stresses and, due to bending of stringers, axial stress S_L in the stringer will vary considerably over the span between the rings. Also, the presence of stringers reduces the hoop stress in the shell at midspan between the rings. Accordingly, the results of the Page 6 analysis, while correct for conditions assumed, are not realistic for determination of the plastic limit load.

Alternate panel analysis, Pages 12 to 17, is based on the assumption of rigid boundary and flat panel. These assumptions are totally inappropriate here, because we deal with curved shell and all boundaries are able to deflect. Accordingly, conclusion based on this analysis are not applicable to subject containment. Applicable ring, stiffener and shell interaction is presented in Enclosure 2.

Bolt yield pressure of 64.5 psi, found by R&D is acceptable to this reviewer.

SHELL REVOLUTION ANALYSIS
FOR EL. 778' TO 798'

Shell of revolution model representing the portion of the containment, Figure 6, was used for the analysis. All basic assumptions used in the second analysis, Enclosure 1, were applied here as well, including the method of "smearing-out" the meridional stiffeners.

Qualitative results for this analysis are similar to those for the second analysis. The stress distribution in the shell is shown in Figure 7. The highest hoop membrane stress of 20,039 psi is found at the junction of 5/8" and 1/2" shell sections. Its increase over that found in the second analysis is due to decrease in shell thickness and also due to the reduction of the ring size. This hoop stress would cause yield at

$$p = \frac{20}{20,039} (32,000) = 31.9 \text{ psi}$$

This pressure exceeds that predicted by R&D Associates and it reflects the positive influence offered by the meridional stiffeners and rings in reducing the hoop stress from 27,600 psi to 20,039 psi. The membrane hoop stress in the span between elevations 778' 0-5/8" to 788' 0-5/8" varies between 20,039 psi and 17,390 psi. This entire section will yield in the range of pressures 31.9 psi to 36.8 psi.

There was no finite element analysis performed for this model. Based on the findings when comparing the second and third analysis, it is reasonable to assume that the lowest pressure required to yield the junction of 5/8" and 1/2" sections will be

$$(31.9) \frac{34.3}{36.1} = 30.3 \text{ psi}$$

The model, Figure 6, extends to the spring line between cylinder and the sphere. It is anticipated that the discontinuity effects of the sphere will not affect adversely the critical section identified in this analysis, in particular since the transition section is strongly reinforced with rings.

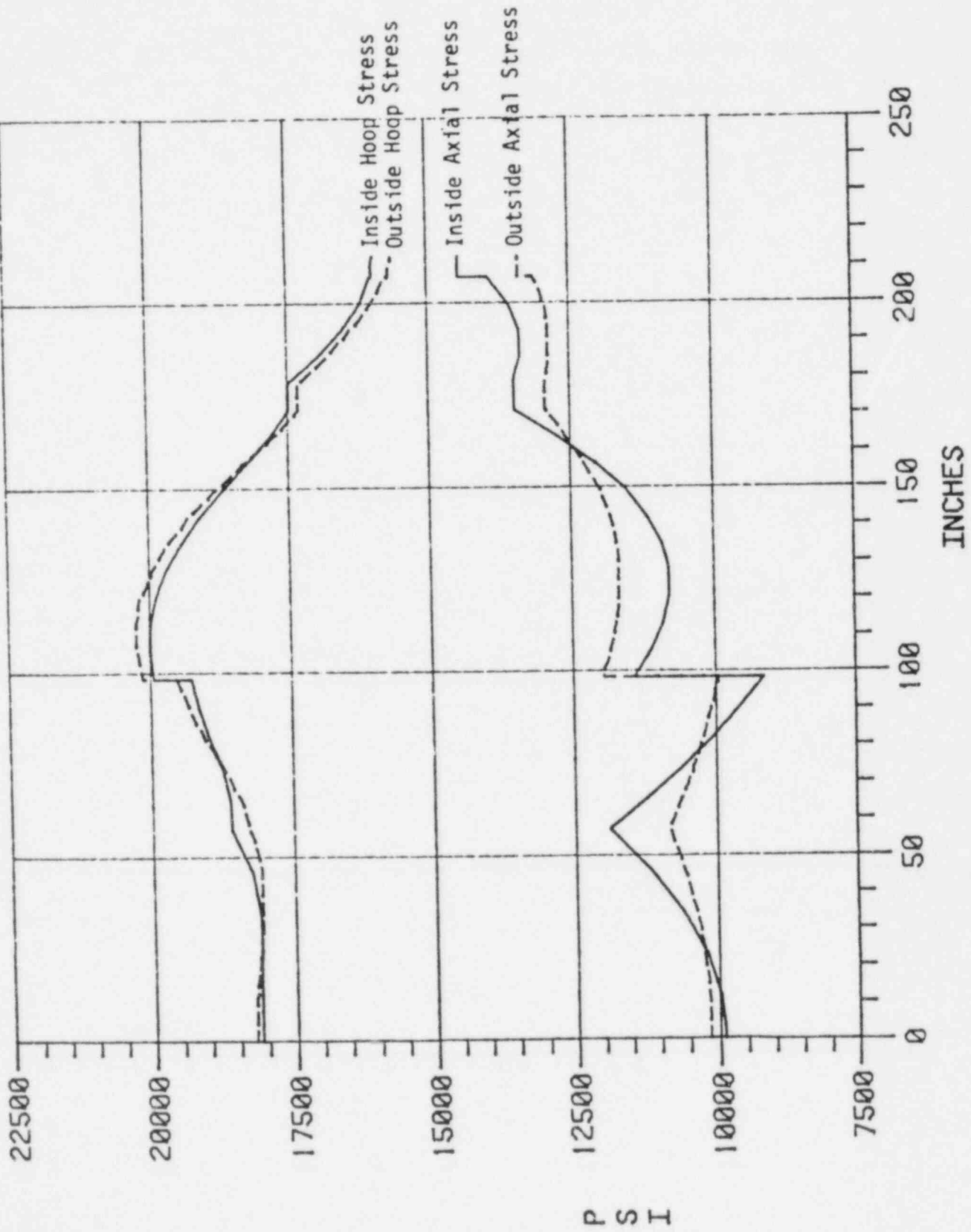
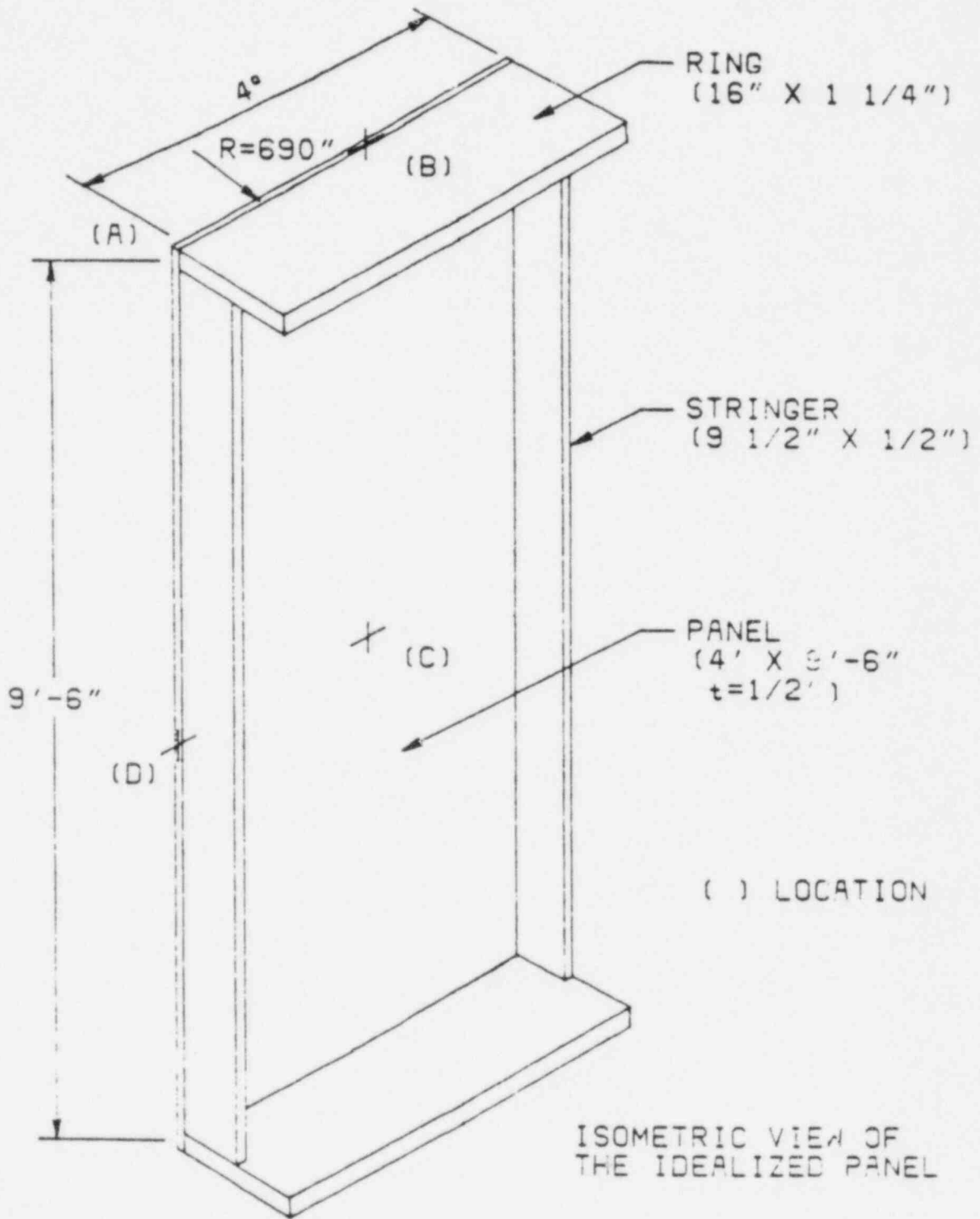
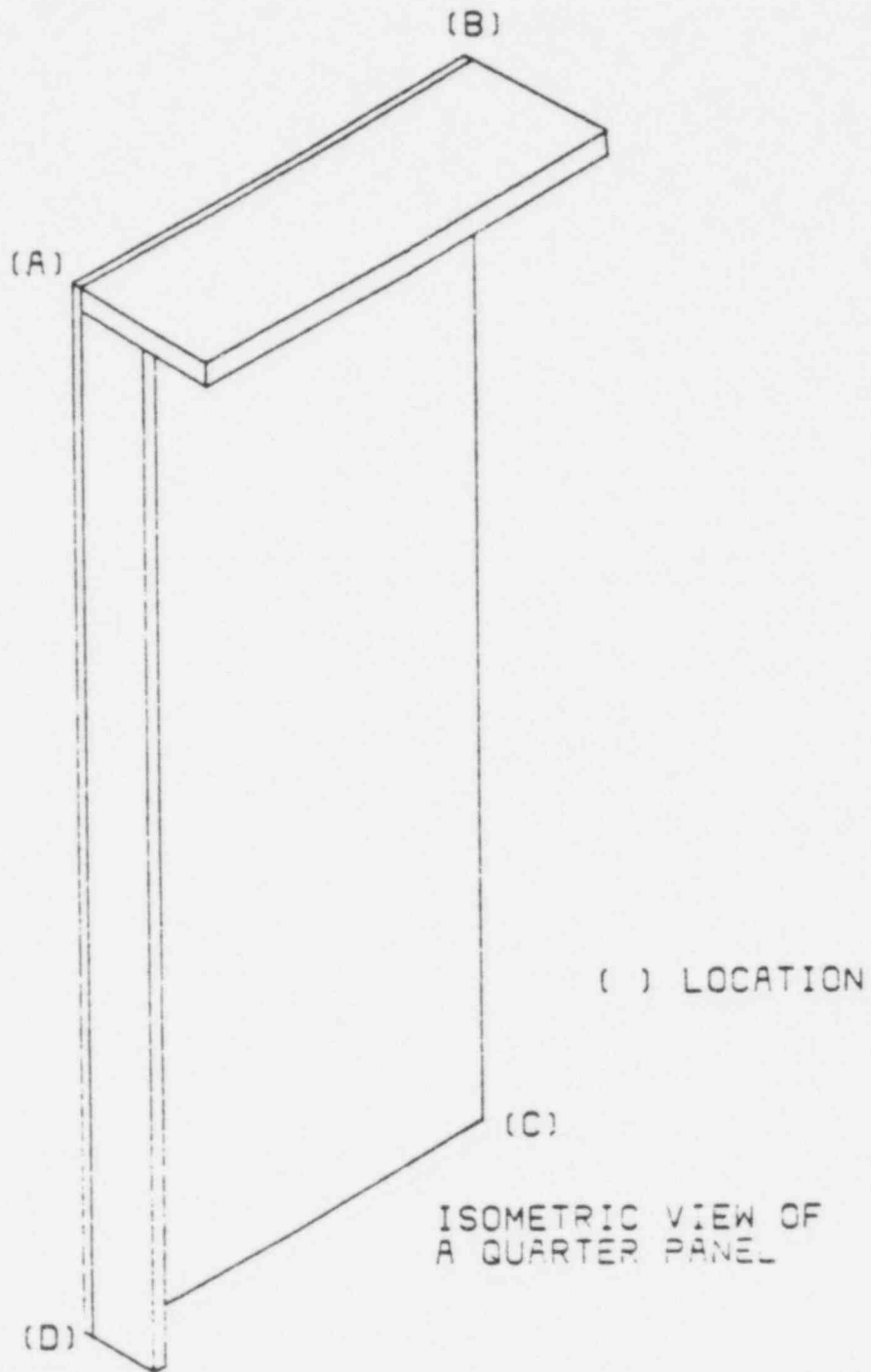


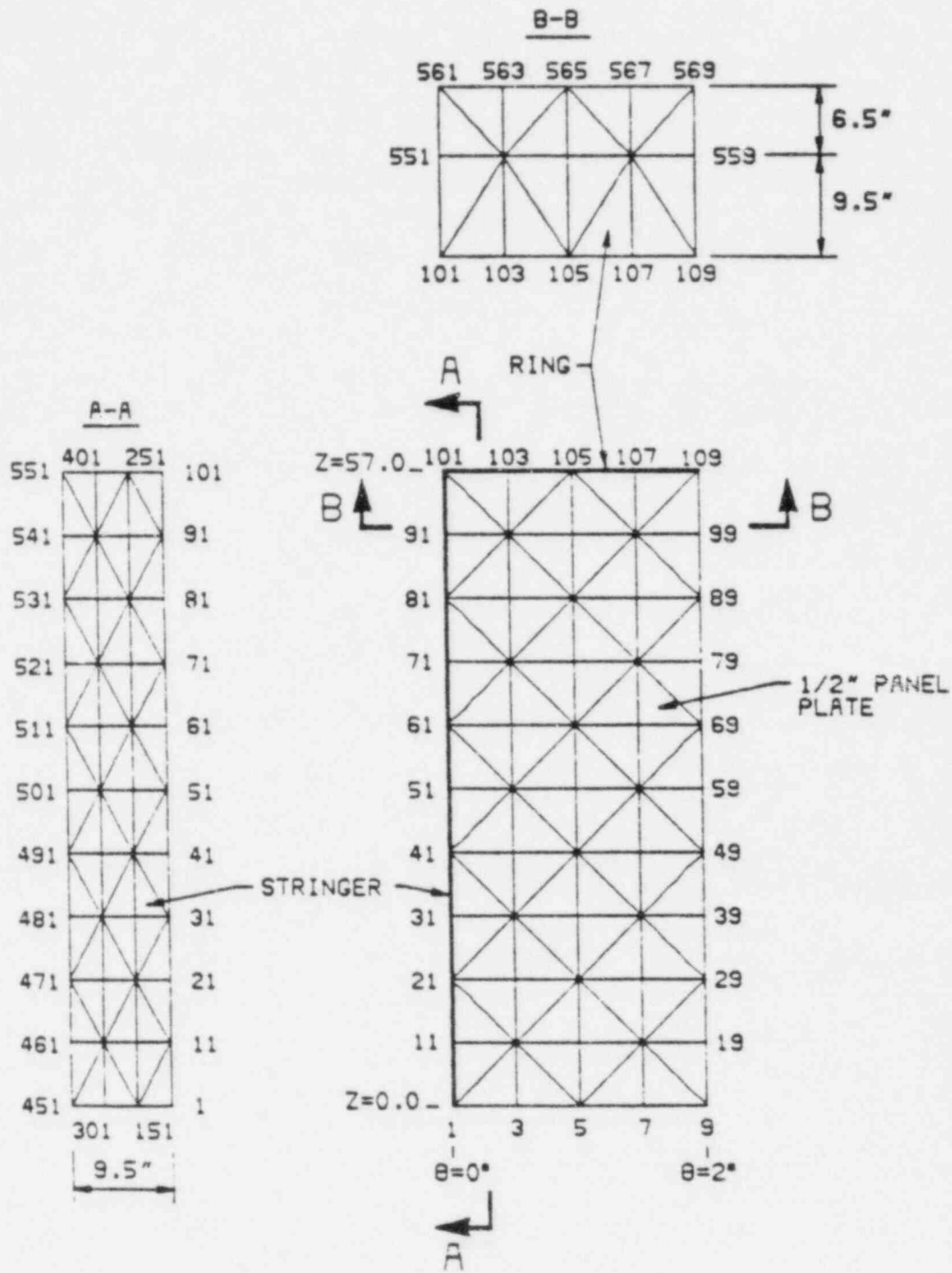
Figure 7. Stresses in Sequoyah Containment 1/2" Shell Section Analyzed

REFERENCE F

Orr, R. (Offshore Power Systems), oral presentation at ACRS meeting, September 2, 1980.







FINITE ELEMENT MODEL OF THE QUARTER PANEL

STRESSES DUE TO 12 PSI INTERNAL PRESSURE LOAD

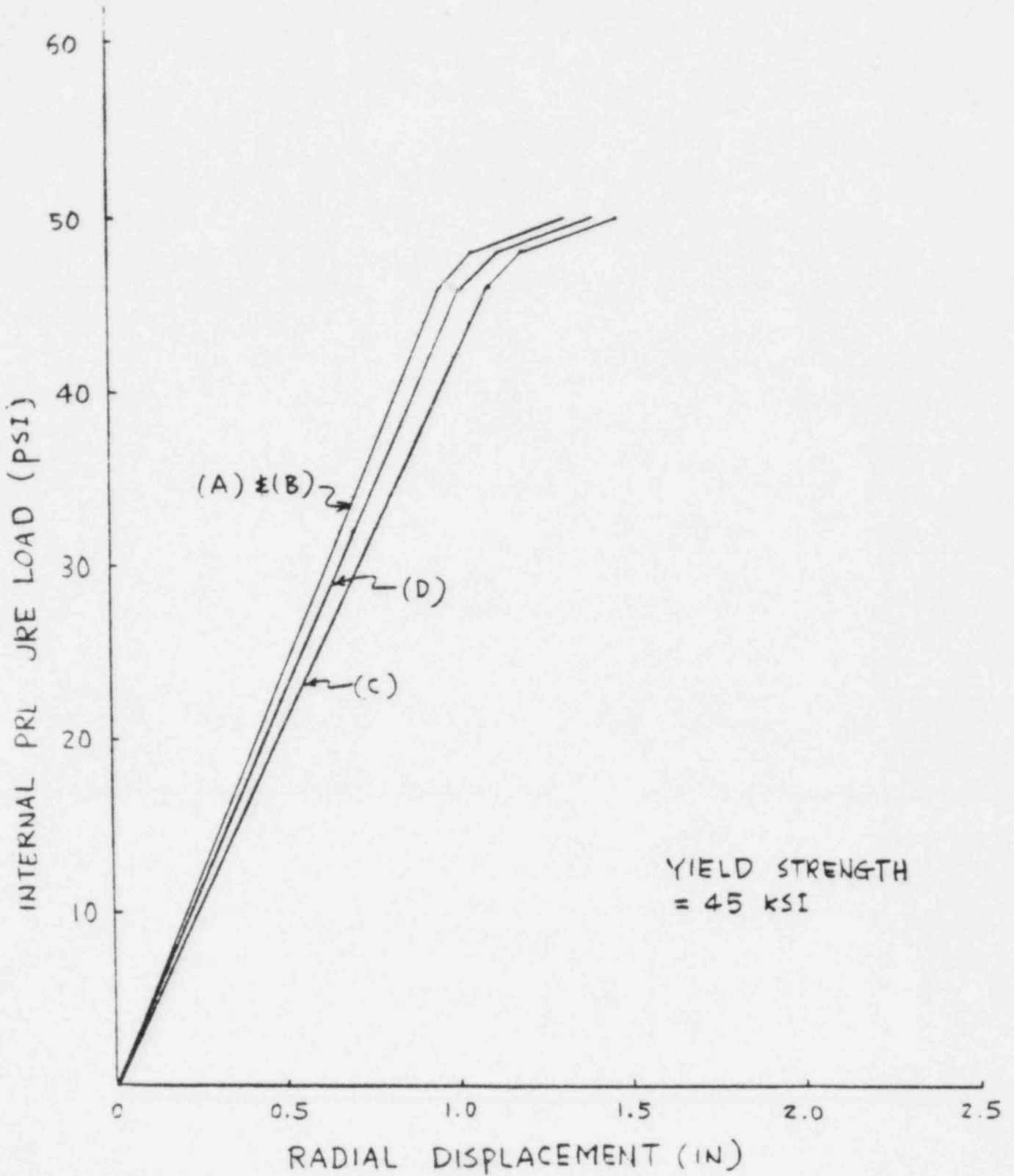
MEMBER	LOCATION	FIBER	STRESS INTENSITY (ksi)	VON MISES (ksi)
1/2" PANEL PLATE	CENTRAL REGION OF THE PANEL (C)	OUTER SURFACE	18.3	15.9
		MID SURFACE	14.0	12.1
		INNER SURFACE	9.6	8.4
	NEAR MID SPAN OF THE RING (B)	OUTER SURFACE	10.5	9.3
		MID SURFACE	12.0	10.5
		INNER SURFACE	13.6	12.8
	NEAR MID SPAN OF THE STRINGER (D)	OUTER SURFACE	8.6	7.5
		MID SURFACE	14.1	12.2
		INNER SURFACE	20.2	17.6

STRESSES DUE TO 12 PSI INTERNAL PRESSURE LOAD

MEMBER	LOCATION	FIBER	STRESS INTENSITY (ksi)	VON MISES (ksi)
RING	MID SPAN (B)	NEAR INNER EDGE	9.2	9.2
		NEAR OUTER EDGE	9.5	9.4
	RING-STRINGER JUNCTION (A)	NEAR INNER EDGE	9.3	9.3
		NEAR OUTER EDGE	9.5	9.1

STRESSES DUE TO 12 PSI INTERNAL PRESSURE LOAD

MEMBER	LOCATION	FIBER	STRESS INTENSITY (ksi)	VON MISES (ksi)
STRINGER	MID SPAN (D)	NEAR INNER EDGE	3.1	3.0
		NEAR OUTER EDGE	6.9	6.8
	RING-STRINGER JUNCTION (A)	NEAR INNER EDGE	6.5	6.0
		NEAR OUTER EDGE	4.9	4.5



PRESSURE - DISPLACEMENT CURVES BASED ON GEOMETRIC & MATERIAL NON-LINEAR ANALYSIS

STRESSES DUE TO 46 PSI INTERNAL PRESSURE LOAD

MEMBER	LOCATION	FIBER	HOOP STRESS (ksi)	VON MISES (ksi)
RING	MID SPAN (B)	NEAR INNER EDGE	39.4	39.5
		NEAR OUTER EDGE	37.0	37.0
	RING-STRINGER JUNCTION (A)	NEAR INNER EDGE	38.2	38.2
		NEAR OUTER EDGE	38.9	38.9

MEMBER	LOCATION	FIBER	LONGI-TUDINAL STRESS (ksi)	VON MISES (ksi)
STRINGER	MID SPAN (D)	NEAR INNER EDGE	11.5	12.0
		NEAR OUTER EDGE	22.0	21.8
	RING-STRINGER JUNCTION (A)	NEAR INNER EDGE	18.1	22.9
		NEAR OUTER EDGE	-10.2	10.2

CONTAINMENT YIELD PRESSURE

BASE CASE

0.5 INCH PLATE

NOMINAL YIELD = 32,000

$$p_0 = 23.2 \text{ psi}$$

FACTOR (F₁) ACTUAL YIELD

$$F_1 = \frac{45}{32} = \underline{1.41}$$

FACTOR (F₂) VON MISES YIELD

$$F_2 = \underline{1.15}$$

TWO WAY STIFFENING

$$16" \times 1\frac{1}{4}" \text{ HOOP OVER } 9'6" \text{ LENGTH} : F_3 = 1 + \frac{16 \times 1.25}{114 \times 0.5} = \underline{1.35}$$

$$16" \times 1\frac{1}{4}" \text{ HOOP OVER } 6'6" \text{ LENGTH} : F_4 = 1 + \frac{16 \times 1.25}{78 \times 0.5} = \underline{1.51}$$

FINITE ELEMENT PANEL

$$\begin{aligned} \text{CAPABILITY} &= p_0 \times F_1 \times F_2 \times F_3 \\ &= 23.2 \times 1.41 \times 1.15 \times 1.35 = \underline{50.5 \text{ psi}} \end{aligned}$$

SEQUYAH - PANEL AT SPRING LINE

$$\begin{aligned} \text{CAPABILITY} &= p_0 \times F_1 \times F_2 \times F_4 \\ &= 23.2 \times 1.41 \times 1.15 \times 1.51 = \underline{56.5 \text{ psi}} \end{aligned}$$

REFERENCE G

Greimann, L.F. (Ames Lab.), letter report to Dr. F.P. Schauer, NRC, Washington, DC, July 18, 1980 and supplement of July 30, 1980.

SUPPLEMENT TO: PRELIMINARY CALCULATIONS, ULTIMATE STRENGTH FOR HYDROGEN EXPLOSION, SEQUOYAH CONTAINMENT VESSEL (submitted 7/18/80)

TO: F. P. Schauer, Chief Structural Engineering Branch
Division of System Safety
Office of Nuclear Reactor Regulation
Nuclear Regulatory Commission
Washington, DC 20555

BY: Lowell Greimann
Ames Laboratory
Iowa State University
Ames, IA 50011

DATE: July 30, 1980

Idealized Pressure Loading

The dynamic pressures associated with detonation are not significant for two reasons (see pg. 6).

The detonation time is much smaller than the period of motion of the structure

$$\frac{t_d}{T} = \frac{0.0000025}{0.040} = 6.25(10^{-5})$$

The impulse associated with detonation, I_d , is negligible with respect to the impulse from the venting pressure, I_v ,

$$\frac{I_d}{I_v} = \frac{1.375(10^{-5})p_v}{0.015 p_v} = 9.2(10^{-4})$$

or, I_d is about 0.1% of I_v .

Ductility Capacity - Lower Bound

A lower bound on the ductility capacity of a pressure vessel is

$$\mu_c = 2$$

This value is a design recommendation by the Welding Institute in the United Kingdom and is based upon experimental evidence.* Also, the ASME

* Rolfe & Barsom, Fracture and Fatigue Control in Structures, Prentice Hall, 1977, pp. 527-530.

Boiler and Pressure Vessel Code** previously defined the collapse pressure of a vessel as the pressure at which the displacement is two times the displacement at first yielding. Note that both of these values are design recommendations. As such, they incorporate some (unspecified) factor of safety--probably between 2 and 3. With this conservative value of ductility capacity, the ultimate venting pressure would be (from page 14) about 31 psi.

** ASME Boiler and Pressure Vessel Code, Section I'I, Division 1, par. 1430, Appendix II, 1974.

PRELIMINARY CALCULATIONS
ULTIMATE STRENGTH FOR HYDROGEN EXPLOSION
SEQUOYAH CONTAINMENT VESSEL

To: F. P. Schauer, Chief Structural Engineering Branch
Division of System Safety
Office of Nuclear Reactor Regulation
Nuclear Regulatory Commission
Washington, DC 20555

By: Lowell Greimann
Ames Laboratory
Iowa State University, Ames, Iowa 50011

July 18, 1980

CONTENTS

	<u>page</u>
Summary	1
Typical Compartment	1
Assumptions	1.1
Ring Idealization	2
Pressure Loading	6
Finite Element Idealization	7
Static Solution	9
Dynamic Solution	11
Failure Criteria	15
Ultimate Strength	20

SUMMARY

This report summarizes the calculations performed to predict the ultimate strength of the containment vessel for the Sequoyah Nuclear Power Plant subject to an explosion in a lower compartment. The analysis is intended to be a first approximation which can be refined when time permits.

Assumptions

- . Behavior is controlled by the containment rings. The shell wall acts as a membrane transmitting forces to the rings. Thus, the analysis considers a typical ring in the vicinity of a lower compartment (pg. 1.1).
- . The shell below a typical ring remains elastic (pg. 4).
- . The steel was taken to have a static yield strength of 32 ksi and a dynamic strength of 39 ksi.
- . The dynamic loads from the explosion can be represented by
 - (1) An impulse of $1.37 (10^{-5}) p_v$ k-sec/in² at time zero which approximates the detonation phase.
 - (2) A dynamic pressure which decreases linearly from p_v at time zero to zero pressure at 0.030 sec. to approximate the venting phase, where p_v is the maximum value of the venting pressure (pg. 6). The pressure was applied over a 60° arc of the vessel.

Ductility limits on the vessel control the allowable strains which may be permitted (pg. 15).

Analysis

A typical ring in the lower compartment region was idealized by a number of beam type finite elements with nonlinear material and geometric capability (pg. 7). The stiffness of the shell below the ring was approximated by linear springs (pg. 7). Time dependent forces ^{were} ~~where~~ applied to the idealization (pg. 8). This idealization was analyzed by the ANSYS computer program.

Results

Static Solution:

The static solution was obtained by incrementing the pressure from 0 to 50 psi. The approximate static plastic pressure is 34 psi (pg. 10).

Dynamic Solution:

A nonlinear transient solution was obtained for the idealization discussed above. Three dynamic analyses were performed with a maximum venting pressure, p_v , of 10, 50 and 100 psi, respectively. The following results were obtained:

<u>p_v</u>	<u>μ_D</u>	<u>δ_{max}</u>
10 psi	0.4	0.6 in.
50 50 psi	4.8	4.6 in.
100 psi	24.9	24.9 in.

where μ_D is the ductility demand (maximum strain/yield strain) and δ_{max} is the maximum displacement (pg. 12).

Ductility Capacity:

The ductility capacity (allowable strain/yield strain) of the ring was taken as

$$\mu_c = 5$$

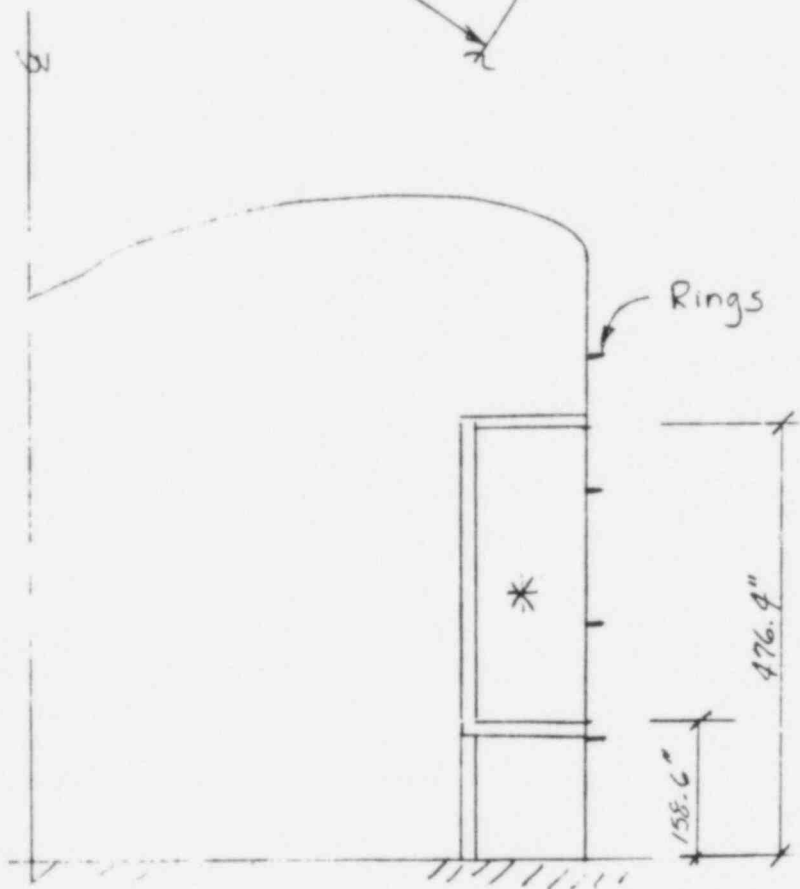
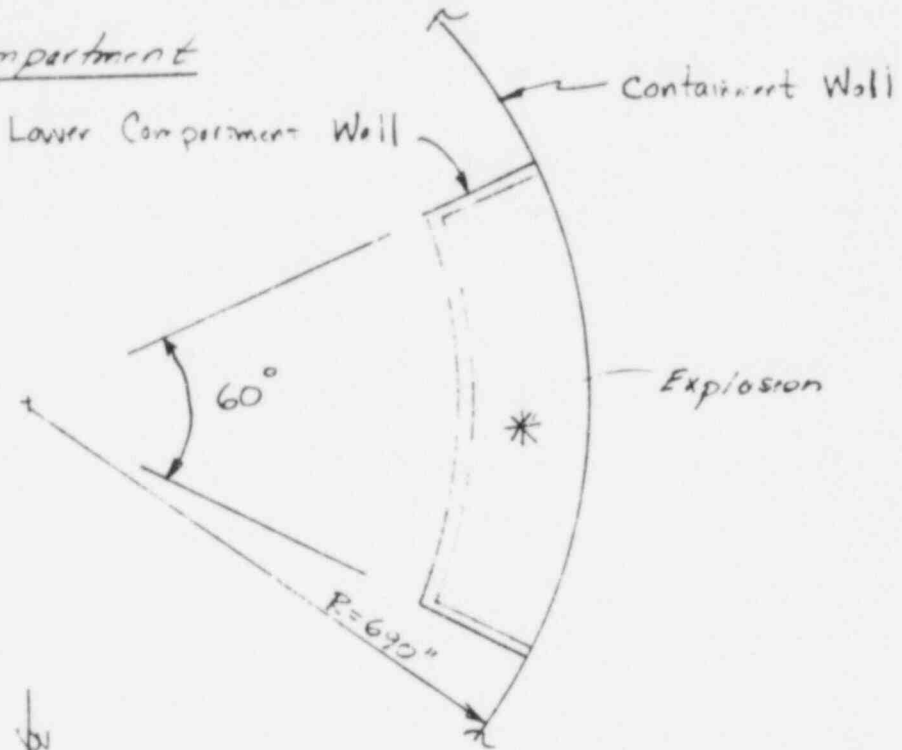
Ultimate Load:

Ultimate load is defined as the maximum value of the venting pressure at which the ductility demand is equal to the ductility capacity. The ultimate pressure is found as 51 psi (pg. 20).

EXPLOSIVE STRENGTH - SEQUOYAH NPP

LOWER COMPARTMENTS

Typical Compartment



The following analysis is considered as a first approximation to the strength of the Sequoyah containment vessel subject to a hydrogen explosion in a lower compartment. Time constraints require that several simplifying assumptions be made to make the problem tractable.

Primary Assumption

Behavior is basically non-symmetric since the loading is non-symmetric. Non-symmetric behavior of a circular cylinder is controlled primarily by its bending stiffness. In this case, the predominate bending stiffness is provided by the rings. Therefore, the non-symmetric behavior will be controlled by the rings.

Assumption: The behavior of the containment vessel is controlled by the rings in the lower compartment region. The shell wall acts only as a membrane which transmits the dynamic pressures to the rings.

(This assumption would not be as valid if the disturbance were axisymmetric, for which case the effect of the ring extends only on the order of \sqrt{rt} (a few feet) along the shell. However, for non-symmetric disturbances, the effect of the rings extends a couple diameters (many ring spacings). Hence, for this non-symmetric loading case, the rings will be quite effective in providing stiffness to the shell between stiffeners.)

(Note: Deformations of the shell wall between rings will, of course, be somewhat larger than deformations of the rings. However, the deformation between rings need only be sufficiently large to carry the pressure to the rings by membrane action.)

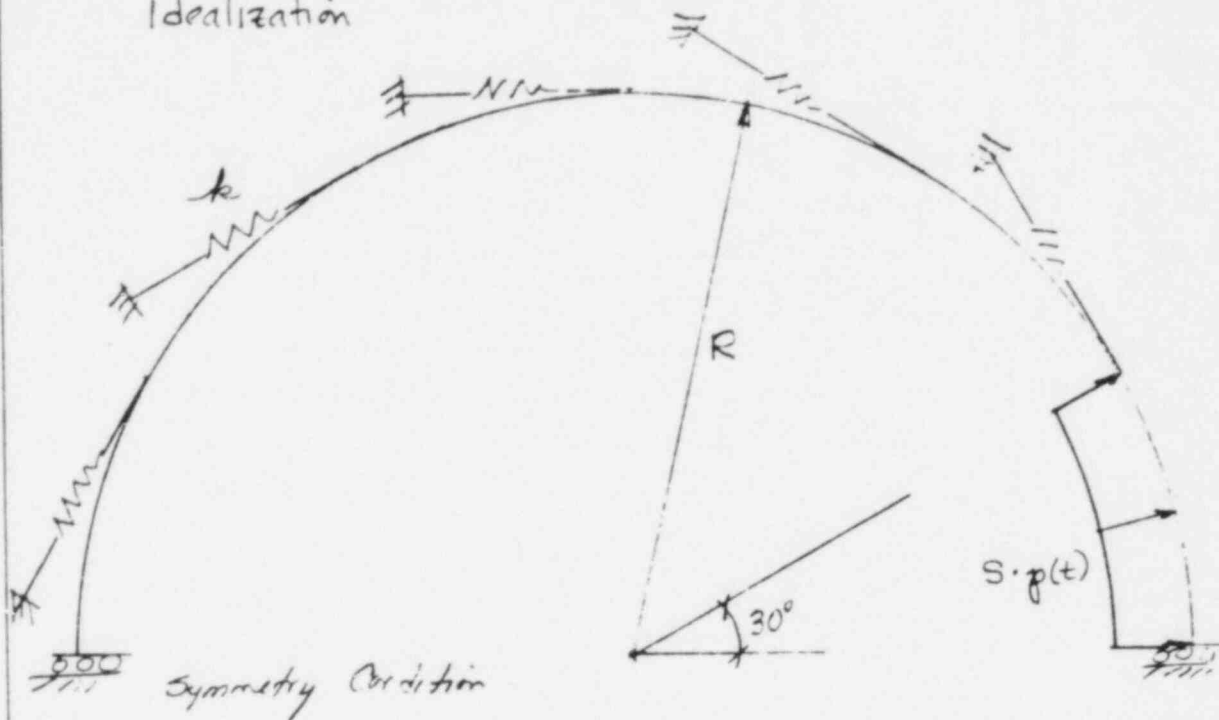
This assumption can be relaxed by a more sophisticated analysis which is beyond the present time constraint.

Other Assumptions

- . Shell below a typical ring is elastic (p. 229).
- . Venting pressure decreases linearly to zero at 0.030 sec (p. 231).
- . Ductility capacity of the ring is limited (p.

Consider Ring in lower compartment

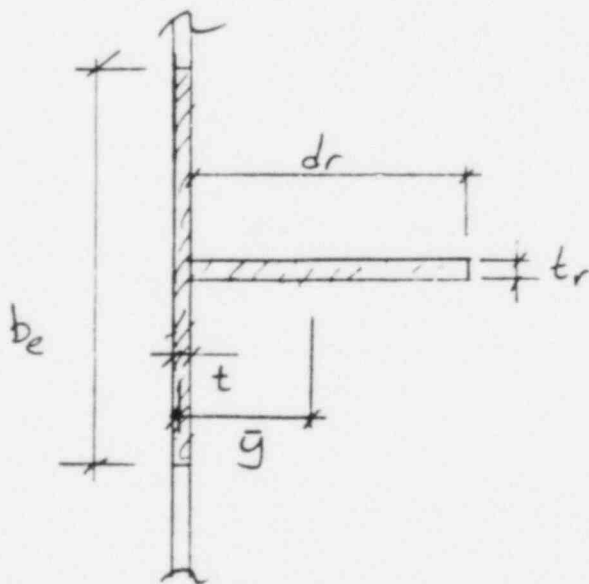
Idealization



k - springs representing restraint of sill below ring

s = ring spacing
 $p(t)$ = dynamic pressure

Ring Cross Section



b_e = effective length of sill

For typical ring in upper part of compartment

$$t = 1\frac{1}{16}''$$

$$d_r = 19.4''$$

$$t_r = 1\frac{1}{4}''$$

$$S = 120''$$

$$t_e = \frac{253}{\sqrt{F_y}} t = 47.5'' \quad (\text{AISC 1.9.2.2})$$

effective section properties

$$A = 74.72 \text{ in}^2$$

$$\bar{y} = 3.32'' \Rightarrow R = 693.9''$$

$$I = 2478.5 \text{ in}^4$$

$$Z = 258.4 \text{ in}^3 \quad (\text{plastic section modulus})$$

Material Properties

$$E = 29000 \text{ ksi}$$

$$F_y \text{ (static)} = 52 \text{ ksi}$$

$$F_y \text{ (dynamic)} = 57 \text{ ksi} \quad \left(\frac{\text{Str. De. for Dy. Loads, McGraw}}{1959, \text{ pg 6}} \right)$$

$$\rho = 7.246 (10^{-7}) \text{ k sec}^2/\text{in}^4 \quad (\text{mass density})$$

$$\rho \text{ (Air eff. section)} = \rho \frac{\text{Area}_a}{\text{A}_{eff}}$$

$$= 1.492 (10^{-6}) \text{ k sec}^2/\text{in}$$

Reasonable approach is by numerical methods (FE).

E.A. Witner, et al., "Large Dynamic Deformations of Beams, Rings, Plates and Shells," AIAA Jour., v. 1, No. 8, Aug. 1963, pp 1848-1857.

Hodge, "The Influence of Blast Characteristics on the Final Deformation of Circular Cylindrical Shells," J. of App. Mech., v.23, n.4, Dec. 1956, p. 617.

Owens & Symonds, "Plastic Deformations of a Free Ring Under Concentrated Dynamic Loading," J. of App. Mech., v.22, n.4, Dec. 1955, pp 523-529.

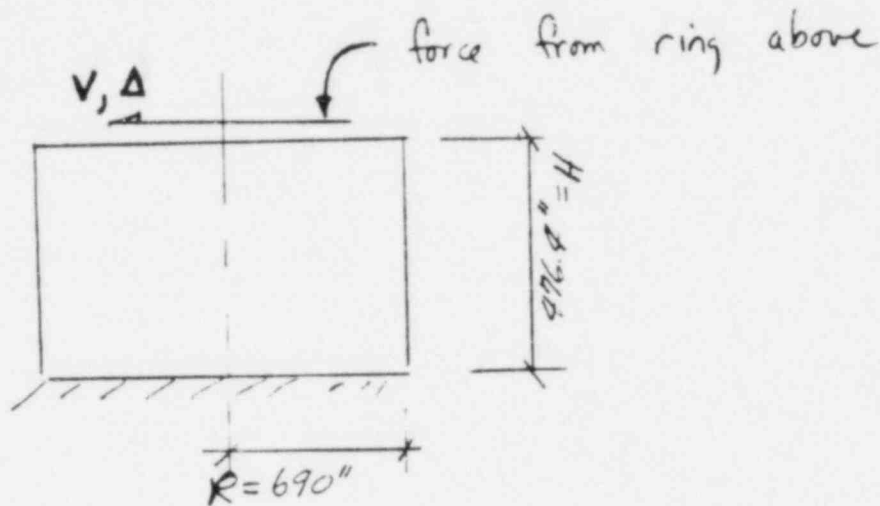
Spring Stiffness, k (lower portion of shell)

Neglect forces in shell above ring.

Neglect inertial forces in shell below ring.

Assume lower shell remains elastic.

Lower Shell



From deep beam theory, containment vessel acts as deep beam, cantilevered from base, under action of asymmetric dynamic load.

$$f = \text{flexibility} = \frac{\Delta}{V} = \frac{VH^3}{3EI} + \nu \frac{VH}{AG}$$

$$I = \pi R^3 t \quad (\text{entire shell})$$

$$A = 2\pi R$$

$$\nu = \text{shear shape factor} = 2$$

$$E = 2.6G$$

$$f = \frac{H}{AG} \left[0.256 \left(\frac{H}{R} \right)^2 + 2 \right] \approx \frac{2H}{AG}$$

$$A = 2\pi (690) \left(1 \frac{1}{16} \right), \quad G = 11500 \text{ KSI}$$

$$f = 1.799 (10^{-5}) \text{ in/k}$$

or

$$V = k \Delta \quad k = \frac{1}{f} = 55600 \text{ k/in. stiffness}$$

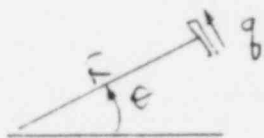
Select k (equivalent springs) such that above stiffness is obtained.

for typical spring

$$q = k \delta$$

$q = \text{force/length}$
 $\delta = \text{spring disp}$

$$V = 4 \int_0^{\frac{\pi}{2}} q \sin \theta R d\theta$$



$$V = 4 \int_0^{\frac{\pi}{2}} k \delta R \sin \theta d\theta$$

but δ for each spring = $\Delta \sin \theta$

$$V = 4 k \Delta R \int_0^{\frac{\pi}{2}} \sin^2 \theta d\theta = 4 k \Delta R \left[\frac{\pi}{4} \right]$$

$$= \pi k R \Delta$$

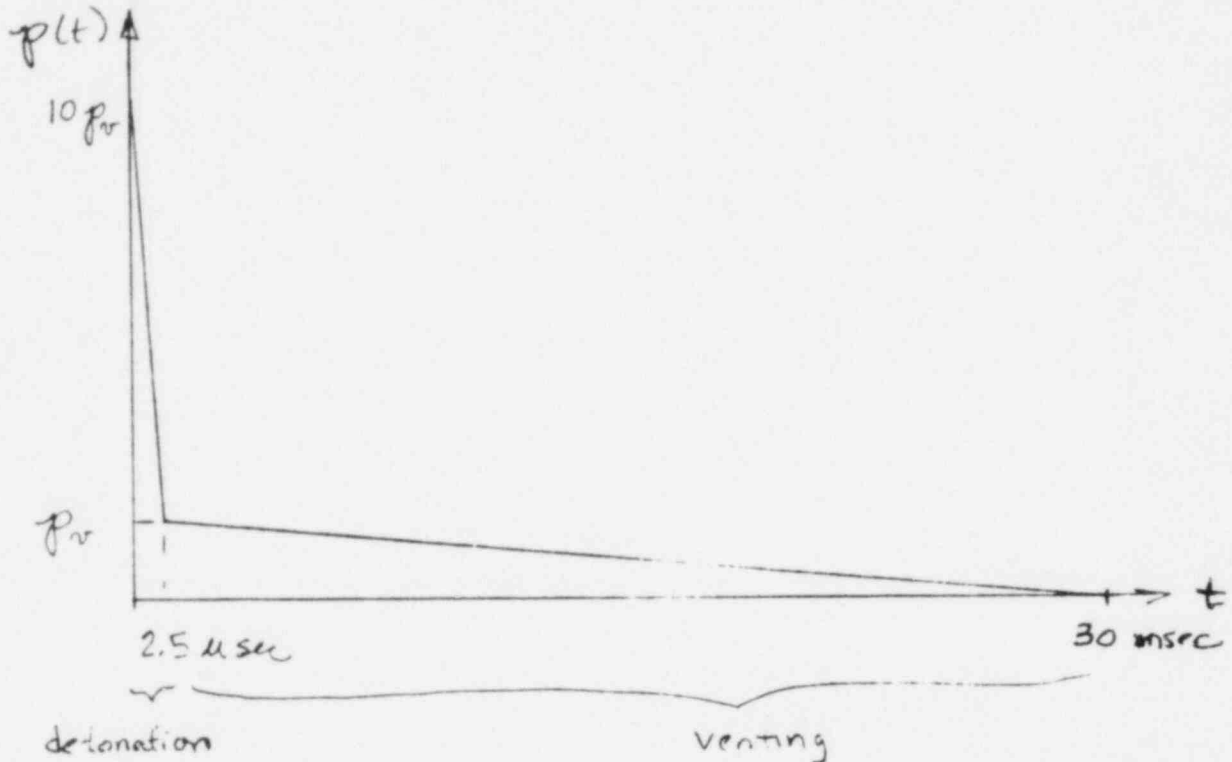
$$\text{or } k = \frac{K}{\pi R} = 25.65 \text{ k/in/in}$$

Note: $q = k \delta = k \Delta \sin \theta = \frac{k V \sin \theta}{K} = \frac{V}{\pi R} \sin \theta$

which is shear flow distribution for beams
 $\left(\frac{VQ}{It} \right)$

PRESSURE LOADING

Simulated Dynamic Pressures



Let p_v = venting pressure.

Assume detonation pressure = $10 p_v$.

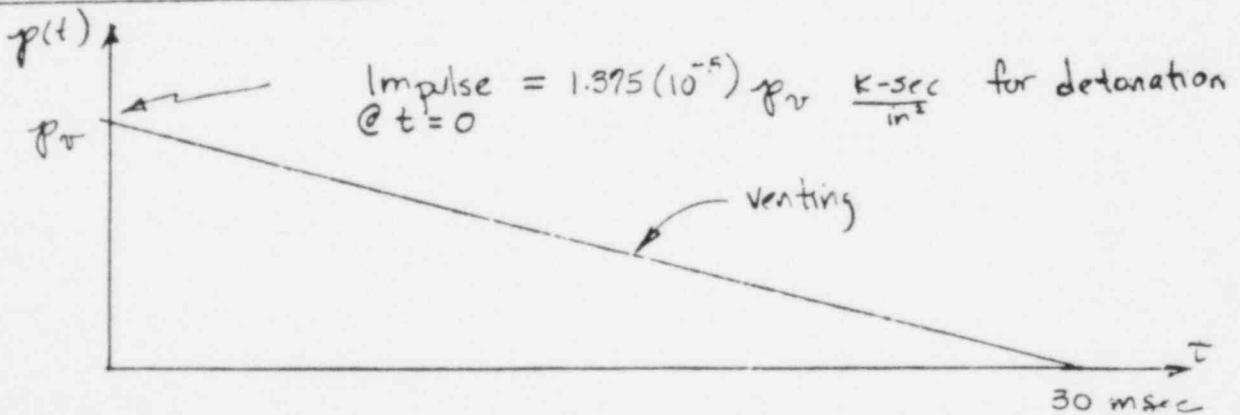
(as per material furnished by NRC)

Assume detonation time interval = $2.5 \mu\text{sec}$.

Assume venting time interval = 30 msec .

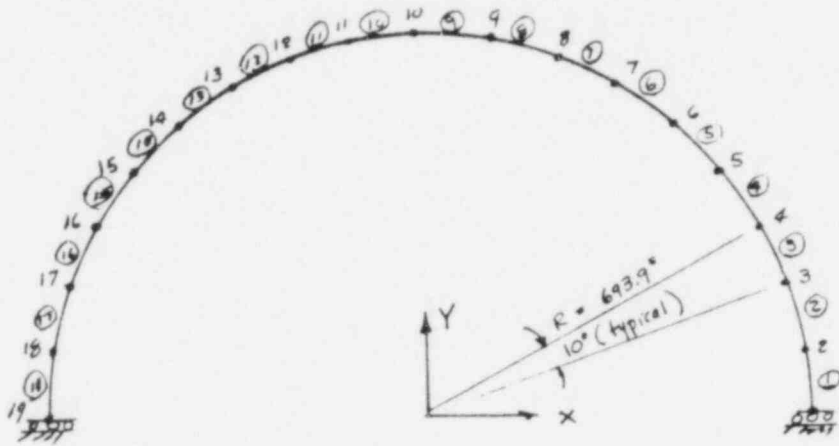
Note: Detonation pressure & time not very important since impulse associated with detonation is very small relative to venting impulse; also, detonation time is very small with reference to structural period.

IDEALIZED DYNAMIC PRESSURE



Finite Element Idealization

Ring



Elements are two-dimensional beam elements (STIF23 in ANSYS) with plastic deformation capability and stress stiffening capability (1st order approx. to large disp.).

$$A = 74.72 \text{ in}^2, I = 2479.5 \text{ in}^4, Z = 258.4 \text{ in}^4$$

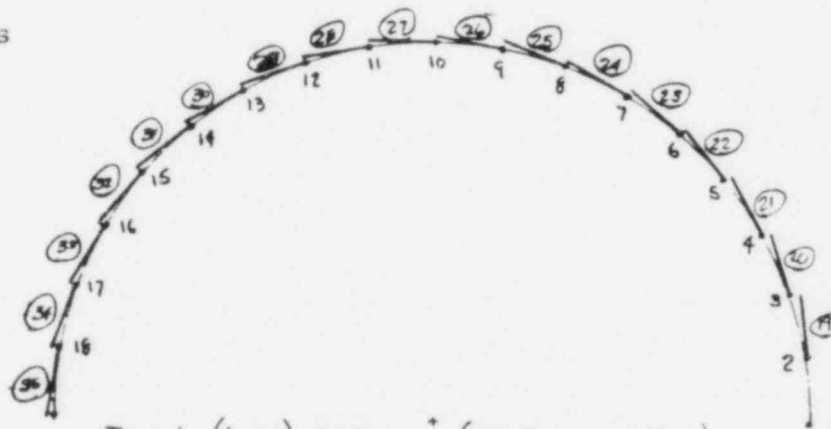
Material

$$E = 29000 \text{ ksi}, \nu = 1.492 (10^{-6}) \text{ ksec}^2/\text{in}^4$$

$$F_y = 32 \text{ ksi (static)}, F_y = 39 \text{ ksi (dynamic)}.$$

No strain hardening.

Support
Springs

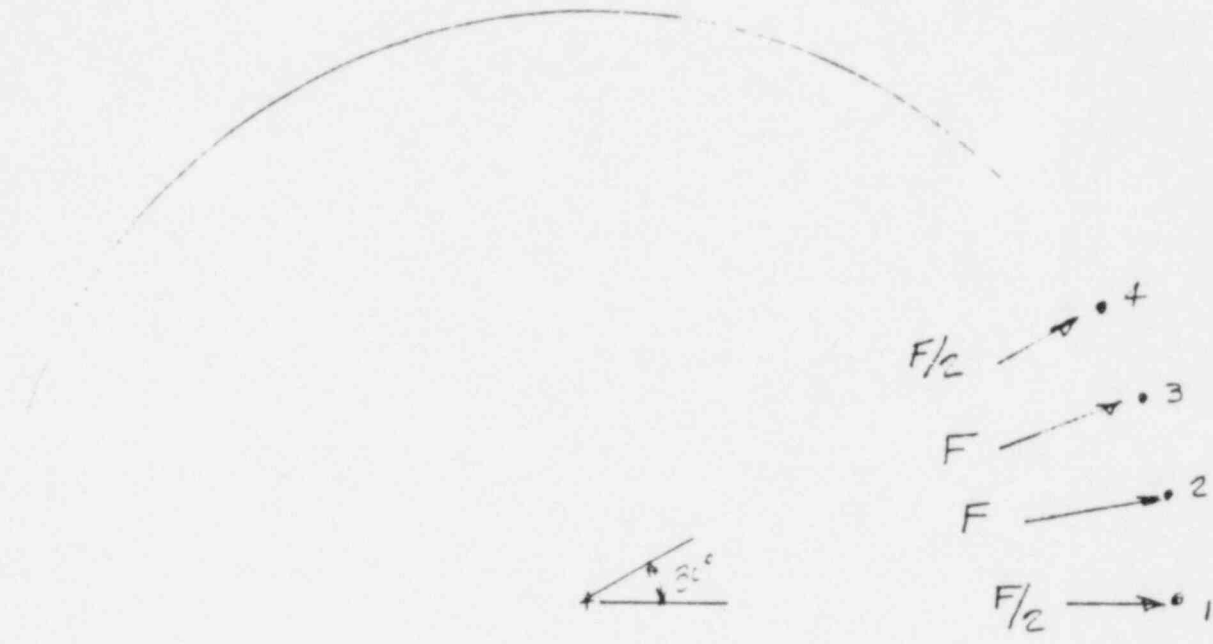


Typical (linear) spring * (STIF14 in ANSYS)

$$k_s = k \left(\frac{\pi}{18} \right) R = 25.65 \left(\frac{\pi}{18} \right) (693.9) = 3106 \text{ k/in}$$

← pg 232

Loads



$$F(t) = p(t) S \left(\frac{\pi}{18} R \right) = p(t) 120 \left(\frac{\pi}{18} \right) (693.9)$$

$$= 14500 p(t)$$

where $p(t)$ varies as on page 233
 (note. $p(t)$ in KSI units)

Initial Conditions (for dynamic analysis)

Initial Disp = 0

Initial Velocity = $\frac{\text{Impulse}}{\text{Nodal Mass}}$

Nodal Mass = $F A \left(\frac{\pi}{18} 693.9 \right)$ node 2 & 3

Impulse = $1.375 (10^{-5}) p_{or} S \left(\frac{\pi}{18} 693.9 \right)$ node 2 & 3

Initial Velocity = $\frac{1.375 (10^{-6}) p_{or} (120)}{1.492 (10^{-6}) 74.72} = 14.80 p_{or}$ ips

p_{or} = initial venting pressure

Note: Initial Velocity is probably negligible

Solution

Idealization on page 234 run in ANSYS with loads on page 235.

Static

Static Solution

p increased from 10 to 50 psi in increments of 5 psi

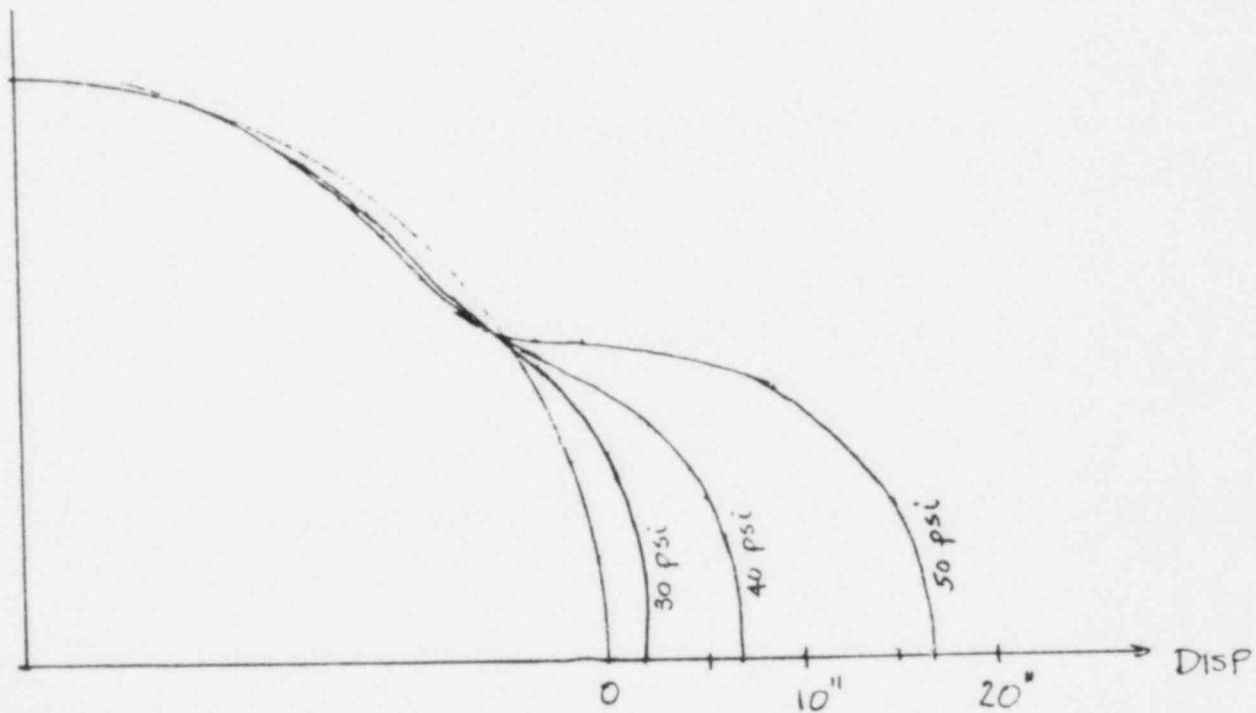
$F_y = 32$ ksi (yield strength)

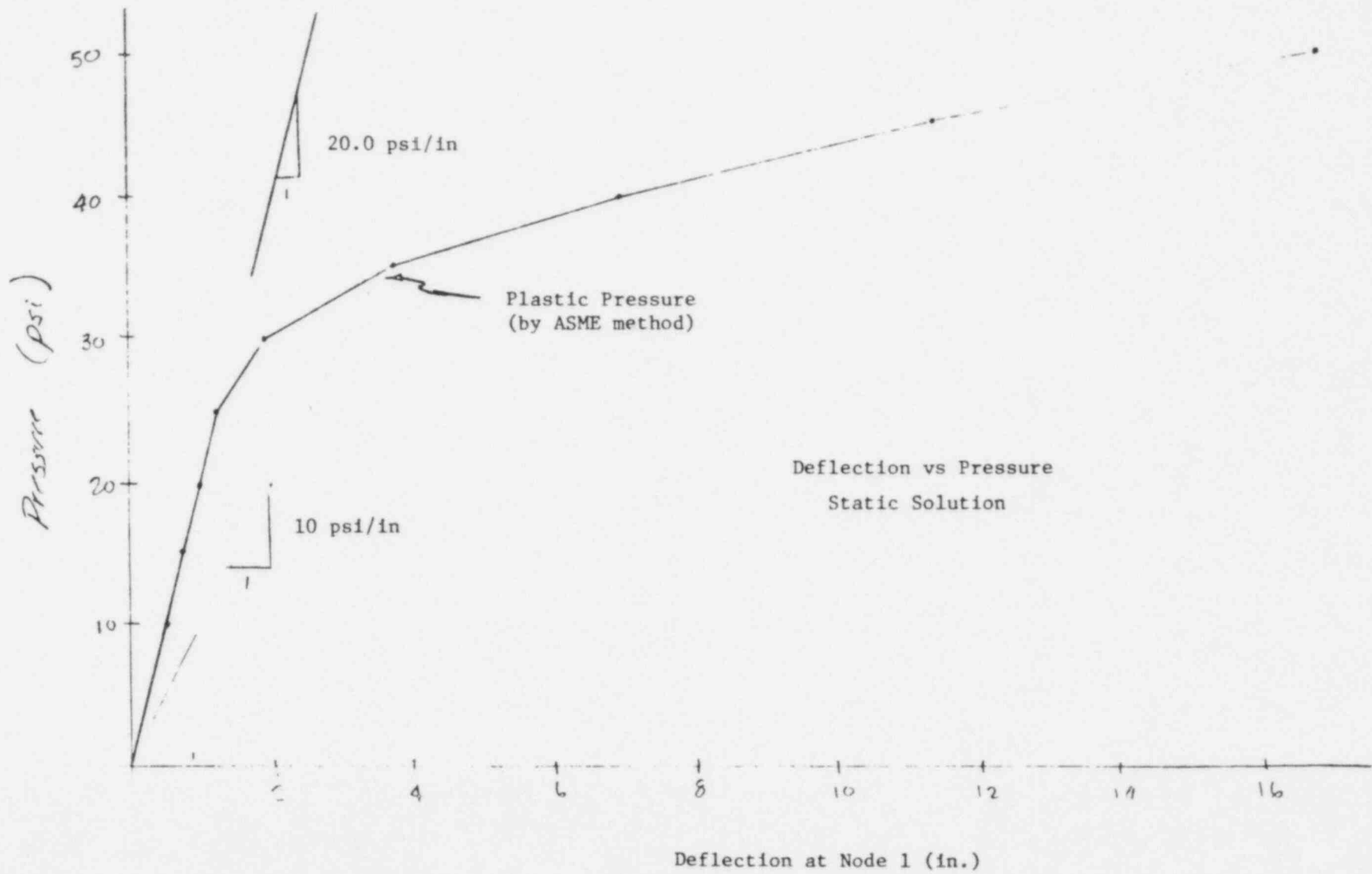
Convergence Criteria $\frac{\Delta \epsilon_p}{\epsilon_e} < 0.01$.

(Not satisfied above 30 psi, but not rerun because static solution not that useful.)

Deflection at Node 1 vs Pressure
(see following page)

Deflected Shape (right 1/2 of model)





Dynamic Solution

Dynamic Loads

Detonation & Venting - p. 233 + 235

p_v = ~~max~~ maximum venting pressure

= 10, 50, 100 psi

(three dynamic solutions)

Integration interval, Δt

FLSYS manual suggests $\Delta t = T/30$
where T is period of interest

$$T \approx \frac{2\pi}{\omega} \sqrt{\frac{M}{K}}$$

$$K \approx (0.020 \text{ ksi/in}) \left(\underset{\substack{\uparrow \\ p_0}}{10} \right) \left(\underbrace{\frac{\pi}{18} 693.9}_{\text{load area}} \right) (3)$$

$$= 871 \text{ k/in}$$

$$M \approx 1.492 (10^{-6}) \left(\underset{\substack{\uparrow \\ \rho}}{74.72} \right) \left(\underbrace{\frac{\pi}{18} 693.9}_{\text{volume in } 30^\circ \text{ arc}} \right) (3)$$

(assumes mass in 30° arc
is effective)

$$= 0.0405 \text{ k sec}^2/\text{in}$$

$$T \approx 2\pi \sqrt{\frac{0.0405}{871}} = 0.043 \text{ sec}$$

$$\Delta t \approx \frac{0.043}{30} = 0.0014 \text{ sec}$$

use $\Delta t = 0.001 \text{ sec}$

(this looks OK - see results for $p_v = 50 \text{ ksi}$
where $T \approx 0.04 \text{ sec}$)

Material Yield Stress

$F_y = 39 \text{ ksi}$ (to account for high strain rate,

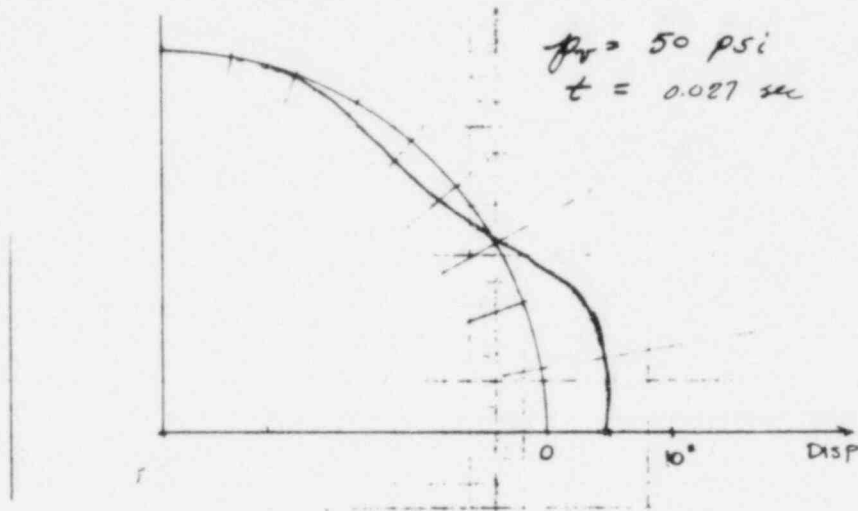
Results

Disp. at Node 1 vs Time

(see following page 240)

only results for $p_v = 50$ psi plotted

Deflected Shape



Maximum Strain

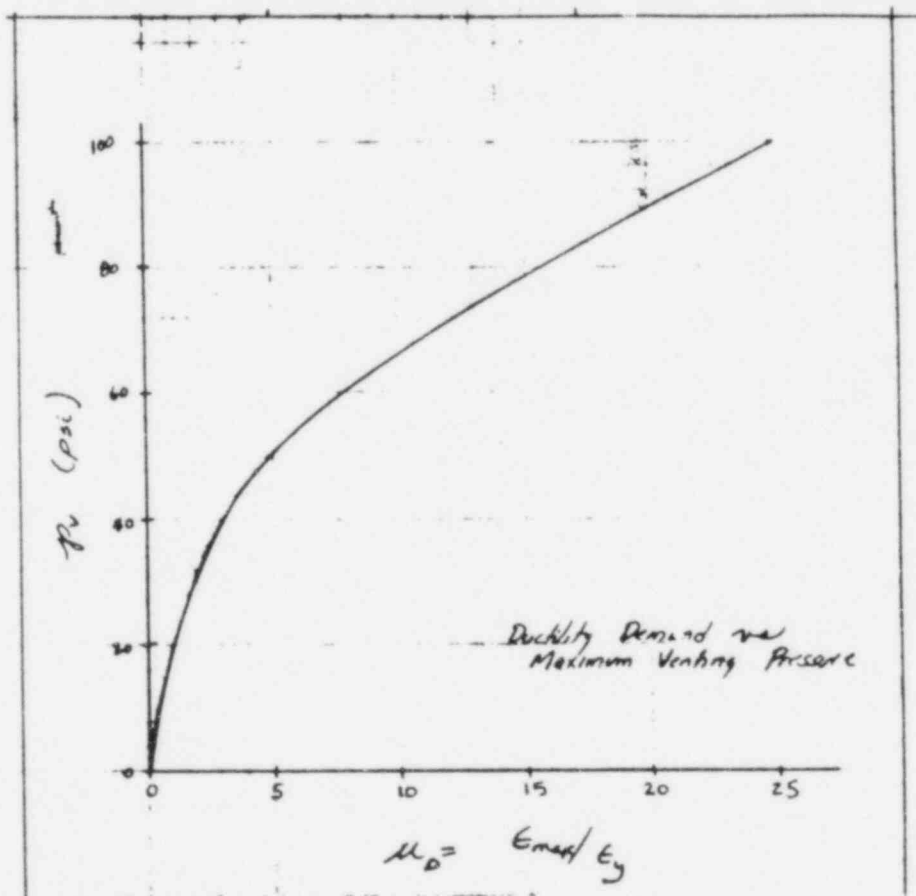
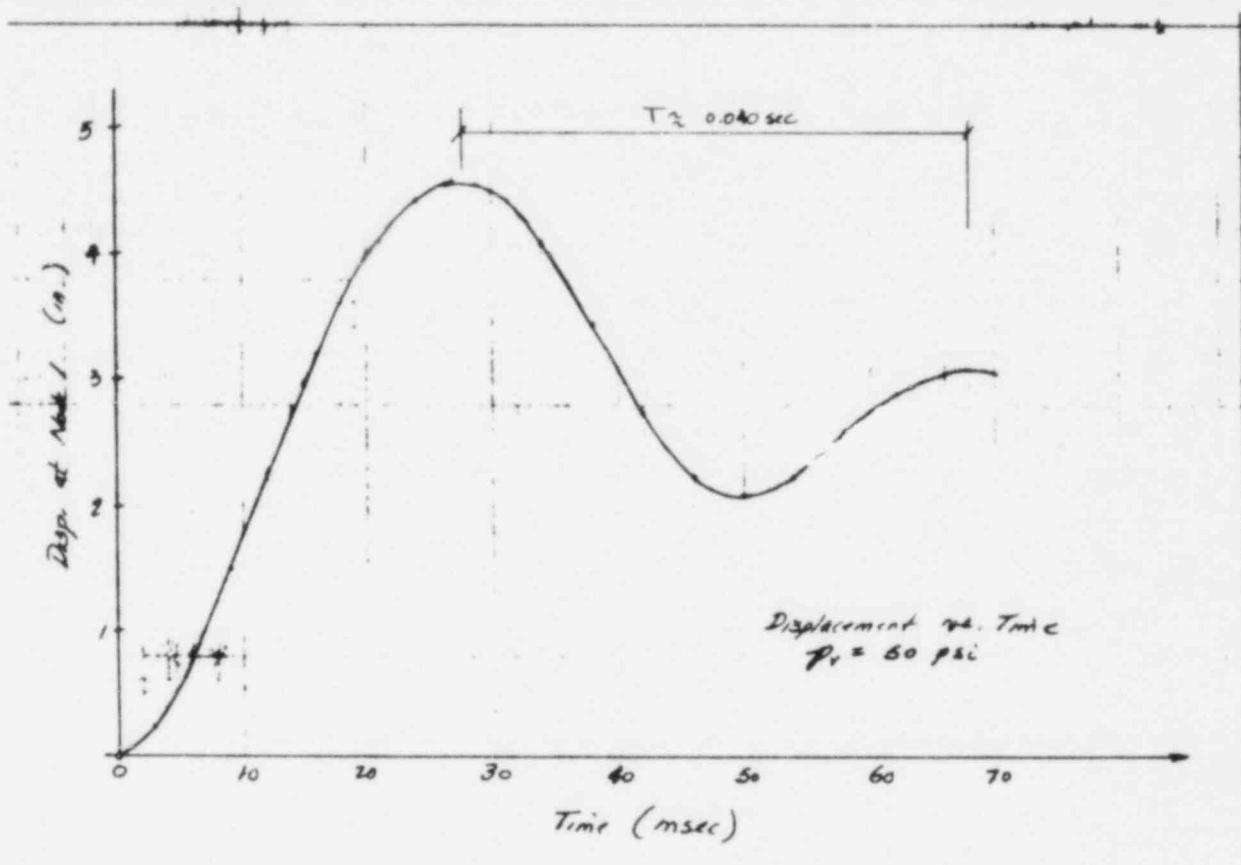
Output was searched for maximum strain in all elements, ϵ_{\max}

Ductility requirement is $\epsilon_{\max}/\epsilon_y = \mu_D$ where ϵ_y is yield strain
(1345 μ in/in)

Only membrane strains used (mid-surface). See later sections
for use of this strain in defining failure.

p_v	ϵ_{\max} (membrane)	μ_D	δ_{\max}
10 psi	504 μ in/in	0.4	0.6"
50 psi	6487 "	4.8	4.6"
100 psi	33520 "	24.9	24.9"

(See following page for plot.)



Failure Criteria

Estimate ductility limits of shell to prevent leakage

Ultimate Strength Failure (burst)
(no cracks)

$$S_r = \frac{f}{F_u} = 1 \tag{1}$$

f = applied stress

F_u = ultimate tensile stress of material
= 66 ksi (assumed max value)

Linear Elastic Fracture Mechanics

(no plastic deformation at crack tip)
(small crack propagates through shell)

$$K_{II} = K_{IId}$$

K_{II} = stress intensity factor

$$= 1.12 f_e \sqrt{\pi a}$$

1.12 - factor for partially through crack

f_e = elastic stress

a = crack size

Ref #1 S.T. Rolfe & J.M. Barsen, Fracture and Fatigue Control in Structures, Prentice Hall, 1977.

assume a = 1/16"

$$f_e \text{ (elastic stress)} \approx E_{max} E$$

(equivalent elastic stress)

$$\approx \mu \epsilon_y E$$

$$= \mu F_y$$

(μ = ductility factor
= E_{max}/E_y)

K_{Ic} = critical stress intensity factor for dynamic loading

approximate curve fit of data for ASME curve

Ref. #2 ASME Boiler & P.V. Code, Section III, Div. 1 - Subsection NA, Appendix G, Article - 2000.

see Ref #1, Fig. 15.1, Pg 437

$$K_{Ic} \approx 1.2 e^{0.0125(T+255)} + 26.8 \text{ ksi}\sqrt{\text{in}}$$

T = temp. above NDT (assume 80°F)

$$K_{Ic} = 105.8 \text{ ksi}\sqrt{\text{in}}$$

failure by LEFM

$$K_I = K_{Ic}$$

or

$$K_r = \frac{K_I}{K_{Ic}} = 1$$

$$K_r = \frac{1.12 f_c \sqrt{\pi a}}{K_{Ic}}$$

$$= \frac{f_c}{F_c} \tag{2}$$

where F_c = failure stress = $\frac{K_{Ic}}{1.12 \sqrt{\pi a}}$

$$= \frac{105.8}{1.12 \sqrt{\pi(\frac{1}{16})}} = 213.2 \text{ ksi}$$

Eq. (1) - failure with no cracks

$$S_r = 1$$

Eq. (2) - failure with plane strain conditions at crack tip (no through thickness yielding in plastic zone)

$$L_r = 1$$

Real case actually has cracks & a plastic zone. In lieu of elastic plastic fracture mechanics use two parameter interaction curve

$$K_r = S_r \left[\frac{8}{\pi^2} \ln \sec \frac{\pi}{2} S_r \right]^{-1/2}$$

Ref #3 R.P. Harrison, B.J.L. Darleston, C.H.A. Townley "Failure Assessment of Pressure Vessels Under Yielding Conditions", 3rd Int. Conf. on PV Technology, ASME, 1977.

Ref #4 H. Larsson & J. Bernard "Fracture of Longitudinally Cracked Ductile Tubes", Int. J. P.V. and Piping, Vol. 6, 1978 pp 223-293

Substituting $f = F_y$ (stresses at yield) into S_r

$$\frac{f}{S_r} = \mu F_y \quad \text{into } K_r$$

gives $(F_y = 39 \text{ ksi for dynamic case})$

$$\begin{aligned} \mu_c &= \text{ductility capacity of containment} \\ &= 5.01 \end{aligned}$$

This implies that the containment can withstand strains about 5 times the yield strain before leakage occurs.

Other approaches to ductility limits crack opening displacement [1, p. 530 & 532].

$$\frac{\epsilon}{\epsilon_y} = \mu_c = \phi + 0.25 = \frac{\delta_c}{2\pi \epsilon_y a} + 0.25$$

where δ_c = critical COD

δ_c (static) ≈ 0.4 mm (at high temp)
(Fig 16.9, 16.10, 16.11, 16.19)

δ_c (dynamic) ≈ 0.2 mm (0.008 in.)
(Fig. 16.12, 16.13, 16.14)

$$\mu_c = \frac{0.008}{2\pi (0.001345) \left(\frac{1}{16}\right)} + 0.25 = 15.4$$

Design Recommendations - includes some (unknown) F.S.

$$\mu_c = 2.$$

Ref #1, Fig. 16.16 a

$$\mu_c = \frac{0.004}{0.001345} = 2.97$$

Ref #1, bottom pg 533

$$\mu_c = \frac{2}{\pi f \epsilon_y} + 0.25$$

Ref #1, pg 535

for $f = 500$

$$\frac{f}{2} = \frac{1}{\pi (\epsilon - 0.25 \epsilon_y)} \quad \text{pg 532}$$

$$\mu_c = 1.2$$

for surface crack

for $f = 100$

$$\mu_c = 4.98$$

Summary

Ductility capacity, μ_c , of vessel is probably between 5 and 15 (dependent upon actual material properties and defects - in material and welds). Penetrations, with the resulting additional welding and complex geometry, will limit ductility. Deformations of the shell between rings (assumption, p. 228) will limit ductility. The ductility capacity of the ring will be selected as

$$\mu_c = 5$$

Ultimate Strength

Ultimate Strength is taken to be the maximum value of the working pressure for which leakage will not occur

$$P_u = (P_w)_{\text{max. w/o leakage}}$$

Ductility Demand on Structure

see μ_D vs M_D , Pg 240

Ductility Capacity of Structure

$$\mu_c = 5 \quad , \text{ pg 244}$$

Ultimate Strength

$$\mu_D = \mu_c$$

$$\mu_D = 5$$

or, from pg. 14, maximum value of working pressure

$$\underline{\underline{P_u = 51 \text{ psi}}}$$

(Note, if μ_c were taken as 10, P_u would be 66 psi)

NRC FORM 335 <small>(11-81)</small>		U.S. NUCLEAR REGULATORY COMMISSION BIBLIOGRAPHIC DATA SHEET		1. REPORT NUMBER (Assigned by DDC) NUREG/CR-1891 IS-4753	
4. TITLE AND SUBTITLE (Add Volume No., if appropriate) Reliability Analysis of Containment Strength Sequoyah and McGuire Ice Condenser Containments				2. (Leave blank)	
7. AUTHOR(S) L. Greimann, F. Fanous, A. Sabri, D. Ketelaar, A. Wolde-Tinsae, D. Bluhm				3. RECIPIENT'S ACCESSION NO.	
9. PERFORMING ORGANIZATION NAME AND MAILING ADDRESS (Include Zip Code) Ames Laboratory Iowa State University Ames, Iowa 50011				5. DATE REPORT COMPLETED MONTH YEAR April 1982	
12. SPONSORING ORGANIZATION NAME AND MAILING ADDRESS (Include Zip Code) Office of Nuclear Reactor Regulation Nuclear Regulatory Commission Washington, D.C. 20555				6. (Leave blank)	
13. TYPE OF REPORT Technical Report				DATE REPORT ISSUED MONTH YEAR August 1982	
PERIOD COVERED (Inclusive dates) September 1, 1979 to September 30, 1980				8. (Leave blank)	
15. SUPPLEMENTARY NOTES				10. PROJECT/TASK/WORK UNIT NO.	
16. ABSTRACT (200 words or less) <p>The Sequoyah and McGuire ice condenser containment vessels were designed to withstand pressures in the range of 12 to 15 psi. Since pressures of the order of 28 psi were recorded during the Three Mile Island incident, a need exists to more accurately define the strength of these vessels. A best estimate and uncertainty assessment of the strength of the containments was performed by applying the second moment reliability method. Material and geometric properties were supplied by the plant owners. A uniform static internal pressure was assumed. Gross deformation was taken as the failure criterion. Both approximate and finite element analyses were performed on the axisymmetric containment structure and the penetrations. The predicted strength for the Sequoyah vessel is 60 psi with a standard deviation of 8 psi. For McGuire, the mean and standard deviation are 84 psi and 12 psi, respectively. In an Addendum, results by others are summarized and compared and a preliminary dynamic analysis is presented.</p>				11. FIN NO. A4131	
17. KEY WORDS AND DOCUMENT ANALYSIS				14. (Leave blank)	
17a. DESCRIPTORS					
17b. IDENTIFIERS: OPEN-ENDED TERMS					
18. AVAILABILITY STATEMENT Unlimited				19. SECURITY CLASS (This report) Unclassified	
				21. NO. OF PAGES	
				20. SECURITY CLASS (This page) Unclassified	
				22. PRICE \$	

UNITED STATES
NUCLEAR REGULATORY COMMISSION
WASHINGTON, D.C. 20555

OFFICIAL BUSINESS
PENALTY FOR PRIVATE USE, \$300

FOURTH CLASS MAIL
POSTAGE & FEES PAID
USNRC
WASH D C
PERMIT No. 667

120555078877 1 ANRD
US NRC
ADM DIV OF TIDC
POLICY & PUBLICATIONS MGT BR
PDR NUREG COPY
LA 212
WASHINGTON DC 20555